BRUNEL UNIVERSITY

SCHOOL OF INFORMATION SYSTEMS, COMPUTING
AND MATHEMATICS

Dissertation

NUMERICAL IMPLEMENTATION OF A COHESIVE ZONE MODEL FOR TIME AND HISTORY DEPENDENT MATERIALS

by

LAYAL HAKIM

Thesis submitted in fulfillment of the
requirements for the degree of
Doctor of Philosophy

to the

Department of Mathematical Sciences
March 2014

Abstract

A cohesive zone model approach is used in order to study the behaviour of cracks in elasto-plastic materials. The cohesive zone model being studied is time-dependent, unlike standard cohesive zone models in elasto-plasticity. The stress distribution over the cohesive zone is related to the normalised equivalent stress functional, and is expressed in the form of an Abel-type integral equation. During the stationary crack stage as well as the propagating crack stage, the aim is to study the behaviour of the cohesive zone length with respect to time as well as the crack tip opening. To aid accomplishing this aim, the stress intensity factor was set to zero at the cohesive zone tip. As well as other material parameters, the external applied load participates in the model equations. We will consider two cases for the external load, namely the case when this load is constant in time, and the case when this load behaves linearly with time. We will implement numerical schemes to obtain the crack growth as well as the cohesive zone growth with respect to time for both the elastic case and the visco-elastic case while considering different sets of parameters. The numerical convergence rates are obtained for each of the problems solved. This justifies the suitability of the numerical schemes used.

Contents

List of Figures

List of Tables

Biographical Sketch

I was born in London, England. I attended Brunel University, and graduated with a Bachelors of Science degree with Honors in Mathematics in July 2010. After that, I started a doctoral course in the same department under the supervision of Professor Sergey Mikhailov. My main interests lie in the area of fracture mechanics, numerical techniques to solve integral equations, and programming using MATLAB. I also enjoy reading about other topics in mathematics and philosophy; and I enjoy painting. I have given 8 presentations during the past 3 years at conferences and symposiums. The following publications are results of the work conducted

1. Hakim L., Mikhailov S.E. *Cohesive Zone Models in History Dependent Materials*, Proceedings, International Conference on Computational Mechanics 2013, CM13., Durham, England, 25-27 March, 2013

2. Hakim L., Mikhailov S.E. *Integral Equations in Cohesive Zones Modelling of Fracture in History Dependent Materials*, Proceedings, World Congress on Engineering 2013, Newswood Limited, International Association of Engineers, pp. 226-231, 2013

3. Hakim L, Mikhailov S.E., *Nonlinear Abel Type Integral Equation in Modelling Creep Crack Propagation*, Integral Methods in Science and Engineering: Computational and Analytic Aspects, edited by Constanda C. and Harris P., Springer, pp. 191-201, 2011.

4. Hakim L., Mikhailov S.E., *Numerical Implementation of a Cohesive Zones in History-Dependent Materials*, arXiv:1403.3708, 2014

Acknowledgements

This thesis was made possible due to the masterly guidance of my supervisor, Professor Sergey Mikhailov. I would like to thank him for his endless encouragement and help. There have been times when I felt lost with my research, but inevitably, a meeting with Sergey would reinvigorate my enthusiasm. I am very honoured to have him as a supervisor.

My time spent at the Department of Mathematical Sciences at Brunel university doing my PhD and undergraduate degree has been memorable. I am very grateful for the inspiration I received from the academic staff in the department. I hope to pass on a similar kind of passion to the future generation of mathematicians. Special thanks to Dr. Jacques Furter who taught me the essence of all perfection, and to Dr. Matthias Maischak for his on-going help with programming. Many thanks to Professor Julius Kaplunov and Professor Lane Hughston for their useful advice. Thanks to all the administrative staff at the department. They have always been very friendly and a pleasure to be around.

I have been blessed with a loving and supportive family. Many thanks go to my parents for being very patient whilst I worked on this project; I am in debt to them. I would also like to thank all my siblings, they have always been the perfect pillow to lean on.

I would like to thank Elena Kossovich for welcoming me into the department and making me feel special. Thanks to Kinga Zaczek, Alex McKee, Nina Grishina, Suren Islyaev, Dima Savin, Rodrigo Megaides, and Paresh Date for being a great pleasure to be around in between my research hours. Thanks also to Diane McKenzie, Mursal Sherzai, and Fiona

White for their support and great times we spent together. Many thanks also goes to Carolyn Chun, Rhiannon Hall, Jean-Baptiste de Vaux, George Itonishvili, Matthias Gläfke, Vitaly Voloshin, and Victor Arulchandran for their moral support. Thinking about the great time spent with them makes me smile and causes a great rush of nostalgia. I would also like to thank Fadi Alammarine for teaching me perseverance and for his encouragement during the final stage of my thesis.

Teaching undergraduate students at Brunel university in between my research hours has been enjoyable and memorable. They will all be missed. Thanks to everyone else whom I did not mention here but have been helpful and supportive.

Chapter 1

Introduction

Fracture mechanics is a mature subject. It is an essential topic for understanding and predicting the failure of buildings and machines. For many centuries, engineers have been studying the durability of materials; the main approach for this is to identify when failure will occur. This mainly concerns nucleation and propagation of cracks in a body. Cracks appear or grow due to stresses caused by external forces. The external load applied on the material could cause a crack to initiate, or could cause growth of an already existing crack and the presence of a crack could lead to rupture when the crack propagates directly through the body. To predict the strength of the material and where fracture will occur, the local approach or the non-local approach can be used. The local approach uses the stress (or stress history) at the point where the crack appears, while the non-local approach uses not only the stress (history) at the point but also in the vicinity of that point.

Problems in fracture mechanics can be classified to belong in two categories: (i) linear elastic fracture mechanics or (ii) elasto-plastic fracture mechanics. Cohesive Zone (CZ) models have been used as a tool to study the behaviour of cracks in elasto-plastic materials.

The CZ in a material is the area between two separating but still sufficiently close

surfaces ahead of the crack tip, this CZ is illustrated by the shaded region in Figure 1.1, where $\hat{c}$, and $\hat{a}$ denote the CZ tip coordinate and the crack length respectively. Also, $\hat{q}$, and $\hat{\delta}$ respectively denote the external load and the crack tip opening. At the CZs, there are cohesive stresses $\hat{\sigma}$ opposing the effect of the external load $\hat{q}$.

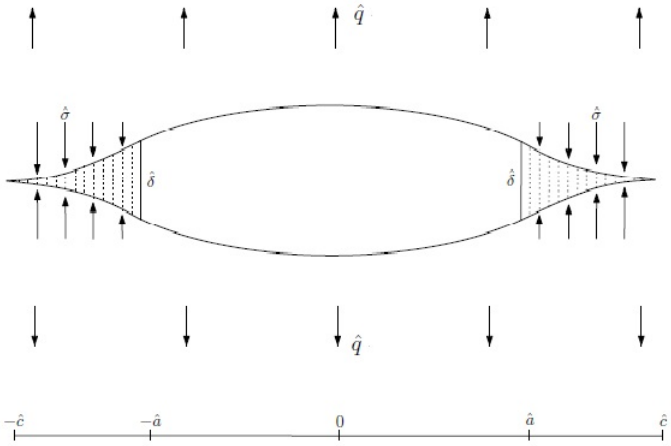

Figure 1.1: Cohesive zone

The external load $\hat{q}$ is constant in space and it is first taken to be independent of time. However, in some real life applications, it can be a function of time. To this end, we can construct a relationship between the load $\hat{q}$ and time $\hat{t}$ and see how the behaviour of the crack changes. The relationship that we will consider in this project is simply a linear relationship, namely $\hat{q} = s\hat{t}$ where s is a constant.

There have been many CZ models introduced in the literature. The cohesive stress $\hat{\sigma}$ is defined by a traction-separation law which can be different depending on the CZ model considered. The simplest case is when the cohesive stress is constant. This case was introduced by Dugdale, Leonov, and Panasyuk (DLP) (1959-1960), see [19,33]. In the DLP model, the maximal normal stress in the CZs is constant and equals to the material yield stress. This model is one of the most popular CZ models and many modifications of this model have been made and widely used in nonlinear fracture mechanics. Another popular CZ model is the Barenblatt (1962) model. The 3 main components needed to study CZ

models are:

- the constitutive equations in the bulk of the material;
- the constitutive equations in the CZ;
- the criterion for the CZ to break, i.e. the crack to propagate.

Many CZ models involve time-independent stresses in the cohesive region; however, since many materials (such as polymers) exhibit creep behaviour, time-dependent stress is a vital factor which has largely been ignored in most CZ models in the literature. The model presented in this thesis is an extension of the DLP model by using a non-linear history-dependent constitutive equation in the CZ. Thus, the stresses in the CZ will now be time and history dependent. Although this is not generally necessary, in this project we will assume that a crack already exists in the material. Furthermore, we assume that there can exist a CZ ahead of the crack tip.

The crack opening is an important part in terms of analysing when crack propagation will initiate. Crack propagation begins when the crack tip opening reaches a critical value known as the critical crack tip opening. Once the crack starts growing, the CZ will grow simultaneously with the crack but not necessarily at the same rate. By analysing CZ models in materials, we would like to know or find out the size of this CZ, the time when the crack will start to propagate, and more importantly, when total rupture of the material will occur.

Our aim is to study the behaviour of the CZ length with time during 2 stages: (i) stationary crack stage; and (ii) propagating crack stage. In each of these 2 stages, we will consider 2 cases of the constitutive equations for the bulk of the material: (i) linear elastic materials; and (ii) linear viscoelastic materials. We will compare the results obtained in the elastic case to that of the viscoelastic case as well as analyse the effect, on the CZ, of having an external load varying in time compared to the case when it is constant. After formulating the problems, we will obtain numerical solutions using appropriate numerical techniques. All algorithms were implemented using MATLAB as a programming language.

Given below is the layout for this thesis according to the contents of each chapter.

Arrangement of the Thesis

- Chapter 2: Literature Review:

  An overview on the work that has been done by researchers in topics related to this thesis are given in this chapter. This includes an introduction to linear elastic fracture mechanics as well as an overview on elasto-plasticity, specifically CZ models. Also covered is the description of a CZ and where such models lie in the field of fracture mechanics. Also presented is a brief history of the most commonly used CZ models considered (such as the Dugdale and Barenblatt models). Viscoelasticity is an important part of the project thus an introduction of viscoelasticity will be given in this chapter.

- Chapter 3: Model Problem Formulation:

  The formulation of the problem is given. The yield condition (CZ appearance criterion), which represents the normalised equivalent stress functional in the form of an Abel-type integral equation, is discussed. Also given in this chapter is a normalisation of the principal variables and equations used to solve the problem.

- Chapter 4: Cohesive Zone Growth with a Stationary Crack:

  While the crack is stationary, we introduce a numerical algorithm which was used to obtain the CZ tip position with time. This also involves computing the stresses ahead of the CZ, at the CZ tip and in the CZ. To this end, graphs of CZ length vs. time as well as stress (at a specific point in space) vs. time are presented.

- Chapter 5: The Crack Tip Opening:

  We introduce the formula used to calculate the crack opening at a specific point in time and space. We consider the crack opening in a linear elastic material as well

as that in a linear viscoelastic material. Using the material parameters of PMMA, we obtain the crack tip opening growth with respect to time for different sets of parameters.

- Chapter 6: Cohesive Zone Growth with a Propagating Crack:

  To begin this chapter, we define and explain the use of the critical crack tip opening displacement which is a crucial aspect while studying crack growth. This critical parameter will be used further on in the project. Crack growth initiates when the crack tip opening reaches a critical value. A numerical algorithm is presented which outputs the crack growth as well as CZ growth with time. Consequently, we present some solutions obtained for different sets of parameters.

- Chapter 7: Time-dependent External Load:

  Another one model problem is considered where the external load $\hat{q}$ is a linear function in time. The resulting equations have been formulated. The solutions for this case are presented; this includes the crack length as well as the CZ length for both the elastic and viscoelastic cases while the load is varying in time.

- Chapter 8: Numerical Convergence Rate:

  Verifying the suitability of numerical schemes is an important part of knowing how accurate the solutions are. In this chapter we obtain the numerical convergence rate at a specific point in time for the solutions of each model problem discussed.

- Chapter 9: Discussion and Evaluation:

  This chapter is used to analyse the behaviour of the solutions. This includes discussing the obtained solutions for the CZ length, crack length and stresses.

- Chapter 10: Conclusions and Ideas for Further Research:

  We give a summary of the conclusions and present some ideas on how the project can be extended further by considering related problems.

Chapter 2

Literature Review

2.1 Linear Elastic Fracture Mechanics

Linear elastic fracture mechanics (LEFM) is usually used to analyse crack initiation and growth in linear elastic materials. There are a few assumptions needed in order for linear elastic fracture mechanics to be applicable. The main assumption is that the plastic deformation zone, which is at the crack tip, needs to be small compared to the whole crack, see [13]. In general, the partial differential equation of motion for a linear elastic body is given by

$$\nabla\sigma + F = \rho\ddot{u}, \tag{2.1}$$

where $\nabla\sigma$ denotes the divergence of the stress tensor σ, see e.g. [38,57]. Also, F denotes the force acting on the body per unit volume, ρ is the mass density, and the vector u denotes the displacement (so $\ddot{u}$ is the acceleration of the deforming body). This equation reduces to the equation of equilibrium when the acceleration is zero. In this text, we will use the

following notation

$$u_{i,j} = \frac{\partial u_i}{\partial x_j},$$

and similarly for other components such as the stress components. Also, in what follows, we will use Einstein's summation convention. This convention, which is applied when we have repeated indices in the product of variables, is given by the following

$$x_i y_i = \sum_i x_i y_i.$$

To this end, equation (2.1) can be written in the form

$$\sigma_{ij,j} + F_i = \rho \ddot{u}_i. \tag{2.2}$$

The stress tensor can be expressed as the product of the stiffness tensor and the infinitesimal strain tensor; this is given by

$$\sigma_{ij} = C_{ijkl}\varepsilon_{kl} \quad i, j, k, l = 1, 2, 3, \tag{2.3}$$

where C_{ijkl} is symmetric with respect to its indices so that $C_{ijkl} = C_{klij} = C_{jikl} = C_{ijlk}$, and the components of the strain tensor ε_{kl} can be expressed as

$$\varepsilon_{kl} = \frac{1}{2}(u_{k,l} + u_{l,k}). \tag{2.4}$$

Equation (2.3) is known as Hook's law for anisotropic linear elastic materials. Using equations (2.2), (2.3), (2.4), and the symmetry of the stiffness tensor, we can write the partial differential equations of motion in a linear elastic material as

$$(C_{ijkl}u_{k,l})_{,j} + F_i = \rho \ddot{u}_i \quad \text{in } \Omega \tag{2.5}$$

where Ω denotes the region of the body. The equations given by (2.5) are known as the Lamé equations. If the body is homogeneous and isotropic, then the stiffness tensor C_{ijkl} can be written as

$$C_{ijkl} = \lambda \delta_{ij}\delta_{kl} + \mu(\delta_{ik}\delta_{jl} + \delta_{il}\delta_{jk}),$$

where λ and μ are the elastic constants known as the Lamé constants. Consequently, equation (2.5) is given by

$$(\lambda + \mu)u_{j,ji} + \mu u_{i,jj} + F_i = \rho \ddot{u}_i.$$

Consider a body with a crack as in Figure 2.1. The traction vector on any surface with unit normal $\vec{n}$ in terms of the stress components is given by the following equation

$$T_i(n, x) = \sigma_{ji}(x)n_j,$$

see e.g. [57]. These equations are known as the Cauchy formulas. The forces or displacements on the boundary are called boundary conditions. The boundary conditions depend on the nature of the problem. We can have traction prescribed on the boundary, or displacements, or both; but not both at the same point. For instance, if we use Dirichlet boundary conditions, for the displacements, the boundary conditions are given by

$$u_i(x) = v_i(x) \quad x \in \Gamma_D,$$

where $v_i(x)$ is a known function. If we consider Neumann boundary conditions, the boundary conditions for the traction are given by

$$T_i(x) = g_i(x) \quad x \in \Gamma_N,$$

where $g_i(x)$ is a known function. Let Γ_{NC} denote the boundary of the crack faces. At the crack faces, the traction is usually known to be zero

$$T_i(x) = 0 \quad x \in \Gamma_{NC}.$$

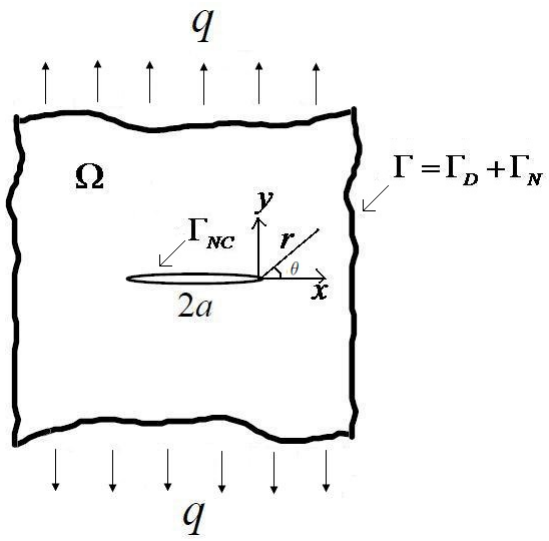

Figure 2.1: Linear elastic body with a crack, see [38].

2.1.1 Fracture Modes and the Stress Intensity Factors

The stress intensity factor is used to predict the stress state at the crack tip. There are 3 types of stress intensity factors, K_I for Mode I type (opening mode), K_{II} for Mode II (shearing mode), and K_{III} for Mode III (tearing mode); each type depends on how the crack vicinity deforms. Figure 2.2 below shows the 3 types. We will further consider the Mode I loading which is when the crack opens in a perpendicular direction to the plane of the crack.

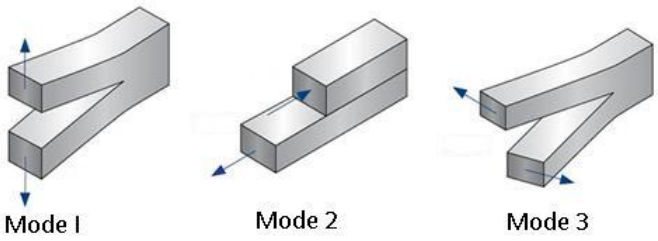

Figure 2.2: Fracture modes I, II, and III, taken from [65].

When the stress intensity factor reaches a critical value, this leads to crack growth and

possibly failure of the material. Denoted by K_C, the critical stress intensity factor is a material parameter and it is also known as the fracture toughness of a material. The fracture toughness for a material under Mode I loading is denoted by K_{IC}.

Considering an infinite plate containing a straight crack of length $2a$, the stress intensity factor under Mode I loading for such a plate subjected to external loads, σ_∞, is given by (e.g. see [2])

$$K_I = \sigma_\infty \sqrt{\pi a}. \tag{2.6}$$

As well as the stress intensity factor, an important characteristic in the field of linear elastic fracture mechanics is the strain energy release rate, G. This represents the rate of change of the mechanical energy U_M of an elastic material with respect to the change of half the crack length a, that is

$$G = \frac{dU_M}{da},$$

see [32]. This mechanical energy U_M consists of the work done by the external applied load (we will denote this as U_L) and the potential energy stored in the elastic material (we will denote this energy term by U_P). The strain energy release rate, G, is also known as the crack-extension force. Under mode I loading, G and K_I are related. For the *plane stress* state, the relationship is given by the following formula

$$G = \frac{K_I^2}{E},$$

and for the *plane strain* state, the relationship is given by

$$G = \frac{K_I^2}{E}(1 - \nu^2),$$

where ν denotes Poisson's ratio; see [2]. The fracture energy G_c, which is also known as the critical energy release rate, is the amount of energy needed to cause the crack to propagate. In other words, the crack will propagate when the strain energy release rate G reaches or exceeds the fracture energy G_c; or alternatively, when the stress intensity factor K_I reaches or exceeds K_{IC}.

2.1.2 The Griffith's Criterion

One of the first scientists to research into the field of fracture mechanics was A.A. Griffith (in 1920). Griffith derived a criterion for the fracture of a body based on the change of the body's total energy, see [13]. Griffith considered materials which are elastic and brittle. Consider a static linear elastic body with a crack of length $2a$ subjected to external loads. The total energy of a body, say U, is given by

$$U = U_M + U_S = (-U_L + U_P) + U_S. \tag{2.7}$$

see [32]. As mentioned before, the term U_M denotes the mechanical energy of the body. Whereas, the second term of equation (2.7), U_S, denotes the surface energy; this is the energy required to separate atomic bonds and form new cracks. As a crack propagates, the mechanical energy of the whole system will decrease while the surface energy will increase. In other words, the two energy terms (mechanical and surface energy) in equation (2.7) must balance; this is known as thermodynamic equilibrium, see [32]. The requirement for equilibrium is given by the Griffith energy-balance concept:

$$\frac{dU}{da} = 0,$$

i.e. the change in total energy with respect to crack length is 0.

Griffith experimented on glass which is a linear elastic and isotropic material that satisfied Hook's law before fracture occurs. Griffith obtained a relationship between the work done by external loads U_L and the potential energy U_P of the elastic body under constant external loads during crack formation. This relationship is given by

$$U_L = 2U_P, \tag{2.8}$$

which implies that all the work done goes to the potential energy. Griffith obtained the following results for a plate of thickness B, see [2, 32],

$$U_S = 4aB\gamma \tag{2.9}$$

where a is half the crack length and γ is the free surface energy. Considering an infinite plane with a straight crack under traction σ_∞ normal to the crack, in the state of plane stress, we have

$$U_P = \frac{\pi a^2 \sigma_\infty^2}{E}. \tag{2.10}$$

Considering a plate of unit thickness ($B = 1$), we can substitute equations (2.8), (2.9), and (2.10) into equation (2.7) to obtain an expression for the total energy in the cracked body. This expression is given by

$$U = \frac{-\pi a^2 \sigma_\infty^2}{E} + 4a\gamma.$$

Then, if we differentiate this expression and equate the result to 0, according to the Griffith energy-balance concept, we obtain an expression for σ_∞ which gives the following fracture criterion

$$\sigma_\infty = \sqrt{\frac{2\gamma E}{\pi a}}. \tag{2.11}$$

In the case of plane strain, we arrive at the same expressions given in equation (2.10) and so in equation (2.11), except E is replaced by $\dfrac{E}{1 - v^2}$.

2.1.3 Irwin's Model

While studying crack propagation at the macroscopic level, Irwin postulated the idea of having non-elastic deformation in the vicinity of the crack tips, see [28]. Thus he modified Griffith's theory, which was suitable only for fully elastic materials. As cracks propagate, a dislocation motion takes place near the crack tips and so this causes energy to be dissipated (as heat). To this end, he introduced an extra energy term called the effective surface energy (denoted as γ_e) representing the work done by plastic deformation in the plastic zones which lie ahead of the crack tips. This gives an extra term added to the total energy given in equation (2.7). Using the modified version of Griffith's model, Irwin and Orowan, see [45], obtained a revised expression for the fracture criterion of a material under plane stress, this expression is given below

$$\sigma_\infty = \left(\frac{2E(\gamma + \gamma_e)}{\pi a} \right)^{\frac{1}{2}}.$$

Similarly to Griffith's criterion, this expression is for an infinite plane under constant traction. Having introduced the concept of the strain energy release rate, Irwin then came up with the idea of using stress intensity factors to describe the asymptotic behaviour of the stresses at the crack tip.

In general, the solution asymptotics for the stress and displacement components near the crack tip in a linear elastic body are given, respectively, by the following expressions

$$\sigma_{ij} = (2\pi r)^{-\frac{1}{2}} \sum_{l=I,II,III} K_l f_{lij}(\theta) + \tilde{\sigma}_{ij}(r,\theta), \tag{2.12}$$

and

$$u_i = u_i^0 + \frac{1}{2E}\left(\frac{r}{2\pi}\right)^{\frac{1}{2}} \sum_{l=I,II,III} K_l g_{li}(\theta) + \tilde{u}_i(r,\theta),$$

where radius r and angle θ are the crack tip local polar coordinates, see [32], as shown in Figure 2.1. The stress terms given by equation (2.12) have a singularity at $r = 0$. The remainder stresses given by $\tilde{\sigma}_{ij}(r,\theta)$ are finite at $r = 0$. The remainder displacement terms $\tilde{u}_i(r,\theta)$ approach zero as r tends to zero. The extra term given by u_i^0 is a constant which defines the displacement of the body at the crack tip. The functions $g_{li}(\theta)$ and $f_{lij}(\theta)$ are dimensionless functions corresponding to the deformation type considered (Mode I, Mode II, or Mode III). In the above expressions, E denotes Young's modulus of elasticity.

2.2 Elasto-Plastic Fracture Mechanics: Cohesive Zone Models

In linear elastic fracture models, the stress at the crack tip is infinite, whereas in CZ models, the stresses are finite. An important assumption needed in order to use linear elastic fracture mechanics is that the inelastic region at the crack tip must be negligible in comparison to the size of the whole crack itself (so we assume the bulk of the material acts elastically). However, in many real life situations this assumption does not apply. In such cases, elasto-plastic fracture mechanics (EPFM) is considered instead; see e.g. [13].

2.2.1 Description of a Cohesive Zone

Cohesive zone (CZ) models have been used in the past 40 to 50 years to study the behaviour of cracks in elasto-plastic materials; see e.g. [11]. In these cases, the need of an initial crack is not necessary and thus CZ modelling can predict crack growth as well as nucleation and initiation. When studying CZ models, we assume that there, generally, exists a CZ ahead of the crack tip. The CZ area in a material is the area between two separating surfaces ahead of the crack tip, see Figure 1.1. At this CZ, cohesive forces are present pulling the cohesive faces together. The external loads being applied to a body causes a crack to propagate and also causes the crack faces to move further away from each other. This CZ is known as the plastic zone when metals are considered, and known as the process zone when considering ceramics and cement. By analysing CZ models in materials, we would like to know the size of this CZ, and more importantly, when the crack will start to propagate. When the crack eventually propagates, the CZ vanishes in the place where it appeared but a new CZ is formed further in the material. So, practically, attached to the crack tip, a CZ will always be present causing the stresses to remain finite. The constitutive equation defining the relationship between the cohesive stresses (acting on the cohesive faces) and the displacement jump δ (separation between the separating faces of the material) are known as the cohesive laws or traction-separation laws. There have been many traction-separation laws (or cohesive laws) introduced in the literature. From the graphs of stress $\hat{\sigma}$ vs. crack separation δ, one can obtain the fracture energy per unit area, G_c, defined by

$$G_c = \int_0^{\delta_c} \sigma d\delta,$$

see e.g. [56], where δ_c represents the displacement jump when fracture occurs. The stress σ is defined by a constitutive equation which can be different depending on the type of cohesive law considered. The simplest case is when the cohesive stress is constant. This case was introduced by Dugdale (1960) and Leonov-Panasyuk (1959), see [19, 33].

2.3 History of Cohesive Zone Models

Two popular CZ models are known as the Dugdale and Barenblatt models where cohesive forces are introduced in the plastic zone in order to remove the stress singularity at the crack tip. The Dugdale and Barenblatt models were the first models to take into consideration CZs; these models have been modified and used in many applications in fracture mechanics, e.g. see [13, 56].

2.3.1 The Dugdale-Leonov-Panasyuk Model

The Dugdale-Leonov-Panasyuk model (DLP model), introduced in 1959-1960, was for ductile materials. Dugdale used a thin plate of mild steel. The whole body is assumed to be elastic but the plastic zone, also known as the process zone or the yield zone, acts plastically; see [13,56]. Consider a crack in such a material where there exists a CZ ahead of each end of the crack. In his model, Dugdale used σ_y to denote the cohesive stresses which act at the cohesive faces. Also, the edges of the whole infinite plate are subjected to uniform tensile stress, denoted by σ_∞, acting perpendicular to this crack. Figure 2.3 illustrates the described model.

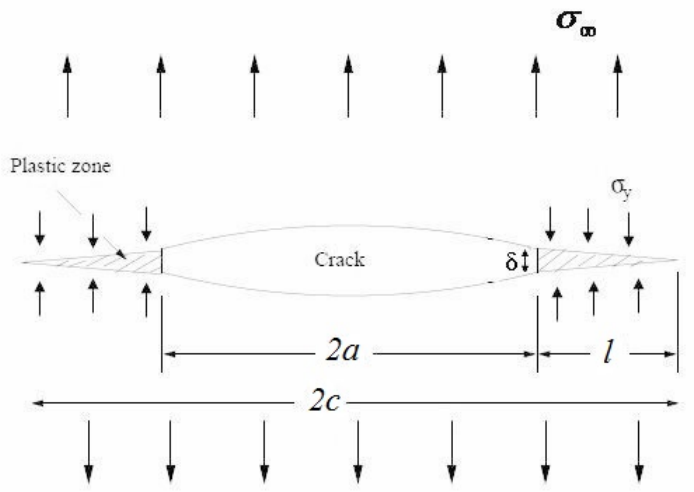

Figure 2.3: Dugdale CZ model.

The equation for the stress of the DLP model and the stress-separation graph are shown respectively below

$$\sigma = \begin{cases} \sigma_y & \text{for } 0 < \delta < \delta_c \\ 0 & \text{for } \delta > \delta_c \end{cases}$$

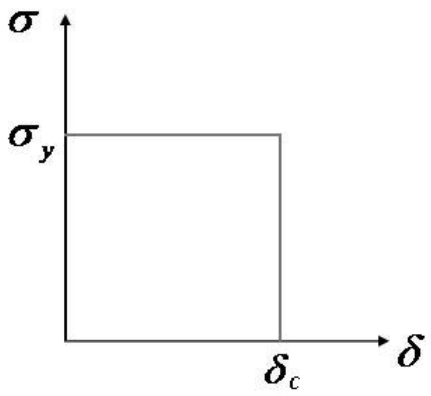

Figure 2.4: Stress-separation graph in the Dugdale model.

In this case, the fracture energy is given by

$$G_c = \text{Area under curve} = \sigma_y \delta_c.$$

The results of Dugdale's experiments showed that as the applied stress increased, the plastic zone length also increased. The aim here was to study the stress near the crack tip and thus to determine when the crack will propagate. The traction acting on the crack faces, as well as the displacement jump, are analysed in order to determine when the crack will propagate and when the plastic region will undergo plastic deformation. The strength condition in the DLP CZ model is when the crack tip opening displacement δ is less than a critical value δ_c which is a material constant; i.e. $\delta < \delta_c$. If this condition is violated, then the crack will propagate. Dugdale's experiments were used to determine the size of the plastic zone, in other words, to determine l, see Figure 2.3. As mentioned before, the stress at the crack tip σ_y remains finite. To that end, we need the stress intensity factor at the end of the

plastic zone, $K_I(c)$, to be zero

$$K_I(c) = 0.$$

This stress intensity factor, $K_I(c)$, is the sum of the 2 stress intensity factors from the 2 load components. Considering an infinite plane under constant traction at infinity, we have

$$\begin{aligned} K_I(c) &= \text{stress intensity factor due to } \sigma_y + \text{stress intensity factor due to } \sigma_\infty \\ &= K_I^{\sigma_y}(c) + K_I^{\sigma\infty}(c) \\ &= K_I^{\sigma_y}(c) + \sigma_\infty\sqrt{\pi c}. \end{aligned}$$

Now, $K_I^{\sigma_y}(c)$ is given by

$$K_I^{\sigma_y}(c) = \int_{-c}^{-a} -\sigma_y(x)\tilde{K}_I(x,c)dx + \int_a^c -\sigma_y(x)\tilde{K}_I(x,c)dx, \tag{2.13}$$

where the stress intensity factor $\tilde{K}_I(x,c)$ caused by the action of concentrated forces, applied at the point x, is given by

$$\tilde{K}_I(x,c) = \frac{1}{\sqrt{\pi c}}\sqrt{\frac{c+x}{c-x}};$$

see e.g. [1, 38]; such expression for the stress intensity factor was obtained from linear elastic fracture mechanics. Substituting this formula for $\tilde{K}_I(x,c)$ into equation (2.13) and integrating the result, we arrive at the following expression for $K_I^{\sigma_y}(c)$

$$K_I^{\sigma_y}(c) = -\frac{2\sigma_y\sqrt{c}}{\sqrt{\pi}}\arccos\left(\frac{a}{a+l}\right),$$

where $l = c - a$. Equating $K_I(c)$ to zero, we get

$$K_I(c) = \sigma_\infty\sqrt{\pi c} - \frac{2\sigma_y\sqrt{c}}{\sqrt{\pi}}\arccos\left(\frac{a}{a+l}\right) = 0.$$

Using this, we can solve the equation for l (the size of the plastic zone), which gives

$$l = a\left[\sec\left(\frac{\sigma_\infty\pi}{2\sigma_y}\right) - 1\right]. \tag{2.14}$$

We can express equation (2.14) in a simplified approximate form by using the series expansion of $\sec\left(\frac{\sigma_\infty\pi}{2\sigma_y}\right)$; to this end let $x = \frac{\sigma_\infty\pi}{2\sigma_y}$, the series expansion is given by

$$\sec(x) = 1 + \frac{1}{2}x^2 + \frac{5}{24}x^4 + \frac{61}{720}x^6 + \ldots \tag{2.15}$$

Note that this series expansion can be used if $|x| < \frac{\pi}{2}$. In this case, we must have that $\frac{\sigma_\infty \pi}{2\sigma_y} < \frac{\pi}{2}$ meaning $\sigma_\infty < \sigma_y$ which is true since the external field stress σ_∞ is assumed to be less than the yield stress σ_y. We therefore have

$$\sec\left(\frac{\sigma_\infty \pi}{2\sigma_y}\right) \approx 1 + \frac{1}{2}\left(\frac{\sigma_\infty^2 \pi^2}{4\sigma_y^2}\right),$$

where we have neglected the terms of order 4 or higher (when $\sigma_\infty < \sigma_y$). Thus using equations (2.15) and (2.6) the cohesive size can be approximated by

$$\begin{aligned} l &\approx c\left(1 + \frac{\sigma_\infty^2 \pi^2}{8\sigma_y^2} - 1\right) \\ &= \frac{a\sigma_\infty^2 \pi^2}{8\sigma_y^2} \\ &= \frac{\pi}{8}\left(\frac{K_I(a)}{\sigma_y}\right)^2 \end{aligned} \tag{2.16}$$

where $K_I(a) = \sigma_\infty \sqrt{\pi a}$.

The crack opening is given by the following formula

$$[u_2(x_1; c)] = [u_2^{(q)}(x_1; c)] + [u_2^{(\sigma_y)}(x_1; c)],$$

where

$$[u_2^{(q)}(x_1; c)] = \int_{-c}^{c} q v_2(x_1, \xi; c) d\xi, \tag{2.17}$$

and

$$[u_2^{(\sigma_y)}(x_1; c)] = \int_{-c}^{-a} -\sigma_y(\xi) v_2(x, \xi, c) d\xi + \int_{a}^{c} -\sigma_y(\xi) v_2(x, \xi, c) d\xi. \tag{2.18}$$

In the above expressions, κ denotes the Kolosov-Muskhelishvili constant. Under plane strain conditions, $\kappa = 3 - 4\nu$, while $\kappa = \frac{3-\nu}{1+\nu}$ under plane stress conditions, and $\mu = \frac{E_0}{2(1+\nu)}$ is the shear modulus, where E_0 and ν denote Young's modulus of elasticity and Poisson's ratio, respectively. Furthermore, $v_2(x, \xi; c)$ denotes the displacement jump generated by the unit concentrated forces applied to the opposite crack shores; $v_2(x, \xi; c)$ is given by the following formula

$$v_2(x, \xi; c) = -\frac{\kappa + 1}{2\pi\mu} \Gamma(x, \xi; c), \tag{2.19}$$

where

$$\Gamma(x,\xi;c) = \ln\left[\frac{c^2 - x\xi - \sqrt{(c^2-x^2)(c^2-\xi^2)}}{c^2 - x\xi + \sqrt{(c^2-x^2)(c^2-\xi^2)}}\right], \tag{2.20}$$

see [38]. After substituting expressions (2.19) and (2.20) into (2.17) and (2.18), we have the following results, respectively,

$$[u_2^{(q)}(x;c)] = \frac{q(1+\kappa)}{2\mu}\sqrt{c^2-x^2}, \tag{2.21}$$

$$[u_2^{(\sigma_y)}(x;c)] = \frac{\sigma_y}{4\pi\mu}\left((x-a)\Gamma(x,a;c) - (x+a)\Gamma(x,-a;c)\right). \tag{2.22}$$

Therefore, the crack opening at the end of the original crack, at $x = a$, is obtained by combining equations (2.21) and (2.22); this yields

$$\delta = [u_2(a;c)] = \frac{(\kappa+1)c\sigma_y}{\pi\mu}\ln\left[\cos\left(\frac{q\pi}{2\sigma_y}\right)\right]^{-1}.$$

Thus, the crack will propagate if the following condition is violated

$$\frac{(\kappa+1)c\sigma_y}{\pi\mu}\ln\left[\cos\left(\frac{q\pi}{2\sigma_y}\right)\right]^{-1} < \delta_c.$$

2.3.2 The Barenblatt Model

The Barenblatt model (introduced in 1962) was for brittle materials, thus the bulk of the material is assumed to be elastic. In Barenblatt's model, the material is subjected to an external load which causes a crack to propagate. Also, there exists strong cohesive forces at each tip of the crack pulling together the faces of the crack. It is assumed in Barenblatt's model that the distribution of the forces acting at the crack tip and the CZ length, l, are independent of the applied load. The distribution of these cohesive forces are unknown; unlike the Dugdale model, where the distribution of the forces, acting in the plastic zone, is known and is constant; see e.g. [13, 56].

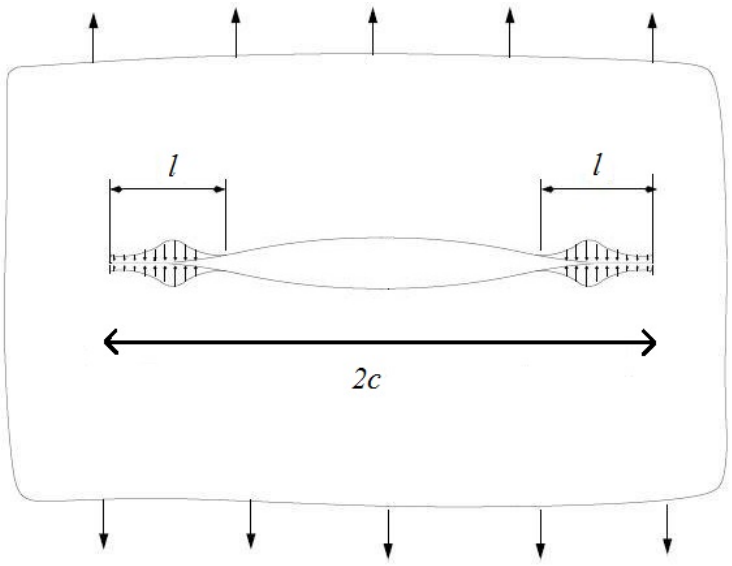

Figure 2.5: Barenblatt CZ model.

Barenblatt introduced 2 hypotheses about the CZ model, see [5]:

- 'The width of the edge (cohesive) region of a crack is small compared to the size of the whole crack.' This simply means that the length of the whole crack (including the CZ) is large compared to l (see Figure 2.5). This hypothesis is true for most cracks, particularly macro-cracks; however, if the crack is very small (a micro-crack) then this hypothesis is not valid since l might be larger than the crack.

- 'The form of the normal section of the crack surface in the edge region (and consequently the local distribution of the forces of cohesion over the crack surface) does not depend on the acting loads and is always the same for a given material under given conditions (temperature, composition and pressure of the surrounding atmosphere and so on).' In a basic explanation, this means that if the external applied load changes, this would not have an effect on the size of the CZ. Moreover, this CZ will remain the same size for a given material regardless of how much the crack will propagate.

2.3.3 Other Models in the Literature

Rice

In 1968, the Barenblatt model was considered by Rice, see [50] and the path-independent J integral was used which was written in terms of the cohesive stresses and the displacement jumps. This J integral was used to predict the stability of crack growth as well as a criteria of crack initiation.

The two main parameters used to characterise crack behaviour in materials are the stress intensity factor and the J integral. The J integral is an integral used to study fracture in a linear or nonlinear elastic body. Rice showed that the J integral is a path independent integral used for obtaining the strain energy release rate. (In linear elastic fracture mechanics, this J integral becomes the strain energy release rate G defined in Section 2.1.1.) Let Γ denote a contour around the crack tip starting at the bottom part of the crack to the top part as shown in Figure 2.6.

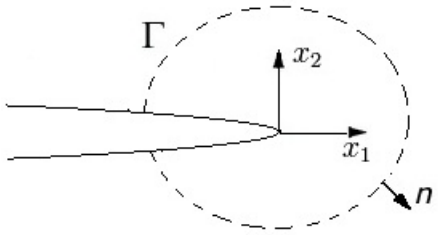

Figure 2.6: Contour surrounding a crack tip.

The J integral is a line integral taken over the contour Γ in the anti-clockwise direction, given by

$$J := \int_{\Gamma} \left(W dx_2 - \mathbf{T} \frac{\partial \mathbf{u}}{\partial x_1} \right) ds$$

where W is the strain energy per unit volume, $\mathbf{T}$ and $\mathbf{u}$ represent the traction vector and the displacement vector, respectively, and $\vec{n}$ is the unit vector normal to the contour.

In Rice's model, CZs are assumed to be present in front of the crack and Γ is taken to be the contour surrounding the CZ region, as shown in Figure 2.7. The body is loaded with external loads and cohesive forces are present at the CZs. The proof of path independence applies for any contour Γ which surrounds the crack tip, see [50].

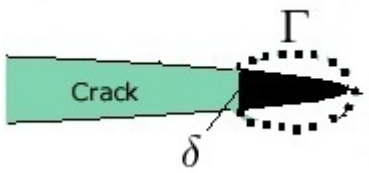

Figure 2.7: Contour surrounding a CZ in front of a crack.

The crack propagation criterion is when the crack tip opening δ reaches a value of δ^* and thus leads to crack growth. It was concluded, see [50], that as long as the CZ is relatively small, the equilibrium condition is equivalent to Griffith's (energy) theory, see section 2.1.2.

Hillerborg

In 1976, Hillerborg et al, see [27], developed the DLP and Barenblatt models by applying them to concrete materials and used numerical implementation with the aid of finite element techniques. The Hillerborg model is sometimes referred to as the *fictitious crack model*.

In Hillerborg's model, the crack starts to propagate, or initiates if no crack is present, when the maximum principal stress σ reaches a strength of σ^*, see [27]. (In [27] f_t is used instead of σ^*.) The stress, σ, in the CZ starts at it's maximum value, and decreases as the crack opening increases. Thus, when the opening reaches a critical value $\delta = \delta^*$, the cohesive stress is zero. Around the crack tip, surrounding the CZ, there is a small region which was referred to as the microcracked region, see Figure 2.8. The stress in the CZ gets transferred to this region.

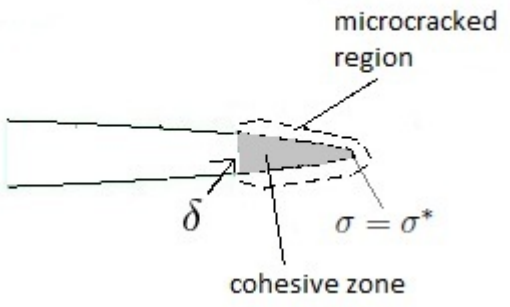

Figure 2.8: Microcracked region around CZ.

The graph below gives the behaviour of σ against the crack opening δ

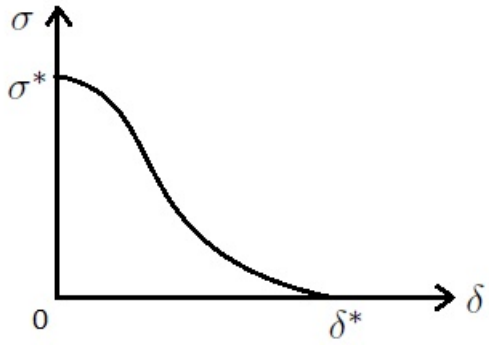

Figure 2.9: Stress vs. crack opening.

However, the relationship between the stress and the crack opening can be modified to take a different form. For example, if we consider a constant stress at $\sigma = \sigma^*$ and then a sudden decreases when $\delta = \delta^*$, Hillerborg's model will be equivalent to the DLP model. The stress-opening relationship usually depends on the material being used.

Finite element analysis was used in order to obtain the stresses and absorbed energy. However, the energy is not very sensitive to the mesh size used thus a fine mesh is not necessary. This is advantageous when solving difficult problems when only a coarse mesh can be easily applied; this also implies less computation time.

Baẑant

Baẑant introduced the *crack band model*. Baẑant's theory was for concrete materials and considered only the mode I case. In the crack band model, the CZ is assumed to have a finite length. This model, introduced by Baẑant and Oh (1983) see [6], uses stress-strain relations to describe the micro-cracking which occurs in the crack. This model has been studied further on after its derivation in 1983, for example De Borst applied numerical techniques to the crack band model in nonlinear phenomena such as plasticity and creep, see [11].

The process zone ahead of a crack in a concrete material is very large (particularly compared with the actual crack). When studying the fracture process in concrete, it should also be noted that concrete is a heterogeneous material which means that its properties vary (nonuniform composition) particularly at the micro scale. Microcracking is when small cracks appear in the neighbourhood of the major crack tip causing the crack to propagate. The energy used for the growth of these minor cracks causes the main (major) crack to grow. Strain softening is when the materials' stress decreases gradually as the strain increases. Strain softening occurs after a specific peak stress value is reached. In [6], the stress-strain relation is derived which describes the behaviour of the process zone during microcracking and crack growth. The strain-softening function depends on the fracture energy, the uniaxial strength and the width of the process zone. Baẑant's hypothesis was that in concrete materials, there is a process zone where blunt-ended microcracks are formed. Strain-softening develops as a result of the microcracking, see [6].

In concrete materials, the crack grows in a random manner so we cannot predict the path of the crack in advance. Since the fracture depends highly on the fracture energy of the materials, the crack propagation condition used in Baẑant's model considers the fracture energy (instead of using the materials' strength as a crack propagation criteria, which is used in many other CZ models).

Finite element analysis was used in Baẑant's model to study the microcracking effect

including the computation of the crack length, the micro-stresses (stresses in the process zone) and the energy release rate. One of the advantages of using this model compared with many other models is the absence of the zero stress intensity factor condition. This model is very similar to Hillerborg's model. The main difference between the two models involves the modelling of the CZ. In Bažant's model, the given width of the process zone is assumed to be finite. Thus the fracture energy can be determined, which depends on this band width.

Schapery

Assuming viscoelasticity in the bulk of the material, Schapery in 1984, studied a CZ model where variable CZ stress was assumed. Schapery used the fracture energy as the crack growth criteria unlike in the DLP model, and many other models, where the critical crack tip opening was considered instead. The viscoelastic functions of the material were used to determine the work done in the CZ and in turn when this work done is equal to the fracture energy then crack growth begins. For polymers, this fracture energy is dependent on time and temperature, see [55].

Schapery's model was for studying crack growth in nonlinear viscoelastic materials, see [55]. By using the elastic solutions, along with the correspondence principal, Schapery obtained the solutions of the stresses $\sigma_{i,j}$ and the displacements u_i of the viscoelastic case. A single hereditary integral was used to study the deformation in a body with viscoelastic effects.

McCartney

In 1988, McCartney considered a model that can be applied to viscoelastic materials containing a crack with CZs at the crack tips, and analysed the stresses in the CZ under the assumption that the stress is dependent on the velocity of crack propagation, see [36].

A linear viscoelastic solid is considered which is under a time-dependent stress applied at infinity in a direction normal to the crack plane. Cohesive zones are assumed to exist at the end of the crack tips where, the material behaves as a non-linear elastic or plastic solid. However, an important assumption made was that the stresses in the CZ were dependent on the crack growth velocity. Taking this into account, there were two aims in this model, namely (i) to obtain an energy fracture criterion and (ii) to obtain the stress distribution as well as the deformation in the CZs; both of which depend on the crack growth speed v.

The displacement discontinuity distribution involves a time-dependent integral which depends on the longitudinal strain response in the material, the creep function, $J(t)$, the external applied stress, σ_∞, the CZ stresses, σ_c, and the cohesive zone length, $c(t)$. It is assumed that the crack grows with uniform velocity. The crack growth speed can be represented in terms of the effective fracture energy Γ. Results of asymptotic analysis, particular to see what happens as $v \to 0$ and as $v \to \infty$, show conditions on the stress intensity factor K such that the numerical results can be implemented.

The dependence of v on the stress intensity factor is analysed. This relationship is found by using the energy balance criterion in terms of Γ. Numerical schemes were used to solve the problem for two cases: (i) when the bulk of the material is a linear elastic solid and (ii) when it is a linearly viscoelastic solid. For case (i), it was shown that the solution for the displacement discontinuities is independent of the speed v. However, for case (ii), the solution of the integral equation (for the displacement discontinuities) is dependent on the velocity. For case (ii), graphs of the dependence of the crack growth speed on the stress intensity factor were obtained. It was shown that the stress intensity factor increases monotonically but tends to a finite value as v increases. Also, graphs of the cohesive stress vs. the CZ length were obtained which show that the cohesive stress decreases monotonically with CZ length for cases when $v \to 0$ and when $v \to \infty$. It was also finally concluded that as velocity increases, the CZ length also increases.

Tvergaard and Hutchinson

Tvergaard and Hutchinson in 1992, see [58], used a ductile material to study how the work in the plastic region contributes to the fracture toughness of the material. Thus, by using a trapezoidal traction-separation law it was shown that the fracture toughness depends highly on the plastic work that surrounds the crack tip.

In [58], two problems were considered: (i) the fracture process in a single void interacting with the crack tip; and (ii) the fracture process consisting of void growth and coalescence where multiple voids interact ahead of the crack tip. In this model, small scale yielding and mode I fracture conditions were considered for a material under plane strain conditions. Also, it was assumed that fracture was rate-independent. This model depends on 2 main parameters, namely the work of separation per unit area Γ_0 and the peak traction $\hat{\sigma}$. The purpose was to obtain a relation between Γ_0 and the total work of fracture. The relation is given by

$$\sigma = \begin{cases} \dfrac{\hat{\sigma}}{\delta_1} & \text{for } \delta < \delta_1 \\ \hat{\sigma} & \text{for } \delta_1 \leq \delta \leq \delta_2 \\ (\delta - \delta_2)\left(\dfrac{\hat{\sigma}}{\delta_2 - \delta_c}\right) + \hat{\sigma} & \text{for } \delta^* < \delta < \delta_c \end{cases}$$

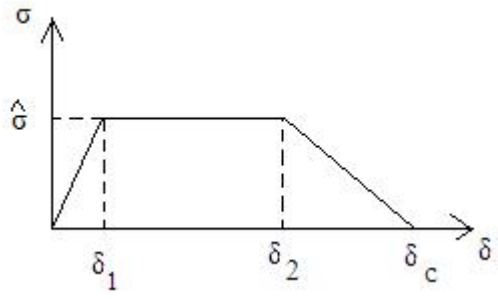

Figure 2.10: Stress-separation graph in the trapezoidal model.

Here, we have, by finding the area under the curve,

$$\Gamma_0 = \frac{1}{2}\hat{\sigma}(\delta_c + \delta_2 - \delta_1).$$

An expression for the crack growth resistance $K_R(\Delta a)$ is given where a denotes the crack length. A finite element approach was used to obtain the crack growth resistance for given material parameters with respect to the crack length. Graphs of crack growth resistance vs. crack length were obtained showing the monotonic increase of K_R yet tending to a finite value. When K_R ceases to increase, steady-state conditions are attained, we have $K_R^{ss} \to K_R$ as $\Delta a \to \infty$.

Two main stages are considered in this paper, namely the crack initiation stage and the crack growth stage. The crack initiates when the crack growth resistance satisfies $K_R = K_0$ (or equivalently when $G = \Gamma_0$) where K_0 denotes the stress intensity factor in the case of no plasticity. During the crack growth stage, steady state crack growth was considered and plots of the crack growth resistance K_R^{ss} vs. $\hat{\sigma}$ were obtained for chosen dependence on the shape of the traction separation law (δ_1, δ_2, and δ_c).

Also considered was the problem of crack propagation in the case of having two identical solids bonded together, as well as the case with two nonidentical solids (where one is much stronger than the other). Such problems allow us to know how interface structures will help in the toughness and durability of materials.

Some Other Models in the Literature

There are many other CZ models introduced in the literature. We will briefly introduce some of these models in this subsection.

Knauss in 1993, studied a time-dependent crack growth by considering a rate dependent CZ model and determined the crack opening using the viscoelastic properties of the material. The stability of the crack was studied by using the traction-separation law, it has

been concluded that in some materials, the crack tip can become unstable even before the critical crack tip opening has been reached; see [29].

A linear cohesive law, was used by Camacho and Ortiz (1996). In this case the stress reduces linearly with displacement. The behaviour is illustrated in Figure 2.11 and the relation is given by, see [14],

$$\sigma = \sigma_y - \delta\left(\frac{\sigma_y}{\delta_c}\right).$$

Thus, the fracture energy is given by

$$G_c = \frac{\sigma_y \delta_c}{2}.$$

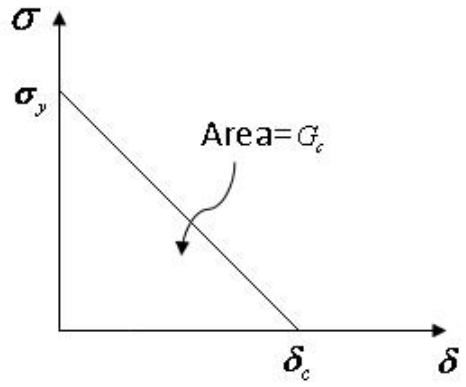

Figure 2.11: Stress-separation graph in the rigid linear model.

An exponential traction-separation law was used by Xu and Needleman in 1994 see [60] and later on by Ortiz and Pandolfi in 1999, see [46].

In 1998, Guebelle and Baylor, see [22], used a bilinear CZ model. Unlike the linear traction-separation law, many researchers have considered the case where the stress starts at zero (before separation takes place) then increases until it reaches a maximum value for σ and eventually decreases to zero when the separation reaches δ_c. An example of such cohesive law is known as the bilinear traction-separation law, see e.g. [59]. The stress-

separation equation is given below and the corresponding graph follows in Figure 2.12.

$$\sigma = \begin{cases} \delta \left(\dfrac{\sigma_y}{\delta^*} \right) & \text{for } 0 < \delta < \delta^* \\ (\delta - \delta^*) \left(\dfrac{\sigma_y}{\delta^* - \delta_c} \right) + \sigma_y & \text{for } \delta^* < \delta < \delta_c \end{cases}$$

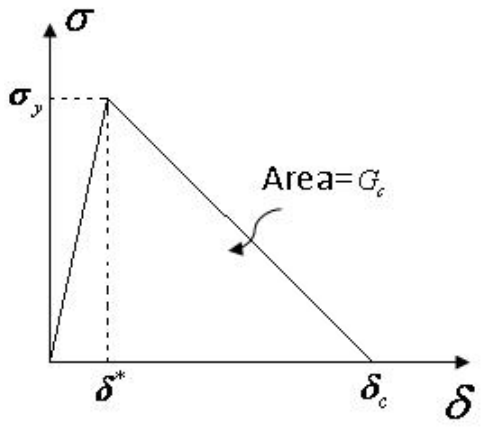

Figure 2.12: Stress-separation graph in the bilinear model.

In this case, the critical fracture energy is also given by

$$G_c = \frac{\sigma_y \delta_c}{2}.$$

In 1999, Yoon and Allen [61] considered a CZ model in a nonlinear viscoelastic material and modelled the behaviour of the crack using hereditary integrals which were in terms of the relaxation functions of the material. It was shown that the energy release rate is time and history dependent.

Other traction-separation laws which have not been mentioned here, such as the parabolic and sinusoidal laws, have also been considered by researchers in the past 40 years, these models consist of different constitutive equations for the stresses. A table of some CZ models and their parameters can be found in [16].

2.4 Viscoelasticity

Viscoelastic materials such as polymers experience a time and history dependant stress-strain relationship. Viscoelastic materials can be classified as linear or nonlinear. We will consider only linear materials.

2.4.1 Stress-Strain Relations

When a material is subject to an external constant stress σ_0 starting from time $t = 0$, a strain is produced and is given by relation

$$\varepsilon(t) = \sigma_0 J(t)$$

where $J(t)$ is called the creep function and is different for different materials. The graphs in Figure 2.13 demonstrate the behaviour of stress and strain in creep.

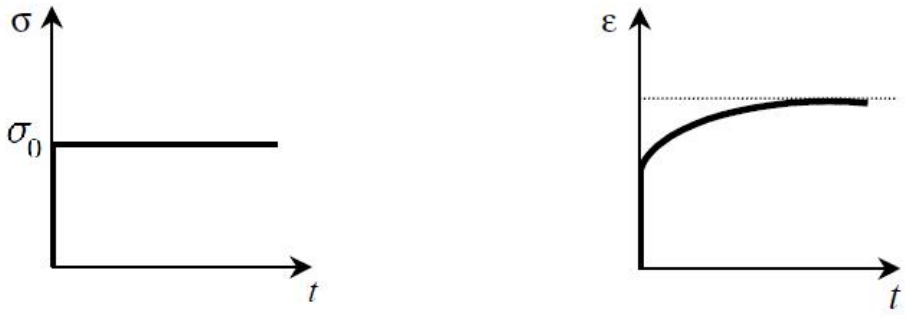

Figure 2.13: Viscoelastic creep.

Consider the case of having a second load, denoted by $\Delta\sigma$ applied at a time $t = \tau$ where $\tau > 0$, the corresponding strain is given by $\varepsilon(t) = \Delta\sigma J(t - \tau)$. Using linearity, the total strain of both loads is

$$\varepsilon(t) = \sigma_0 J(t) + \Delta\sigma J(t - \tau).$$

Now, if we consider an indefinite number of applied loads, the total strain is given by

$$\varepsilon(t) = \sigma_0 J(t) + \int_{0^+}^{t} J(t - \tau)\dot{\sigma}(\tau)d\tau, \tag{2.23}$$

see [20], assuming $\sigma(t) = 0$ for $t < 0$, where $\dot{\sigma}$ denotes the derivative of σ with respect to time. If we apply integration by parts to the integral in equation (2.23), we will arrive at the following representation

$$\varepsilon(t) = J(0)\sigma(t) - \int_0^t \dot{J}(t-\tau)\sigma(\tau)d\tau.$$

Denoting $\dot{J}(t-\tau) = \dfrac{dJ(t-\tau)}{d\tau} = -K(t-\tau)$, we arrive at the standard constitutive equation

$$\varepsilon(t) = \frac{\sigma(t)}{E_0} + \int_0^t K(t-\tau)\sigma(\tau)d\tau \tag{2.24}$$

we have also used $J(0) = \dfrac{1}{E_0}$ where E_0 denotes the instantaneous elastic modulus. If the material is a viscoelastic solid, the strain tends to a finite value as t tends to infinity, as shown by the dotted line in the graph in Figure 2.13, this value is usually denoted as ε_∞. Otherwise if we have a viscoelastic fluid, the strain continues to grow, see [2].

We can also consider the case of varying stress with time as we keep the strain $\varepsilon(t) = \varepsilon_0$ for $t \geq 0$ constant, and $\varepsilon(t) = 0$ for $t < 0$. The corresponding stress is given by

$$\sigma(t) = \varepsilon_0 Y(t), \quad t > 0$$

where $Y(t)$ is called the relaxation function and also depends on the material. The graphs in Figure 2.14 demonstrate the behaviour of strain and stress in relaxation

Figure 2.14: Relaxation.

If the material is a viscoelastic solid then the stress tends to a finite value as t tends to infinity, as shown by the dotted line in the graph above, this value is usually denoted as σ_∞. Otherwise if we have a viscoelastic fluid, then the stress continues to decrease to 0.

We obtain the inverse relation of equation (2.24) and arrive at the following constitutive equation for stress with respect to time

$$\sigma(t) = \varepsilon(0)Y(t) + \int_{0^+}^{t} Y(t-\tau)\dot{\varepsilon}(\tau)d\tau \tag{2.25}$$

or alternatively expressed by

$$\sigma(t) = E_0\varepsilon(t) + \int_{0}^{t} E^*(t-\tau)\varepsilon(\tau)d\tau$$

where we have used $\dot{Y}(t-\tau) = \dfrac{dY(t-\tau)}{d\tau} = -E^*(t-\tau)$.

2.4.2 Relation Between the Creep and Relaxation Functions

The relation between the creep function $J(t)$ and the relaxation function $Y(t)$ can be found with the aid of Laplace transformation, see [7].

For equations (2.23) and (2.25), applying the convolution theorem and obtaining the inverse Laplace transform yields the following result

$$\int_0^t J(t-x)Y(x)dx = \int_0^t Y(t-x)J(x)dx = t. \tag{2.26}$$

Therefore, if we know the creep function or the relaxation function, we can use relation (2.26) to find the relaxation function and the creep function respectively.

2.4.3 Linear Viscoelastic Models

The behaviour of such materials is often modelled using a combination of 2 mechanical models: springs, to present the elastic characteristics; and dashpots, to present the viscous characteristics. Examples of such mechanical models are the Maxwell model and the Kelvin-Voight model.

The Maxwell Model

The Maxwell model is constructed using a spring and a dashpot in series.

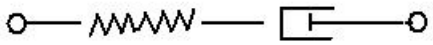

Figure 2.15: Maxwell Model.

The differential equation that defines the stress-strain relationship in a Maxwell model is given by

$$\dot{\varepsilon}(t) = \frac{1}{E}\dot{\sigma}(t) + \frac{1}{\eta}\sigma(t),$$

see [8, 20], where E denotes Young's modulus of elasticity and η denotes the viscosity coefficient. This differential equation can be written as

$$\varepsilon(t) = \frac{1}{E}\sigma(t) + \frac{1}{\eta}\int_0^t \sigma(\tau)d\tau.$$

Using integration by parts on the integral, we have

$$\varepsilon(t) = \frac{1}{E}\sigma(t) + \frac{t}{\eta}\sigma(t) - \frac{1}{\eta}\int_0^t \tau\dot{\sigma}(\tau)d\tau$$

$$= \frac{1}{E}\int_0^t \dot{\sigma}(\tau)d\tau + \frac{1}{E}\sigma_0 + \frac{1}{\eta}t\int_0^t \dot{\sigma}(\tau)d\tau + \frac{1}{\eta}t\sigma_0 - \frac{1}{\eta}\int_0^t \tau\dot{\sigma}(\tau)d\tau$$

$$= \sigma_0\left(\frac{1}{E} + \frac{1}{\eta}t\right) + \int_0^t \dot{\sigma}(\tau)\left(\frac{1}{E} + \frac{1}{\eta}(t-\tau)\right)d\tau;$$

and comparing this to equation (2.23), we find that the creep function for the Maxwell model is given by

$$J(t) = \frac{1}{E} + \frac{1}{\eta}t.$$

Using a similar approach, or using relation (2.26), we find that the relaxation function for the Maxwell model is given by

$$Y(t) = Ee^{-\frac{E}{\eta}t};$$

generally, $\frac{\eta}{E}$ is known as the relaxation time of the material.

The Kelvin-Voight Model

The Kelvin-Voight model is constructed using a spring and a dashpot in parallel.

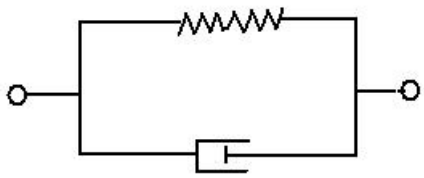

Figure 2.16: Kelvin-Voight Model.

The differential equation that defines the stress-strain relationship in the Kelvin-Voight model is given by

$$\dot{\varepsilon}(t) + \frac{E}{\eta}\varepsilon(t) = \frac{1}{\eta}\sigma(t),$$

see [8, 20]. Solving this differential equation, using an integrating factor, yields

$$\varepsilon(t) = \frac{1}{\eta}\int_0^t e^{\frac{E}{\eta}(\tau - t)}\sigma(\tau)d\tau;$$

using integration by parts on the integral gives

$$\varepsilon(t) = \frac{1}{E}\sigma(t) - \frac{1}{E}\sigma_0 e^{-\frac{E}{\eta}t} - \frac{1}{E}\int_0^t \dot{\sigma}(\tau)e^{\frac{E}{\eta}(\tau - t)}d\tau$$

$$= \sigma_0\frac{1}{E}\left(1 - e^{-\frac{E}{\eta}t}\right) + \frac{1}{E}\int_0^t \dot{\sigma}(\tau)\left(1 - e^{-\frac{E}{\eta}(t-\tau)}\right)d\tau,$$

and comparing this to equation (2.23), we find that the creep function for the Kelvin-Voight model is given by

$$J(t) = \frac{1}{E}\left(1 - e^{-\frac{E}{\eta}t}\right).$$

The relaxation function for the Kelvin-Voight model is given by

$$Y(t) = E + \eta\delta(t),$$

where $\delta(t)$ denotes the Dirac delta function which possesses the fundamental property

$$\int_{-\infty}^{\infty} \delta(t)\phi(t)dt = \phi(0)$$

for any continuous function $\phi(t)$.

Standard Linear Solid

This model is also known as the 3-parameter material or the Zener model. Consider the case of having a spring in series with a Kelvin-Voight model, as shown in Figure 2.17.

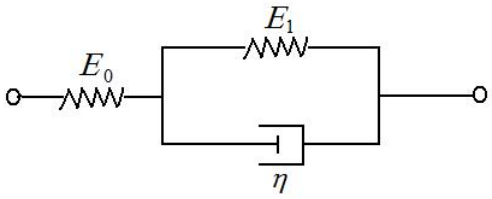

Figure 2.17: Standard linear solid: Kelvin form.

The corresponding differential equation modelling the stress-strain relation in such a material is given by

$$\sigma(t) + \frac{\eta}{E_0 + E_1}\dot{\sigma}(t) = \frac{E_0 E_1}{E_0 + E_1}\varepsilon(t) + \frac{\eta E_0}{E_0 + E_1}\dot{\varepsilon}(t),$$

see [8,20]. Using similar techniques as for the Maxwell and Kelvin-Voight models, we derive the creep function for a standard linear solid of the Kelvin-Voight form

$$J(t) = \frac{1}{E_0} + \frac{1}{E_1}\left(1 - e^{-\frac{E_1}{\eta}t}\right).$$

These results can be generalised for the case of having n Kelvin-Voight elements in series with a spring. The generalised creep function can be found in e.g. [8].

Now, consider the case of having a spring in parallel with a Maxwell model, as shown in Figure 2.18.

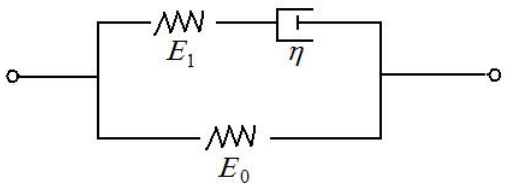

Figure 2.18: Standard linear solid: Maxwell form.

The differential equation describing the stress-strain relation in such a material is

$$\sigma(t) + \frac{\eta}{E_1}\dot{\sigma}(t) = E_0\varepsilon(t) + \frac{\eta(E_0+E_1)}{E_1}\dot{\varepsilon}(t),$$

see [8,20], and again, we can derive the creep function using the same techniques as before which yields

$$J(t) = \frac{1}{E_0} - \frac{E_1}{E_0(E_0+E_1)}e^{-\frac{E_0E_1}{\eta(E_0+E_1)}t}. \tag{2.27}$$

In the literature, see e.g. [4, 49], experiments using polymers have been undertaken and the corresponding results show that polymers behave like standard linear solids. The material which will be considered in this project is Poly(methyl methacrylate), also known as plexiglas or PMMA.

Consider again the case of a spring in parallel with a Maxwell model. If we have constant stress σ_0, from $\varepsilon(t) = \sigma_0 J(t)$, and the creep function given by equation (2.27), we have

$$\varepsilon(t) = \frac{\sigma_0}{E_0} - \frac{E_1\sigma_0}{E_0(E_0+E_1)}e^{-\frac{E_0E_1}{\eta(E_0+E_1)}t}.$$

Now, at $t = 0$ and $t = \infty$, we have

$$\varepsilon(0) = \frac{\sigma_0}{E_0+E_1}, \qquad \varepsilon(\infty) = \frac{\sigma_0}{E_0},$$

and since E_0 and E_1 are finite, we represent such behaviour for the strain on a graph as shown below

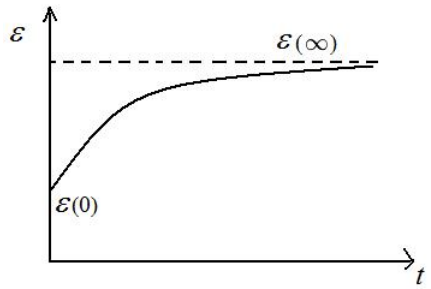

Figure 2.19: Strain vs. time for a standard linear solid: Maxwell form.

which resembles the strain behaviour in polymers, see e.g. [47]. Therefore, the standard linear solid is a reasonable model to predict the creep behaviour of polymers.

2.4.4 Viscoelastic Correspondence Principle

When studying problems in elasticity, the material properties (such as Young's modulus of elasticity E_0 and Poisson's ratio ν) which appear in the equations are assumed to be time independent. The correspondence principle is a technique used in solving viscoelastic stress analysis problems by using the corresponding elastic problem, see e.g. [20]. Accordingly, we replace the elastic constants, which appear in the elastic solution, by the corresponding viscoelastic operators, to arrive at the viscoelastic solution.

2.5 Crack Growth in History-Dependent Materials

There is some work in the literature involving history dependent strength conditions in materials under creep conditions and fatigue conditions. The main difference between the two types is that under creep conditions, the stress and rupture are time-dependent, whereas, under fatigue loading, the number of load cycles is the major factor. While studying crack propagation, it is useful to construct a graph of crack length against time (creep case),

or crack length against the number of load cycles (fatigue case). More information about the characteristics of creep and fatigue loading can be found in [10, 15, 62]. To predict the strength of the material and where fracture will occur, the *local approach* or the *non-local approach* can be used. The local approach uses the stress (or stress history) at the point where the crack appears, while, the non-local approach uses the stress (history) not only at the point of the crack but also in the vicinity of that point. Under creep conditions, the durability of a material depends on the duration of the applied load as well as the temporal load history. The *Basquin diagram*, see [47, 51], is a power type relation which relates the life time of a material under a uniaxial load which is constant in space and time. This relation is given by $\sigma^*(t) = \sigma_0 t^{-1/b}$, where σ_0 and b are constant material parameters. Given in Figure 2.20 is an example of a durability diagram.

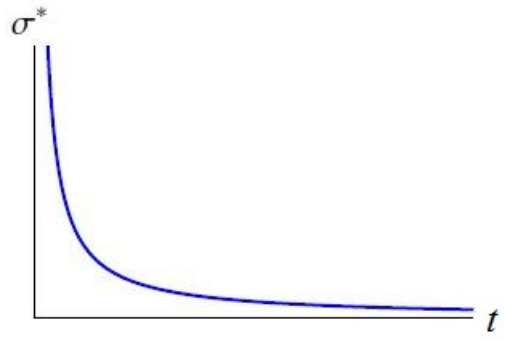

Figure 2.20: Material strength σ^* under constant uniaxial stress as a function of life time.

In [43], a temporal strength condition is given for materials which exhibit time-dependent crack growth. This condition is given by

$$\underline{\Lambda}(\sigma; t) = 1,$$

where $\underline{\Lambda}(\sigma, t)$ denotes the temporal normalised equivalent stress functional which depends on the stress σ, history, and time t. A particular form of $\underline{\Lambda}(\sigma, t)$ has been suggested in [40], and its parameters were obtained from experimental data. This functional is given by

$$\underline{\Lambda}(\sigma; t) := \left[\frac{d}{dt} \int_0^t \left| \frac{\sigma(\tau)}{\sigma^*(t-\tau)} \right|^\beta d\tau \right]^{1/\beta} < 1,$$

where $\sigma^*(t)$ is the durability diagram under constant loading. The parameter β is a material constant in the nonlinear accumulation rule for durability under variable load, see [40]. For the Basquin diagram, it takes the form

$$\begin{aligned} \underline{\Lambda}(\sigma;t) &= \left[\frac{d}{dt}\int_0^t \left|\frac{\sigma(\tau)}{\sigma_0}\right|^\beta (t-\tau)^{\frac{\beta}{b}} d\tau\right]^{1/\beta} \\ &= \left[\frac{\beta}{b\sigma_0^\beta}\int_0^t |\sigma(\tau)|^\beta (t-\tau)^{\frac{\beta}{b}-1} d\tau\right]^{1/\beta} < 1. \end{aligned} \tag{2.28}$$

When $\beta = b$, equation (2.28) coincides with the Robinson rule of linear accumulation of partial life times. The local approach was used in [25] to study creep crack propagation for a body with initially no crack. The strength condition (2.28) was used to formulate a nonlinear Abel type integral equation which models the crack behaviour in time. Let a denote the crack length. For an infinite elastic isotropic or anisotropic plane, the stress distribution $\sigma_{22}(\tau; x_1)$ ahead of the crack has the following form (see e.g. [54]), which remains valid also for a viscoelastic material,

$$\sigma_{22}(\tau;x_1) = \frac{qx_1}{\sqrt{(x_1^2 - a^2(\tau))}}. \tag{2.29}$$

Substituting the stress distribution (2.29) into the durability condition (2.28) with $x_1 = a(t)$ (and replacing the inequality with equality), we arrive at the following nonlinear Volterra integral equation

$$\int_0^t \frac{(t-\tau)^{\frac{\beta}{b}-1}}{[a^2(t)-a^2(\tau)]^{\frac{\beta}{2}}} d\tau = \frac{b}{\beta}\left(\frac{q}{\sigma_0}\right)^{-\beta} a^{-\beta}(t). \tag{2.30}$$

The equation that models crack propagation under fatigue loading in an elastic material is analogous to equation (2.30) except the crack length, a, will depend on the number of loading cycles, n, instead of time, t.

In [41, 42], equation (2.30) was solved analytically for the case $\beta = b$. For other values of β, no exact solution has yet been found. A modified version of the Nyström method was introduced and implemented in [25] in order to numerically solve the problem for the cases when $\beta \neq b$. Graphs of crack length against normalised time were produced for $\beta = b$ (in

order to compare with the analytical solution) as well as for other values of β. These graphs were used to analyse the rate of the crack growth taking different values of the parameters, β and b. The theoretical results from the exact solution for $\beta = b$, given in [41], show that the normalised breaking time for a plane with a crack is $t_r = 1$. On the other hand, it was also shown that for other certain values of β, the normalised breaking time is also $t = 1$. Since the equation modelling crack growth in a body undergoing fatigue loading conditions is analogous to the equation modelling crack growth in a body undergoing creep loading conditions, similar interpretations were made on how the crack length increases with respect to the number of cycles being applied. Papers [41, 42] model the creep and fatigue cases respectively. Both the local and non local approaches were considered. In both papers, it is observed that as the material parameter b increases, the crack growth increases more rapidly with time and number of cycles. However, the local approach is only applicable for cases when $b < 2$; whereas, in the non local approach, this restriction is not required. Therefore, solutions were obtained for values such as $b = 3$ and $b = 6$.

Chapter 3

Model Problem Formulation

Let the problem geometry be as in Figure 1.1, i.e, the crack occupies the interval $[-\hat{a}(\hat{t}), \hat{a}(\hat{t})]$ and the CZ occupies the intervals $[-\hat{c}(\hat{t}), -\hat{a}(\hat{t})]$ and $[\hat{a}(\hat{t}), \hat{c}(\hat{t})]$ in an infinite linearly elastic or viscoelastic plane loaded at infinity by a traction $\hat{q}$ in the direction normal to the crack applied at time $\hat{t} = 0$. We will now give a generalisation of the DLP Model to history-dependent materials.

3.1 Cohesive Zone Stress Condition

We introduce the normalised equivalent stress, which is given by the following formula

$$\underline{\Lambda}(\boldsymbol{\sigma}(\hat{x}, \cdot); \hat{t}) = \left(\frac{\beta}{b\sigma_0^\beta} \int_0^{\hat{t}} |\boldsymbol{\sigma}(\hat{x}, \hat{\tau})|^\beta (\hat{t} - \hat{\tau})^{\frac{\beta}{b}-1} d\hat{\tau} \right)^{\frac{1}{\beta}} \tag{3.1}$$

see [40]. Here, $|\boldsymbol{\sigma}|$ is the maximum of the principal stresses, $\hat{t}$ and $\hat{x}$ denote the time and space coordinates respectively. The parameters σ_0 and b are material constants in the assumed power-type relation

$$\hat{t}_\infty(\hat{q}) = \left(\frac{\hat{q}}{\sigma_0} \right)^{-b} \tag{3.2}$$

between the rupture time $\hat{t}_\infty$ and the constant uniaxial tensile stress $\hat{q}$ applied to a sample without cracks. The rupture time $\hat{t}_\infty(\hat{q})$ satisfies the following equation

$$\int_{\hat{t}_0}^{\hat{t}} \hat{q}^\beta (\hat{t}-\hat{\tau})^{\frac{\beta}{b}-1} d\hat{\tau} = \frac{b\sigma_0^\beta}{\beta}.$$

We will replace the classical DLP CZ (yield) stress condition, $\hat{\sigma} = \sigma_y$, with the history-dependent condition

$$\underline{\Lambda}(\hat{\boldsymbol{\sigma}}(\hat{x},\cdot);\hat{t}) = 1, \tag{3.3}$$

while in the rest (the bulk) of the material the strength condition

$$\underline{\Lambda}(\hat{\boldsymbol{\sigma}}(\hat{x},\cdot);\hat{t}) < 1$$

should be satisfied.

So, for $\hat{x}$ between the crack tip and the CZ tip, the CZ stress satisfies the equation

$$\int_0^{\hat{t}} \sigma_{22}^\beta(\hat{x},\hat{\tau})(\hat{t}-\hat{\tau})^{\frac{\beta}{b}-1} d\hat{\tau} = \frac{b\sigma_0^\beta}{\beta}.$$

The integral on the left hand side of the above equation can be split into 2 parts, and thus we can rewrite the above equation as

$$\int_{\hat{t_c}}^{\hat{t}} \sigma_{22}^\beta(\hat{x},\hat{\tau})(\hat{t}-\hat{\tau})^{\frac{\beta}{b}-1} d\hat{\tau} = \frac{b\sigma_0^\beta}{\beta} - \int_0^{\hat{t_c}} \sigma_{22}^\beta(\hat{x},\hat{\tau})(\hat{t}-\hat{\tau})^{\frac{\beta}{b}-1} d\hat{\tau} \tag{3.4}$$

where $\hat{x} > \hat{c}(\hat{\tau})$ and $\hat{t_c}(\hat{x})$ denotes the time when the point $\hat{x}$ became part of the CZ. The stress in the integrand on the right hand side of equation (3.4) is the stress ahead of the CZ; however, the stress in the left hand side of equation (3.4) is the stress in the CZ.

To analyse the range of b and β for which the CZ model based on conditions (3.3), (3.1) can exist, let us first remark that if $\beta = b$, then

$$\frac{d}{d\hat{t}}\underline{\Lambda}(\hat{\boldsymbol{\sigma}}(\hat{x},\cdot);\hat{t}) = \frac{1}{b\sigma_0^\beta}\underline{\Lambda}^{1-\beta}(\hat{\boldsymbol{\sigma}};\hat{t})|\hat{\boldsymbol{\sigma}}(\hat{x},\hat{t})|^\beta,$$

which means that $\underline{\Lambda}(\hat{\boldsymbol{\sigma}}(\hat{x},\cdot);\hat{t})$ is a strictly growing function for any t, when $|\hat{\boldsymbol{\sigma}}(\hat{x},\hat{t})| > 0$. Particularly, if the cohesive condition (3.3) has been reached at some time $t_c(x)$, it can not

stay satisfied at larger times, $t > t_c(x)$, for $|\hat{\boldsymbol{\sigma}}(\hat{x}, \hat{t})| > 0$ on the CZ; but if $|\hat{\boldsymbol{\sigma}}(\hat{x}, \hat{t})| = 0$ for $t > t_c(x)$ this means that the point belongs to the crack and not to the CZ. That is, the CZ can not exist for $\beta = b$.

Similarly, if $\beta > b$, then

$$\frac{d}{d\hat{t}}\underline{\Lambda}(\hat{\boldsymbol{\sigma}}; \hat{t}) = \frac{\frac{\beta}{b}}{\beta\sigma_0^{\beta}}\underline{\Lambda}^{1-\beta}(\hat{\boldsymbol{\sigma}}; \hat{t}) \int_0^{\hat{t}} |\hat{\boldsymbol{\sigma}}(\hat{\tau})|^{\beta}(\hat{t} - \hat{\tau})^{\frac{\beta}{b}-2} d\hat{\tau} > 0,$$

which also prevents the CZ condition (3.3) to hold at any time $t > t_c$, after it had been reached at a time $t_c(x)$, even if $\sigma(t) = 0$ for $t > t_c(x)$. Thus, the CZ defined by (3.4) can exist only if $0 < \beta < b$. Thus we will further consider values for b and β from this interval only.

Relations (3.1)-(3.4) were implemented in [25, 41] to solve a similar crack propagation problem without a CZ; i.e. it was assumed that when condition (3.1) is reached at a point, this point becomes part of the crack. However, such approach in a local form appeared to be inapplicable for $b \geq 2$ (but it can still be used for $b \geq 2$ in a non-local form, see [41]). In this paper, a CZ approach is developed instead, in order to cover the larger range of b values relevant to structural materials. Note that the CZ approach can be considered as a kind of non-local approach.

3.2 Stress Ahead of the CZ

As shown in Figure 3.1, the problem for a cracked plane subject to external loads can be modelled as the sum of the problems for a body with a crack and a body without a crack subjected to external loads.

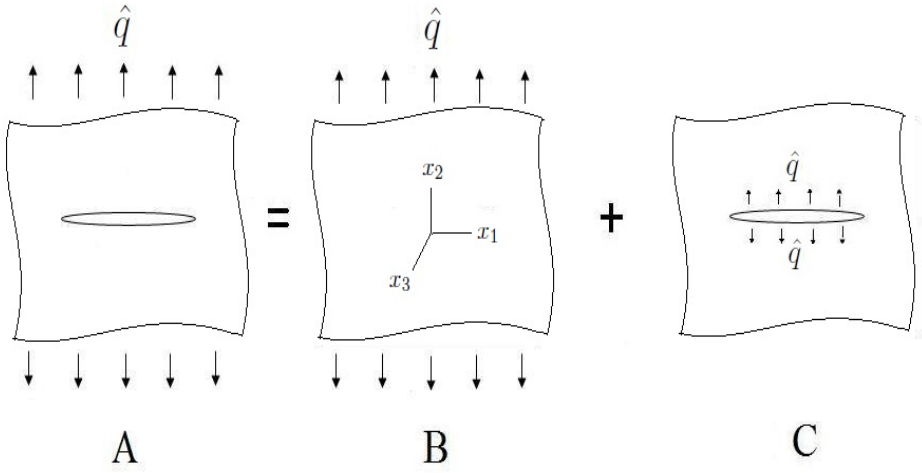

Figure 3.1: Infinite plane subject to external loads.

Regarding component B shown in Figure 3.1 (for an infinite plane without a crack), this is a uniform tension in the x_2 direction so the stress components, for any point in the plane, are given by $\sigma_{22} = \hat{q}$ and $\sigma_{11} = \sigma_{12} = 0$; we have

$$\boldsymbol{\sigma}^{(B)}(x) = \begin{pmatrix} 0 & 0 \\ 0 & \hat{q} \end{pmatrix}$$

where $\hat{q}$ is constant with respect to x. If $\hat{q}$ is negative then the body is in compression. For the problem of a plane with a crack (illustrated by component C in Figure 3.1), the stresses at infinity are zero, but there are stresses acting on the crack surfaces lying on $x_2 = 0$. From the symmetry of the problem, for any point lying on $x_2 = 0$, σ_{11} and σ_{22} are the only non-zero components. Thus we have

$$\boldsymbol{\sigma}^{(C)}(x_1) = \begin{pmatrix} \tilde{\sigma}_{11}(x_1) & 0 \\ 0 & \tilde{\sigma}_{22}(x_1) \end{pmatrix}$$

The stress of the combination of the above two cases (illustrated by component A in Figure 3.1) for the points lying on $x_2 = 0$ can then be represented as

$$\boldsymbol{\sigma}^{(A)}(x_1) = \begin{pmatrix} \tilde{\sigma}_{11}(x_1) & 0 \\ 0 & \hat{q} + \tilde{\sigma}_{22}(x_1) \end{pmatrix}.$$

The maximum of principle stress ahead of the CZ can be taken as $\hat{\sigma}(\hat{x}, \hat{t})$ which is given by

$$\hat{\sigma}(\hat{x}, \hat{t}) = \hat{q} + \tilde{\sigma}_{22}(\hat{x}, \hat{t}). \tag{3.5}$$

The formula for the stress component $\tilde{\sigma}_{22}(\hat{x}, \hat{t})$ can be derived using [44] as follows. In terms of the complex potentials, the stress components can be expressed as

$$\tilde{\sigma}_{22} - i\tilde{\sigma}_{12} = \Phi(z) + \Omega(\bar{z}) + (z - \bar{z})\overline{\Phi'(z)} \tag{3.6}$$

with $\Phi(z)$ and $\Omega(z)$ defined by

$$\Phi(z) = \Omega(z) = \frac{1}{2\pi i\sqrt{(z + \hat{c}(\hat{t}))(z - \hat{c}(\hat{t}))}} \int_{-\hat{c}(\hat{t})}^{\hat{c}(\hat{t})} \frac{\sqrt{(\xi + \hat{c}(\hat{t}))(\xi - \hat{c}(\hat{t}))}}{\xi - z} p(\xi) d\xi,$$

where $z = x_1 + ix_2$, $\hat{c}(\hat{t})$ denotes half the length of the crack with the CZ, while $p(\hat{x}, \hat{t})$ is given by

$$p(\hat{x}, \hat{t}) = \begin{cases} -\hat{q} & \text{when } \hat{x} \text{ is on the crack excluding the CZ} \\ \hat{\sigma}(\hat{x}, \hat{t}) - \hat{q} & \text{when } \hat{x} \text{ is on the CZ} \end{cases} \tag{3.7}$$

Denoting $\bar{z}$ as the complex conjugate of z, we have

$$\Omega(\bar{z}) = \frac{1}{2\pi i\sqrt{(\bar{z} + \hat{c}(\hat{t}))(\bar{z} - \hat{c}(\hat{t}))}} \int_{-\hat{c}(\hat{t})}^{\hat{c}(\hat{t})} \frac{\sqrt{(\xi + \hat{c}(\hat{t}))(\xi - \hat{c}(\hat{t}))}}{\xi - \bar{z}} p(\xi) d\xi.$$

In our case, $x_2 = 0$; so taking $z = x_1 = \bar{z}$, the last term $(z - \bar{z})\overline{\Phi'(z)}$ vanishes and

$$\Phi(z) = \Phi(x_1) = \Omega(\bar{z}) = \Omega(x_1).$$

After making the simplifications, we see that the imaginary term of equation (3.6) vanishes and we retrieve the following

$$\tilde{\sigma}_{22}(\hat{x},\hat{t}) = \frac{1}{\pi\sqrt{\hat{x}^2-\hat{c}^2(\hat{t})}}\int_{-\hat{c}(\hat{t})}^{\hat{c}(\hat{t})} \frac{\sqrt{\hat{c}^2(\hat{t})-\hat{\xi}^2}}{\hat{\xi}-\hat{x}} p(\hat{\xi},\hat{t})d\hat{\xi}, \quad |\hat{x}| > \hat{c}(\hat{t}).$$

Thus, we can rewrite equation (3.5) as

$$\hat{\sigma}(\hat{x},\hat{t}) = \frac{1}{\pi\sqrt{\hat{x}^2-\hat{c}^2(\hat{t})}}\int_{-\hat{c}(\hat{t})}^{\hat{c}(\hat{t})} \frac{\sqrt{\hat{c}^2(\hat{t})-\hat{\xi}^2}}{\hat{\xi}-\hat{x}} p(\hat{\xi},\hat{t})d\hat{\xi} + \hat{q}, \quad |\hat{x}| > \hat{c}(\hat{t}). \tag{3.8}$$

Using equation (3.7), we can rewrite equation (3.8) as

$$\begin{aligned}\hat{\sigma}(\hat{x},\hat{t}) = \frac{1}{\pi\sqrt{\hat{x}^2-\hat{c}^2(\hat{t})}}\Bigg[&\int_{-\hat{c}(\hat{t})}^{-\hat{a}(\hat{t})} \frac{\sqrt{\hat{c}^2(\hat{t})-\hat{\xi}^2}}{\hat{\xi}-\hat{x}}(\hat{\sigma}(\hat{\xi},\hat{t})-\hat{q})d\hat{\xi} + \int_{-\hat{a}(\hat{t})}^{\hat{a}(\hat{t})} \frac{\sqrt{\hat{c}^2(\hat{t})-\hat{\xi}^2}}{\hat{\xi}-\hat{x}}(-\hat{q})d\hat{\xi} \\ &+ \int_{\hat{a}(\hat{t})}^{\hat{c}(\hat{t})} \frac{\sqrt{\hat{c}^2(\hat{t})-\hat{\xi}^2}}{\hat{\xi}-\hat{x}}(\hat{\sigma}(\hat{\xi},\hat{t})-\hat{q})d\hat{\xi}\Bigg] + \hat{q} \quad |\hat{x}| > \hat{c}(\hat{t}).\end{aligned} \tag{3.9}$$

The integrals with respect to $\hat{\xi}$, where $\hat{\sigma}(\hat{\xi},\hat{t})$ does not appear in the integrand, can be evaluated analytically, and equation (3.9) can then be rewritten as

$$\begin{aligned}\hat{\sigma}(\hat{x},\hat{t}) = \frac{1}{\pi\sqrt{\hat{x}^2-\hat{c}^2(\hat{t})}}\Bigg[&\hat{q}\pi\left(\hat{x}-\sqrt{\hat{x}^2-\hat{c}^2(\hat{t})}\right) + \int_{-\hat{c}(\hat{t})}^{-\hat{a}(\hat{t})} \frac{\sqrt{\hat{c}^2(\hat{t})-\hat{\xi}^2}}{\hat{\xi}-\hat{x}}\hat{\sigma}(\hat{\xi},\hat{t})d\hat{\xi} \\ &+ \int_{\hat{a}(\hat{t})}^{\hat{c}(\hat{t})} \frac{\sqrt{\hat{c}^2(\hat{t})-\hat{\xi}^2}}{\hat{\xi}-\hat{x}}\hat{\sigma}(\hat{\xi},\hat{t})d\hat{\xi}\Bigg] + \hat{q} \quad |\hat{x}| > \hat{c}(\hat{t}).\end{aligned} \tag{3.10}$$

Also, using the substitution $u = -\hat{\xi}$, and noting that the stress, $\hat{\sigma}(\hat{x},\hat{\tau})$, is symmetric about the centre of the whole crack and so acts as an even function, we can combine the integrals ranging from $-\hat{c}(\hat{\tau})$ to $-\hat{a}(\hat{t})$ and from $\hat{a}(\hat{t})$ to $\hat{c}(\hat{t})$. Consequently, after simplifications, equation (3.10) can be rewritten as

$$\hat{\sigma}(\hat{x},\hat{t}) = \frac{\hat{x}}{\sqrt{\hat{x}^2-\hat{c}^2(\hat{t})}}\left(\hat{q} - \frac{2}{\pi}\int_{\hat{a}(\hat{t})}^{\hat{c}(\hat{t})} \frac{\sqrt{\hat{c}^2(\hat{t})-\hat{\xi}^2}}{\hat{x}^2-\hat{\xi}^2}\hat{\sigma}(\hat{\xi},\hat{t})d\hat{\xi}\right), \quad |\hat{x}| > \hat{c}(\hat{t}). \tag{3.11}$$

3.3 Stress Intensity Factor

The essence of using CZ modelling of fracture is that it can remove the stress singularity at the crack tip, see [19,33]. As one can see from (3.11), $\hat{\sigma}(\hat{x},\hat{t})$ generally has a square root singularity as $\hat{x}$ tends to the CZ tip $\hat{c}$. The stress intensity factor, $\hat{K}$, at this singularity can be obtained by multiplying the stress in equation (3.11) by $\sqrt{\hat{x}-\hat{c}(\hat{t})}$ and taking the limit as $\hat{x}$ tends to $\hat{c}(\hat{t})$, this yields

$$\hat{K}(\hat{t}) = \sqrt{\frac{\hat{c}(\hat{t})}{2}}\left(\hat{q} - \frac{2}{\pi}\int_{\hat{a}(\hat{t})}^{\hat{c}(\hat{t})} \frac{\hat{\sigma}(\hat{\xi},\hat{t})}{\sqrt{\hat{c}^2(\hat{t})-\hat{\xi}^2}} d\hat{\xi}\right). \tag{3.12}$$

A sufficient condition for the normalised equivalent stress, $\underline{\Lambda}$, to have no such singularity at the CZ tip is that the stress $\hat{\sigma}$ given by (3.11) does not have it either, while the necessary condition for the latter is that the stress intensity factor, $\hat{K}$, is zero there.

3.4 Normalisation

For simplicity, we will derive normalised forms of equations (3.4), (3.11) and (3.12). First, we will normalise time using

$$t = \frac{\hat{t}}{\hat{t}_\infty}; \tag{3.13}$$

and we will normalise the space coordinate and dimensions using

$$x = \frac{\hat{x}}{\hat{a}_0}, \quad a(t) = \frac{\hat{a}(t\,\hat{t}_\infty)}{\hat{a}_0}, \quad c(t) = \frac{\hat{c}(t\,\hat{t}_\infty)}{\hat{a}_0}. \tag{3.14}$$

Thus, t, $a(t)$, and $c(t)$ denote the normalised time, the normalised crack length, and the normalised CZ tip coordinate respectively. Here, $\hat{a}_0$ is the physical initial crack length. Also, since the stress $\hat{\sigma}(\hat{x},\hat{t})$ depends on the external load $\hat{q}$, we will use

$$\sigma(x,t) = \frac{\hat{\sigma}\left(\hat{x},\hat{t}\right)}{\hat{q}} = \frac{\hat{\sigma}(x\,\hat{a}_0, t\,\hat{t}_\infty)}{\hat{q}}. \tag{3.15}$$

After applying the normalisations given above, we arrive at the following normalised form of equation (3.4).

$$\int_{t_c(x)}^{t} \sigma^{\beta}(x,\tau)(t-\tau)^{\frac{\beta}{b}-1}d\tau = \frac{b}{\beta} - \int_{0}^{t_c(x)} \sigma^{\beta}(x,\tau)(t-\tau)^{\frac{\beta}{b}-1}d\tau \quad \text{for } a(t) \leq |x| \leq c(t).$$

Now, we will apply the same normalisation for the stress ahead of the crack tip. Using equations (3.13), (3.14), and (3.15) respectively, we arrive at the following form of equation (3.11)

$$\sigma(x,t) = \frac{x}{\sqrt{x^2 - c^2(t)}}\left(1 - \frac{2}{\pi}\int_{a(t)}^{c(t)} \frac{\sqrt{c^2(t)-\xi^2}}{x^2-\xi^2}\sigma(\xi,t)d\xi\right) \text{ for } |x| > c(t).$$

For the stress intensity factor, we will also use equations (3.13), (3.14), and (3.15) and denote

$$K(c,t) = \frac{\hat{K}(c\,\hat{a}_0, t\,\hat{t}_\infty)}{\hat{q}\sqrt{\hat{a}_0}};$$

this yields the following expression for the normalised stress intensity factor:

$$K(c(t),t) = \sqrt{\frac{c(t)}{2}}\left(1 - \frac{2}{\pi}\int_{a(t)}^{c(t)} \frac{\sigma(\xi,t)}{\sqrt{c^2(t)-\xi^2}}d\xi\right).$$

Chapter 4

Cohesive Zone Growth with a Stationary Crack

In this chapter, we assume that $a(t) = 1$, i.e. the CZ propagates, while the crack does not. The results of this problem have been published in [23,24,26]. In the previous chapter, we obtained the following normalised principal equations for the considered problem:

(a) the condition on the normalised equivalent stress, $\underline{\Lambda}(\sigma(x), t) = 1$ in the form

$$\int_{t_c(x)}^{t} \sigma^{\beta}(x,\tau)(t-\tau)^{\frac{\beta}{b}-1} d\tau = \frac{b}{\beta} - \int_{0}^{t_c(x)} \sigma^{\beta}(x,\tau)(t-\tau)^{\frac{\beta}{b}-1} d\tau, \tag{4.1}$$

for $a(t) \leq |x| \leq c(t)$, $t > t_c(x)$.

(b) the expression for the stress ahead of the CZ tip:

$$\sigma(x,t) = \frac{x}{\sqrt{x^2 - c^2(t)}} \left(1 - \frac{2}{\pi} \int_{a(t)}^{c(t)} \frac{\sqrt{c^2(t) - \xi^2}}{x^2 - \xi^2} \sigma(\xi, t) d\xi \right) \text{ for } |x| > c(t); \tag{4.2}$$

(c) the zero stress intensity factor condition, $K(c(t), t) = 0$, where

$$K(c(t), t) = \sqrt{\frac{c(t)}{2}} - \frac{\sqrt{2c(t)}}{\pi} \int_{a(t)}^{c(t)} \frac{\sigma(\xi, t)}{\sqrt{c^2(t) - \xi^2}} d\xi. \tag{4.3}$$

4.1 Numerical Method

To solve the system of equations given by (4.1) and (4.3) we will introduce a numerical algorithm which makes wide use of: (i) the analytical solution of an Abel-type integral equation; (ii) linear interpolation; and (iii) the secant method. We will use the next 3 subsections to briefly discuss these techniques.

Solution of a Generealised Abel-Type Integral Equation

Stated below is an important theorem regarding the exact solution of an Abel-type integral equation, see for e.g. [21, Theorem 1.2.1].

Theorem 1 *Let $T_0, T_1 \in \mathbb{R}$. If $f(t)$ is absolutely continuous on $[T_0, T_1]$, then the Abel type integral equation*

$$\int_{T_0}^{t} g(\tau)(t-\tau)^{-\lambda} d\tau = f(t), \quad t \in [T_0, T_1], \quad \lambda \in (0,1)$$

has a unique solution g in $L_1(T_0, T_1)$, which is given by the formula

$$g(\tau) = \frac{\sin(\pi\lambda)}{\pi} \frac{d}{d\tau} \int_{T_0}^{\tau} \frac{f(t)}{(\tau - t)^{1-\lambda}} dt. \tag{4.4}$$

Integrating by parts, expression (4.4) can be written as

$$g(\tau) = \frac{\sin(\pi\lambda)}{\pi} \left(f(T_0)(\tau - T_0)^{\lambda-1} + \int_{T_0}^{\tau} f'(t)(\tau - t)^{\lambda-1} dt \right). \tag{4.5}$$

Linear Interpolation

A continuous function $y(x)$ can be approximated using linear interpolation

$$y(x) \approx y(x_i) + \frac{y(x_{i+1}) - y(x_i)}{x_{i+1} - x_i}(x - x_i), \quad x \in [x_i, x_{i+1}].$$

This can particularly be used to approximate functions participating in integrands.

The Secant Method

The secant method is a root finding algorithm. This method requires two initial approximations. As an example, let's assume we have coordinates (x_1, y_1) and (x_2, y_2). In the secant method, after calculating the next approximation, x_3, using

$$x_3 = \frac{y_2 x_1 - y_1 x_2}{y_2 - y_1}$$

we allocate $x_1 = x_2$ and $x_2 = x_3$ to be used for the next iteration. A numerical method which is more stable than the secant method is the *regula falsi* method, see [3, 18]. This method is a combination of the secant method and the bisection method. In the regula falsi method, we choose the next 2 approximation x_1 and x_2 such that, when possible, the function values at these 2 points are different in sign. Although, in many occasions, this method takes a longer time to converge than the secant method, the advantage is that the range $[x_1, x_2]$ will always span the root so convergence is guaranteed.

4.1.1 Algorithm

Introduce a time mesh $t_i = ih$, $i = 0, 1, 2, ..., n$, where $h > 0$ is the time step size. In what follows, we will use c_i to denote the numerical approximation of $c(t_i)$, i.e. $c_i \approx c(t_i)$, and similarly for other variables.

At $t = t_0 = 0$, the normalised CZ length is zero, i.e., $c_0 = 1$, hence from equation (4.2), the stress distribution ahead of the crack is given by

$$\frac{x}{\sqrt{x^2 - c^2(t)}}.$$

For the following time steps $t = t_i$, we apply the algorithm given below. The details of each item in the algorithm will follow.

1. Take 2 initial approximations for c_i: $(c_i)_1$ and $(c_i)_2$.

2. For each approximation of c_i, calculate the stress at the CZ tip points at the preceding time instants, $\sigma(c_i, t_j)$ for $j = 0, 1, ..., i-1$, using equation (4.2).

3. Calculate the stress in the CZ, $\sigma(c_k, t_i)$ $k = 1, ..., i-1$ from (4.1), where $t_c(c_k) = t_k$; as well as the stress at the CZ tip $\sigma(c_i, t_i)$.

4. Now, for each of these 2 approximations, compute the corresponding stress intensity factors $K((c_i)_1, t_i)$ and $K((c_i)_2, t_i)$ from (4.3).

5. Compute the next approximation for c_i using
$$(c_i)_3 = \frac{K((c_i)_2, t_i)(c_i)_1 - K((c_i)_1, t_i)(c_i)_2}{K((c_i)_2, t_i) - K((c_i)_1, t_i)}.$$

6. If $|(c_i)_3 - (c_i)_1| < \epsilon$ or $|(c_i)_3 - (c_i)_2| < \epsilon$ allocate $c_i = (c_i)_3$ and go to the step $t = t_{i+1}$. Otherwise go to the next item.

7. Take the new $(c_i)_1$ as former $(c_i)_1$ or $(c_i)_2$ (depending on the signs of the computed stress intensity factors) and new $(c_i)_2$ as $(c_i)_3$ and return to item 2.

Using this algorithm, we obtain the behaviour of the crack length as well as the stress distribution in the CZ.

The details of items 2, 3, and 4 are given below.

Item 2

For the integral in equation (4.2), we piece-wise linearly interpolate $\sigma(\xi, t_j)$, $a \le \xi \le c(t_j)$, over $\sigma(c_k, t_j)$, $k = 0, ..., i-1$, for integration. We have
$$\sigma(c_i, t_j) = \frac{c_i}{\sqrt{c_i^2 - c_j^2}} \left(1 - \frac{2}{\pi} \sum_{k=1}^{j} \int_{c_{k-1}}^{c_k} \frac{\sqrt{c_j^2 - \xi^2}}{c_i^2 - \xi^2} \sigma(\xi, t_j) d\xi \right)$$
where
$$\sigma(\xi, t_j) \approx \sigma(c_{k-1}, t_j) + \frac{\sigma(c_k, t_j) - \sigma(c_{k-1}, t_j)}{c_k - c_{k-1}} (\xi - c_{k-1}), \quad c_{k-1} \le \xi \le c_k.$$

So, we have:

$$\sigma(c_i, t_j) = \frac{c_i}{\sqrt{c_i^2 - c_j^2}} \left(1 - \frac{2}{\pi} \sum_{k=1}^{j} S_k\right)$$

where

$$S_k = \left(\frac{\sigma(c_{k-1}, t_j)c_k - \sigma(c_k, t_j)c_{k-1}}{c_k - c_{k-1}}\right) I_1 + \left(\frac{\sigma(c_k, t_j) - \sigma(c_{k-1}, t_j)}{c_k - c_{k-1}}\right) I_2$$

where

$$I_1 = \int_{c_{k-1}}^{c_k} \frac{\sqrt{c_j^2 - \xi^2}}{\xi^2 - c_i^2} d\xi \quad \text{and} \quad I_2 = \int_{c_{k-1}}^{c_k} \frac{\xi\sqrt{c_j^2 - \xi^2}}{\xi^2 - c_i^2} d\xi.$$

Evaluating the integrals, we have

$$I_1 = \arctan\left(\frac{c_k}{\sqrt{c_j^2 - c_k^2}}\right) - \arctan\left(\frac{c_{k-1}}{\sqrt{c_j^2 - c_{k-1}^2}}\right) + \frac{\sqrt{c_i^2 - c_j^2}}{c_i}\left(\arctan\left(\frac{c_{k-1}\sqrt{c_i^2 - c_j^2}}{c_i\sqrt{c_j^2 - c_{k-1}^2}}\right) - \arctan\left(\frac{c_k\sqrt{c_i^2 - c_j^2}}{c_i\sqrt{c_j^2 - c_k^2}}\right)\right),$$

$$I_2 = \sqrt{c_j^2 - c_{k-1}^2} - \sqrt{c_j^2 - c_k^2} + \sqrt{c_i^2 - c_j^2}\left(\arctan\left(\frac{\sqrt{c_j^2 - c_k^2}}{\sqrt{c_i^2 - c_j^2}}\right) - \arctan\left(\frac{\sqrt{c_j^2 - c_{k-1}^2}}{\sqrt{c_i^2 - c_j^2}}\right)\right)$$

when $k \neq j$ and

$$I_1 = \frac{\sqrt{c_i^2 - c_k^2}}{c_i} \arctan\left(\frac{c_{k-1}\sqrt{c_i^2 - c_k^2}}{c_i\sqrt{c_k^2 - c_{k-1}^2}}\right) - \arctan\left(\frac{c_{k-1}}{\sqrt{c_k^2 - c_{k-1}^2}}\right) - \frac{\pi}{2c_i}\left(\sqrt{c_i^2 - c_k^2} - c_i\right),$$

$$I_2 = \sqrt{c_j^2 - c_{k-1}^2} - \sqrt{c_i^2 - c_j^2} \arctan\left(\frac{\sqrt{c_j^2 - c_{k-1}^2}}{\sqrt{c_i^2 - c_j^2}}\right)$$

when $k = j$.

Item 3

To obtain the stress at the CZ tip, we solve the integral equation (4.1) for $\sigma^\beta(c_i, t_i)$ by piecewise linearly interpolating $\sigma^\beta(c_i, \tau)$ for τ between t_0 and t_i. We have

$$\sum_{j=1}^{i} \int_{t_{j-1}}^{t_j} \sigma^\beta(c_i, \tau)(t_i - \tau)^{\frac{\beta}{b}-1} d\tau = \frac{b}{\beta}. \tag{4.6}$$

We use the linear interpolant

$$\sigma^\beta(c_i,\tau) \approx \sigma^\beta(c_i,t_{j-1}) + \frac{\sigma^\beta(c_i,t_j)-\sigma^\beta(c_i,t_{j-1})}{t_j-t_{j-1}}(\tau-t_{j-1}), \quad t_{j-1}\le\tau\le t_j.$$

Substituting these interpolation formulas into (4.6) and integrating the result, we have

$$\sigma^\beta(c_i,t_i) = \left[\frac{b}{\beta} - \sum_{j=1}^{i-1} G_j\right]\frac{\beta(\beta+b)}{b^2}(t_i-t_{i-1})^{-\frac{\beta}{b}} - \frac{\beta}{b}\sigma^\beta(c_i,t_{i-1}),$$

where

$$\begin{aligned} G_j = {}& \sigma^\beta(c_i,t_{j-1})\left(\frac{b}{\beta}(t_i-t_{j-1})^{\frac{\beta}{b}} - \frac{b}{\beta}(t_i-t_j)^{\frac{\beta}{b}}\right) \\ & + \left(\frac{\sigma^\beta(c_i,t_{j-1})-\sigma^\beta(c_i,t_j)}{t_{j-1}-t_j}\right)\left(\frac{b}{\beta}(t_{j-1}-t_j)(t_i-t_j)^{\frac{\beta}{b}}\right. \\ & \left. -\frac{b^2}{\beta(\beta+b)}(t_i-t_j)^{\frac{\beta}{b}+1} + \frac{b^2}{\beta(\beta+b)}(t_i-t_{j-1})^{\frac{\beta}{b}+1}\right). \end{aligned}$$

To obtain the stress in the CZ, we solve the integral equation (4.1) for $\sigma^\beta(x,t_i)$ for $x=c_k$, $k=0,1,2,3,...,i-1$ where $t_c(x)=t_k$. For the integral on the right hand side, $\sigma^\beta(x,\tau)$ is piecewise linearly interpolated between t_0 and $t_c(x)=t_k$. Using the analytical solution of a generalised Abel-type integral equation, we arrive at the following solution

$$\begin{aligned} \sigma^\beta(c_k,t_i) = {}& -\frac{1}{\pi}\sin\left(\frac{\pi\beta}{b}\right)\left[\sum_{l=1}^{k}\sigma^\beta(c_k,t_{l-1})\left(V(t_{l-1},t_i,t_k)-V(t_l,t_i,t_k)\right)+\right. \\ & \left.\frac{b}{\beta}\left(\frac{\sigma^\beta(c_k,t_l)-\sigma^\beta(c_k,t_{l-1})}{t_l-t_{l-1}}\right)\left(W(t_{l-1},t_i,t_k)-W(t_l,t_i,t_k)-\frac{\beta}{b}(t_l-t_{l-1})V(t_l,t_i,t_k)\right)\right] \end{aligned} \tag{4.7}$$

where

$$V(y,t_i,t_k) = \int_{t_k}^{t_i}\frac{(\tau-y)^{\frac{\beta}{b}-1}}{(t_i-\tau)^{\frac{\beta}{b}}}d\tau \qquad \text{and} \qquad W(y,t_i,t_k) = \int_{t_k}^{t_i}\frac{(\tau-y)^{\frac{\beta}{b}}}{(t_i-\tau)^{\frac{\beta}{b}}}d\tau.$$

Evaluating the integrals yields

$$V(y,t_i,t_k) = \pi\csc\left(\frac{\pi\beta}{b}\right) - \frac{b}{\beta}\left(\frac{t_k-y}{t_i-y}\right)^{\frac{\beta}{b}}\ {}_2F_1\left[\frac{\beta}{b},\frac{\beta}{b};1+\frac{\beta}{b};\frac{t_k-y}{t_i-y}\right], \tag{4.8}$$

and

$$W(y,t_i,t_k) = \frac{\beta}{b}\pi\csc\left(\frac{\pi\beta}{b}\right)(t_i-y) - \frac{b}{b+\beta}(t_k-y)^{1+\frac{\beta}{b}}(t_i-y)^{-\frac{\beta}{b}}\ {}_2F_1\left[1+\frac{\beta}{b},\frac{\beta}{b};2+\frac{\beta}{b};\frac{t_k-y}{t_i-y}\right] \tag{4.9}$$

where ${}_2F_1$ is the Gauss hypergeometric function, see e.g. [31, Section 1.6].

Item 4

Piecewise linearly interpolating $\sigma(\xi, t_i)$ over already calculated $\sigma(c_k, t_i)$, $k = 0, ..., i-1$ and $\sigma(c_i, t_i)$, calculate $K(t_i, c_i)$ from (4.3). This gives

$$K(t_i, c_i) = \frac{\sqrt{c_i}}{\sqrt{2}} - \frac{\sqrt{2c_i}}{\pi} \sum_{k=0}^{i-2} \int_{c_k}^{c_{k+1}} \frac{1}{\sqrt{c_i^2 - \xi^2}} \sigma(\xi, t_i) d\xi - \frac{\sqrt{2c_i}}{\pi} \int_{c_{i-1}}^{c_i} \frac{1}{\sqrt{c_i^2 - \xi^2}} \sigma(\xi, t_i) d\xi. \tag{4.10}$$

For the first integral we have

$$\sigma(\xi, t_i) \approx \sigma(c_k, t_i) + \frac{\sigma(c_{k+1}, t_i) - \sigma(c_k, t_i)}{c_{k+1} - c_k}(\xi - c_k), \quad c_k \leq \xi \leq c_{k+1}$$

and for the second integral, we have a similar interpolant but with c_k replaced with c_{i-1} and c_{k+1} replaced with c_i. Substituting these linear interpolation formulas into (4.10) and integrating the results, we have

$$\begin{aligned}
K(t_i, c_i) = \frac{\sqrt{c_i}}{\sqrt{2}} - \frac{\sqrt{2c_i}}{\pi} \sum_{k=0}^{i-2} \Bigg[& \sigma(c_k, t_i) \left(\arcsin\left(\frac{c_{k+1}}{c_i}\right) - \arcsin\left(\frac{c_k}{c_i}\right) \right) \\
& + \frac{\sigma(c_{k+1}, t_i) - \sigma(c_k, t_i)}{c_{k+1} - c_k} \left(\sqrt{c_i^2 - c_k^2} - \sqrt{c_i^2 - c_{k+1}^2} - c_k \arcsin\left(\frac{c_{k+1}}{c_i}\right) + c_k \arcsin\left(\frac{c_k}{c_i}\right) \right) \Bigg] \\
& - \frac{\sqrt{2c_i}}{\pi} \Bigg[\sigma(c_{i-1}, t_i) \left(\frac{\pi}{2} - \arcsin\left(\frac{c_{i-1}}{c_i}\right) \right) \\
& + \frac{\sigma(c_i, t_i) - \sigma(c_{i-1}, t_i)}{c_i - c_{i-1}} \left(\sqrt{c_i^2 - c_{i-1}^2} - c_{i-1}\frac{\pi}{2} + c_{i-1} \arcsin\left(\frac{c_{i-1}}{c_i}\right) \right) \Bigg].
\end{aligned} \tag{4.11}$$

4.1.2 Analysis of Stress in the Cohesive Zone

We denote the right hand side of equation (4.1) by $f(x, t)$. Hence,

$$f(x, t) = \frac{b}{\beta} - \int_0^{t_c(x)} \sigma^\beta(x, \tau)(t - \tau)^{\frac{\beta}{b} - 1} d\tau.$$

Note that since the condition $\underline{\Lambda}(\sigma(x, t); t) = 1$ must be satisfied, this means that $f(c(t_k), t_c) = 0$. Therefore, in our case, using the form given in equation (4.5) for the solution to the integral equation (4.1) is more accurate than using the form in equation (4.4) since the

integral in the right hand side is found numerically by interpolation, but we know that $f(c(t_k), t_c)$ is analytically zero.

We wish to analyse the continuity of the solution for $\sigma(x,t)$ as $t \to t_c(x)$ (we may use t_c to denote $t_c(x)$). We expect that the stress approaches a finite value. From (4.7), we have the following

$$\lim_{t\to t_c} \sigma^\beta(x,t) = \lim_{t\to t_c} -\frac{1}{\pi}\sin\left(\frac{\pi\beta}{b}\right)\left[\sum_{l=1}^{c}\sigma^\beta(x,t_{l-1})\left(V(t_{l-1},t,t_c)-V(t_l,t,t_c)\right)\right.$$
$$\left.+\frac{b}{\beta}\left(\frac{\sigma^\beta(x,t_l)-\sigma^\beta(x,t_{l-1})}{t_l-t_{l-1}}\right)\left(W(t_{l-1},t,t_c)-W(t_l,t,t_c)-\frac{\beta}{b}(t_l-t_{l-1})V(t_l,t,t_c)\right)\right]. \tag{4.12}$$

In the above limit, only $V(t_l,t,t_c)$ and $W(t_l,t,t_c)$ depend on t. We compute the limits

$$\lim_{t\to t_c} V(t_l,t,t_c) = \begin{cases} 0 & \text{for } l < c \\ \pi \csc\left(\frac{\pi\beta}{b}\right) & \text{when } l = c \end{cases}$$

and

$$\lim_{t\to t_c} W(t_l,t,t_c) = 0 \quad \forall\ l \le c$$

see Appendix A for the intermediate steps of obtaining the above limits.

Consequently, in equation (4.12), the summation over l for $l < c$ will be zero but the non-zero $V(t_l,t,t_c)$ for $l = c$ yields the following

$$\begin{aligned}\lim_{t\to t_c}\sigma^\beta(x,t) &= -\frac{1}{\pi}\sin\left(\frac{\pi\beta}{b}\right)\left[-\pi\csc\left(\frac{\pi\beta}{b}\right)\sigma^\beta(x,t_{c-1})\right.\\ &\left.+\frac{b}{\beta}\cdot\frac{\sigma^\beta(x,t_c)-\sigma^\beta(x,t_{c-1})}{t_c-t_{c-1}}\left(\frac{\beta}{b}(t_c-t_{c-1})\pi\csc\left(\frac{\pi\beta}{b}\right)\right)\right]\\ &= \sigma^\beta(x,t_c).\end{aligned}$$

Therefore, $\lim_{t\to t_c}\sigma^\beta(x,t_i) = \sigma^\beta(x,t_c)\ \forall\, b > \beta$.

The computed integrals are in terms of the Gauss hypergeometric function ${}_2F_1$. MATLAB is rather slow while computing hypergeometric functions. Therefore, we will often

look at cases of the parameters β and b such that the resulting hypergeometric functions can be represented in simplified analytical forms. Such cases are $\beta = \frac{b}{2}$, $\beta = \frac{b}{4}$, and $\beta = \frac{b}{8}$.

Now, we will give the representation of the solution in equation (4.7) for the 3 cases: $\beta = \frac{b}{2}$, $\beta = \frac{b}{4}$, and $\beta = \frac{b}{8}$. Excluding the intermediate steps, the parameters V and W in equation (4.7), have the following forms.

For $\beta = \frac{b}{2}$:

$$V(y,t_i,t_k) = \frac{\pi}{2} + \arcsin\left(1 + \frac{2(y-t_k)}{t_i - y}\right),$$
$$W(y,t_i,t_k) = \sqrt{(t_i-t_k)(t_k-t)} + \frac{\pi}{4}(t_i-y) + \frac{1}{2}(t_i-y)\arcsin\left(1 + \frac{2(y-t_k)}{t_i-y}\right).$$

For $\beta = \frac{b}{4}$:

$$V(y,t_i,t_k) = \pi\sqrt{2} - 4\left(\frac{t_k-y}{t_i-y}\right)^{1/4} {}_2F_1\left[\frac{1}{4},\frac{1}{4};\frac{5}{4};\frac{t_k-y}{t_i-y}\right],$$
$$W(y,t_i,t_k) = (t_k-y)^{1/4}(t_i-t_k)^{3/4} + \frac{\pi\sqrt{2}}{4}(t_i-y) - (t_k-y)^{1/4}(t_i-y)^{3/4}\,{}_2F_1\left[\frac{1}{4},\frac{1}{4};\frac{5}{4};\frac{t_k-y}{t_i-y}\right].$$

However, ${}_2F_1\left[\frac{1}{4},\frac{1}{4};\frac{5}{4};z\right]$ can be represented analytically using

$$\begin{aligned} {}_2F_1\left[\frac{1}{4},\frac{1}{4};\frac{5}{4};z\right] &= \frac{\ln\left(1 + \frac{\sqrt{2}z^{1/4}}{(1-z)^{1/4}} + \frac{\sqrt{z}}{\sqrt{1-z}}\right) - \ln\left(1 - \frac{\sqrt{2}z^{1/4}}{(1-z)^{1/4}} + \frac{\sqrt{z}}{\sqrt{1-z}}\right)}{4\sqrt{2}z^{1/4}} \\ &+ \frac{2\arctan\left(1 - \frac{z^{1/4}}{\sqrt{2}(1-z)^{1/4}}, -\frac{z^{1/4}}{\sqrt{2}(1-z)^{1/4}}\right) + 2\arctan\left(1 + \frac{z^{1/4}}{\sqrt{2}(1-z)^{1/4}}, -\frac{z^{1/4}}{\sqrt{2}(1-z)^{1/4}}\right)}{-4\sqrt{2}z^{1/4}} \end{aligned} \tag{4.13}$$

see [63].

For $\beta = \frac{b}{8}$:

$$V(y,t_i,t_k) = \pi\csc\left(\frac{\pi}{8}\right) - 8\left(\frac{t_k-y}{t_i-y}\right)^{1/8} {}_2F_1\left[\frac{1}{8},\frac{1}{8};\frac{9}{8};\frac{t_k-y}{t_i-y}\right],$$

$$W(y,t_i,t_k)=\left(\frac{t_k-y}{t_i-t_k}\right)^{\frac{1}{8}}(t_i-t_k)+\frac{\pi}{8}(t_i-y)\csc\left(\frac{\pi}{8}\right)-(t_i-y)^{7/8}(t_k-y)^{1/8}\,{}_2F_1\left[\frac{1}{8},\frac{1}{8};\frac{9}{8};\frac{t_k-y}{t_i-y}\right].$$

Although, ${}_2F_1\left[\frac{1}{8},\frac{1}{8};\frac{9}{8};z\right]$ cannot directly be represented analytically by a formula, we can use the Pfaff hypergeometric transformation given by

$${}_2F_1\left[\frac{1}{8},\frac{1}{8};\frac{9}{8};z\right]=(1-z)^{-1/8}\,{}_2F_1\left[\frac{1}{8},1;\frac{9}{8};\frac{z}{z-1}\right]$$

see [31]; and ${}_2F_1\left[\frac{1}{8},1;\frac{9}{8};\frac{z}{z-1}\right]$ can be computed analytically using the following formula

$$\begin{aligned}{}_2F_1\left[\frac{1}{8},1;\frac{9}{8};z\right]=\frac{1}{8z^{1/8}}\Big(&2\arctan\left(z^{1/8}\right)+\sqrt{2}\arctan\left(1-z^{1/4},\sqrt{2}z^{1/8}\right)-\ln\left(1-z^{1/8}\right)\\&+\ln\left(1+z^{1/8}\right)+\frac{-\ln\left(1-\sqrt{2}z^{1/8}+z^{1/4}\right)+\ln\left(1+\sqrt{2}z^{1/8}+z^{1/4}\right)}{\sqrt{2}}\Big)\end{aligned}\tag{4.14}$$

see [63].

4.2 Numerical Solution

Although the exact solution is unknown, we can judge the suitability of the algorithm by inspecting the solution as the number of points in the mesh doubles. This inspection is given in Appendix B. However, a more accurate and elegant way of checking convergence of the solutions is by looking at the numerical convergence rate considered in Chapter 8.

The solutions will be presented for the cases $b=4$, and $b=1.5$ with $\beta=\frac{b}{2}$, $\beta=\frac{b}{4}$, and $\beta=\frac{b}{8}$ for each case. In the following section, we will present some of the solutions obtained after implementing the algorithm. As well as the evolution of the CZ tip coordinate in time, we are also interested in showing how the stress, at a specific point, is behaving as a function of time. We expect the stress, at a particular point in space, to grow monotonically before this point becomes part of the CZ, and to decrease monotonically inside the CZ. To analyse the behaviour of the stress, we will take a point, say $c(t^*)$ for $t^*=0.6$, and plot the values

of σ before the point became part of the CZ (before $t = 0.6$), at the CZ tip (at $t = 0.6$) and when it is inside the CZ (after $t = 0.6$).

In Figures 4.1-4.4, we present graphs of $c(t)$ and $\sigma(c(t^*), t)$ vs. time for three cases of β while using a time step of $h = \dfrac{1}{800}$.

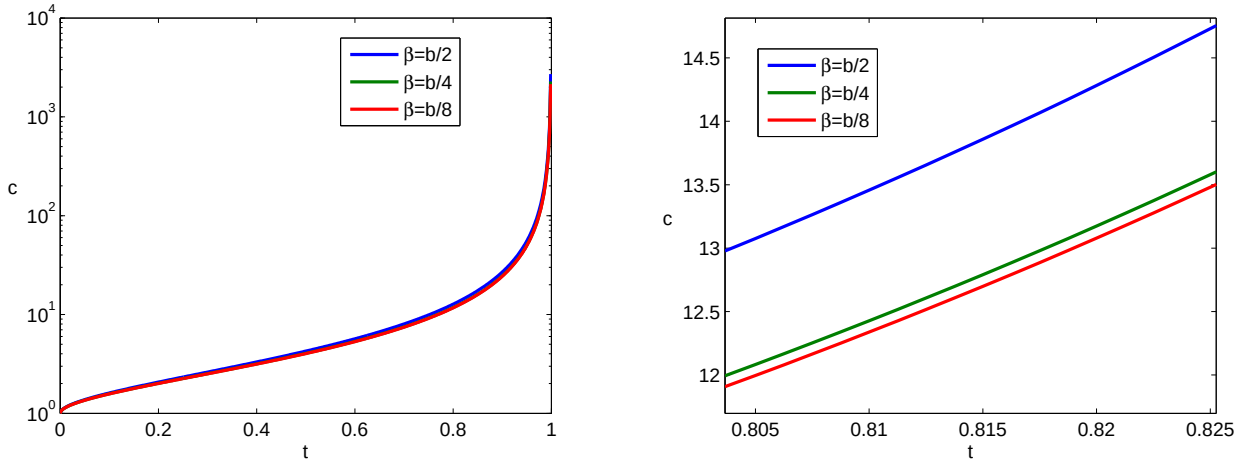

Figure 4.1: CZ tip coordinate vs. time for $b = 4$.

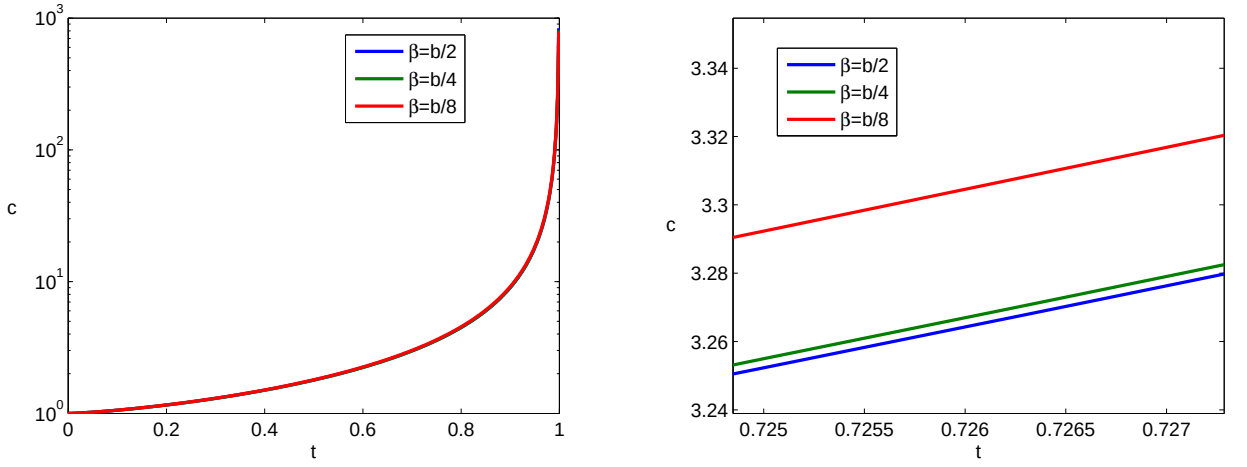

Figure 4.2: CZ tip coordinate vs. time for $b = 1.5$.

We see that ahead of the CZ tip, the rate of stress increase with time is greater as we

take higher values for β and, after the CZ tip, the rate of stress decrease with time is greater as we take higher values of β. We can see that we have monotonic increase of the stress before the point reaches the CZ tip, and we also have monotonic decrease of the stress after the CZ tip.

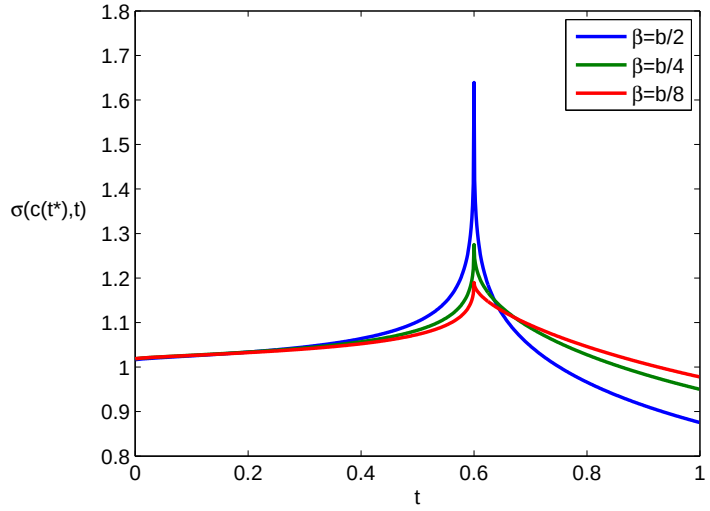

Figure 4.3: $\sigma(c(t^*), t)$ for $b = 4$ at $t^* = 0.6$.

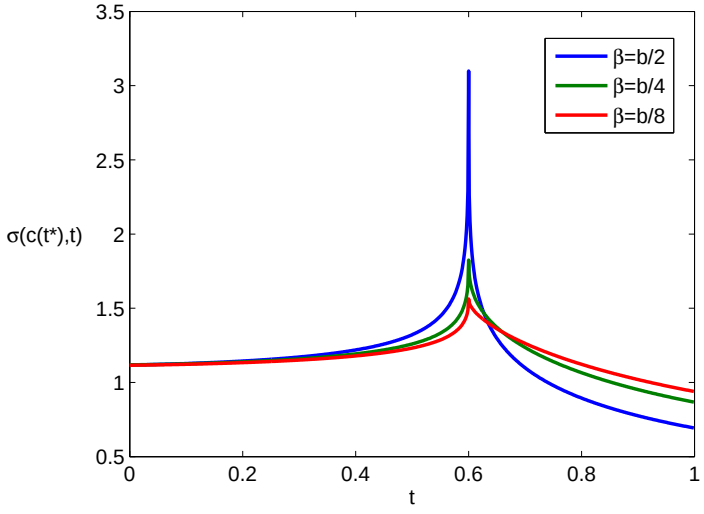

Figure 4.4: $\sigma(c(t^*), t)$ for $b = 1.5$ at $t^* = 0.6$.

Chapter 5

The Crack Tip Opening

As in the previous sections, consider a crack of length $2a$ with a CZ length $l = c - a$ at each end of the crack. We want to find the crack opening, that is the displacement jump over the crack shores. We will first consider the case when the bulk of the material is linearly elastic and then convert the obtained solution to the case of linear visco-elastic materials using the so-called Volterra principle. We denote the crack opening by $\hat{u}$ and the displacement jump at the crack tip (the crack tip opening) by $\hat{\delta}$, see Figure 5.1. We will use δ_e and δ_v to denote the elastic and viscoelastic crack tip opening respectively.

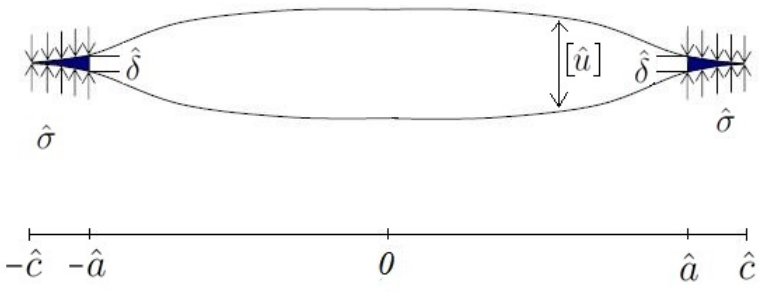

Figure 5.1: Crack with CZs, [38].

5.1 Linear Elastic Material

5.1.1 Formulation

The crack opening is calculated in a similar manner as done for the Dugdale model, see subsection 2.3.1, and is given by the following formula

$$[\hat{u}_e](\hat{x},\hat{t}) = [\hat{u}_e^{(\hat{q})}](\hat{x},\hat{t}) + [\hat{u}_e^{(\hat{\sigma})}](\hat{x},\hat{t})]$$

where

$$[\hat{u}_e^{(\hat{q})}](\hat{x},\hat{t}) = \int_{-\hat{c}(\hat{t})}^{\hat{c}(\hat{t})} \hat{q}\hat{v}_2(\hat{x},\hat{\xi};\hat{c}(\hat{t}))d\hat{\xi} \tag{5.1}$$

and

$$[\hat{u}_e^{(\hat{\sigma})}](\hat{x},\hat{t}) = \int_{-\hat{c}(\hat{t})}^{-\hat{a}(\hat{t})} -\hat{\sigma}(\hat{\xi},\hat{t})\hat{v}_2(\hat{x},\hat{\xi},\hat{c}(\hat{t}))d\hat{\xi} + \int_{\hat{a}(\hat{t})}^{\hat{c}(\hat{t})} -\hat{\sigma}(\hat{\xi},\hat{t})\hat{v}_2(\hat{x},\hat{\xi},\hat{c}(\hat{t}))d\hat{\xi}. \tag{5.2}$$

In the above expressions, $\hat{v}_2(\hat{x},\hat{\xi};\hat{c}(\hat{t}))$ is given by the following formula

$$\hat{v}_2(\hat{x},\hat{\xi};\hat{c}(\hat{t})) = -\frac{\kappa+1}{2\pi\mu}\tilde{\Gamma}(\hat{x},\hat{\xi};\hat{c}(\hat{t})) \tag{5.3}$$

where

$$\tilde{\Gamma}(\hat{x},\hat{\xi};\hat{c}(\hat{t})) = \ln\left[\frac{\hat{c}^2(\hat{t}) - \hat{x}\hat{\xi} - \sqrt{(\hat{c}^2(\hat{t})-\hat{x}^2)(\hat{c}^2(\hat{t})-\hat{\xi}^2)}}{\hat{c}^2(\hat{t}) - \hat{x}\hat{\xi} + \sqrt{(\hat{c}^2(\hat{t})-\hat{x}^2)(\hat{c}^2(\hat{t})-\hat{\xi}^2)}}\right] \tag{5.4}$$

see [38].

After substituting the expression (5.3) into (5.1) and (5.2), we have the following results

$$[\hat{u}_e^{(\hat{q})}](\hat{x},\hat{t}) = \frac{\hat{q}(1+\kappa)}{2\mu}\sqrt{\hat{c}^2(\hat{t})-\hat{x}^2},$$

$$[\hat{u}_e^{(\hat{\sigma})}](\hat{x},\hat{t}) = \frac{\kappa+1}{2\pi\mu}\left(\int_{-\hat{c}(\hat{t})}^{-\hat{a}(\hat{t})} \hat{\sigma}(\hat{\xi},\hat{t})\tilde{\Gamma}(\hat{x},\hat{\xi};\hat{c}(\hat{t}))d\hat{\xi} + \int_{\hat{a}(\hat{t})}^{\hat{c}(\hat{t})} \hat{\sigma}(\hat{\xi},\hat{t})\tilde{\Gamma}(\hat{x},\hat{\xi};\hat{c}(\hat{t}))d\hat{\xi}\right).$$

Combining the integrals ranging from $-\hat{c}(\hat{t})$ to $-\hat{a}(\hat{t})$ and $\hat{a}(\hat{t})$ to $\hat{c}(\hat{t})$, $[\hat{u}_e^{(\hat{\sigma})}](\hat{x},\hat{t})$ can be written as

$$[\hat{u}_e^{(\hat{\sigma})}](\hat{x},\hat{t}) = \frac{\kappa+1}{2\pi\mu}\left(\int_{\hat{a}(\hat{t})}^{\hat{c}(\hat{t})} \hat{\sigma}(\hat{\xi},\hat{t})\Gamma(\hat{x},\hat{\xi};\hat{c}(\hat{t}))d\hat{\xi}\right),$$

where

$$\Gamma(\hat{x},\hat{\xi};\hat{c}(\hat{t})) = \ln\left[\frac{2\hat{c}^2(\hat{t}) - \hat{\xi}^2 - \hat{x}^2 - 2\sqrt{(\hat{c}^2(\hat{t}) - \hat{x}^2)(\hat{c}^2(\hat{t}) - \hat{\xi}^2)}}{2\hat{c}^2(\hat{t}) - \hat{\xi}^2 - \hat{x}^2 + 2\sqrt{(\hat{c}^2(\hat{t}) - \hat{x}^2)(\hat{c}^2(\hat{t}) - \hat{\xi}^2)}}\right].$$

So, after combining the expressions for $[\hat{u}_e^{(\hat{q})}](\hat{x},\hat{t})$ and $[\hat{u}_e^{(\hat{\sigma})}](\hat{x},\hat{t})$, we have the following formula for the crack opening

$$[\hat{u}_e](\hat{x},\hat{t}) = \frac{1+\kappa}{2\mu}\left(\hat{q}\sqrt{\hat{c}^2(\hat{t}) - \hat{x}^2} + \frac{1}{\pi}\int_{\hat{a}(\hat{t})}^{\hat{c}(\hat{t})} \hat{\sigma}(\hat{\xi},\hat{t})\Gamma(\hat{x},\hat{\xi};\hat{c}(\hat{t}))d\hat{\xi}\right).$$

The *crack tip* opening occurs at $x = a(t)$ and is therefore given by

$$\hat{\delta}_e(\hat{t}) := [\hat{u}_e](\hat{a}(\hat{t}),\hat{t}) = \frac{1+\kappa}{2\mu}\left(\hat{q}\sqrt{\hat{c}^2(\hat{t}) - \hat{a}^2(\hat{t})} + \frac{1}{\pi}\int_{\hat{a}(\hat{t})}^{\hat{c}(\hat{t})} \hat{\sigma}(\hat{\xi},\hat{t})\Gamma(\hat{a}(\hat{t}),\hat{\xi};\hat{c}(\hat{t}))d\hat{\xi}\right). \quad (5.5)$$

Using the space, time, and stress normalisation given in subsection 3.4 as well as the following normalisation

$$[u_e](x,t) = \frac{8\mu\ [\hat{u}_e]\left(\hat{x}\,\hat{a}_0, t\hat{t}_\infty\right)}{\hat{q}\hat{a}_0(1+\kappa)}, \quad \delta_e(t) = \frac{8\mu\,\hat{\delta}_e(t\,\hat{t}_\infty)}{\hat{q}\hat{a}_0(1+\kappa)}, \quad (5.6)$$

we have the following formulae for the normalised crack opening and the normalised crack tip opening respectively

$$[u_e](x;t) = \frac{4}{\pi}\left(\pi\sqrt{c^2(t) - x^2} + \int_{a(t)}^{c(t)} \sigma(\xi,t)\Gamma(x,\xi;c(t))d\xi\right), \quad (5.7)$$

$$\delta_e(t) = \frac{4}{\pi}\left(\pi\sqrt{c(t)^2 - a(t)^2} + \int_{a(t)}^{c(t)} \sigma(\xi,t)\Gamma(a(t),\xi;c(t))d\xi\right). \quad (5.8)$$

In the previous chapter, we considered discrete time steps and found $c(t_i)$ and $\sigma(c(t_k),t_i)$. These results will be used when numerically computing the crack tip opening. To evaluate the crack tip opening at each time step t_i, using equation (5.8), we linearly interpolate $\sigma(\xi,t_i)$ between $c(t_k)$ and $c(t_{k+1})$ for $k = 0,1,...i-1$ and $i = 1,...,n$. To this end, at time step t_i, we can rewrite the integral in (5.8) as

$$\int_{a_i}^{c_i} \sigma(\xi,t_i)\Gamma(a_i,\xi;c_i)d\xi = \sum_{k=0}^{i-1}\left(\frac{\sigma(c_k,t_i)c_{k+1} - \sigma(c_{k+1},t_i)c_k}{c_{k+1}-c_k}A + \frac{\sigma(c_{k+1},t_i) - \sigma(c_k,t_i)}{c_{k+1}-c_k}B\right) \quad (5.9)$$

where

$$A = \int_{c_k}^{c_{k+1}} \ln \left[\frac{2c_i^2 - \xi^2 - a_i^2 - 2\sqrt{(c_i^2 - a_i^2)(c_i^2 - \xi^2)}}{2c_i^2 - \xi^2 - a_i^2 + 2\sqrt{(c_i^2 - a_i^2)(c_i^2 - \xi^2)}} \right] d\xi \tag{5.10}$$

and

$$B = \int_{c_k}^{c_{k+1}} \xi \ln \left[\frac{2c_i^2 - \xi^2 - a_i^2 - 2\sqrt{(c_i^2 - a_i^2)(c_i^2 - \xi^2)}}{2c_i^2 - \xi^2 - a_i^2 + 2\sqrt{(c_i^2 - a_i^2)(c_i^2 - \xi^2)}} \right] d\xi. \tag{5.11}$$

Since we are now looking at the stationary crack stage, we will replace a_i with a. After integration, we have

$$A = -4\sqrt{c_i^2 - a^2} \arctan \left(\frac{c_k \sqrt{c_i^2 - c_k^2} - c_{k+1}\sqrt{c_i^2 - c_{k+1}^2}}{c_k^2 + c_{k+1}^2 - c_i^2} \right) + (a - c_k)\tilde{\Gamma}(a, c_k; c_i)$$
$$- (a + c_k)\tilde{\Gamma}(a, -c_k; c_i) - (a - c_{k+1})\tilde{\Gamma}(a, c_{k+1}; c_i) + (a + c_{k+1})\tilde{\Gamma}(a, -c_{k+1}; c_i)$$

and

$$B = 2\sqrt{(c_i^2 - c_{k+1}^2)(c_i^2 - c_0^2)} - 2\sqrt{(c_i^2 - c_k^2)(c_i^2 - c_0^2)} - \frac{1}{2}(c_k^2 - a^2)\tilde{\Gamma}(a, c_k; c_i)$$
$$- \frac{1}{2}(c_k^2 - a^2)\tilde{\Gamma}(a, -c_k; c_i) + \frac{1}{2}(c_{k+1}^2 - a^2)\tilde{\Gamma}(a, c_{k+1}; c_i) + \frac{1}{2}(c_{k+1}^2 - a^2)\tilde{\Gamma}(a, -c_{k+1}; c_i).$$

Using different forms and simplifications of the above results for A and B for the special cases when $k + 1 = i$ or $k = 0$, we have the following results.

When $c_k = a$ and $c_{k+1} = c_i$

$$A = 4a \ln \left[\frac{c_i}{a} \right] - 4\sqrt{c_i^2 - a^2} \arccos \left(\frac{a}{c_i} \right),$$
$$B = 2(a^2 - c_i^2).$$

When $c_k = a$ and $c_{k+1} \neq c_i$

$$A = 4a \ln \left(\frac{c_i}{a} \right) - 4\sqrt{c_i^2 - a^2} \arctan \left(\frac{a\sqrt{c_i^2 - a^2} - c_{k+1}\sqrt{c_i^2 - c_{k+1}^2}}{a^2 - c_i^2 + c_{k+1}^2} \right)$$
$$- (a^2 - c_{k+1}^2)\tilde{\Gamma}(a, c_{k+1}; c_i) + (a^2 + c_{k+1}^2)\tilde{\Gamma}(a, -c_{k+1}; c_i),$$

$$B = 2a^2 - 2c_i^2 + 2\sqrt{(c_i^2 - c_{k+1}^2)(c_i^2 - a^2)} - \frac{1}{2}(a^2 - c_{k+1}^2)\left(\tilde{\Gamma}(a, c_{k+1}; c_i) + \tilde{\Gamma}(a, -c_{k+1}; c_i) \right).$$

When $c_{k+1} = c_i$ and $c_k \neq a$

$$A = -4\sqrt{c_i^2 - a^2}\arccos\left(\frac{c_k}{c_i}\right) + (a - c_k)\tilde{\Gamma}(a, c_k; c_i) - (a + c_k)\tilde{\Gamma}(a, -c_k; c_i),$$

$$B = -2\sqrt{(c_i^2 - a^2)(c_i^2 - c_k^2)} - \frac{1}{2}(c_k^2 - a^2)\left(\tilde{\Gamma}(a, c_k; c_i) - \tilde{\Gamma}(a, -c_k; c_i)\right).$$

where $\tilde{\Gamma}(x, \xi; c)$ is given in equation (5.4). For a given mesh, A and B can be calculated and substituted into equation (5.9) and consequently this will be substituted into (5.8) to give the normalised crack tip opening δ_e.

5.1.2 Numerical Solution

Using a time mesh consisting of equidistantly spaced nodes with step size $h = \frac{1}{800}$, we have the following graphs.

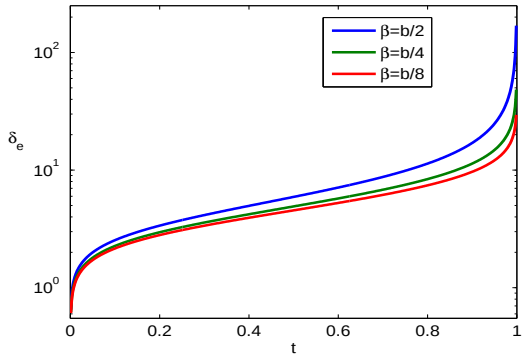

Figure 5.2: Crack tip opening δ_e vs. time t for $b = 4$.

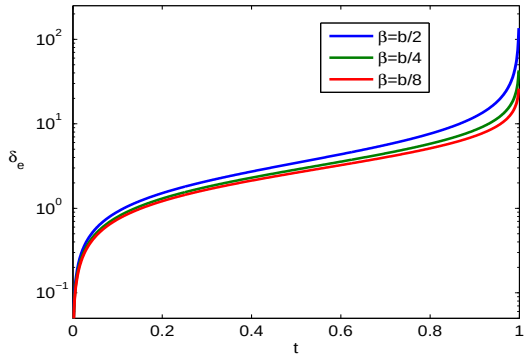

Figure 5.3: Crack tip opening δ_e vs. time t for $b = 1.5$.

5.2 Linear Viscoelastic Material

5.2.1 Formulation

To obtain the crack tip opening in the viscoelastic case, we will implement the so-called Volterra principle, according to which we have to replace the elastic constants μ and ν in the elastic solution by the corresponding viscoelastic operators, to arrive at the viscoelastic solution. Although this approach does not always bring a viscoelastic solution for the problems with moving boundaries, it is possible to show, see [52], that this approach leads to a viscoelastic solution for the plane symmetric problem with a straight propagating crack. This means that for the viscoelastic problem we can directly use the results by Muskhelishvili, see [44], for the stress representation ahead of the CZ tip given in equation (4.2) since they do not include the elastic constants at all.

For simplicity, we will consider the viscoelastic material with constant (purely elastic) Poisson's ratio ν (and thus the parameter κ will also remain constant). Then, to obtain the crack opening in the viscoelastic case, we have to replace $\dfrac{1}{\mu}$ in (5.5) by the second kind Volterra integral operator $\boldsymbol{\mu}^{-1}$ defined by

$$\left(\boldsymbol{\mu}^{-1}\hat{\sigma}\right)\left(\hat{t}\right) = \frac{\hat{\sigma}\left(\hat{t}\right)}{\mu} - \int_0^{\hat{t}} \dot{J}\left(\hat{t}-\hat{\tau}\right)\hat{\sigma}\left(\hat{\tau}\right)d\hat{\tau}$$

To this end, the crack opening in the viscoelastic case can be computed using

$$\begin{aligned}\hat{\delta}_v\left(\hat{t}\right) &= \left(\boldsymbol{\mu}^{-1}\mu\hat{\delta}_e\right)\left(\hat{t}\right)\\ &= \left(\hat{\delta}_e\left(\hat{t}\right) - \mu\int_0^{\hat{t}} \dot{J}\left(\hat{t}-\hat{\tau}\right)\hat{\delta}_e\left(\hat{\tau}\right)d\hat{\tau}\right).\end{aligned} \tag{5.12}$$

In our case, we will use the creep function of a standard linear solid, we have

$$J\left(\hat{t}-\hat{\tau}\right) = \frac{1}{E_0} + \frac{1}{E_1}\left(1 - e^{-\frac{1}{\theta}\left(\hat{t}-\hat{\tau}\right)}\right),$$

and so

$$\dot{J}\left(\hat{t}-\hat{\tau}\right) = -\frac{1}{\eta}e^{-\frac{1}{\theta}\left(\hat{t}-\hat{\tau}\right)}$$

where θ and $\eta = E_1\theta$ denote the relaxation time and viscosity respectively. So, equation (5.12) becomes

$$\hat{\delta}_v\left(\hat{t}\right) = \hat{\delta}_e\left(\hat{t}\right) + \frac{\mu}{\eta}\int_0^{\hat{t}} e^{-\frac{1}{\theta}\left(\hat{t}-\hat{\tau}\right)}\hat{\delta}_e\left(\hat{\tau}\right)d\hat{\tau}. \tag{5.13}$$

We will use the same normalisations given in subsection 3.4 to normalise space, time, and stress. Furthermore, similarly to equation (5.6), we will normalise the viscoelastic crack tip opening using

$$\delta_v(t) = \frac{8\mu\tilde{\delta}_v\left(tt_\infty\right)}{\hat{q}\hat{a}_0\left(1+\kappa\right)}. \tag{5.14}$$

Consequently, the normalised crack tip opening for the viscoelastic case is given by

$$\delta_v(t) = \delta_e(t) + m\int_0^t e^{-\frac{(t-\tau)}{\theta}}\delta_e(\tau)d\tau \tag{5.15}$$

where $m = \dfrac{E_0\hat{t}_\infty}{\eta}$ and $\theta = \dfrac{\hat{\theta}}{\hat{t}_\infty}$ are dimensionless.

For a time mesh with nodes t_i, $\delta_v(t)$ will be evaluated by piecewise linearly interpolating $\delta_e(\tau)$ between t_0 and t_i. For $k = 1, 2, ..., i$, we have

$$\delta_e(\tau) \approx \frac{\delta_e(t_k) - \delta_e(t_{k-1})}{t_k - t_{k-1}}\tau + \frac{t_k\delta_e(t_{k-1}) - t_{k-1}\delta_e(t_k)}{t_k - t_{k-1}}.$$

Then, equation (5.15) can be approximated as

$$\delta_v(t_i) \approx \delta_e(t_i) + m\sum_{k=1}^{i}\int_{t_{k-1}}^{t_k} e^{-\frac{(t_i-\tau)}{\theta}}\delta_e(\tau)d\tau.$$

Substituting the interpolant into the integral, and integrating the result yields

$$\delta_v(t_i) = \delta_e(t_i) + m\sum_{k=1}^{i} H_k$$

where

$$H_k = e^{-\frac{t_i}{\theta}}\left(\left(e^{\frac{t_{k-1}}{\theta}} - e^{\frac{t_k}{\theta}}\right)\left(\frac{\delta_e(t_k) - \delta_e(t_{k-1})}{t_k - t_{k-1}}\right) + \delta_e(t_k)e^{\frac{t_k}{\theta}} - \delta_e(t_{k-1})e^{\frac{t_{k-1}}{\theta}}\right).$$

5.2.2 Reference Data for PMMA

We will use PMMA as a reference material in our calculations. The table below demonstrates the static creep rupture time under tensile stress for PMMA at a temperature of $22.5°C$. This experimental data was reported in [37].

Stress (MPa)	40	45	50	55	60.34
Time (hrs)	998	110.6	18.3	2.47	0.51

Table 5.1: Experimental results for PMMA.

Fitting these values into the power type relationship

$$\hat{t}_\infty(\hat{\sigma}) = \left(\frac{\hat{\sigma}}{\sigma_0}\right)^{-b},$$

we find that

$$b \approx 18.5 \quad \text{and} \quad \sigma_0 \approx 58.1\text{MPa hr}^{1/b}.$$

Taking the applied load as $\hat{q} = 50$ MPa, we have

$$t_\infty = \left(\frac{50}{58.1}\right)^{-18.5} = 16.08\,\text{hrs}.$$

With a relaxation time of $\hat{\theta} = 5.8 \cdot 10^4$ s, we arrive at the following normalised relaxation time

$$\theta = \frac{\hat{\theta}}{\hat{t}_\infty} \approx 1.$$

PMMA has a Poisson ratio of $\nu = 0.35$, modulus of elasticity of $E_0 = 3100$ MPa, and viscosity of the same order as $\eta = 3.5 \cdot 10^7$ MPa see e.g. [30, 35, 64]. From this information, we can deduce that the shear modulus is given by $\mu = 1148$ MPa, and this gives

$$m = \frac{E_0 \hat{t}_\infty}{\eta} \approx 5.$$

5.2.3 Numerical Solution

As in the case of an elastic material, we will use a mesh with step size $h = \frac{1}{800}$ to obtain the solutions. We will now present the graphs of the elastic crack tip opening and the viscoelastic crack tip opening on the same figure for comparison. We can see that as β becomes larger, the crack tip opening increases more rapidly with time.

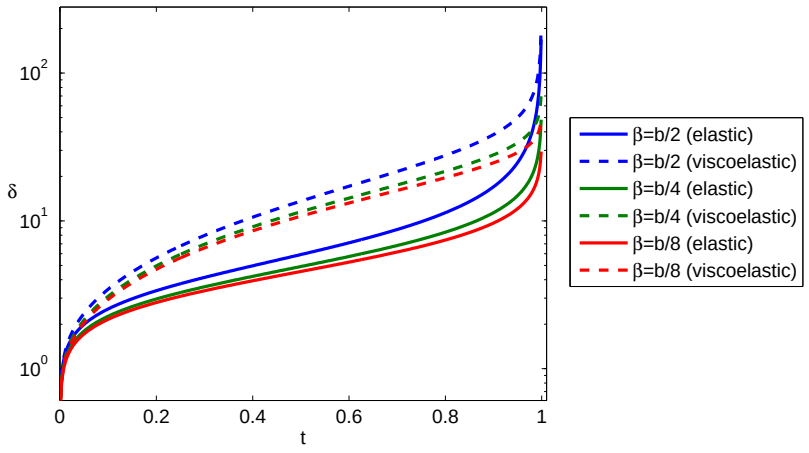

Figure 5.4: Crack opening vs. time for $b = 4$.

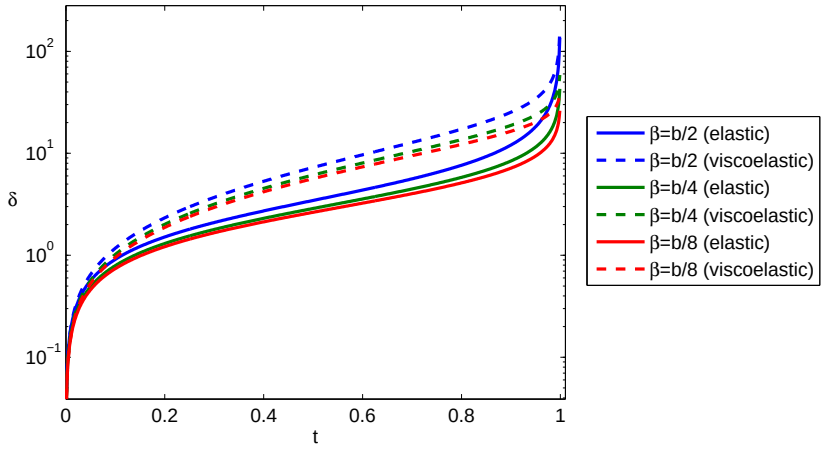

Figure 5.5: Crack opening vs. time for $b = 1.5$.

Chapter 6

Cohesive Zone Growth with a Propagating Crack

We have so far assumed that the crack is stationary and only the CZ is growing ahead of the crack. However, at some point in time, the crack will start to grow with the CZ still propagating ahead of the crack. The results of this model problem have been published in [24, 26].

6.1 Crack Growth Criterion

As mentioned in section 2.2, the crack will start to propagate when the crack tip opening $\hat{\delta}$ reaches a critical value $\hat{\delta}_c$. We will use the experimentally found value of $\hat{\delta}_c = 0.0016$ mm, for PMMA, see [17]. Using the normalisations given in equation (5.6), in the case of plane strain, the normalised critical crack tip opening is

$$\delta_c \approx 1.13$$

where we have used a constant external load with magnitude $\hat{q} = 50$MPa and an initial crack of length $\hat{a}_0 = 0.1$ mm. The time instant, when the crack tip opening reaches a critical value, will be referred to as the fracture delay time and denoted by $\hat{t}_d$, where t_d corresponds to the normalised delay time. Given below is a closer look at the graphs given in Figures 5.4-5.5 in the neighbourhood of the critical crack tip opening displacement.

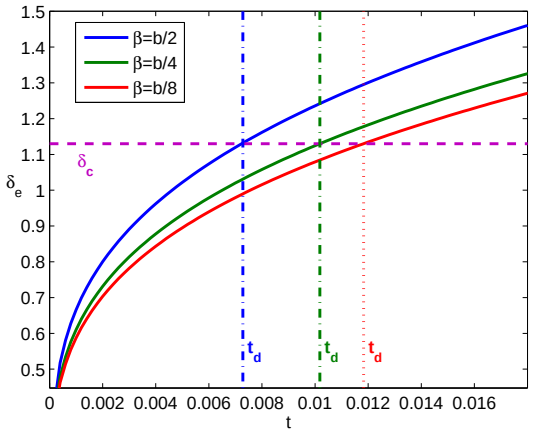

Figure 6.1: Crack tip opening for $b = 4$ (elastic).

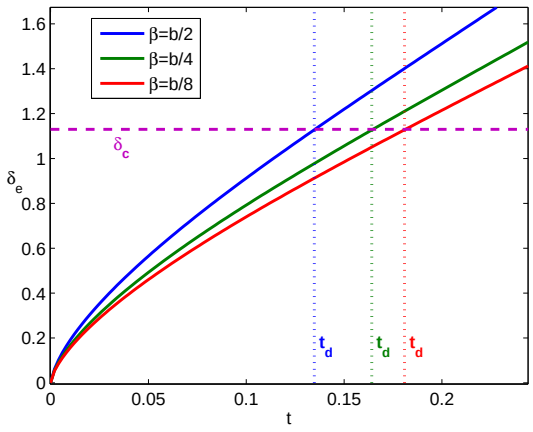

Figure 6.2: Crack tip opening for $b = 1.5$ (elastic).

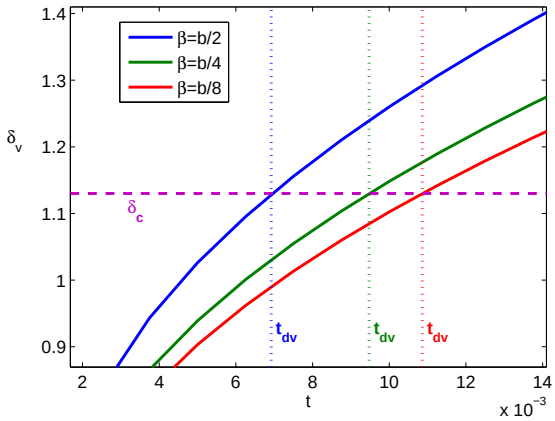

Figure 6.3: Crack tip opening for $b = 4$ (viscoelastic).

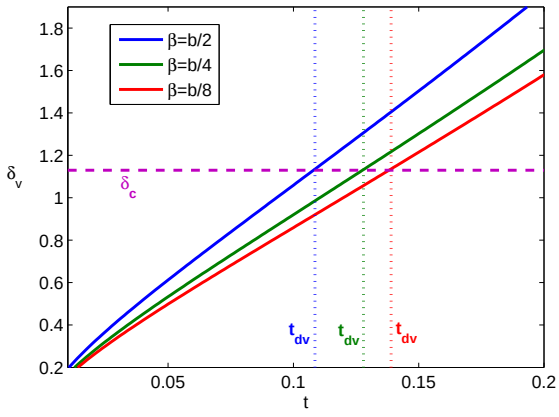

Figure 6.4: Crack tip opening for $b = 1.5$ (viscoelastic).

In both cases, $b = 4$ and $b = 1.5$, as β decreases, the delay time t_d increases.

As in the DLP model, we assume that the crack begins to grow when the crack tip opening $\delta(t)$ reaches the critical value δ_c. During the crack propagation stage, the crack tip opening satisfies equation

$$\delta_e(t) = \delta_c, \quad t \geq t_d \tag{6.1}$$

for the purely elastic case; and

$$\delta_v(t) = \delta_c, \quad t \geq t_d \tag{6.2}$$

for the viscoelastic case. In the crack propagation stage, the crack length $a(t)$ varies with time and is no longer a constant value. The next section will explain the algorithm used to study how the crack length and CZ length evolve with time.

6.2 Numerical Method

Taking for example the elastic case with $h = \dfrac{1}{500}$, $b = 4$ and $\beta = 2$, we have the following values for the crack tip opening

i	0	1	2	3	4
t_i	0	0.002	0.004	0.006	0.008
c_i	1	1.05545	1.0848	1.1073	1.1264
δ_e	0	0.7377	0.9423	1.0625	1.1543

Table 6.1: Solutions using a uniform time mesh.

It is evident that the crack begins to grow before the 4th time step $t_4 = 0.008$. In order to have more time steps before the delay time, we need to refine the mesh. The crack length a is equal to 1 for all steps $t \leq t_d$, and after this point in time, the crack begins to grow.

The first aim in the crack propagation stage is to find the delay time, t_d. This is obtained by solving equations (6.1) or (6.2) using the secant method, while $a(t_d) = 1$; the

corresponding value of $c(t_d)$ is obtained by setting the stress intensity factor to zero and applying secant iterations as explained in Section 4.1.1.

To calculate the crack length and the CZ length at $t > t_d$, we use a uniform time mesh with time steps $t_i = t_d + i \cdot h$, where h is the same step size used during the stationary crack stage. We then implement an iterative method to solve equation (6.1) (in the elastic case) or (6.2) (in the visco-elastic case) for $a(t_i)$. To this end, we need $c(t_i)$ at each iteration, and this is obtained by setting the stress intensity factor to zero. Thus the equations which form the system to be solved are

(a) The condition $\underline{\Lambda}(\sigma(x), t) = 1$

$$\int_{t_c(x)}^{t} \sigma^{\beta}(x,\tau)(t-\tau)^{\frac{\beta}{b}-1} d\tau = \frac{b}{\beta} - \int_{0}^{t_c(x)} \sigma^{\beta}(x,\tau)(t-\tau)^{\frac{\beta}{b}-1} d\tau, \tag{6.3}$$

for $a(t) \leq |x| \leq c(t)$, $t > t_c(x)$;

(b) the stress ahead of the crack tip:

$$\sigma(x,t) = \frac{x}{\sqrt{x^2 - c^2(t)}} \left(1 - \frac{2}{\pi} \int_{a(t)}^{c(t)} \frac{\sqrt{c^2(t) - \xi^2}}{x^2 - \xi^2} \sigma(\xi, t) d\xi \right) \text{ for } |x| > c(t); \tag{6.4}$$

(c) the zero stress intensity factor

$$K(t, a(t), c(t)) = \sqrt{\frac{c(t)}{2}} - \frac{\sqrt{2c(t)}}{\pi} \int_{a(t)}^{c(t)} \frac{\sigma(\xi, t)}{\sqrt{c^2(t) - \xi^2}} d\xi = 0; \tag{6.5}$$

(d) setting the crack tip opening to the critical value

$$U(t, a(t), c(t)) = \delta_e(t) - \delta_c = 0 \qquad \text{for the elastic case}$$
$$U(t, a(t), c(t)) = \delta_v(t) - \delta_c = 0 \qquad \text{for the viscoelastic case.}$$

We will now go through the details of the method used for finding the length of the crack with respect to time, and the corresponding CZ length at that time.

6.2.1 Algorithm

Step 1 Take 2 points, of the CZ tip in the previous time instants, as initial approximations for a_i: $(a_i)_1 = c_m$ and $(a_i)_2 = c_{m+1}$. The index m is chosen such that the product of $U(t_i, (a_i)_1, c_i)$ and $U(t_i, (a_i)_2, c_i)$ is negative. At the start of crack growth, we begin with $(a_i)_1 = c_0$ and $(a_i)_2 = c_1$.

Step 2 For each of the 2 approximations of a_i, find the corresponding c_i using the secant method:

- Take 2 initial approximations as $(c_i)_1 = c_{i-1}$ and $(c_i)_2$ as the linear extrapolation of c over the previous time instants:

$$(c_i)_2 = c_{i-2}\frac{t_i - t_{i-1}}{t_{i-2} - t_{i-1}} + c_{i-1}\frac{t_i - t_{i-2}}{t_{i-1} - t_{i-2}}.$$

- Find $K(t_i, a_i, (c_i)_1)$ and $K(t_i, a_i, (c_i)_2)$ using equation (6.5). To find them, we simultaneously make use of equations (6.3) and (6.4) to find the stress $\sigma(\xi, t_i)$.
- Find $(c_i)_3$ as usual in the secant method, i.e.,

$$(c_i)_3 = \frac{K(t_i, a_i, (c_i)_2)(c_i)_1 - K(t_i, a_i, (c_i)_1)(c_i)_2}{(c_i)_2 - (c_i)_1}.$$

- Take $(c_i)_3$ and $(c_i)_2$ (or $(c_i)_1$) as the next 2 approximations and repeat the above 3 sub-items until convergence is reached and c_i is obtained.

Step 3 Once c_i has been found for each of the 2 approximations for a_i, find the corresponding $U(t_i, (a_i)_1, c_i)$ and $U(t_i, (a_i)_2, c_i)$.

Step 4 If $U(t_i, (a_i)_1, c_i) \cdot U(t_i, (a_i)_2, c_i) < 0$ then take

$$(a_i)_3 = \frac{U(t_i, (a_i)_2, c_i)(a_i)_1 - U(t_i, (a_i)_1, c_i)(a_i)_2}{U(t_i, (a_i)_2, c_i) - U(t_i, (a_i)_1, c_i)}$$

implying $(a_i)_1 < (a_i)_3 < (a_i)_2$. However, if $U(t_i, (a_i)_1, c_i) \cdot U(t_i, (a_i)_2, c_i) > 0$ then go back to Step 1 and take $(a_i)_1 = c_{m+1}$ and $(a_i)_2 = c_{m+2}$, and repeat the above procedure until $U(t_i, (a_i)_1, c_i) \cdot U(t_i, (a_i)_2, c_i) < 0$.

Step 5 If $|(a_i)_3 - (a_i)_1| < \varepsilon$ or $|(a_i)_3 - (a_i)_2| < \varepsilon$, allocate $a(t_i) = (a_i)_3$ and go to the next time instant $t = t_{i+1}$. Otherwise, go to the next step.

Step 6 Take $(a_i)_3$ and $(a_i)_2$ (or $(a_i)_1$) as the next 2 approximations and repeat Steps 2-5 until convergence is reached and a_i is obtained.

6.2.2 Remarks on the Algorithm

When we have known (previous) c_m, $m < i$, points for the initial approximations for a_i, the stress values $\sigma(\xi, t_i)$ for all the node points in the integration range of ξ are known except at $\sigma(c_i, t_i)$. The stress at c_i can be found by solving the integral equation

$$\int_{t_0}^{t_i} \sigma^{\beta}(c_i, \tau)(t_i - \tau)^{\frac{\beta}{b}-1} d\tau = \frac{b}{\beta}$$

by piecewise linearly interpolating $\sigma(c_i, \tau)$ in τ between t_0 and t_i, similarly to equation (4.6). As done in the previous algorithm, $\sigma(c_i, t_j)$ for $j = 0, 1, 2, ...i-1$ will be found using

$$\sigma(c_i, t_j) = \frac{c_i}{\sqrt{c_i^2 - c_j^2}} \left(1 - \frac{2}{\pi} \int_{a_j}^{c_j} \frac{\sqrt{c_j^2 - \xi^2}}{c_i^2 - \xi^2} \sigma(\xi, t_j) d\xi \right). \tag{6.6}$$

Moreover, in order to find $K(t_i, (a_i)_3, c_i)$ and $U(t_i, (a_i)_3, c_i)$, we will have an integral from $(a_i)_3$ to c_i; thus we need to find $\sigma((a_i)_3, t_i)$. To this end, we use:

$$\int_{t_0}^{t_i} \sigma^{\beta}((a_i)_3, \tau)(t_i - \tau)^{\frac{\beta}{b}-1} d\tau = \frac{b}{\beta}, \tag{6.7}$$

where we will approximate $\sigma^{\beta}((a_i)_3, \tau)$ using piecewise linear interpolation between $\tau = t_{k-1}$ and $\tau = t_k$ for $k = 0, 1, ...i-1$. For each $\sigma^{\beta}((a_i)_3, t_k)$, we will use equation (6.7) with t_i replaced by t_k; however, for cases when $a_i > c(t_k)$, we will use equation (6.6).

Furthermore, note that at some point, we will come across the step where a_i will exceed c_{i-1}; and as observed, the CZ length is decreasing, which means we will have $a_i > c_{i-1}$ in all the steps which follow. Thus, for these steps, only one previous value of c (which

is c_{i-1}) can be taken as an initial approximation of a_i. To this end, we will modify the algorithm by fixing a_i and computing the corresponding t_i and c_i by solving $U(t_i, a_i, c_i) = 0$ and $K(t_i, a_i, c_i) = 0$ respectively.

Referring to Step 3, we obtain $U(t_i, a_i, c_i)$ using

$$U_e(t_i, a_i, c_i) = \delta_e(t_i) - \delta_c$$

for the elastic case, and

$$U_v(t_i, a_i, c_i) = \delta_e(t_i, a_i, c_i) + m \int_{t_c(a_i)}^{t_i} e^{-\frac{1}{\theta}(t_i - \tau)} \delta_e(\tau, a_i, c_i) d\tau - \delta_c \tag{6.8}$$

for the viscoelastic case; where the lower limit of the integral is replaced with $t_c(a(t))$ (instead of t_0) since $[u_e](x, \tau) = 0$ when $\tau \leq t_c(x)$. To evaluate the integral in (6.8), $\delta_e(\tau, a_i, c_i)$ is piecewise linearly interpolated between $t_c(a_i)$ and t_i. All the values of $\delta_e(t_k, a_i, c_i)$ are obtained from the following equation

$$\delta_e(t_k, a_i, c_i) = \frac{4}{\pi} \left(\pi \sqrt{c_i^2 - a_i^2} + \int_{a_i}^{c_i} \sigma(\xi, t_k) \hat{\Gamma}(c(t_k), \xi; c_i) d\xi \right).$$

For the viscoelastic case, note that when the approximations for a_i are previous values of c, i.e. $(a_i)_1 = c_m$ and $(a_i)_2 = c_{m+1}$, then the integration over τ in (6.8) will be from t_m to t_i and t_{m+1} to t_i respectively. For example, in the case when $a_i = c_m$, for $k = m, ...i$ we have

$$\delta(\tau, a_i, c_i) \approx \delta_e(t_k, a_i, c_i) + \frac{\delta_e(t_{k+1}, a_i, c_i) - \delta_e(t_k, a_i, c_i)}{t_{k+1} - t_k} (\tau - t_k). \tag{6.9}$$

On the other hand, when a_i is not equal to a known value of c, the integration over τ will be from t_m to t_i where $c_m < a_i < c_{m+1}$, but $\delta_e(t_m, a_i, c_i)$ will be 0. Thus, the integral would be written as

$$\sum_{k=m}^{i-1} \int_{t_k}^{t_{k+1}} e^{-\frac{1}{\theta}(t_i - \tau)} \delta_e(\tau, a_i, c_i) d\tau$$

where

$$\delta_e(\tau, a_i, c_i) \approx \frac{\delta_e(t_{m+1}, a_i, c_i)}{t_{m+1} - t_m} (\tau - t_m)$$

for $k = m$ and $\delta(\tau, a_i, c_i)$ is given by equation (6.9) for $k = m + 1, ..., i$.

6.3 Numerical Solution

Using $h = \frac{1}{8000}$ and $h = \frac{1}{800}$ as the step sizes for $b = 4$ and $b = 1.5$ respectively, we arrive at the following graphs.

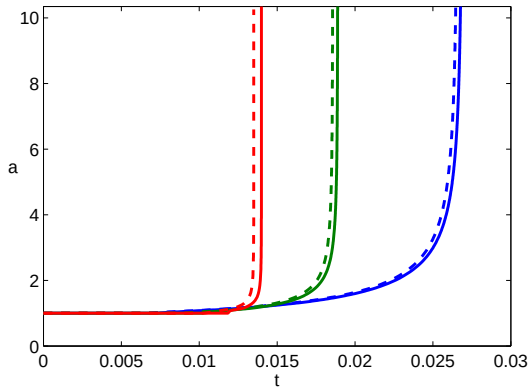

Figure 6.5: Crack length vs. time for $b = 4$.

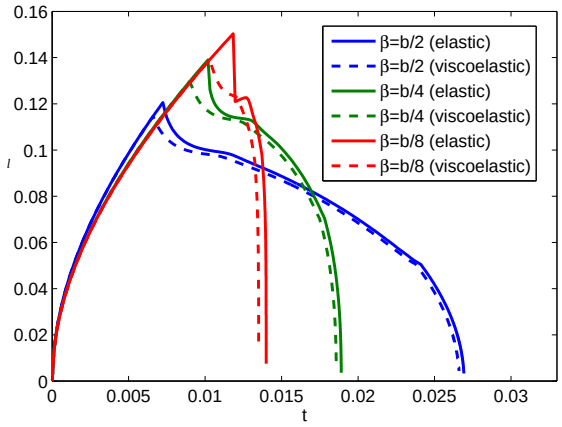

Figure 6.6: CZ length vs. time for $b = 4$.

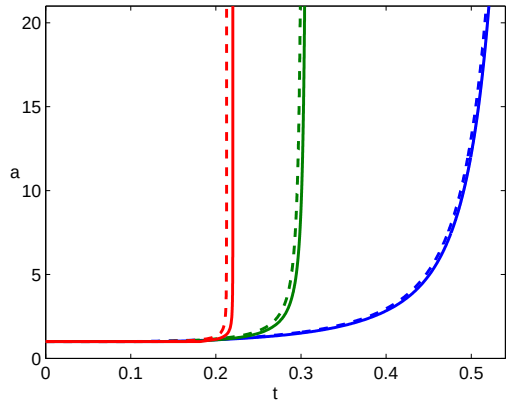

Figure 6.7: Crack length vs. time for $b = 1.5$.

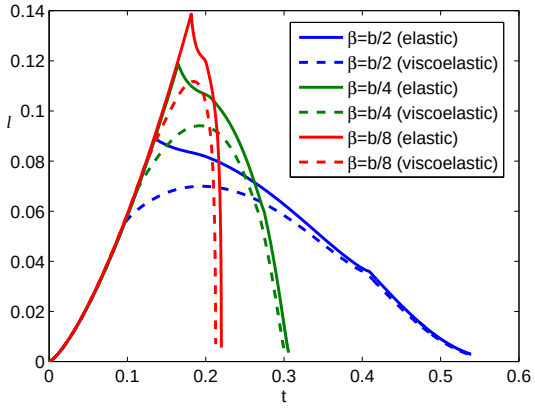

Figure 6.8: CZ length vs. time for $b = 1.5$.

Now we will present the graphs of the CZ tip coordinate vs. time.

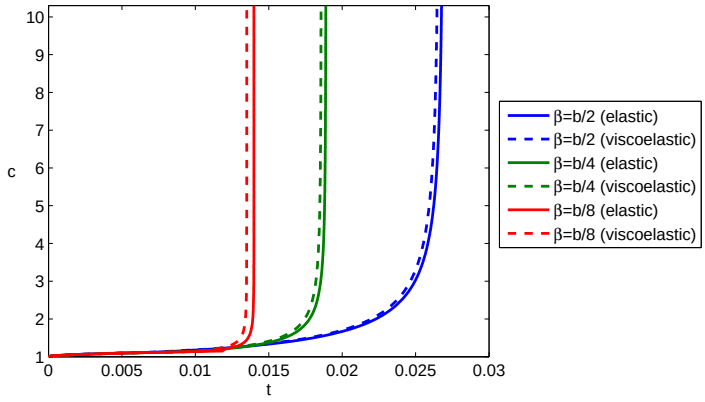

Figure 6.9: CZ tip coordinate vs. time for $b = 4$.

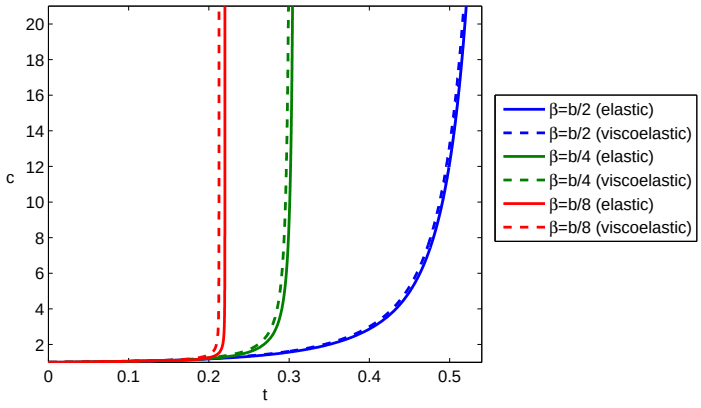

Figure 6.10: CZ tip coordinate vs. time for $b = 1.5$.

The Delay Time and the Rupture Time

The rate of crack growth, the delay time t_d, as well as the normalised rupture time t_r, depend on the material parameters. Figure 6.11 shows the delay time dependence on β for $b = 4$; and Figure 6.12 shows the delay time dependence on b for $\beta = \frac{1}{2}$. Figure 6.13 shows the rupture time dependence on β for $b = 4$; and Figure 6.14 shows the rupture time dependence on b for $\beta = \frac{1}{2}$. The calculations were done for $\beta = \frac{3b}{4}$, $\beta = \frac{b}{2}$, $\beta = \frac{b}{3}$, $\beta = \frac{b}{4}$, and $\beta = \frac{b}{8}$. The graphs show a strong dependence of the normalised rupture time in the

infinite plane on the presence of the crack and on the material parameter. This is in contrast to the crack propagation results obtained, using the local approach, without the CZ, where the rupture time in the plane with and without crack was the same [25, 41, 42]. We will use e and v in the subscripts to refer to the elastic and viscoelastic cases respectively.

Delay Time: Fixed $b = 4$, Varying β

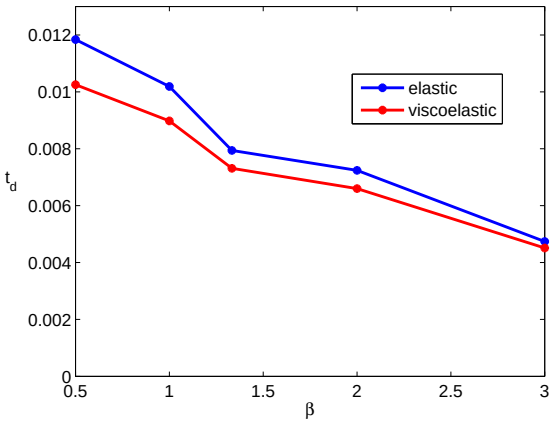

Figure 6.11: Delay time t_d vs. β for $b = 4$.

β	$t_{d,e}$	$t_{d,v}$
$3b/4 = 3$	0.00474	0.00451
$b/2 = 2$	0.00724	0.00660
$b/3 = 4/3$	0.00794	0.00731
$b/4 = 1$	0.01019	0.00898
$b/8 = 1/2$	0.01184	0.01025

Table 6.2: Delay time t_d for $b = 4$.

Delay Time: Fixed $\beta = \frac{1}{2}$, Varying b

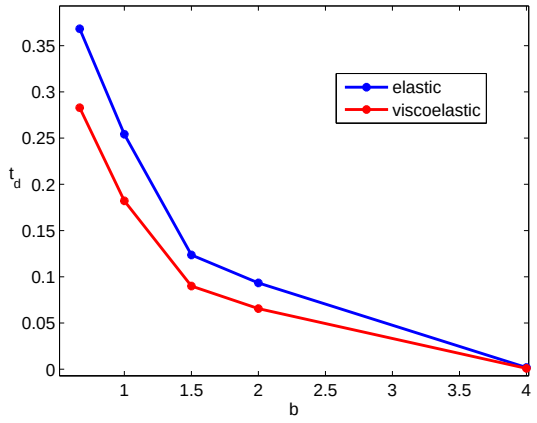

Figure 6.12: Delay time t_d vs. b for $\beta = \frac{1}{2}$.

b	$t_{d,e}$	$t_{d,v}$
$8\beta = 4$	0.01184	0.01025
$4\beta = 2$	0.09344	0.06566
$3\beta = 3/2$	0.12360	0.08994
$2\beta = 1$	0.25420	0.18210
$4\beta/3 = 2/3$	0.36820	0.28290

Table 6.3: Delay time t_d for $\beta = \frac{1}{2}$.

Rupture Time: Fixed $b = 4$, Varying β

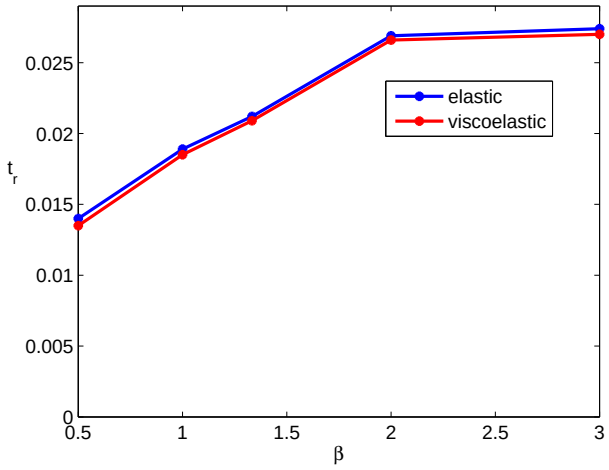

Figure 6.13: Rupture time t_r vs. β for $b = 4$.

β	$t_{r,e}$	$t_{r,v}$
$3b/4 = 3$	0.02740	0.02709
$b/2 = 2$	0.02698	0.02662
$b/3 = 4/3$	0.02120	0.02092
$b/4 = 1$	0.01896	0.01858
$b/8 = 1/2$	0.01408	0.01357

Table 6.4: Rupture time t_r vs. β for $b = 4$.

Rupture Time: Fixed $\beta = \frac{1}{2}$, Varying b

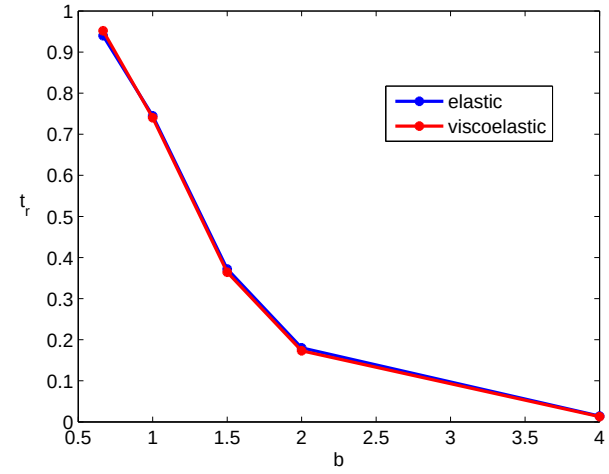

Figure 6.14: Rupture time t_r vs. β for $\beta = \frac{1}{2}$.

b	$t_{r,e}$	$t_{r,v}$
$8\beta = 4$	0.01408	0.01357
$4\beta = 2$	0.18021	0.17322
$3\beta = 3/2$	0.37205	0.36431
$2\beta = 1$	0.74498	0.74030
$4\beta/3 = 2/3$	0.93971	0.95192

Table 6.5: Rupture time t_r vs. β for $\beta = \frac{1}{2}$.

The dependency of the CZ length at $t = t_d$, and the maximum CZ length, for different parameter sets is given below.

Fixed $b = 4$, Varying β

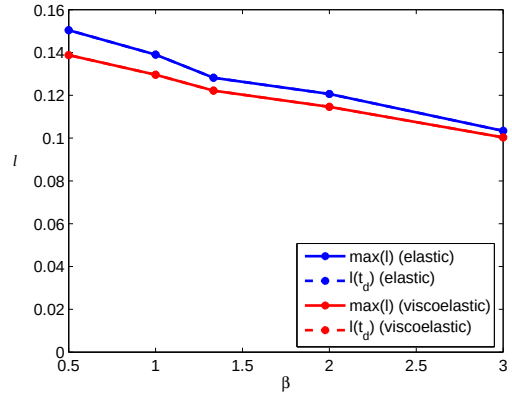

Figure 6.15: Maximum CZ length and $l(t_d)$ vs. β for $b = 4$.

β	$\max(l_e)$	$l(t_d)_e$	$\max(l_v)$	$l(t_d)_v$
$3b/4 = 3$	0.1034	0.1034	0.1003	0.1003
$b/2 = 2$	0.1206	0.1206	0.1146	0.1146
$b/3 = 4/3$	0.1282	0.1282	0.1222	0.1222
$b/4 = 1$	0.1390	0.1390	0.1296	0.1296
$b/8 = 1/2$	0.1504	0.1504	0.1388	0.1388

Table 6.6: Maximum CZ length and $l(t_d)$ vs. β for $b = 4$.

Fixed $\beta = \frac{1}{2}$, Varying b

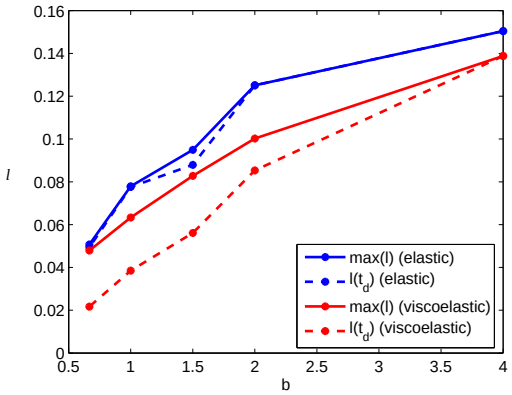

Figure 6.16: Maximum CZ length and $l(t_d)$ vs. b for $\beta = \frac{1}{2}$.

b	$\max(l_e)$	$l(t_d)_e$	$\max(l_v)$	$l(t_d)_v$
$8\beta = 4$	0.1504	0.1504	0.1388	0.1388
$4\beta = 2$	0.1251	0.1251	0.1002	0.0853
$3\beta = 3/2$	0.0949	0.0879	0.0828	0.0561
$2\beta = 1$	0.0779	0.0776	0.0633	0.0385
$4\beta/3 = 2/3$	0.0507	0.0494	0.04787	0.0217

Table 6.7: Maximum CZ length and $l(t_d)$ vs. b for $\beta = \frac{1}{2}$.

An observation which cannot be missed is how the crack length, and thus the CZ length, evolves with time as β decreases. We observed that in the stationary crack stage, changing β doesn't have a substantial effect on the CZ tip coordinate. However, in the growing crack stage, Figures 6.5-6.8 show that there is a significant effect of the parameter β on the solutions. A vanishing CZ is an indication of the crack propagating. We can see from these figures that, while fixing b, as β decreases the crack grows more rapidly with time; and so it can also be concluded that as β decreases, the rupture time also decreases.

As seen in Figures 6.1-6.4, as well as Tables 6.2-6.3, the delay time t_d is higher for the elastic case than for the viscoelastic one. For example, for $b = 4$ and $\beta = 1$, we obtained $t_d = 0.01019$ for the elastic case and $t_d = 0.00898$ for the viscoelastic case. Furthermore, the rupture time in the viscoelastic case is slightly smaller than that for the purely elastic case. For example, for $b = 4$ and $\beta = 1$, the normalised rupture time is $t_r = 0.0189$ for the elastic case and $t_r = 0.0185$ for the viscoelastic one. The results given in Tables 6.6 and 6.7 indicate that as the difference between b and β increases, the maximum CZ length reached increases. This effect can also be observed from the graphs in Figures 6.6 and 6.8.

Chapter 7

Time-Dependent External Load

In this chapter, we consider the case when the external load varies linearly in time.

7.1 Problem Formulation

Let a time-dependent load be linear in time

$$\hat{q}(\hat{t}) = s\,\hat{t}, \tag{7.1}$$

where s is a constant. Similarly to the case of a constant load, see Section 3.1, we denote by $\hat{t}_{s\,\infty}$ the rupture time of the infinite plane without a crack. It is obtained by solving for $\hat{t} = \hat{t}_{s\,\infty}$ the following equation

$$\int_{\hat{t}_0}^{\hat{t}} (s\hat{\tau})^{\beta} (\hat{t} - \hat{\tau})^{\frac{\beta}{b}-1} d\hat{\tau} = \frac{b\sigma_0^{\beta}}{\beta};$$

this yields

$$\hat{t}_{s\,\infty} = \left(\frac{\sigma_0}{s\gamma}\right)^{\frac{b}{1+b}}, \tag{7.2}$$

where

$$\gamma := \left(\frac{b}{\beta} \frac{\Gamma\left[1+\beta+\frac{\beta}{b}\right]}{\Gamma\left[\frac{\beta}{b}\right]\Gamma[1+\beta]} \right)^{-1/\beta}.$$

Then, the maximum load reached before rupture in the infinite plane without a crack under such load is

$$\hat{q}_{s\,\infty} = s\hat{t}_{s\,\infty}. \tag{7.3}$$

Given below is a graph which shows how γ varies with the constants b and β.

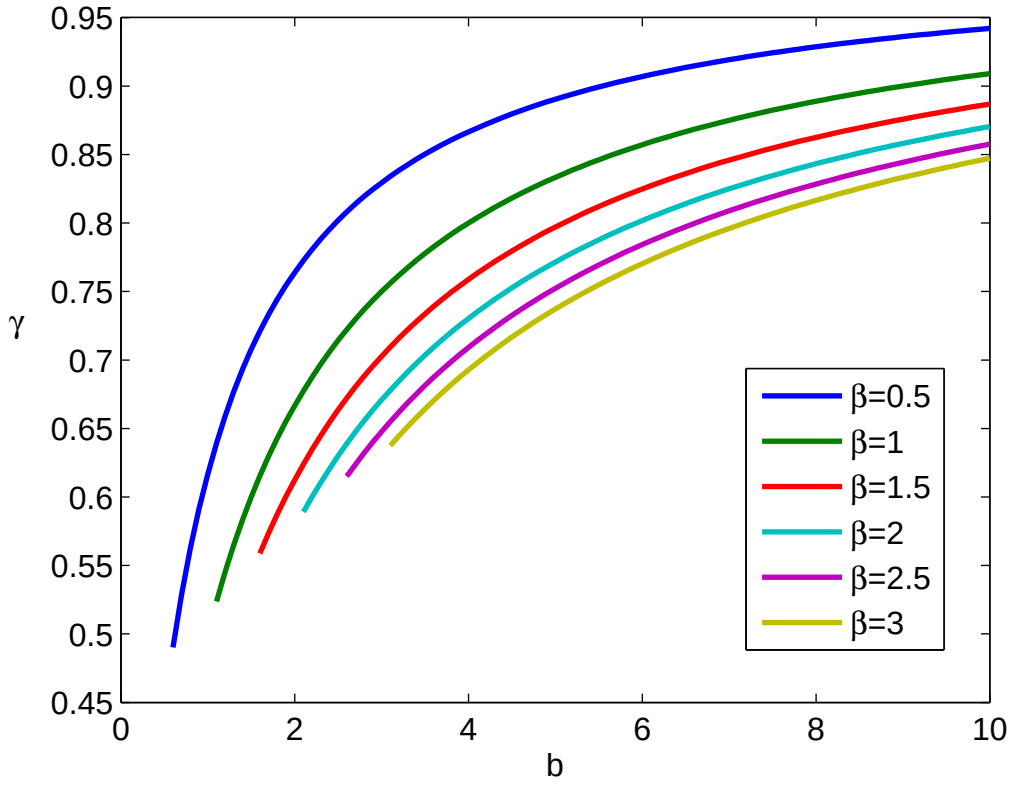

Figure 7.1: γ vs. b for various β.

Let us also introduce the reference constant load $\hat{q}_*$ as

$$\hat{q}_* = \sigma_0 \hat{t}_{s\,\infty}^{-1/b} \tag{7.4}$$

under which such plane ruptures at the same time $\hat{t}_{s\,\infty}$. Expressing s and $\hat{t}_{s\,\infty}$ in terms of

$\hat{q}_{s\infty}$ and $\hat{q}_*$ from equations (7.3)-(7.4) then substituting them into equation (7.2), yields

$$\hat{q}_* = \gamma \hat{q}_{s\infty}.$$

For constant external loading, we used the normalisation $\hat{\sigma}(\hat{x},\hat{t}) = \tilde{\sigma}(\hat{x},\hat{t})\hat{q}$, whereas for variable external loading, we will use $\hat{\sigma}(\hat{x},\hat{t}) = \tilde{\sigma}(\hat{x},\hat{t})\hat{q}_*$. This gives the following form of the condition $\underline{\Lambda}(\hat{\sigma}(\hat{x},\hat{t});\hat{t}) = 1$ on the CZ,

$$\int_{\hat{t}_0}^{\hat{t}} \tilde{\sigma}^{\beta}(\hat{x},\hat{\tau})(\hat{t}-\hat{\tau})^{\frac{\beta}{b}-1} d\hat{\tau} = \frac{b}{\beta}\left(\hat{t}_{s\infty}\right)^{\frac{\beta}{b}} \quad \hat{a} \le |\hat{x}| \le \hat{c}. \tag{7.5}$$

Now, we will normalise time and space using

$$\hat{t} = t\hat{t}_{s\infty}, \quad \hat{x} = x\hat{a}_0, \quad \hat{c}(\hat{t}) = \hat{c}(t\hat{t}_{s\infty}) = c(t)\hat{a}_0. \tag{7.6}$$

Also, we will use the notation $\sigma(x,t) = \tilde{\sigma}(x\hat{a}_0, \hat{t}_{s\infty}t)$; this gives the following relation between the physical stress $\hat{\sigma}(\hat{x},\hat{t})$ and the normalised stress $\sigma(x,t)$

$$\sigma(x,t) = \frac{\hat{\sigma}(x\hat{a}_0, \hat{t}_{s\infty}t)}{\hat{q}_*}. \tag{7.7}$$

Consequently, (7.5) reduces to the following equation

$$\int_{t_0}^{t} \sigma^{\beta}(x,\tau)(t-\tau)^{\frac{\beta}{b}-1} d\tau = \frac{b}{\beta}, \qquad a(t) \le x \le c(t).$$

The stress ahead of the crack tip, as in the constant load case, is given by

$$\hat{\sigma}(\hat{x},\hat{t}) = \frac{\hat{x}}{\sqrt{\hat{x}^2 - \hat{c}^2(\hat{t})}}\left(\hat{q}(\hat{t}) - \frac{2}{\pi}\int_{\hat{a}(\hat{t})}^{\hat{c}(\hat{t})} \frac{\sqrt{\hat{c}^2(\hat{t}) - \hat{\xi}^2}}{\hat{x}^2 - \hat{\xi}^2}\hat{\sigma}(\hat{\xi},\hat{t})d\hat{\xi}\right), \qquad |\hat{x}| > \hat{c}.$$

After normalising, we have

$$\sigma(x,t) = \frac{x}{\sqrt{x^2 - c^2(t)}}\left(q(t) - \frac{2}{\pi}\int_{a(t)}^{c(t)} \frac{\sqrt{c^2(t) - \xi^2}}{x^2 - \xi^2}\sigma(\xi,t)d\xi\right), \qquad |x| > c,$$

where

$$q(t) = \frac{\hat{q}(\hat{t})}{\hat{q}_*} = \frac{s\hat{t}}{\gamma s\hat{t}_{s\infty}} = \frac{\hat{t}}{\gamma \hat{t}_{s\infty}} = \frac{t}{\gamma}.$$

Furthermore, the stress intensity factor is given by

$$\hat{K}(\hat{t},\hat{a}(\hat{t}),\hat{c}(\hat{t}))=\sqrt{\frac{\hat{c}(\hat{t})}{2}}\left(\hat{q}(\hat{t})-\frac{2}{\pi}\int_{\hat{a}(\hat{t})}^{\hat{c}(\hat{t})}\frac{\hat{\sigma}(\hat{\xi},\hat{t})}{\sqrt{\hat{c}^2(\hat{t})-\xi^2}}d\hat{\xi}\right).$$

Using the same normalisations as in (7.6) and (7.7), we have

$$\hat{K}(t,a(t),c(t))=\sqrt{\frac{c(t)\hat{a}_0}{2}}\left(\hat{q}(\hat{t})-\frac{2\hat{q}_*}{\pi}\int_{a(t)}^{c(t)}\frac{\sigma(\xi,t)}{\sqrt{c^2(t)-\xi^2}}d\xi\right).$$

Finally, we normalise the stress intensity factor using

$$K(t,a(t),c(t))=\frac{\hat{K}(\hat{t})}{\sqrt{\hat{a}_0}\,\hat{q}_*},$$

which then yields

$$K(t,a(t),c(t))=\sqrt{\frac{c(t)}{2}}\left(q(t)-\frac{2}{\pi}\int_{a(t)}^{c(t)}\frac{\sigma(\xi,t)}{\sqrt{c^2(t)-\xi^2}}d\xi\right).$$

For the crack tip opening, we have the following equation in terms of the physical variables

$$\hat{\delta}_e(\hat{x},\hat{t})=\frac{(1+\kappa)}{2\mu}\left(\hat{q}(\hat{t})\sqrt{\hat{c}^2(\hat{t})-\hat{x}^2}+\frac{1}{\pi}\int_{\hat{a}(\hat{t})}^{\hat{c}(\hat{t})}\hat{\sigma}(\hat{\xi},\hat{t})\hat{\Gamma}(\hat{x},\hat{\xi},\hat{c}(\hat{t}))d\hat{\xi}\right),$$

$$\hat{\delta}_v\left(\hat{t}\right)=\left(\hat{\delta}_e\left(\hat{t}\right)+\frac{\mu}{\eta}\int_0^{\hat{t}}e^{-\frac{1}{\theta}\left(\hat{t}-\hat{\tau}\right)}\hat{\delta}_e\left(\hat{\tau}\right)d\hat{\tau}\right).$$

for the elastic and viscoelastic cases respectively. We use the same normalisations as in (7.6) and (7.7) for time, length, and stress. In addition to that, we will normalise $\hat{\delta}$ using

$$\delta=\frac{8\mu\hat{\delta}}{\hat{q}_*\hat{a}_0(1+\kappa)}.$$

Consequently, we have

$$\delta_e(x,t)=\frac{4}{\pi}\left(q(t)\pi\sqrt{c^2(t)-x^2}+\int_{a(t)}^{c(t)}\sigma(\xi,t)\hat{\Gamma}(x,\xi,c(t))d\xi\right)$$

and

$$\delta_v(t)=\left(\delta_e(t)+m_s\int_0^t e^{-\frac{1}{\theta_s}(t-\tau)}\delta_e(\tau)d\tau\right)$$

where

$$m_s=\frac{E_0\hat{t}_{s\,\infty}}{\eta},\qquad \theta_s=\frac{\hat{\theta}}{\hat{t}_{s\,\infty}};$$

and as before, $q(t)=\dfrac{t}{\gamma}$.

7.2 Numerical Solutions

After implementing the algorithm in Section 4.1.1 for the problem of a stationary crack, and in Section 6.2.1 for the problem of a propagating crack, we obtained the evolution of (i) the CZ tip while the crack is stationary; (ii) the crack tip opening for the elastic and viscoelastic cases; (iii) the crack length, the CZ tip coordinate, and the CZ length, for a propagating crack. To obtain the crack tip opening for the viscoelastic case, we assume that the constant s which appears in (7.1) takes the value such that $\hat{t}_\infty = \hat{t}_{s\,\infty}$. Thus, we will have $m_s = 5$ and $\theta_s = 1$ as in the case of a constant external load, see Section 5.2.2. We have used a graded time mesh before crack growth begins in order to have less time steps before crack growth begins; in other words, we need a denser mesh. Instead of taking $t_i = ih$, we took $t_i = \sqrt{\tilde{h}i}$ where $\tilde{h}$ is a constant. The results presented below are for the case $\tilde{h} = \dfrac{1}{400}$. See Appendix B for the graphs collected using various mesh sizes.

7.2.1 Stationary Crack

CZ Tip Coordinate

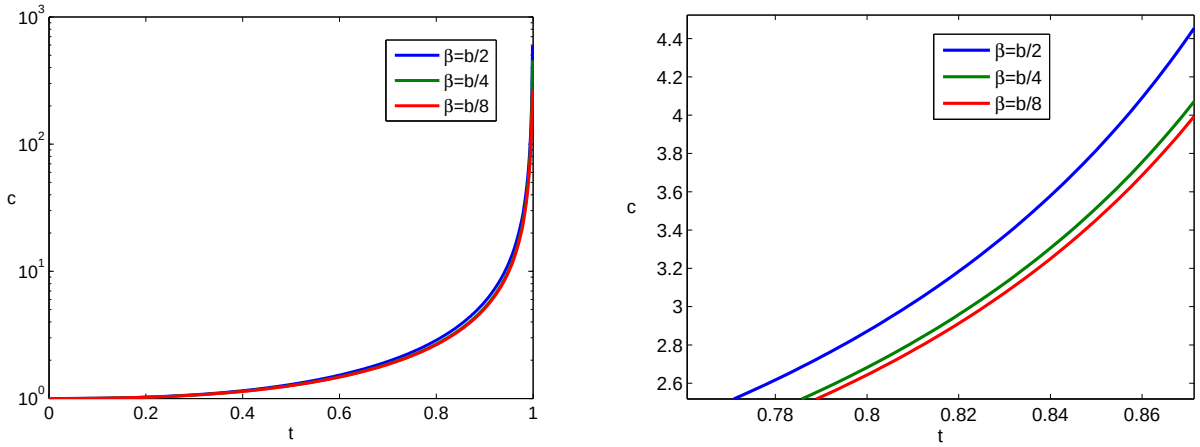

Figure 7.2: CZ tip coordinate vs. time for $b = 4$.

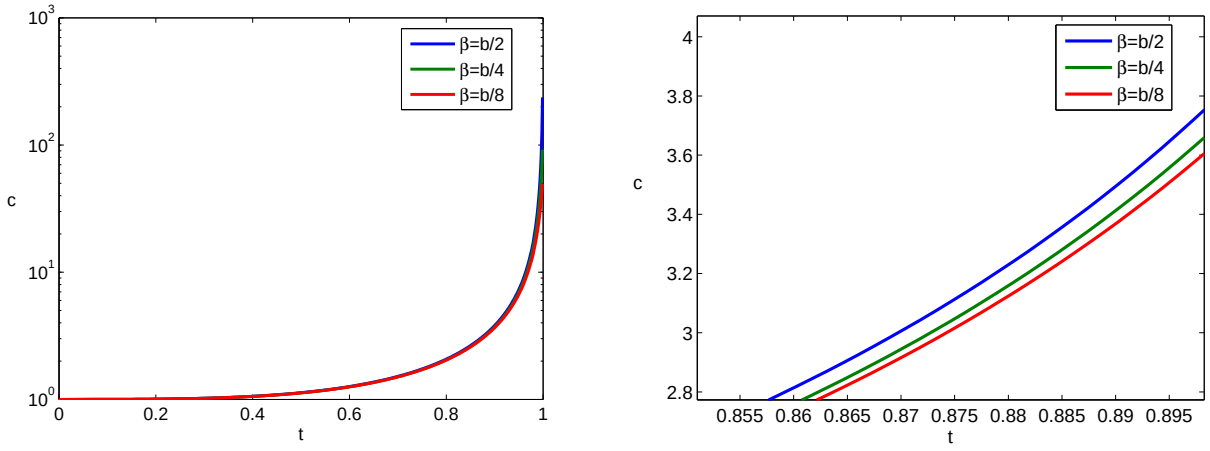

Figure 7.3: CZ tip coordinate vs. time for $b = 1.5$.

Stress

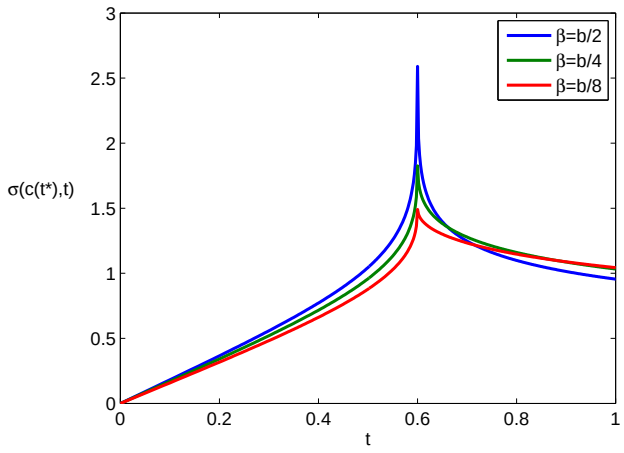

Figure 7.4: $\sigma(c(t^*), t)$ for $b = 4$ at $t^* = 0.6$.

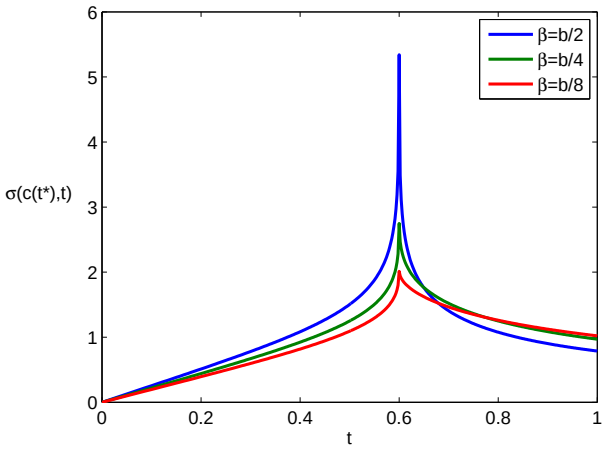

Figure 7.5: $\sigma(c(t^*), t)$ for $b = 1.5$ at $t^* = 0.6$.

Crack Tip Opening

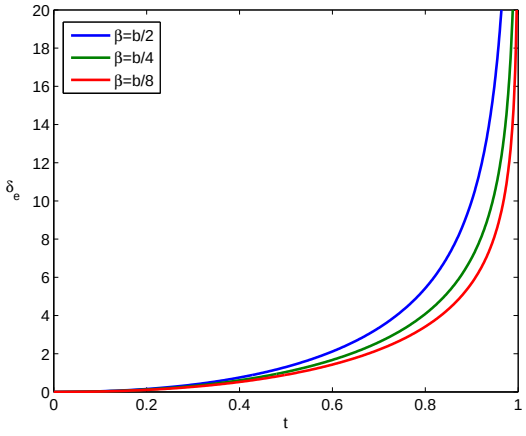

Figure 7.6: Crack opening δ_e vs. time t for $b = 4$.

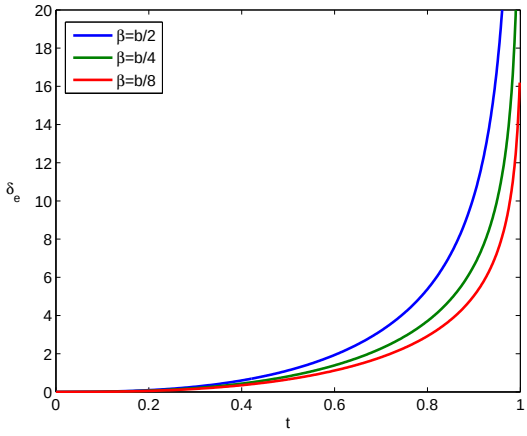

Figure 7.7: Crack opening δ_e vs. time t for $b = 1.5$.

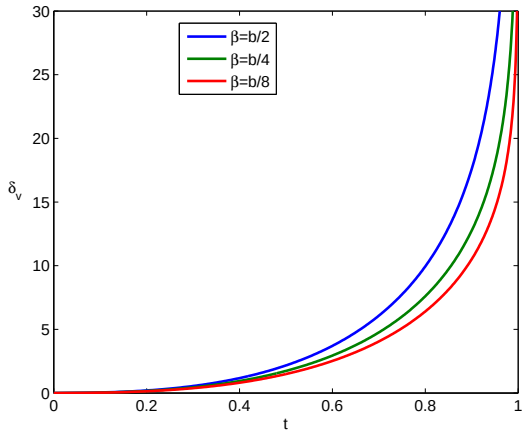

Figure 7.8: Crack opening δ_v vs. time t for $b = 4$.

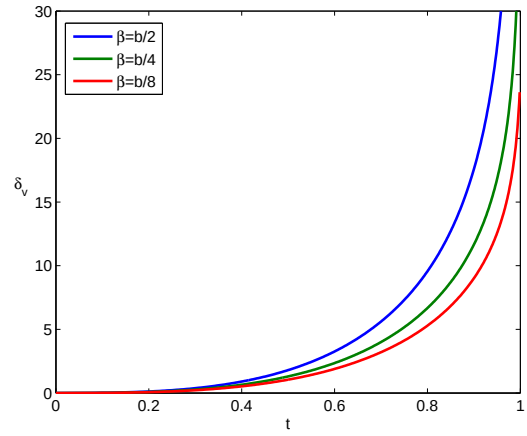

Figure 7.9: Crack opening δ_v vs. time t for $b = 1.5$.

7.2.2 Propagating Crack Stage

Crack Length

The graphs in Figures 7.10-7.13 show the evolution of the crack length in time for $b = 4$ and $b = 1.5$, for three cases of β.

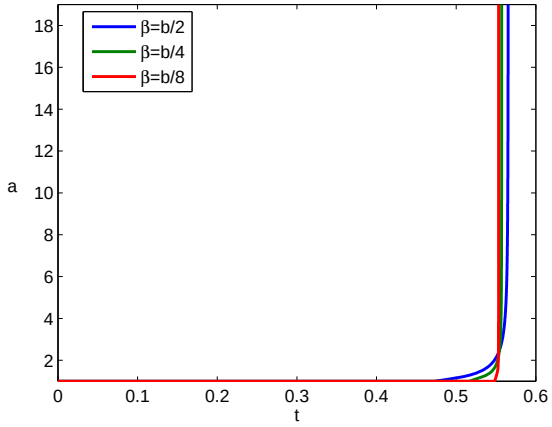

Figure 7.10: Crack length vs. t for $b = 4$.

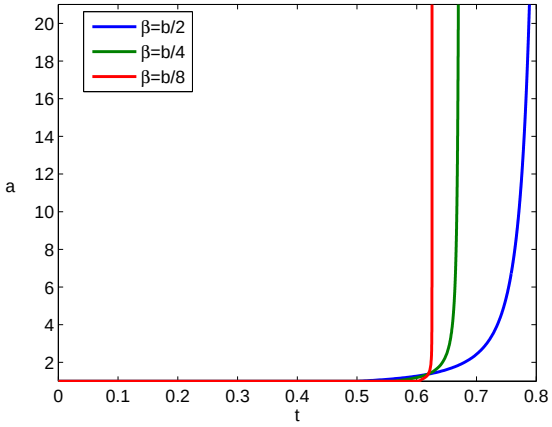

Figure 7.11: Crack length vs. time for $b = 1.5$.

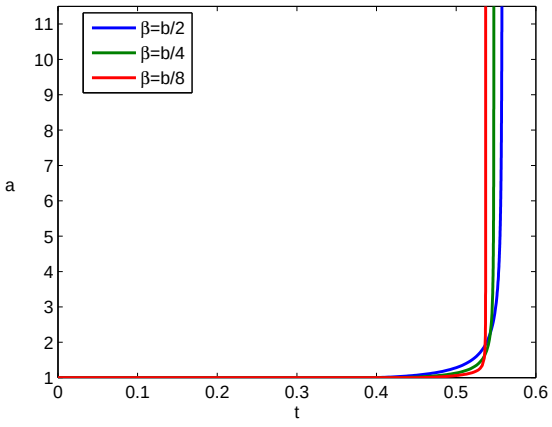

Figure 7.12: Crack length vs. time for $b = 4$.

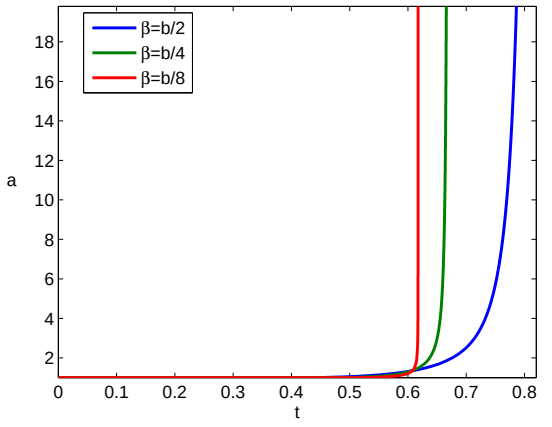

Figure 7.13: Crack length vs. time for $b = 1.5$.

CZ Tip Coordinate

The graphs in Figures 7.14-7.17 show the evolution of the CZ tip in time for $b = 4$ and $b = 1.5$ respectively, for three cases of β.

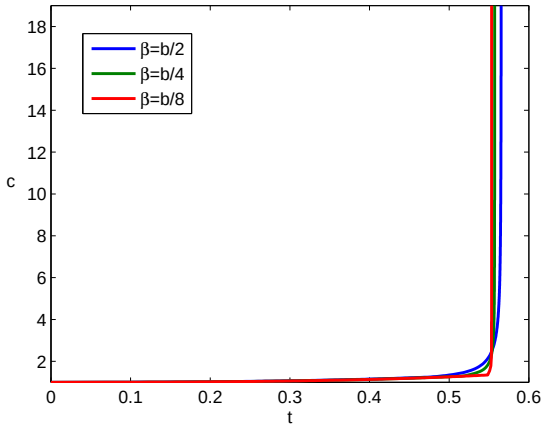

Figure 7.14: CZ tip coordinate vs. time for $b = 4$ (elastic case).

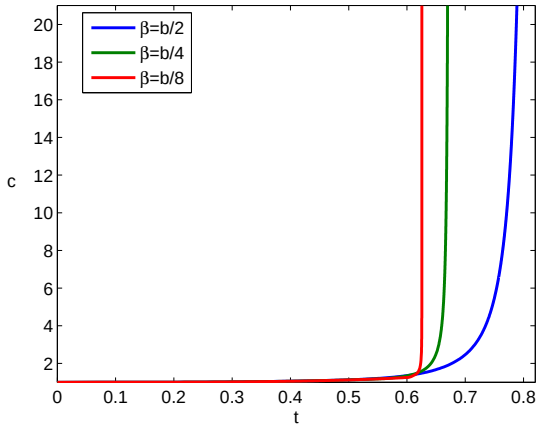

Figure 7.15: CZ tip coordinate vs. time for $b = 1.5$ (elastic case).

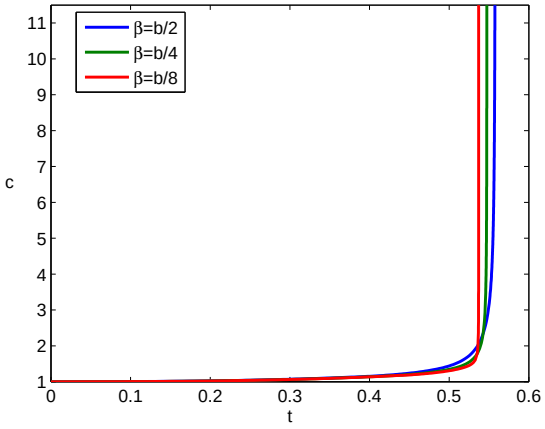

Figure 7.16: CZ tip coordinate vs. time for $b = 4$ (viscoelastic case).

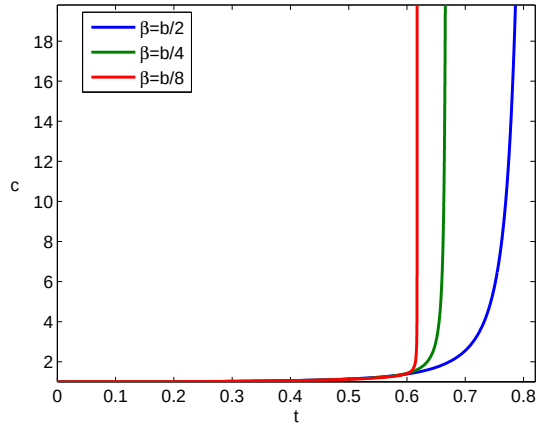

Figure 7.17: CZ tip coordinate vs. time for $b = 1.5$ (viscoelastic case).

CZ Length

The graphs in Figures 7.18-7.21 show the evolution of the CZ length in time for $b = 4$ and $b = 1.5$ respectively, for three cases of β.

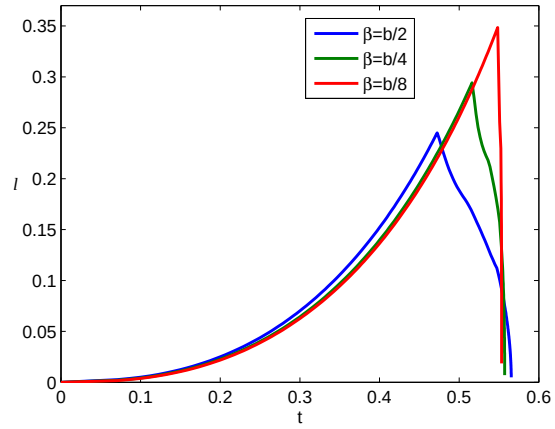

Figure 7.18: CZ length vs. t for $b = 4$ (elastic case).

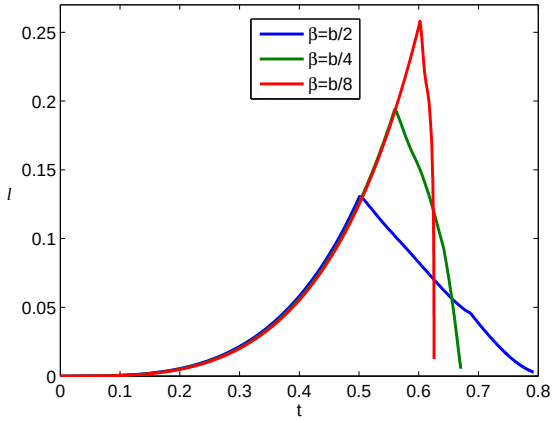

Figure 7.19: CZ length vs. t for $b = 1.5$ (elastic case).

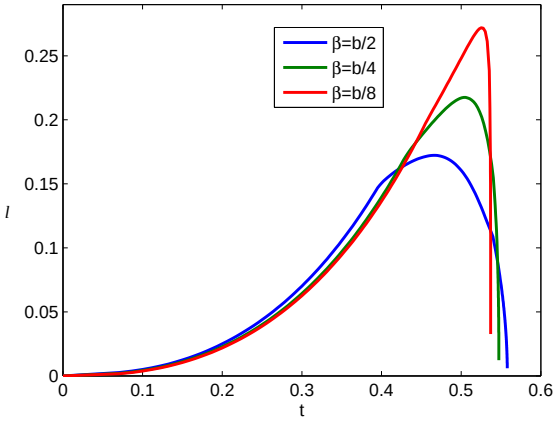

Figure 7.20: CZ length vs. t for $b = 4$ (viscoelastic case).

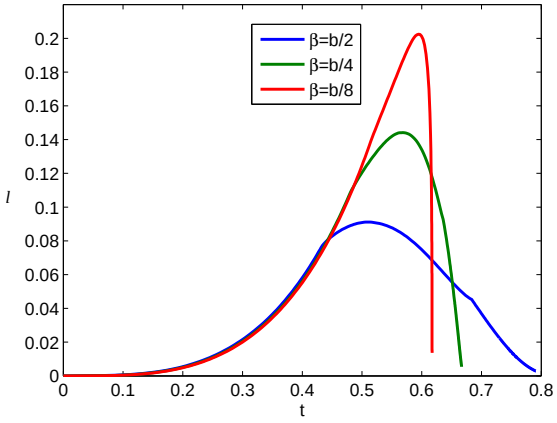

Figure 7.21: CZ length vs. t for $b = 1.5$ (viscoelastic case).

Chapter 8

Numerical Convergence Rate

Numerical schemes for solving mathematical problems result in some degree of uncertainty due to inaccuracies accumulating within the computations. In order to judge the applicability of the numerical methods used for each of the problems solved, we will approximate the error in the solutions as well as compute the corresponding numerical convergence rate.

In the model problems which were numerically solved, we considered discrete solutions using successively refined meshes. In order to obtain the convergence rate of our numerical results, we have to first estimate the error. Let y and y^{appr} denote the exact and approximate value of a variable y respectively. The absolute error is defined as

$$\varepsilon = |y - y^{\text{appr}}|;$$

however, since the exact solutions to our problems are unknown, we cannot obtain an exact form of the error but an approximation to it. To this end, we will use Aitken's extrapolation technique to obtain a good approximation to the exact solution. This nonlinear acceleration scheme, also known as the Aitken Δ^2 process, is a fast and reliable way to accelerate the convergence of a sequence which can be in turn used to estimate the exact solution of a

problem based on a sequence of numerical solutions, e.g. see [9]. Aitken's extrapolation technique gives an approximation y_a of the exact solution y based on 3 consecutive terms of a convergent sequence, the Aitken extrapolation formula is given by

$$y_a = \frac{y_N^{\text{appr}} y_{N-2}^{\text{appr}} - \left(y_{N-1}^{\text{appr}}\right)^2}{y_N^{\text{appr}} - 2y_{N-1}^{\text{appr}} + y_{N-2}^{\text{appr}}},$$

see [9, 12, 48], where y_N^{appr} corresponds to the numerical solution with step size $h = h_N$ for $h = h_1, h_2, ..., h_N$. Therefore, y_a is computed using the solutions corresponding to the 3 finest meshes considered. Consequently, our error will be approximated by

$$\varepsilon = |y_a - y^{\text{appr}}|. \tag{8.1}$$

For convergence, we assume that there exists a constant C such that for all h

$$|y_a - y^{\text{appr}}| \leq Ch^{\alpha},$$

where α is known as the *numerical convergence rate*, see e.g. [34, 53]. Therefore, we have

$$\varepsilon = Ch^{\alpha} + O(h^{\alpha+1}).$$

Neglecting the higher order terms, we have

$$\varepsilon = Ch^{\alpha}.$$

Consider $\varepsilon_i = Ch_i^{\alpha}$ and $\varepsilon_{i+1} = Ch_{i+1}^{\alpha}$; dividing the first equation by the second equation and taking logarithms yields

$$\alpha = \frac{\log\left(\frac{\varepsilon_i}{\varepsilon_{i+1}}\right)}{\log\left(\frac{h_i}{h_{i+1}}\right)}. \tag{8.2}$$

In what follows, we may refer to the numerical convergence rate as CR. We obtain the approximation of the error using equation (8.1) and the numerical convergence rate using equation (8.2). In this chapter we will give the numerical convergence rates and the approximation of the error for the case of constant loading. Similar results were obtained for the variable load case; the graphs and tables for this case can be found in Appendix C.

8.1 Constant Loading

Cohesive Zone Length of a Stationary Crack

Taking the solutions corresponding to $t = 0.6$, we will plot the error against the time spacing in the mesh and present the numerical convergence in a table.

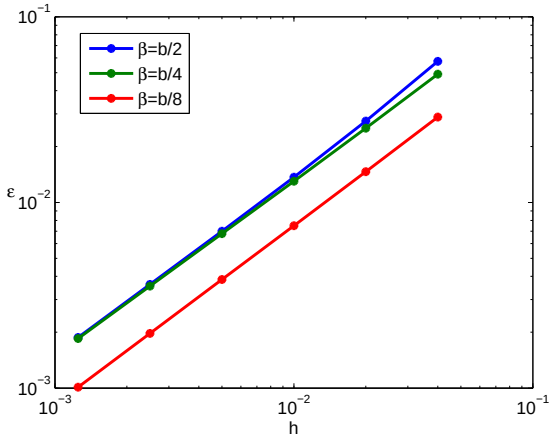

Figure 8.1: Error of the CZ length vs. step size for $b = 4$ and $t = 0.6$ (stationary crack).

h \ β	$\frac{b}{2}$	$\frac{b}{4}$	$\frac{b}{8}$
1/25	-	-	-
1/50	1.06782	0.96783	0.97768
1/100	1.00550	0.94748	0.96672
1/200	0.96689	0.93922	0.96292
1/400	0.94986	0.93766	0.96279
1/800	0.94986	0.93766	0.96279

Table 8.1: CR α at $b = 4$ and $t = 0.6$ (CZ length for stationary crack).

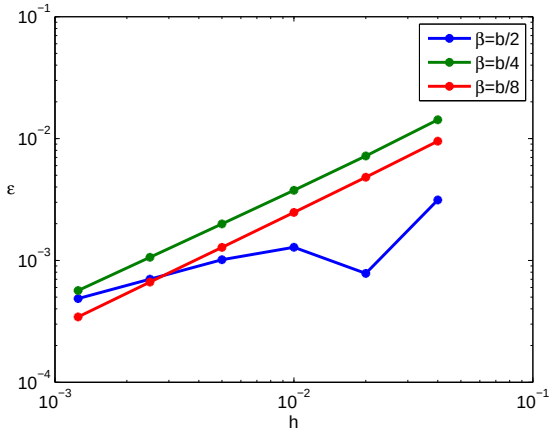

Figure 8.2: Error of the CZ length vs. step size for $b = 1.5$ and $t = 0.6$ (stationary crack).

h \ β	$\frac{b}{2}$	$\frac{b}{4}$	$\frac{b}{8}$
1/25	-	-	-
1/50	2.00554	0.98495	0.98514
1/100	-0.71453	0.93666	0.96027
1/200	0.33857	0.91483	0.95042
1/400	0.53098	0.90886	0.94855
1/800	0.53098	0.90886	0.94855

Table 8.2: CR α at $b = 1.5$ and $t = 0.6$ (CZ length for stationary crack).

For the case $b = 4$, the numerical convergence rate is very close to 1 for all three cases of β. This implies that the numerical solutions obtained converge linearly. The decreasing error, as the mesh becomes finer, supports this conclusion.

This effect is also apparent for the case $b = 1.5$; however, for this case, while $\beta = \frac{b}{2}$, we observe an increase in the error between $h = \frac{1}{50}$ and $h = \frac{1}{100}$. This could be due to computational errors which lead to a negative convergence rate. From $h = \frac{1}{100}$ to $h = \frac{1}{800}$, the convergence rate approaches $\frac{1}{2}$ which implies that we have convergence but at a slower rate than in the cases $\frac{\beta}{4}$ and $\frac{\beta}{8}$.

Stress at the Cohesive Zone Tip

We will study the stress at the CZ tip, for $x = c(t^*)$, $t^* = 0.6$. We are particularly interested in what is happening at the CZ tip. For better observations, we will use the parameter sets $\beta = \frac{3b}{4}$ and $\beta = \frac{b}{3}$ as well as the 3 usual sets $\beta = \frac{b}{2}$, $\beta = \frac{b}{4}$ and $\beta = \frac{b}{8}$. We will first look at the graphs of the stress at the CZ tip for various mesh sizes.

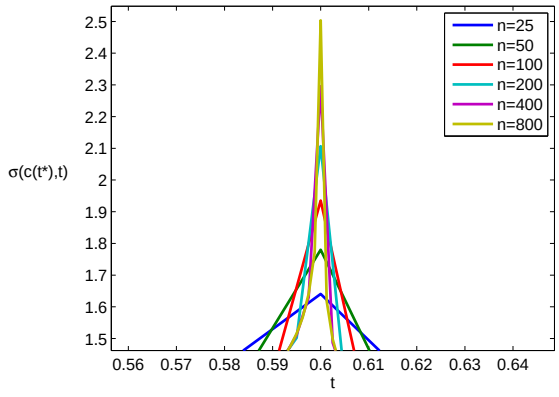

Figure 8.3: $\sigma(c(t^*), t)$ for $b = 4$, $\beta = \frac{3b}{4}$, $t^* = 0.6$: closer look at the CZ tip.

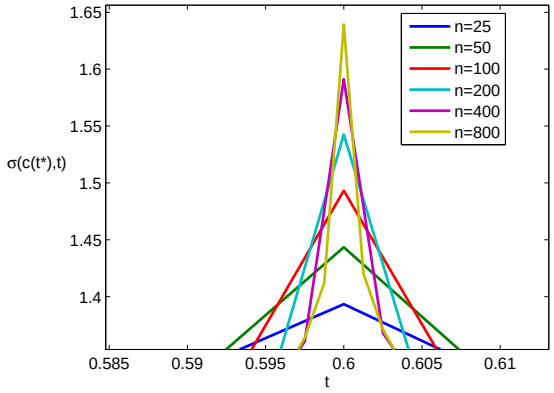

Figure 8.4: $\sigma(c(t^*), t)$ for $b = 4$, $\beta = \frac{b}{2}$, $t^* = 0.6$: closer look at the CZ tip.

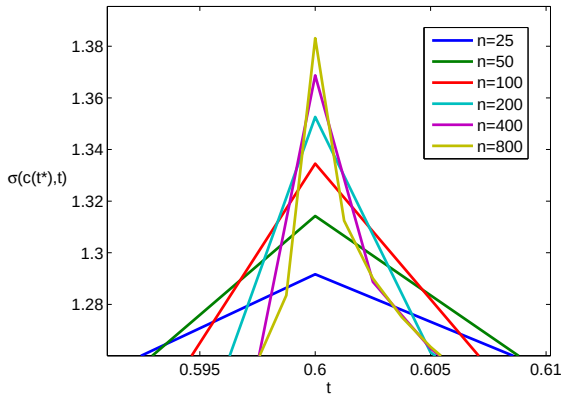

Figure 8.5: $\sigma(c(t^*), t)$ for $b = 4$, $\beta = \dfrac{b}{3}$, $t^* = 0.6$: closer look at the CZ tip.

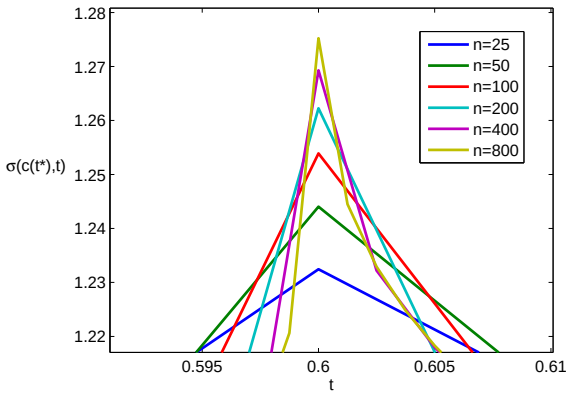

Figure 8.6: $\sigma(c(t^*), t)$ for $b = 4$, $\beta = \dfrac{b}{4}$, $t^* = 0.6$: closer look at the CZ tip.

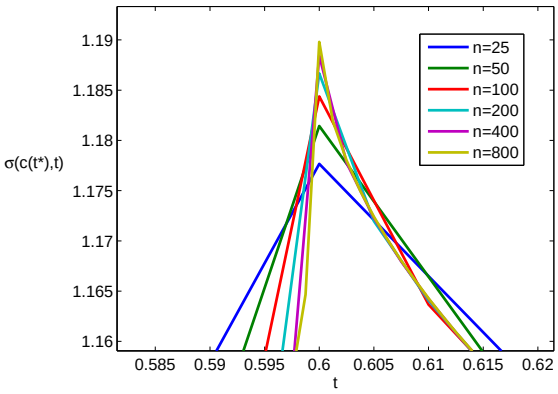

Figure 8.7: $\sigma(c(t^*), t)$ for $b = 4$, $\beta = \dfrac{b}{8}$, $t^* = 0.6$: closer look at the CZ tip.

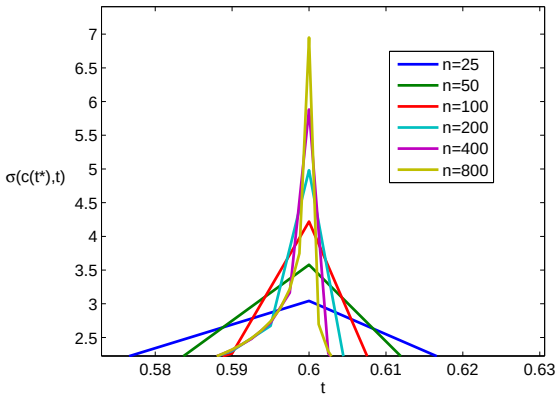

Figure 8.8: $\sigma(c(t^*), t)$ for $b = 1.5$, $\beta = \dfrac{3b}{4}$, $t^* = 0.6$: closer look at the CZ tip.

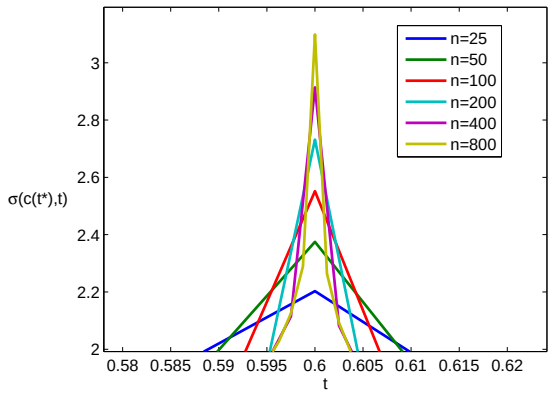

Figure 8.9: $\sigma(c(t^*), t)$ for $b = 1.5$, $\beta = \dfrac{b}{2}$, $t^* = 0.6$: closer look at the CZ tip.

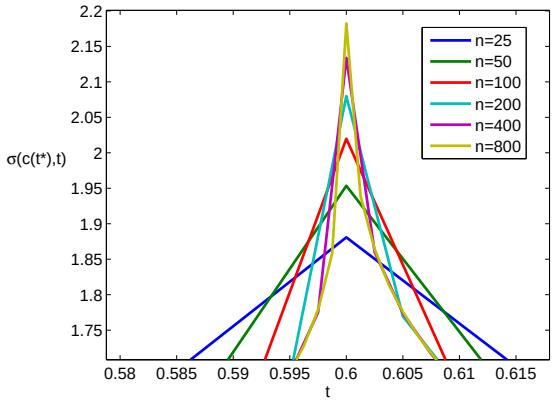

Figure 8.10: $\sigma(c(t^*), t)$ for $b = 1.5$, $\beta = \dfrac{b}{3}$, $t^* = 0.6$: closer look at the CZ tip.

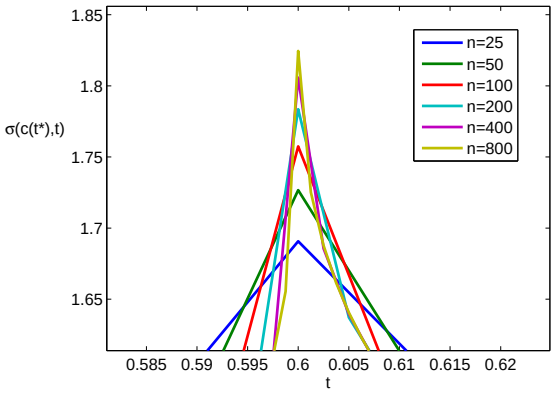

Figure 8.11: $\sigma(c(t^*), t)$ for $b = 1.5$, $\beta = \dfrac{b}{4}$, $t^* = 0.6$: closer look at the CZ tip.

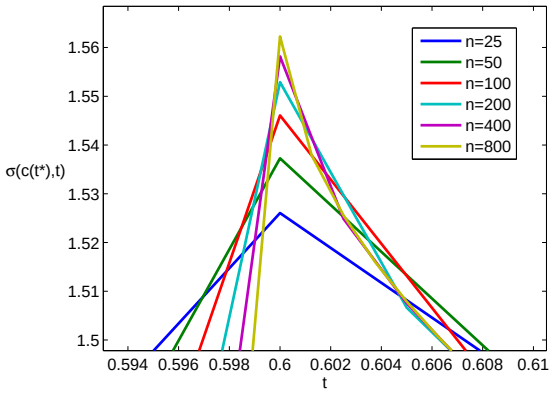

Figure 8.12: $\sigma(c(t^*), t)$ for $b = 1.5$, $\beta = \dfrac{b}{8}$, $t^* = 0.6$: closer look at the CZ tip.

The following table shows the approximations of the stress at the CZ tip for different mesh sizes. Also, σ_a denotes the approximation to the exact solution obtained from using Aitken's extrapolation formula. We will start with the case $b = 4$ followed by the case $b = 1.5$.

β \ h	$\frac{1}{25}$	$\frac{1}{50}$	$\frac{1}{100}$	$\frac{1}{200}$	$\frac{1}{400}$	$\frac{1}{800}$	σ_a
$3b/4$	1.64055	1.78002	1.93513	2.10670	2.29576	2.50354	0.19859
$b/2$	1.39334	1.44340	1.49319	1.54250	1.59121	1.63929	5.25425
$b/3$	1.29166	1.31424	1.33450	1.35260	1.36874	1.38311	1.49965
$b/4$	1.23245	1.24403	1.25390	1.26224	1.26929	1.27521	1.30680
$b/8$	1.17767	1.18144	1.18438	1.18667	1.18843	1.18980	1.19443

Table 8.3: Stress at the CZ tip and its Aitken approximation for $b = 4$.

Given below is the graph of the maximum stress (i.e. the stress at the CZ tip) vs. $n = 25,\ 50,\ 100,\ 200,\ 400,\ 800$.

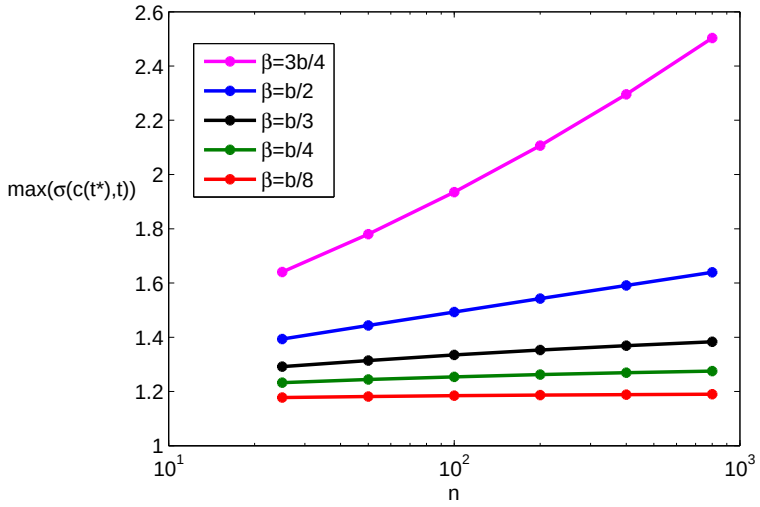

Figure 8.13: Stress at the CZ tip vs. n for $b = 4$.

We can see from Table 8.3 and Figure 8.13 that the stress at the CZ tip increases with mesh refinement. For $\beta = \frac{b}{3}$, $\beta = \frac{b}{4}$, and $\beta = \frac{b}{8}$, Aitken's approximation is very close to the numerically obtained values of σ. However, for $\beta = \frac{3b}{4}$ and $\frac{b}{2}$, Aitken's approximation is far from the numerical approximations. Bearing in mind the vital condition $0 < \beta < b$,

we can conclude that at the CZ tip, there could be another singularity, other than the square root singularity. The impact and strength of this singularity seems to be detectable as the condition $\beta < b$ is close to being violated.

Now, while using the above values for σ_a, let's have a look at the approximation of the error and the numerical convergence rates.

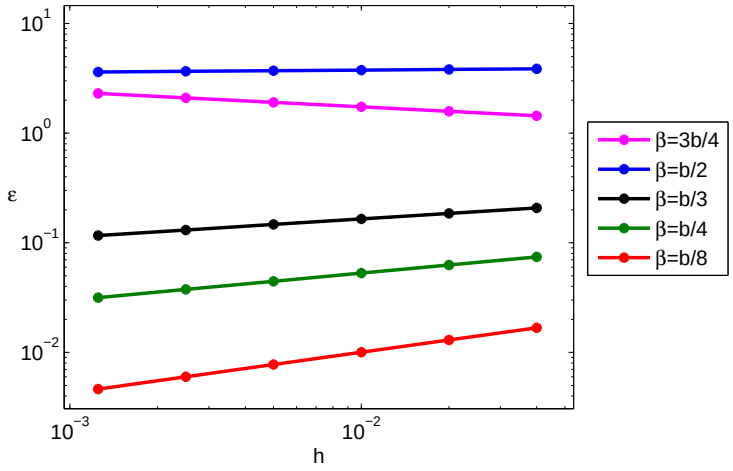

Figure 8.14: Error of the stress at the CZ tip vs. step size for $b = 4$.

h \ β	$\frac{3b}{4}$	$\frac{b}{2}$	$\frac{b}{3}$	$\frac{b}{4}$	$\frac{b}{8}$
1/25	-	-	-	-	-
1/50	-0.13319	0.01883	0.16577	0.24435	0.36745
1/100	-0.13498	0.01897	0.16694	0.24663	0.37080
1/200	-0.13593	0.01904	0.16750	0.24775	0.37243
1/400	-0.13629	0.01906	0.16769	0.24815	0.37303
1/800	-0.13629	0.01906	0.16769	0.24815	0.37303

Table 8.4: CR α for $b = 4$ (Stress at the CZ tip, stationary crack).

The rate of convergence is higher as β decreases, although the rate is still rather slow

compared to those observed for the CZ tip coordinate. Furthermore, we can see that the negative convergence rate, as well as the negative gradient in Figure 8.14, for the case $\beta = \frac{3b}{4}$, indicates that there's no convergence for this case. The low convergence rate at $\beta = \frac{b}{2}$ also signifies very low convergence for the stress at the CZ tip. The results for the case $b = 1.5$ resemble those for the case $b = 4$, thus similar conclusions pertain.

β \ h	$\frac{1}{25}$	$\frac{1}{50}$	$\frac{1}{100}$	$\frac{1}{200}$	$\frac{1}{400}$	$\frac{1}{800}$	σ_a
$3b/4$	3.04260	3.57850	4.21904	4.98066	5.88300	6.94964	0.02482
$b/2$	2.20259	2.37480	2.55152	2.73159	2.91416	3.09873	-13.96742
$b/3$	1.88078	1.95354	2.01986	2.07983	2.13382	2.18227	2.60622
$b/4$	1.69074	1.72663	1.75740	1.78358	1.80576	1.82449	1.92635
$b/8$	1.52605	1.53727	1.54606	1.55289	1.55818	1.56227	1.57617

Table 8.5: Stress at the CZ tip and its Aitken approximation for $b = 1.5$.

Given below is the graph of the maximum stress (i.e. the stress at the CZ tip) vs. $n = 25, 50, 100, 200, 400, 800$.

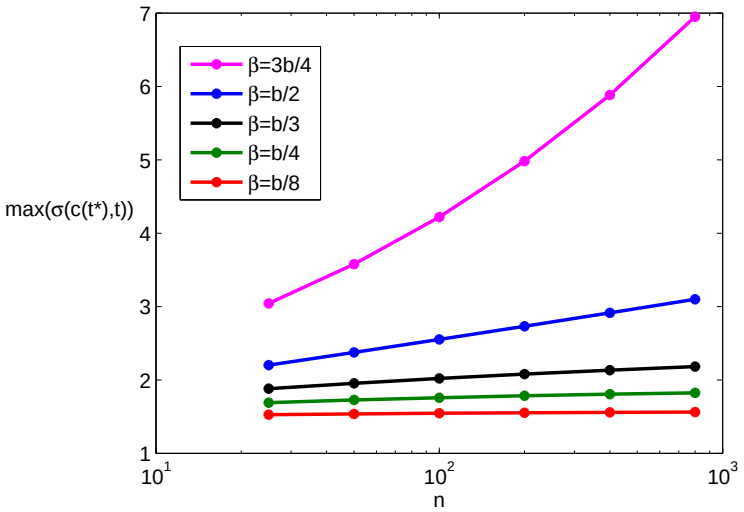

Figure 8.15: Stress at the CZ tip vs. n for $b = 1.5$.

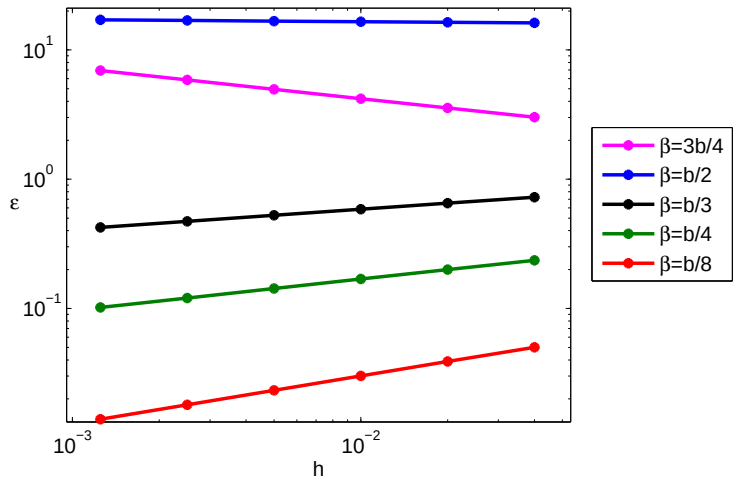

Figure 8.16: Error of the stress at the CZ tip vs. step size for $b = 1.5$.

h \ β	$\frac{3b}{4}$	$\frac{b}{2}$	$\frac{b}{3}$	$\frac{b}{4}$	$\frac{b}{8}$
1/25	-	-	-	-	-
1/50	-0.23583	-0.01528	0.15248	0.23840	0.36586
1/100	-0.23909	-0.01552	0.15457	0.24140	0.36943
1/200	-0.24073	-0.01564	0.15568	0.24294	0.37119
1/400	-0.24132	-0.01569	0.15611	0.24354	0.37186
1/800	-0.24132	-0.01569	0.15611	0.24354	0.37186

Table 8.6: CR α for $b = 1.5$ (Stress at the CZ tip, stationary crack).

Crack Tip Opening for the Elastic Case

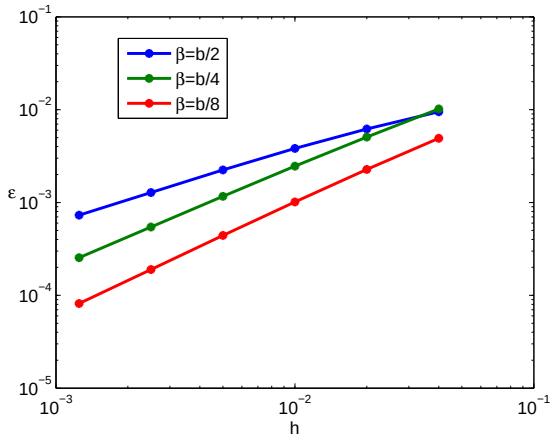

Figure 8.17:

Error of δ_e vs. step size for $b = 4$ at $t = 0.6$.

h \ β	$\frac{b}{2}$	$\frac{b}{4}$	$\frac{b}{8}$
1/25	-	-	-
1/50	0.61765	1.00204	1.11651
1/100	0.69634	1.04398	1.16272
1/200	0.76918	1.07794	1.19813
1/400	0.80870	1.09752	1.21867
1/800	0.80870	1.09752	1.21867

Table 8.7:

CR α of δ_e for $b = 4$ at $t = 0.6$.

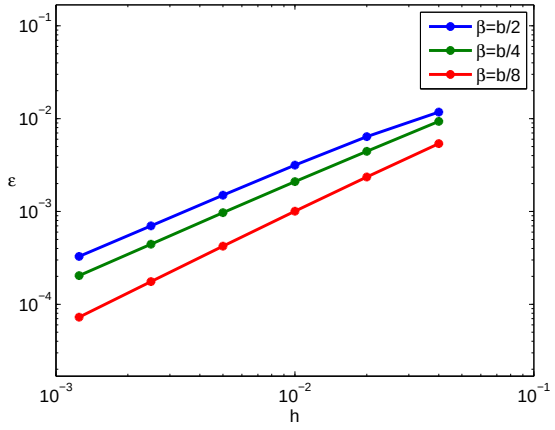

Figure 8.18:

Error of δ_e vs. step size for $b = 1.5$ at $t = 0.6$.

h \ β	$\frac{b}{2}$	$\frac{b}{4}$	$\frac{b}{8}$
1/25	-	-	-
1/50	0.88202	1.06906	1.19473
1/100	1.01906	1.08583	1.22421
1/200	1.07580	1.11027	1.25169
1/400	1.09585	1.12768	1.26958
1/800	1.09585	1.12768	1.26958

Table 8.8:

CR α of δ_e for $b = 1.5$ at $t = 0.6$.

Crack Tip Opening for the Viscoelastic Case

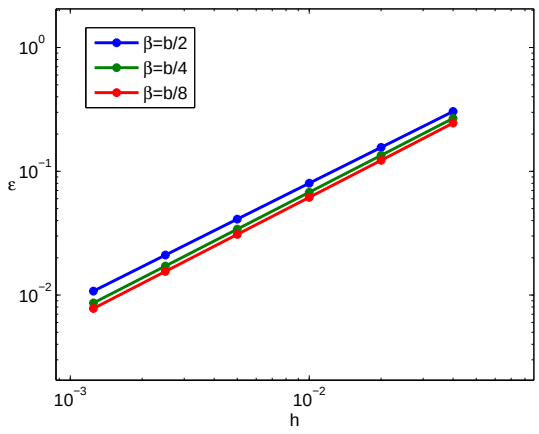

Figure 8.19:

Error of δ_v vs. step size for $b = 4$ at $t = 0.6$.

h \ β	$\frac{b}{2}$	$\frac{b}{4}$	$\frac{b}{8}$
1/25	-	-	-
1/50	0.96579	0.99327	1.00007
1/100	0.96146	0.99002	0.99491
1/200	0.96320	0.99027	0.99344
1/400	0.96562	0.99113	0.99327
1/800	0.96562	0.99113	0.99327

Table 8.9:

CR α of δ_v for $b = 4$ at $t = 0.6$.

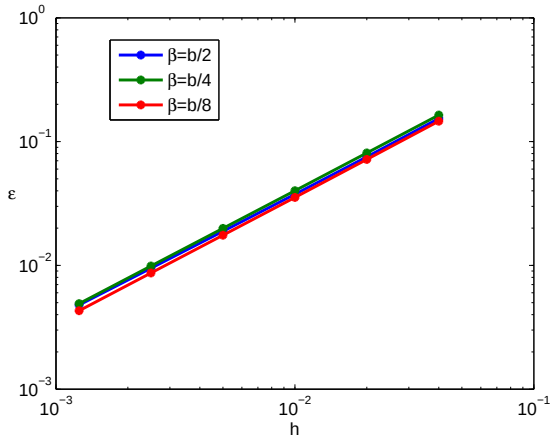

Figure 8.20:

Error of δ_v vs. step size for $b = 1.5$ at $t = 0.6$.

h \ β	$\frac{b}{2}$	$\frac{b}{4}$	$\frac{b}{8}$
1/25	-	-	-
1/50	1.03148	1.01847	1.02646
1/100	1.00445	1.01172	1.01819
1/200	0.99307	1.01054	1.01480
1/400	0.98937	1.01079	1.01347
1/800	0.98937	1.01079	1.01347

Table 8.10:

CR α of δ_v for $b = 1.5$ at $t = 0.6$.

For both the elastic and viscoelastic cases, we can see that the numerical convergence rate tends to 1 which manifests that we have convergence of the crack tip opening obtained. This is seen for both cases $b = 4$ and $b = 1.5$ and for all cases of β.

Crack Propagation Stage for the Elastic Case

Now, we will compute the CR at a time before crack growth begins as well as at a time during crack growth. During crack growth, the time $t = t_d$ is included within the time mesh, therefore time steps which follow will no longer be equidistantly distributed. Hence, in this case, for the chosen value t, we will linearly interpolate the CZ length for times t_a and t_b where $t_a < t < t_b$. We will start with $b = 4$ and then the case $b = 1.5$ will follow.

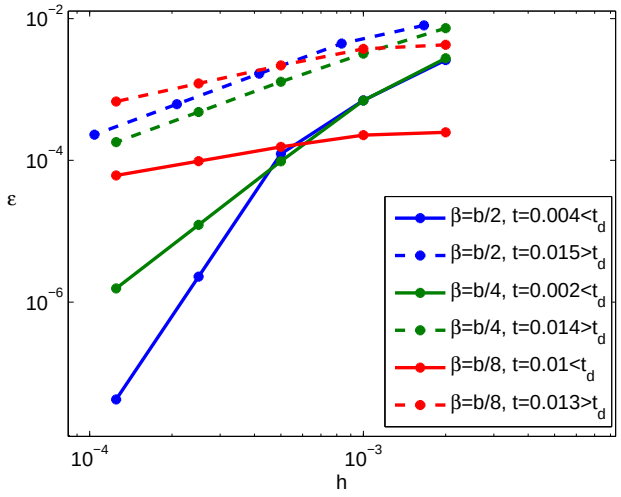

Figure 8.21: Error of CZ length vs. step size for $b = 4$ (stationary and growing crack stage (elastic)).

h \ β	$\frac{b}{2},\ t < t_d$	$\frac{b}{2},\ t > t_d$	$\frac{b}{4},\ t < t_d$	$\frac{b}{4},\ t > t_d$	$\frac{b}{8},\ t < t_d$	$\frac{b}{8},\ t > t_d$
1/500	-	-	-	-	-	-
1/1000	6.96313	1.36470	1.98295	1.19125	0.12785	0.18568
1/2000	2.50666	1.39154	2.84403	1.32103	0.55313	0.77385
1/4000	5.75240	1.34905	2.98105	1.41315	0.67061	0.84807
1/8000	5.75240	1.34905	2.98105	1.41315	0.67061	0.84807

Table 8.11: CR α of the CZ length for $b = 4$ (stationary and growing crack stage (elastic)).

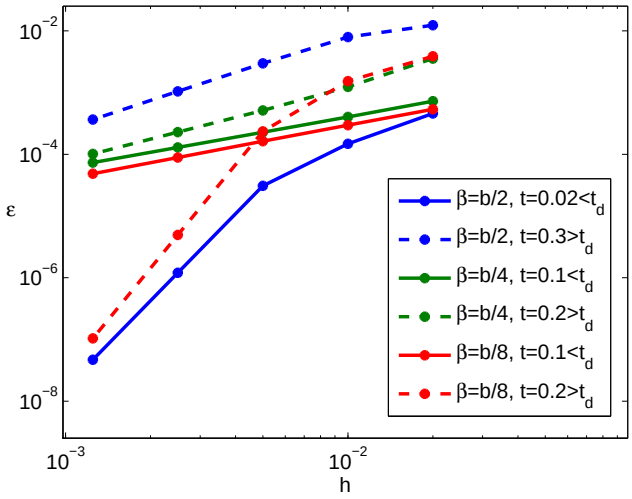

Figure 8.22: Error of CZ length vs. step size for $b = 1.5$ (stationary and growing crack stage (elastic)).

h \ β	$\frac{b}{2},\ t < t_d$	$\frac{b}{2},\ t > t_d$	$\frac{b}{4},\ t < t_d$	$\frac{b}{4},\ t > t_d$	$\frac{b}{8},\ t < t_d$	$\frac{b}{8},\ t > t_d$
1/50	-	-	-	-	-	-
1/100	1.62800	0.63777	0.85262	1.52504	0.85567	1.33368
1/200	2.26296	1.41131	0.82017	1.26149	0.86294	2.70421
1/400	4.68284	1.51220	0.81501	1.17033	0.87217	5.57225
1/800	4.68284	1.51220	0.81501	1.17033	0.87217	5.57225

Table 8.12: CR α of the CZ length for $b = 1.5$ (stationary and growing crack stage (elastic)).

For both cases $b = 4$ and $b = 1.5$, we can see from the graphs that the approximation of the error is decreasing as we take finer meshes. In some cases, such as when $b = 4$, $\beta = \frac{b}{2}$, and $b = 1.5$, $\beta = \frac{b}{2}, \frac{b}{8}$ we have a relatively high convergence rate of greater than 4 for $t < t_d$. The higher the convergence rate, the quicker the method is converging for this particular case and chosen time step. This is evidently justified from the graphs in Figures 8.21-8.22.

Crack Propagation Stage for the Viscoelastic Case

Given below are the graphs presenting the errors as well as the tables showing the numerical convergence rates of the CZ length for the viscoelastic case. We only present the convergence rate for a time step during crack growth since the solutions of the CZ growth for a stationary crack is the same for both elastic and viscoelastic cases (up to $t = t_d$). Refer to Tables 8.11 and 8.12 for the convergence rates in the stationary crack stage.

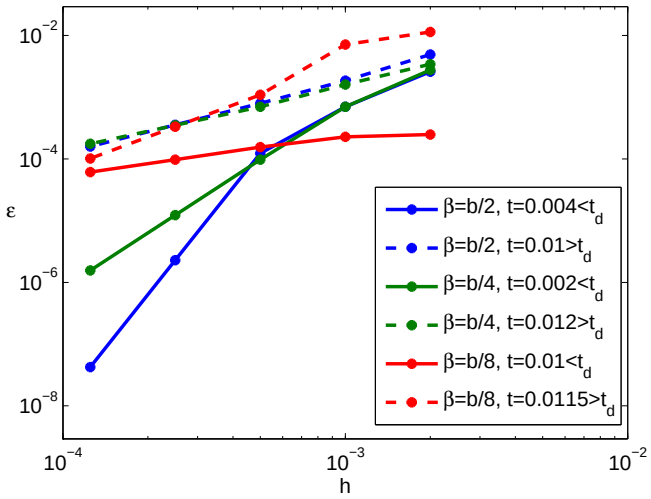

Figure 8.23: Error of CZ length vs. step size for $b = 4$ (growing crack stage (viscoelastic)).

h \ β	$\frac{b}{2},\ t > t_d$	$\frac{b}{4},\ t > t_d$	$\frac{b}{8},\ t > t_d$
1/500	-	-	-
1/1000	1.40449	1.09721	0.68019
1/2000	1.21844	1.19432	2.70292
1/4000	1.16394	0.99579	1.71441
1/8000	1.16394	0.99579	1.71441

Table 8.13:

CR α of the CZ length for $b = 4$ (viscoelastic).

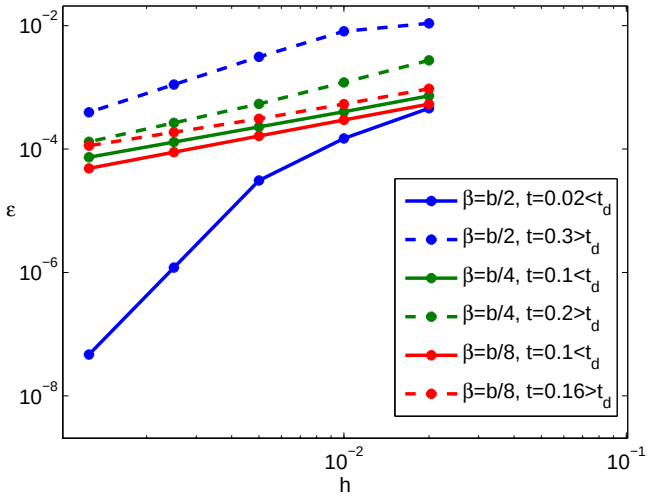

Figure 8.24: Error of CZ length vs. step size for $b = 1.5$ (growing crack stage (viscoelastic)).

h \ β	$\frac{b}{2},\ t > t_d$	$\frac{b}{4},\ t > t_d$	$\frac{b}{8},\ t > t_d$
1/50	-	-	-
1/100	0.42797	1.18890	0.82246
1/200	1.38178	1.16192	0.78850
1/400	1.49043	1.01566	0.72298
1/800	1.49043	1.01566	0.72298

Table 8.14:

CR α of the CZ length for $b = 1.5$ (growing crack stage (viscoelastic)).

The results showing the convergence rates and the approximation of the error in the viscoelastic case produce similar outcomes as those in the elastic case. However, we can see from Table 8.14 that the convergence rate decreases with decreasing β. This could be due to the computational errors which emerge from linearly interpolating the CZ length between times t_a and t_b for $t_a < t < t_b$.

Chapter 9

Discussion and Evaluation

9.1 Comparison of the Constant and Variable Loading Cases

In this section, we will look at how the solutions differ in the case of a variable external load with that of the case of a constant external load. We will compare

1. The CZ tip coordinate in the stationary crack stage
2. The stress ahead of the CZ as well as in the CZ
3. The crack tip opening for the elastic and viscoelastic cases
4. The CZ tip position in the propagating crack stage
5. The CZ length in the propagating crack stage

Note that in the graphs obtained, the legends will state 'constant' and 'variable' to distinguish the cases of the external loads being constant and varying in time respectively.

9.1.1 Stationary Crack Stage

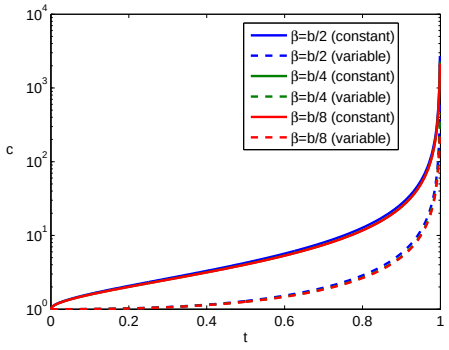

Figure 9.1: CZ tip coordinate vs. time for $b = 4$.

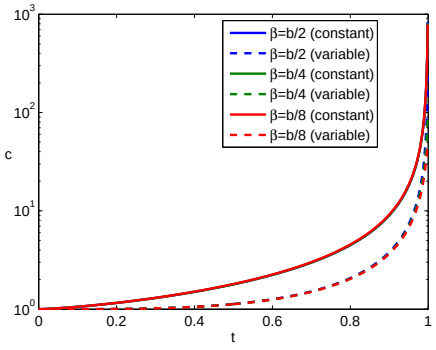

Figure 9.2: CZ tip coordinate vs. time for $b = 1.5$.

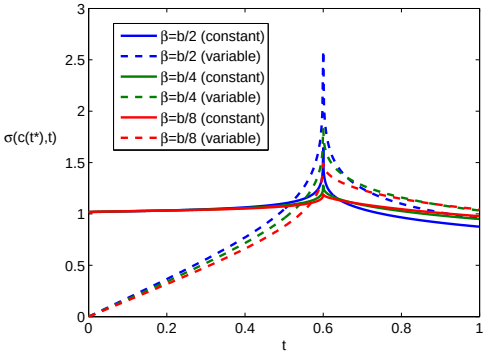

Figure 9.3: $\sigma(c(t^*), t)$ at $t^* = 0.6$ $b = 4$.

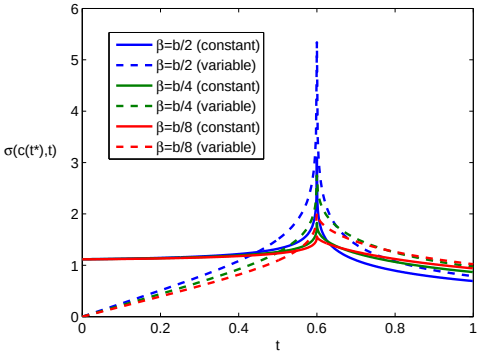

Figure 9.4: $\sigma(c(t^*), t)$ at $t^* = 0.6$ $b = 1.5$.

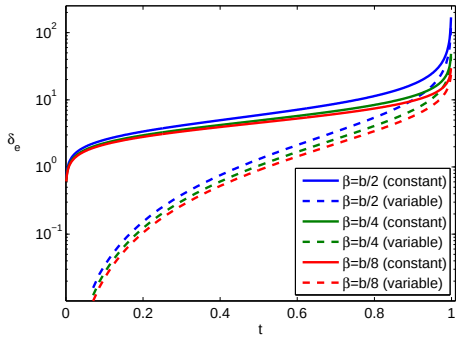

Figure 9.5: δ_e vs. t $b = 4$.

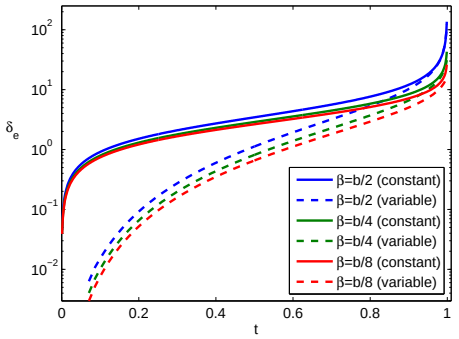

Figure 9.6: δ_e vs. t $b = 1.5$.

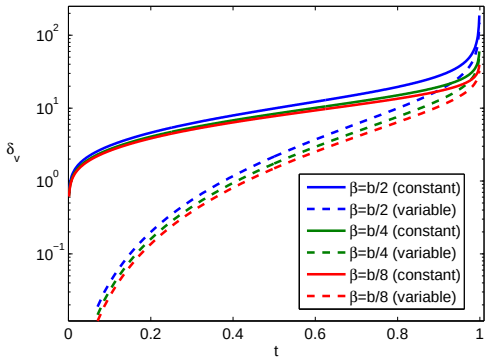

Figure 9.7: δ_v vs. t $b = 4$.

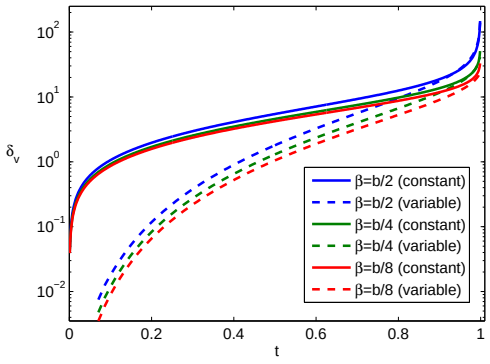

Figure 9.8: δ_v vs. t $b = 1.5$.

9.1.2 Propagating Crack Stage

The graphs in Figures 9.9 and 9.10 show the evolution of the CZ length in time for $b = 4$ and $b = 1.5$ respectively, for three cases of β. We start with presenting the results of the elastic case followed by the results for the viscoelastic case.

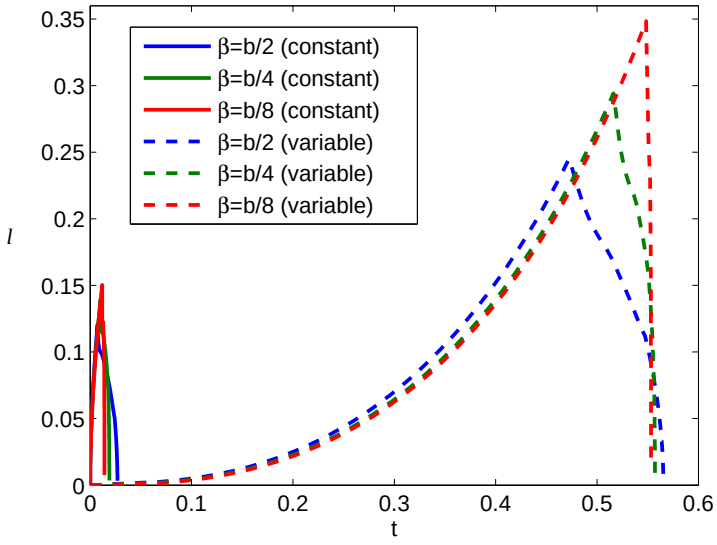

Figure 9.9: CZ length vs. time for $b = 4$ (elastic case).

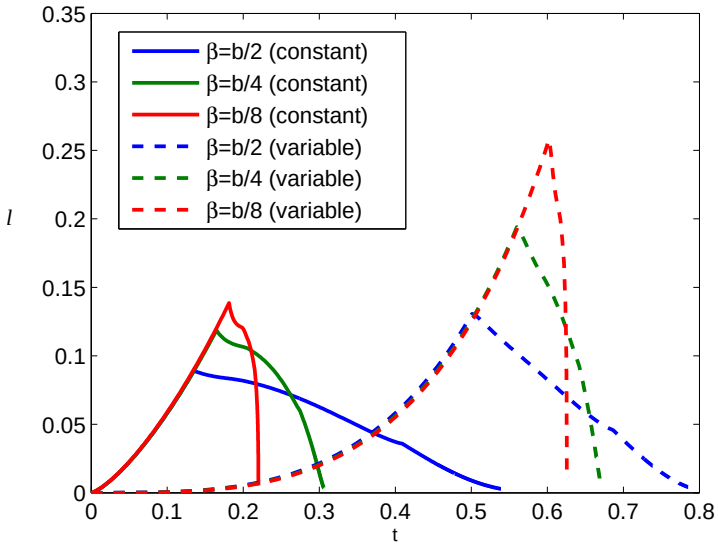

Figure 9.10: CZ tip coordinate vs. time for $b = 1.5$ (elastic).

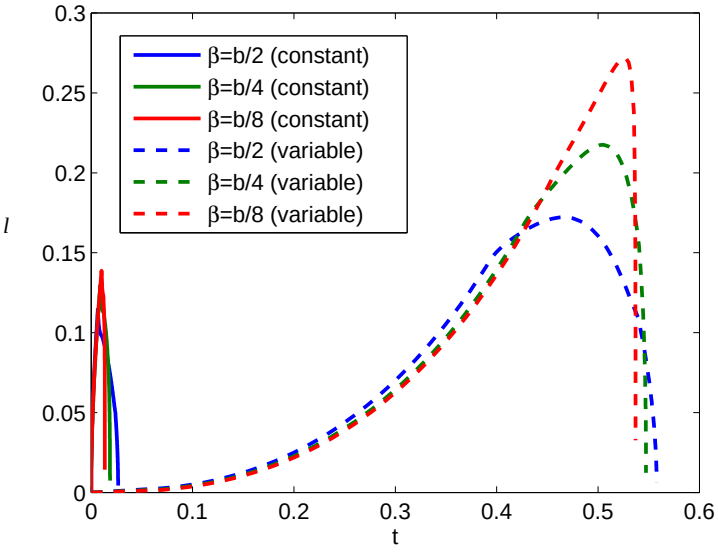

Figure 9.11: CZ tip coordinate vs. time for $b = 4$ (viscoelastic).

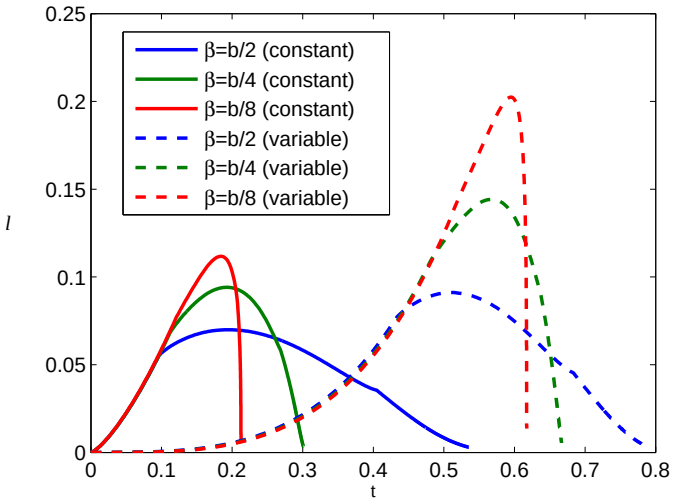

Figure 9.12: CZ tip coordinate vs. time for $b = 1.5$ (viscoelastic).

For the stationary crack stage, we conclude that the CZ tip coordinate grows more rapidly with time in the constant loading case than in the variable loading case. In addition to that, we observe from the obtained graphs that the crack tip opening, in both the elastic and viscoelastic cases, increases more rapidly in the constant loading case. The results for the propagating crack stage show significant differences while comparing the case of a constant load with that of a variable load. We can conclude that in the variable loading case, the crack begins to grow at a much later time than in the constant loading case. This effect holds for $b = 4$ and $b = 1.5$ as seen in Figures 9.9-9.12. However, the difference between the constant external load and variable external load is remarkable when $b = 4$.

9.2 Analysing the Onset of Crack Growth

Inspecting the graphs of the CZ length with respect to time, we can see that for the case $b = 4$, $\beta = \frac{b}{8}$, we have a jump, at the start of crack growth, of the CZ length, see Figure 6.6. We wish to study the behaviour for this set of parameters and also see if this effect appears for the viscoelastic case as well as the case of changing the parameter b.

The Elastic Case with $b = 4$, $\beta = \frac{b}{8}$

For instance, when $h = \frac{1}{2500}$, Figure 9.13 shows how the CZ length is changing with time.

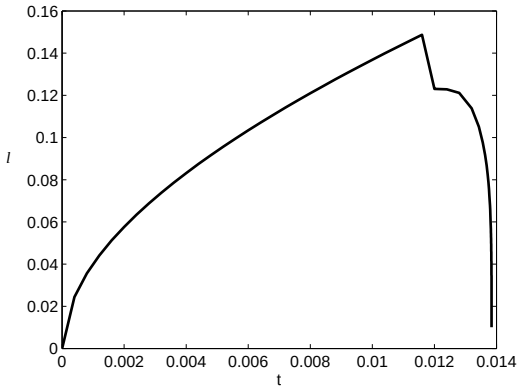

Figure 9.13: CZ length vs. time for $b = 4$, $\beta = \frac{1}{2}$.

Let l_d correspond to the CZ length at the delay time t_d. The CZ length at this point was numerically obtained using the algorithm explained in Section 6.2, this gives the values $(t_d, l_d) = (0.01184, 0.15043)$. At time step $t_{d^+} = t_d + \frac{1}{h} = t_d + \frac{1}{2500}$, we have the value $l_{d^+} = 0.12168$. However, we will modify the value of t_{d^+} 100 times using $t_{d^+,i} = t_d + \frac{1}{2500i}$ for $i = 1, 2, ...100$; to see that the CZ length does not tend to $l_d = 0.150428$ as $t_{d+1,i} \to t_d$, but it decreases and $l_{d^+,i} \to 0.11925$ as $t_{d^+,i} \to t_d$. Additionally, $a(d^+, i)$ does not tend to 1 but $a_{d^+,i} \to 1.05$ as $t_{d^+,i} \to t_d$. The dashed vertical line in Figure 9.14 joins the points for the CZ length at time t_d. See Figure 9.14.

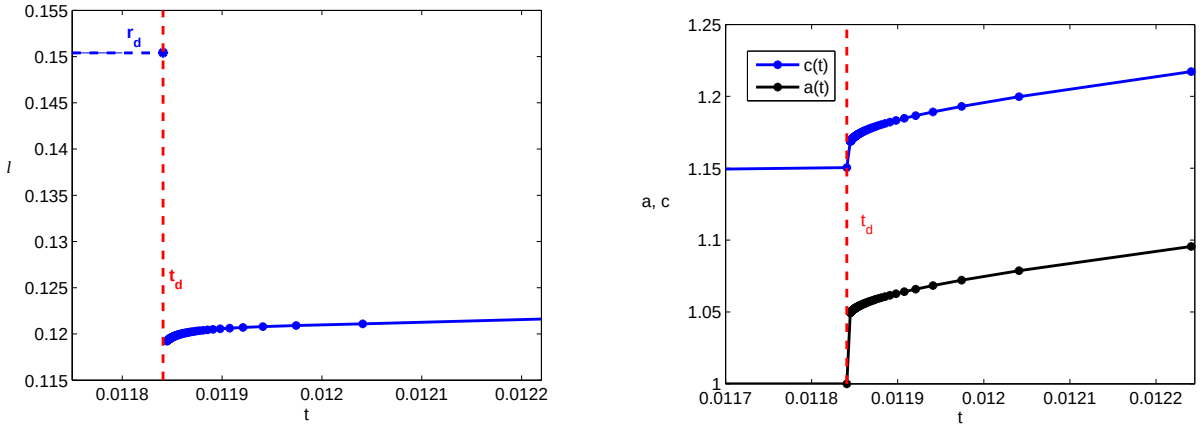

Figure 9.14: CZ length (left), crack length and CZ tip coordinate (right), vs. t for $b = 4$, $\beta = \dfrac{1}{2}$ (elastic).

If we take the points corresponding to $i = 99$ and $i = 100$ (i.e. $t_{d^+,99}$ and $t_{d^+,100}$), and extrapolate to find an approximation of the CZ length at t_d, we obtain the values $(\tilde{t}_d, \tilde{l}_d) = (0.011841, 0.118796)$. Using $(\tilde{t}_d, \tilde{l}_d)$ as the first step during crack growth, we obtain the graph given in Figure 9.15.

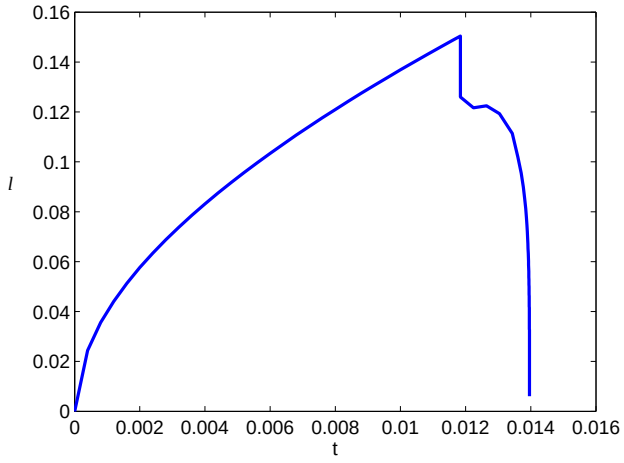

Figure 9.15: CZ length, $l(t)$ vs. time, t for $b = 4$, $\beta = \dfrac{1}{2}$.

The jump of the crack length at $t = t_d$, seen on the figures, indicates that there is

unstable crack growth at the onset of crack propagation followed by stable crack growth, for the chosen set of parameters. It also causes a jump in the CZ length at t_{d^+} followed by a continuous CZ length evolution.

The Viscoelastic Case with $b = 4$, $\beta = \dfrac{b}{8}$

Now we will take the viscoelastic case and see wether the same behaviour will arise at the onset of crack growth. As in the elastic case, we will take $h = \dfrac{1}{2500}$. Figure 9.16 shows that there is an initial decrease of the viscoelastic CZ length. However, with comparison to the elastic case, the drop is not as pronounced.

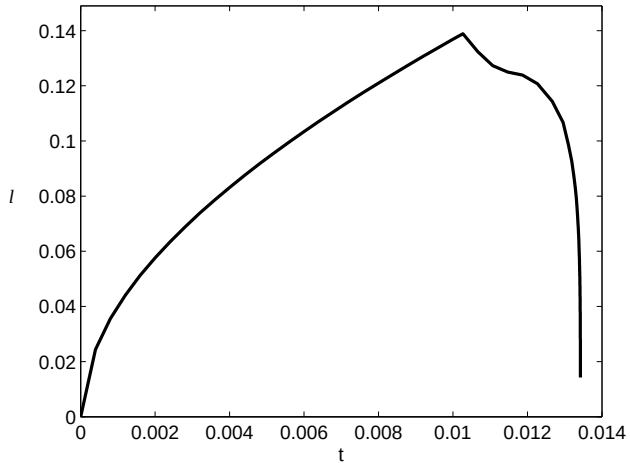

Figure 9.16: CZ length vs. t for $b = 4$, $\beta = \dfrac{1}{2}$.

For this case, we have $(t_d, l_d) = (0.01067, 0.13889)$. As previously done, we will modify the value of t_{d^+} 100 times using $t_{d^+,i} = t_d + \dfrac{1}{2500i}$ for $i = 1, 2, ...100$. See Figure 9.17.

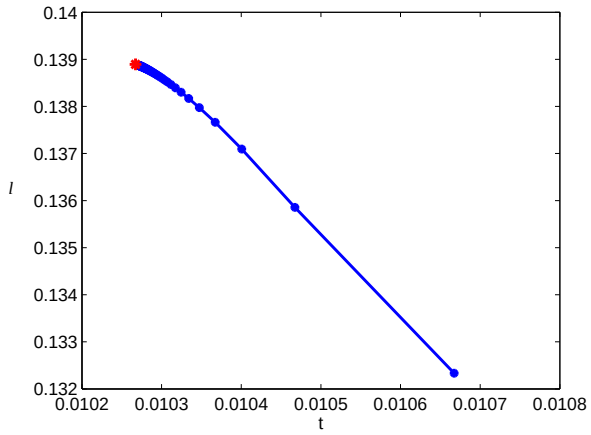

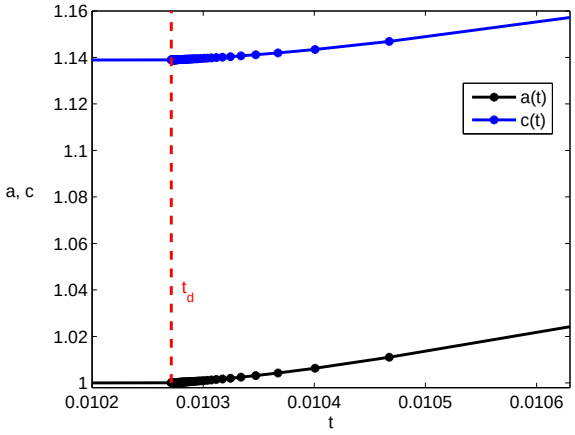

Figure 9.17: CZ length (left), crack length and CZ tip coordinate (right), vs. t for $b = 4$, $\beta = \dfrac{1}{2}$ (viscoelastic).

From the above graphs, we see that the behaviour emerging at the onset of crack growth for the elastic case does not occur for the viscoelastic case. In fact, we have that as $t_{d^+} \to t_d$, $l_{d^+} \to l_d$ and concurrently $a_{d+1} \to a_d = 1$, i.e. $l(t)$ and $a(t)$ are continuous at $t = t_d$

The Case $b = 1.5$

For a step size of $h = \dfrac{1}{200}$, we will look at the limiting behaviour for the elastic and viscoelastic cases. The graphs below show that as we take t_{d^+} closer to t_d, the CZ length at t_{d^+} approaches the CZ length which was computed before crack growth for $t = t_d$.

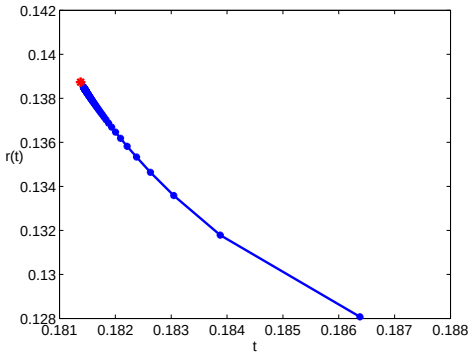

Figure 9.18: CZ length vs. t for $b = 1.5$, $\beta = \dfrac{b}{8}$ (elastic).

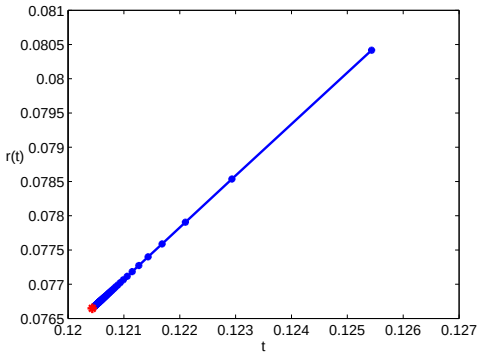

Figure 9.19: CZ length vs. t for $b = 1.5$, $\beta = \dfrac{b}{8}$ (viscoelastic).

Discontinuity for Various Parameter Sets

Now, let's have a look at the initiation of crack growth for different sets of parameters. As mentioned before, the red line connects the points at $t = t_d$ and $t = t_d + \dfrac{1}{2500}$, while the blue curve demonstrates whether $l_{d^+} \to l_d$ as $t \to t_d$. We are plotting these graphs to observe which sets of parameters cause convergence of the CZ length at the onset of crack growth. Convergence is shown by those graphs where the discrete points (demonstrated by the blue points) tend to the maximum red point.

Table 9.1: CZ length at the onset of crack growth (elastic case).

b \ β	$\frac{b}{2}$	$\frac{b}{4}$	$\frac{b}{8}$
4	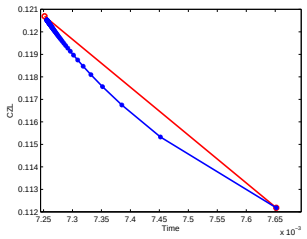	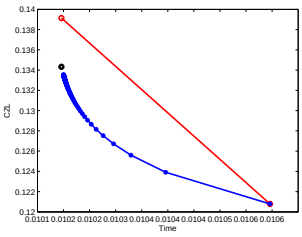	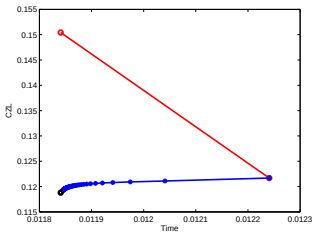
3	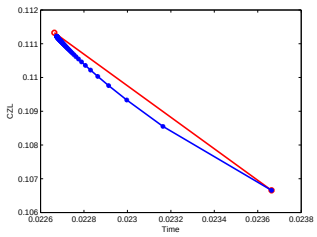	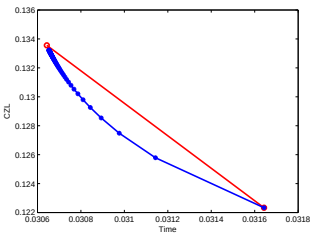	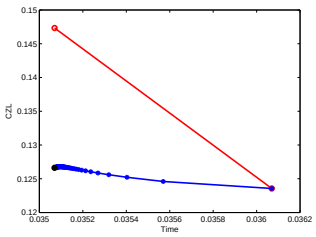
2.1	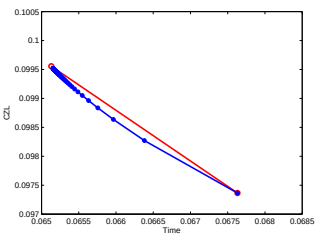	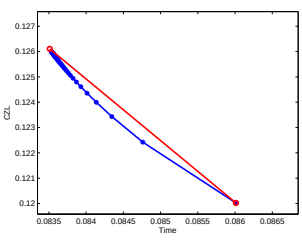	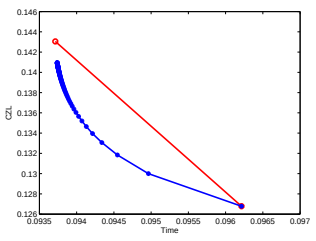

2.01	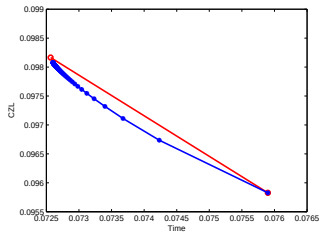 CZL Time	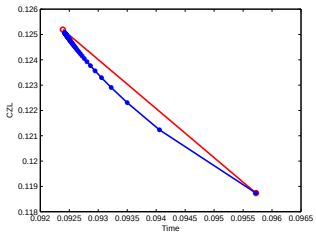 CZL Time	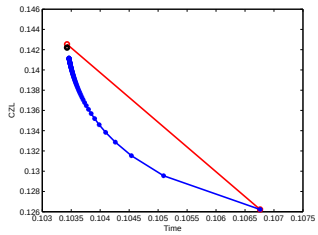 CZL Time
1.99	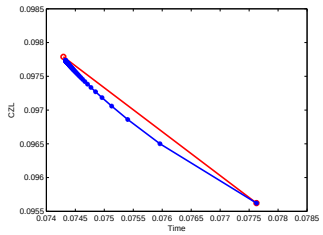 CZL Time	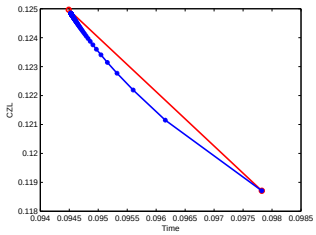 CZL Time	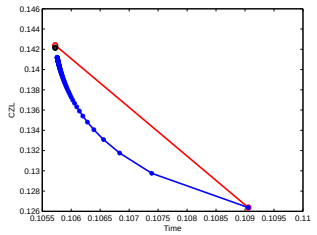 CZL Time
1	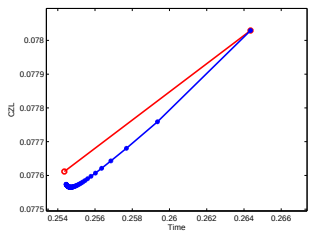 CZL Time	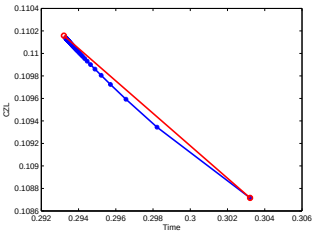 CZL Time	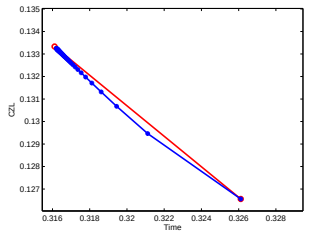 CZL Time
0.75	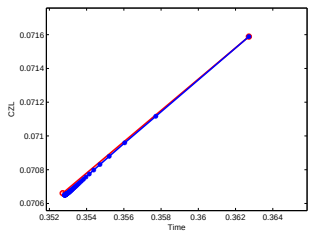 CZL Time	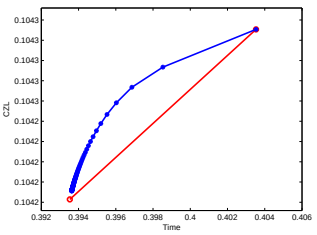 CZL Time	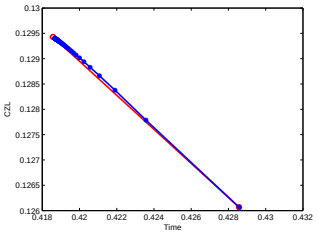 CZL Time

Table 9.2: CZ length at the onset of crack growth (viscoelastic case).

β / b	$\frac{b}{2}$	$\frac{b}{4}$	$\frac{b}{8}$
4	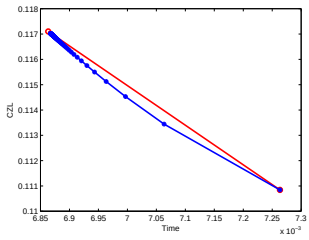	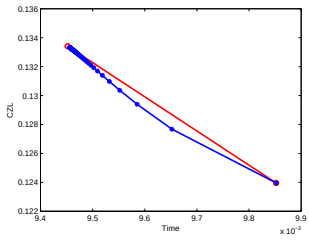	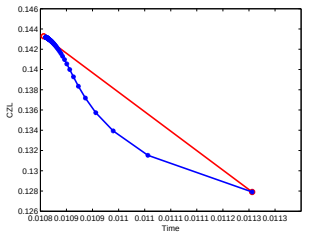
3	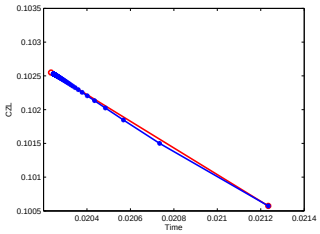	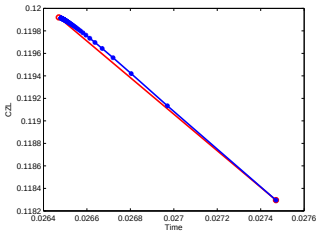	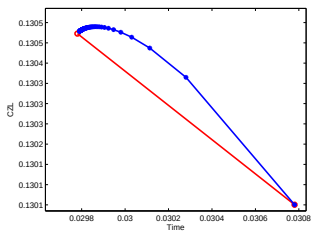
2.1	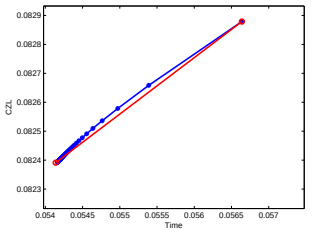	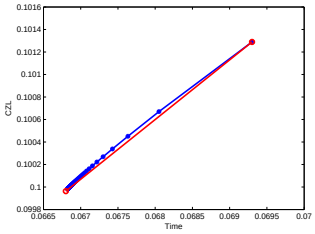	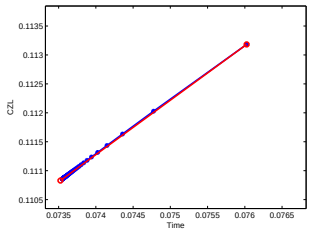
2.01	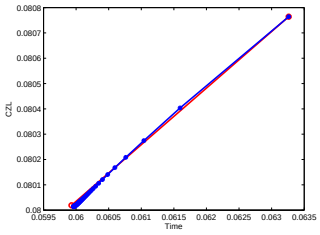	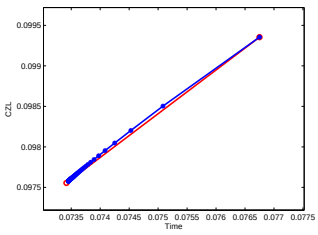	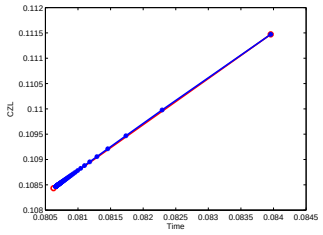
1.99	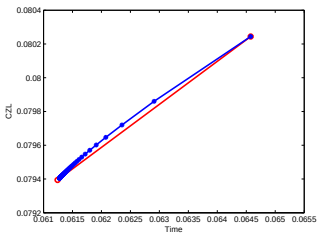	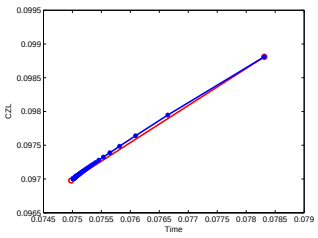	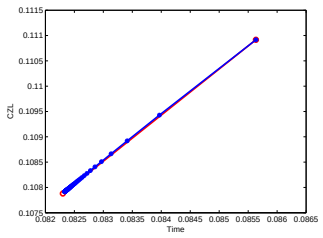

b \ β	$\frac{b}{2}$	$\frac{b}{4}$	$\frac{b}{8}$
1	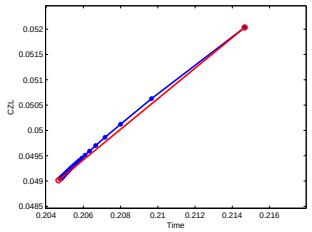	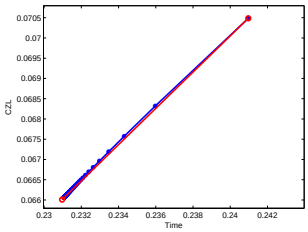	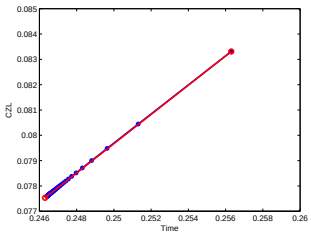
0.75	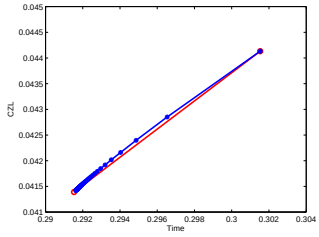	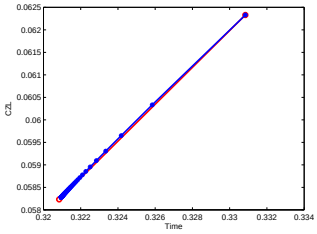	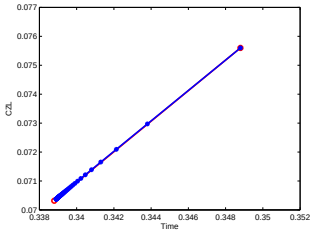

Evidently, when we assume that the material behaves as a linear viscoelastic material, we have continuity of the CZ length at $t = t_d$ for all sets of parameters considered. This stability at the onset of crack growth holds in the elastic case for $\beta = \frac{b}{2}$, as demonstrated in Table 9.1. On the other hand, as β decreases $\left(\text{i.e. for } \beta = \frac{b}{4} \text{ and } \beta = \frac{b}{8}\right)$, there is unstable crack growth as the crack begins to propagate for some cases of b. It is observed that this instability becomes more pronounced as b increases.

Chapter 10

Conclusions and Ideas for Further Research

10.1 Conclusions

A modified version of the Dugdale-Leonov-Panasyuk (DLP) cohesive zone (CZ) model was developed in this thesis. The model problem consists of a time- dependent CZ condition which is in the form of an Abel type integral equation. The unknown function in the integrand is the stress in the CZ. This integral equation depends on the stress ahead of the CZ. The formula which computes these stresses was formulated using results by Muskhelishvili, see [44]. Furthermore, for this stress to be bounded at the CZ tip, the stress intensity factor is assumed to be zero there.

The two main material parameters in the model problem are the exponent in the power-type durability curve, b, and the exponent in the accumulation law, β. The CZ defined in the model problem can exist only if $0 < \beta < b$. We mainly implemented the algorithm for

the set of parameters $\beta = \frac{b}{2}$, $\beta = \frac{b}{4}$ and $\beta = \frac{b}{8}$ and used $b = 4$ and $b = 1.5$. Two stages were thoroughly analysed: (i) the stage of a stationary crack; and (ii) the stage of a crack propagating in time.

For the stationary crack stage, we used a numerical method to study how the CZ tip moves with time and how the stress influences this movement. This numerical method was based on a discrete time mesh and assumed zero stress intensity factor. Applying the secant method, we obtain the CZ tip coordinate, the stress in the CZ and the stress ahead of the CZ. We used the general solution of an Abel type integral equation to find the stress in the CZ. When $b = 4$, the CZ length grows more rapidly with time as β increases; whereas when $b = 1.5$, the CZ length grows more rapidly with time as β decreases. We can see from Figures 4.3 and 4.4 that for a specific point in space, the stress increases while this point is ahead of the CZ tip then reaches a maximum at the CZ tip and monotonically decreases with the distance from the tip.

After that, we looked at the crack opening especially the opening at the crack tip. To obtain the crack opening, we made use of the formulas in the DLP approach where necessary modifications were made, namely including the time and history dependence of the CZ stress and crack length. We first considered the case when the bulk of the material acts elastically and then used a time- dependent Volterra integral operator to arrive at the crack tip opening in the case of having a viscoelastic material. As expected, we have an increase, with time, of the crack tip opening. Moreover, for both cases of b considered, as β increases the crack tip opening increases more rapidly with time. The obtained graphs demonstrate that the crack opens at a higher rate in the viscoelastic case than in the elastic case.

Subsequently, the crack initiation stage, and thus the crack propagation stage, were considered. The crack tip opening is very important in order to predict when the crack will propagate. The crack begins to grow when the crack tip opening reaches a critical value. The time instant when this occurs is referred to as the delay time t_d. For all times following

t_d, the crack is in it's propagating stage. This condition for crack growth holds for both the elastic and viscoelastic cases.

Consequently, under such assumptions, we can find the crack length as well as the CZ length with respect to time. This was carried out by modifying the algorithm used for a stationary crack by allowing the crack length a to be a function depending on time. For the growing crack stage, $t > t_d$, we can see that the crack growth rate increases, while the CZ length decreases with time. The time, when the CZ length becomes zero seems to coincide with the time when the crack length becomes infinite and can be associated with the complete fracture of the body.

The parameter β has a larger effect on the cohesive zone length during the propagating crack stage compared to the stationary crack stage. Furthermore, in the propagating crack stage, the crack grows more rapidly with time as β decreases; and so it can also be concluded that as β decreases, the rupture time also decreases.

An interesting observation made was regarding the delay time and the rupture time as we change the set of values taken for b and β. The delay time t_d is higher for the elastic case than for the viscoelastic case. The rupture time in the viscoelastic case is slightly smaller than that for the purely elastic case. Also, as b and β become further apart, the maximum CZ length reached increases.

It has been noticed that for the elastic case with $b = 4$, $\beta = \dfrac{1}{2}$, we have unstable crack growth as crack propagation initiates. This is accompanied by a significant drop of the CZ length during the first time step, t_{d^+} of crack growth. Studying the limiting value of the crack length, we conclude that the crack length does not tend to its normalised value of 1 as t_{d^+} approached t_d. The following steps for this case indicate the occurrence of stable crack growth. Moreover, for the other cases of the parameters, we have stable crack growth with the crack length at the onset of crack growth approaching $a_0 = 1$ as t_{d^+} approaches t_d.

The problem with an external load varying linearly in time was also considered. While the crack is stationary, considering a variable load produces a slower rate of CZ growth compared to the case of considering a constant load. Evidently, the crack tip opening increases more rapidly in the constant loading case for both the elastic and viscoelastic materials. For the variable loading case, the delay time is larger than in the constant loading case. This effect is more conspicuous when $b = 4$ compared to when $b = 1.5$. Additionally, from Figures 7.10-7.17, we discover that the difference between the curves for the three cases of β is minor when $b = 4$ compared to when $b = 1.5$. In other words, decreasing the value of β does not have a significant effect on the rupture time of the body when $b = 4$. On the other hand, when $b = 1.5$, there is a clear difference in the rupture time for the different cases of β considered.

Last, but not least, the numerical convergence rate was studied for the numerical solutions obtained. The convergence rates, as well as the approximation of the error, were obtained by using Aitken's extrapolation technique. We can conclude that for the stationary crack stage, as well as the propagating crack stage, we have convergence of all computed values as the mesh becomes finer, except for the stress at the CZ tip when the difference between β and b is sufficiently small. The very slow convergence (almost non-convergence) of the stress at the CZ tip, when $\beta = \dfrac{3b}{4}$ and $\dfrac{b}{2}$, may be a manifestation of a CZ tip stress singularity, at some range of values for the parameter β. Although the square root singularity has been eliminated in the model by the requirement that the corresponding stress intensity factor at the CZ tip is zero, a singularity of a different order may still be present there, however this needs a separate analysis, which is an open problem.

10.2 Ideas for Further Research

Although fracture mechanics is a relatively prevalent subject, much still remains to be discovered. Issues such as creep, and time dependence contain open problems of high importance, some of which are mentioned below.

(a) Multiple cracks: It is very interesting to study the behaviour of cohesive zones in materials which contain not one but multiple cracks which are collinear. The equations modelling such geometrical representation of cracks will be different to those used for a single crack, see [39].

(b) Problems of other varying external loads in time: By using a linear function in time for the external load for this thesis, we were thinking about how the solutions would change if a different function was used for the external load. Such dependence of the variable load on time could involve sinusoidal functions to demonstrate a periodic effect of the load on the material. Also, another idea is to consider an impulsive load.

(c) Energy release rate: An open problem is to study the energy release rate for the time-dependent CZ model. The amount of fracture energy dissipated during crack growth depends on the CZ model considered.

(d) The stress at the CZ tip is of great interest. As mentioned in the conclusion, there could be other singularities at the CZ tip which haven't been removed.

(e) An intriguing thought, whilst applying the problems in this thesis to the material PMMA, involves how other materials behave when having a time and history dependent CZ model. Various polymers could be considered and therefore the change of parameters, used in Section 5.2.2, will have an effect on the solutions obtained in the viscoelastic case.

Bibliography

[1] Alten F., Grandt Jr., *Fundamentals of Structural Integrity: Damage Tolerant Design and Nondestructive Evaluation*, John Wiley and Sons, Canada, 2004

[2] Anderson T.L., *Fracture Mechanics: Fundamentals and Applications*, CRC Press, USA, 2005

[3] Antia H.M., *Numerical Methods for Scientists and Engineers Vol. 1*, Springer, USA, 2002

[4] Ashrafi H., Farid M., *A mathematical boundary integral equation analysis of standard viscoelastic solid polymers*, Computational Mathematics and Modeling, Vol. 20, Issue 4, pp. 397-415, 2009

[5] Barenblatt G.I., *The Mathematical Theory of Equilibrium Cracks in Brittle Fracture*, In: Advances in Applied Mechanics, edited by Lemm J.M., Vol. 7 pp. 55-129, 1962

[6] Baẑant Z.P. Oh B.H., *Crack Band Theory for Fracture of Concrete*, Material and Structures, Vol. 16 pp. 155-177, 1983

[7] Beerends R.J., ter Morsche H.G., van den Berg J.C., van de Vrie E.M., *Fourier and Laplace Transforms*, Cambridge University Press, USA, 2003

[8] Betten J., *Creep Mechanics 3rd Edition*, Springer, Germany, 2008

[9] Brezinski C., Zaglia M.R., *Generalizations of Aitken's Process for Accelerating the Convergence of Sequences*, Computational and Applied Mathematics, Vol. 26 pp. 171-189, 2007

[10] Campbell F.C., *Fatigue and Fracture: Understanding the Basics*, ASM International, USA, 2012

[11] Borst R.D., Gutiérrez M.A., Wells G.N., Remmers J.J.C., Askes H., *Cohesive Zone Models, Higher Order Continuum Theories and Reliability Methods for Computational Failure Analysis*, International Journal for Numerical Methods in Engineering, Vol. 60 pp. 289-315, 2004

[12] Bultheel A., Cools R., *The Birth of Numerical Analysis*, World Scientific Publishing Company, Singapore, 2010

[13] Broek D., *The Practical Use of Fracture Mechanics*, Springer, The Netherlands, 1989

[14] Camacho G.T., Ortiz M., *Computational Modelling of Impact Damage in Brittle Materials*, International Journal of Solids and Structures, Vol. 33 pp. 2899-2938, 1996

[15] Carter B.C., Norton G.M., *Ceramic Materials: Science and Engineering*, Springer, USA, 2007

[16] Chandra N., Li H., Shet C., Ghonem H, *Some Issues in the Application of Cohesive Zone Models for Metal Ceramic Interfaces*, International Journal of Solids and Structures, Vol. 39 pp. 2827-2855, 2002

[17] Cotterell B., *Fracture and life*, World Scientific, Singapore, 2010

[18] Dahlquist G., Björck. A , *Numerical Methods*, Dover Publications, USA, 2003

[19] Dugdale D.S., *Yielding of Steel Sheets Containing Slits*, Journal of the Mechanics and Physics of Solids, Vol. 8 pp. 100-104, 1960

[20] Flügge W., *Viscoelasticity*, Blaisdell Publishing Company, USA, 1967

[21] Gorenflo R., Vessella S., *Abel Integral Equations Analysis and Aplications*, Springer Berlin Heidelberg, Berlin, 1991

[22] Geubelle P.H, Baylor J.S., *Impact-Induced Delamination of Composites: A 2D Simulation*, Composites Part B Engineering, Elsevier Science Ltd., Vol. 29 pp 589-602, 1998

[23] Hakim L., Mikhailov S.E. *Cohesive Zone Models in History Dependent Materials*, Proceedings, International Conference on Computational Mechanics 2013, CM13., Durham, England, 25-27 March, 2013

[24] Hakim L., Mikhailov S.E. *Integral Equations in Cohesive Zones Modelling of Fracture in History Dependent Materials*, Proceedings, World Congress on Engineering 2013, WCE 2013., Newswood Limited, International Association of Engineers, pp. 226-231, 2013

[25] Hakim L, Mikhailov S.E., *Nonlinear Abel Type Integral Equation in Modelling Creep Crack Propagation*, Integral Methods in Science and Engineering: Computational and Analytic Aspects, edited by Constanda C. and Harris P., Springer, pp. 191-201, 2011

[26] Hakim L., Mikhailov S.E., *Numerical Implementation of a Cohesive Zones in History-Dependent Materials*, arXiv:1403.3708, 2014

[27] Hillerborg A., Modeer R.M., Petersson P.E., *Analysis of Crack Formation and Crack Growth in Concrete by Means of Fracture Mechanics and Finite Elements*, Cement and Concrete Research, Division of Building Materials Lund Institute of Technology, Vol. 6 pp. 773-782, 1976

[28] Irwin G.R., *Fracture Dynamics, Fracturing of Metals*, Proceedings of the ASM Symposium on Fracturing of Metals, pp. 147-166, 1948

[29] Knauss W.G. *Time Dependent Fracture and Cohesive Zones*, Journal of Engineering Materials and Technology, ASME, Vol. 115 pp. 262-267, 1993

[30] Kobayashi H., Takahashi H., Hiki Y. *Viscosity Measurement of Organic Glasses Below and Above Glass Transition Temperature*, Journal of Non-Crystalline Solids, Vol. 290, pp. 32-40, 2001

[31] Koekoek R., Lesky P.A., Swarttouw R.F., *Hypergeometric Orthogonal Polynomials and Their Q-Analogues*, Springer, Germany, 2010

[32] Lawn B.R., Wilshaw T.R., *Fracture of Brittle Solids*, Cambridge University Press, England, 1975

[33] Leonov M.Ya., Panasyuk V.V., *Development of the Smallest Cracks in the Solid*, Applied Mechanics (Prikladnaya Mekhanika), Vol. 5, pp. 391-401, 1959

[34] Maischak M., *A Priori Error Estimates and Convergence*, Lecture Notes for MA5501, Brunel University, 2011

[35] Mark J.E., *Polymer Data Handbook*, Oxford University Press, New York, 1999

[36] McCartney L.N., *Crack-Growth Predictions for Viscoelastic Materials Exhibiting Non-Uniform Craze Deformation*, International Journal of Fracture, Vol. 37 pp. 279-301, 1988

[37] Mckenna G.B., Crissman J. M., *A Reduced Variable Approach to Relating Creep and Creep Rupture in PMMA*, MRS Proceedings, Vol. 79, pp. 333-343, 1986

[38] Mikhailov S.E., *Mechanics of Solids and Fracture*, Lecture Notes, London Taught Course Centre, 2008

[39] Mikhailov S. E., Namestnikova I. V., *Application of Local and Non-Local Approaches to Multiple Fatigue Crack Initiation and Propagation*, Proceedings of ESIS International Conference on Fatigue Crack Paths, Parma, Italy, 2003

[40] Mikhailov S. E., Namestnikova I. V., *History-Sensitive Accumulation Rules for Life-Time Prediction under Variable Loading*, Archive of Applied Mechanics, Vol. 81 pp. 1679-1696, 2011

[41] Mikhailov S.E., Namestnikova I.V., *Local and Non-Local Approaches to Creep Crack Initiation and Propagation*, Proceedings of the 9th International Conference on the Mechanical Behaviour of Materials, Geneva, Switzerland, 2003

[42] Mikhailov S.E., Namestnikova I.V., *Local and Non-Local Approaches to Fatigue Crack Initiation and Propagation*, IUTAM Symposium on Asymptotics, Singularities and Homogenisation in Problems of Mechanics, edited by A.B. Movchan, Solid Mechanics and Its Applications, Vol. 113, pp. 285-294, 2003

[43] Mikhailov S.E. *Theoretical Backgrounds of Durability Analysis by Normalized Equivalent Stress Functionals*, Mathematics and Mechanics of Solids, Vol. 8 pp 105-142, 2003

[44] Muskhelishvili N.I., *Some Basic Problems of the Mathematical Theory of Elasticity*, Springer, The Netherlands, 1977

[45] Orowan E., *Fracture and Strength of Solids*, Reports on Progress in Physics, Vol. 12 pp. 185-232, 1949

[46] Ortiz M., Pandolfi A., *Finite-Deformation Irreversible Cohesive Elements for Three-Dimensional Crack-Propagatin Analysis*, International Journal for Numerical Methods in Engineering, Vol. 44 pp. 1267-1282, 1999

[47] Penny R.K., Marriott D.L., *Design for Creep*, McGraw-Hill Book Company Ltd., UK, 1971

[48] Quarteroni A., Sacco R., *Numerical Mathematics (Texts in Applied Mathematics)*, Springer, Berlin, 2007

[49] Rabinowitz S., Brown N., *Young's Modulus of Polyethylene in the Microstrain Region*, Journal of Polymer Science Part B: Polymer Physics, Vol. 39 Issue 20 pp. 2420-2429, 2011

[50] Rice J.R., *Mathematical Analysis in the Mechanics of Fracture*, In: Fracture: An Advanced Treatise, edited by Liebowitz H., Vol. 2 pp. 191-311, *Academic Press*, New York, 1968

[51] Rabotnov, Y.N., *Creep Problems in Structural Members (North-Holland Series in Applied Mathematics & Mechanics)*, Elsevier Science Publishing Co Inc., USA, 1969

[52] Rabotnov Yu. N. *Elements of hereditary solid mechanics*, Mir Publishers; [Rev. from the 1977 Russian ed.], Moscow, 1977

[53] Runborg O., *Numerical Solutions of Differential Equations*, Lecture Notes, Royal Institute of Technology, 2012

[54] Savin G.N., *Stress Concentration Around Holes*, Pergamon Press, USA, 1961

[55] Schapery R.A., *Correspondence Principles and a Generalised J-integral for Large Deformation and Fracture Analysis of Viscoelastic Media*, International Journal of Fracture, Vol. 25 pp. 195-223, 1984

[56] Sharpe Jr., William N., *Springer Handbook of Experimental Solid Mechanics*, Springer, USA, 2008

[57] Spencer A.J.M., *Continuum Mechanics*, Dover Publications, London, 1980

[58] Tvergaard V., Hutchinson J. W., *The Relation Between Crack Growth Resistance and Fracture Process Parameters in Elastic-Plastic Solids*, Journal of the Mechanics and Physics of Solids, Vol. 40 pp. 1377-1397, 1992

[59] Williams J.G., Hadavinia H., *Analytical Solutions for Cohesive Zone Models*, Journal of the Mechanics and Physics of Solids, Vol. 50 pp. 809-825, Great Britain, 2001

[60] Xu X.P., Needleman A., *Numerical Simulation of Fast Crack Growth in Brittle Solids*, Journal of the Mechanics and Physics of Solids, Vol. 42 pp. 1397-1434, 1994

[61] Yoon C., Allen D.H., *Damage Dependent Constitutive Behavior and Energy Release Rate for a Cohesive Zone in a Thermoviscoelastic Solid*, International Journal of Fracture, Vol. 96 pp. 55-74, 1999

[62] www.ami.ac.uk/courses/topics/0124_seom/index.html, (Accessed 12th November 2009)

[63] http://functions.wolfram.com/HypergeometricFunctions/Hypergeometric2F1/03/, (Accessed 18th November 2011)

[64] http://www.matbase.com/material/polymers/commodity/pmma/properties, (Accessed 13th November 2011)

[65] http://www.ndt-ed.org/EducationResources/CommunityCollege/Materials/Mechanical/FractureToughness.htm, (Accessed 1st October 2010)

Appendix A

Continuity of the Stress in the Cohesive Zone

Let us now analyse the behaviour of the solution of (4.1) for $\sigma(x,t)$ as $t \to t_c(x)+0$. We have the following

$$\begin{aligned}
&\lim_{t\to t_c(x)+0} \sigma^\beta(x,t) \\
&= \lim_{t\to t_c(x)+0} -\frac{1}{\pi}\sin\left(\pi\frac{\beta}{b}\right)\left[\sum_{l=1}^{c}\sigma^\beta(x,t_{l-1})\left(V(t_{l-1},t,t_c(x))-V(t_l,t,t_c(x))\right)\right. \\
&+\frac{b}{\beta}\left(\frac{\sigma^\beta(x,t_l)-\sigma^\beta(x,t_{l-1})}{t_l-t_{l-1}}\right)\bullet \\
&\left.\left(W(t_{l-1},t,t_c(x))-W(t_l,t,t_c(x))-\frac{\beta}{b}(t_l-t_{l-1})V(t_l,t,t_c(x))\right)\right]. \qquad \text{(A.1)}
\end{aligned}$$

In the above formula, only $V(t_l,t,t_c(x))$ and $W(t_l,t,t_c(x))$ depend on t. Moreover, since $\beta>0$, from (4.8) and (4.9) we have for any t,

$$V(t_c,t,t_c)=\pi\csc\left(\pi\frac{\beta}{b}\right), \quad W(t_c,t,t_c)=0.$$

For the case when $l \neq c$, we have

$$\begin{aligned}\lim_{t\to t_c+0} V(t_l,t,t_c) &= \lim_{t\to t_c+0}\left\{\pi\csc\left(\pi\frac{\beta}{b}\right)-\frac{b}{\beta}\left(\frac{t_c-t_l}{t-t_l}\right)^{\frac{\beta}{b}}\ {}_2F_1\left[\frac{\beta}{b},\frac{\beta}{b};1+\frac{\beta}{b};\frac{t_c-t_l}{t-t_l}\right]\right\}\\ &= \pi\csc\left(\pi\frac{\beta}{b}\right)-\frac{b}{\beta}\Gamma\left[1+\frac{\beta}{b}\right]\Gamma\left[1-\frac{\beta}{b}\right]\\ &= \pi\csc\left(\pi\frac{\beta}{b}\right)-\frac{b}{\beta}\left(\pi\frac{\beta}{b}\csc\left(\pi\frac{\beta}{b}\right)\right)=0,\end{aligned}$$

$$\begin{aligned}&\lim_{t\to t_c+0} W(t_l,t,t_c)\\ &= \lim_{t\to t_c+0}\left\{\frac{\beta}{b}\pi\csc\left(\pi\frac{\beta}{b}\right)(t-t_l)-\frac{1}{1+\frac{\beta}{b}}(t_c-t_l)^{1+\frac{\beta}{b}}(t-t_l)^{-\frac{\beta}{b}}\ {}_2F_1\left[1+\frac{\beta}{b},\frac{\beta}{b};2+\frac{\beta}{b};\frac{t_c-t_l}{t-t_l}\right]\right\}\\ &= \frac{\beta}{b}\pi\csc\left(\pi\frac{\beta}{b}\right)(t_c-t_l)-\frac{1}{1+\frac{\beta}{b}}(t_c-t_l)\Gamma\left[2+\frac{\beta}{b}\right]\Gamma\left[1-\frac{\beta}{b}\right]\\ &= \frac{\beta}{b}\pi\csc\left(\pi\frac{\beta}{b}\right)(t_c-t_l)-\frac{\beta}{b}\pi(t_c-t_l)\csc\left(\pi\frac{\beta}{b}\right)=0,\end{aligned}$$

where we have used that

$${}_2F_1[a,b,c,1]=\frac{\Gamma[c]\Gamma[c-a-b]}{\Gamma[c-a]\Gamma[c-b]},$$

as well as other properties of the Gamma function such as

$$\Gamma[z+1]=z\Gamma[z]\quad\text{and}\quad\Gamma[1-z]\Gamma[z]=\pi\csc[(\pi z)].$$

Consequently, in equation (A.1), the summation over l yields

$$\begin{aligned}\lim_{t\to t_c(x)+0}\sigma^\beta(x,t) = -\frac{1}{\pi}\sin\left(\pi\frac{\beta}{b}\right)\Bigg[&-\pi\csc\left(\pi\frac{\beta}{b}\right)\sigma^\beta(x,t_{c-1})+\\ &\frac{b}{\beta}\cdot\frac{\sigma^\beta(x,t_c(x))-\sigma^\beta(x,t_{c-1})}{t_c(x)-t_{c-1}}\left(\frac{\beta}{b}(t_c(x)-t_{c-1})\pi\csc\left(\pi\frac{\beta}{b}\right)\right)\Bigg]=\sigma^\beta(x,t_c(x)).\end{aligned}$$

Therefore, $\lim_{t\to t_c(x)+0}\sigma^\beta(x,t)=\sigma^\beta(x,t_c(x))$ for $0<\beta<b$.

Appendix B

Graphs of Solutions using Various Meshes

In this section, we present the solutions obtained for the problems considered during the stationary crack stage as well as the propagating crack stage. For each of the cases, we will present the solutions for $b = 4$ to begin with, then the solutions for $b = 1.5$ will follow. The caption of the graphs and tables indicate the parameter sets.

From these graphs, we can see that the solutions obtained converge as we take more points in the mesh.

B.1 Constant Loading

Cohesive Zone Tip Coordinate

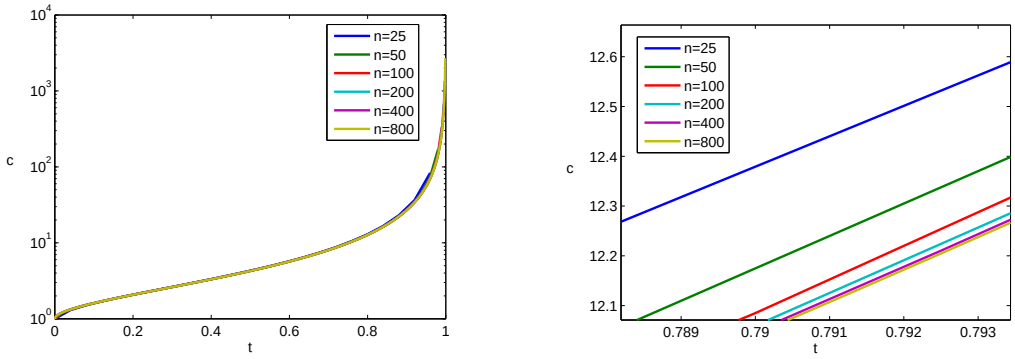

Figure B.1: CZ tip coordinate vs. time for $b = 4$, $\beta = \frac{b}{2}$.

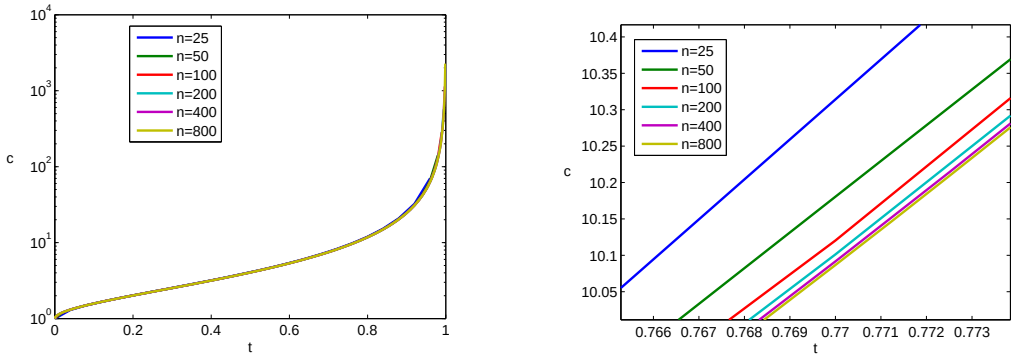

Figure B.2: CZ tip coordinate vs. time for $b = 4$, $\beta = \frac{b}{4}$.

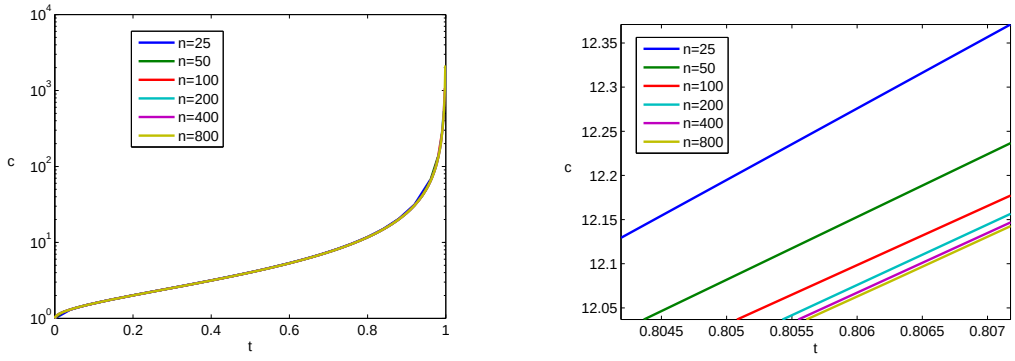

Figure B.3: CZ tip coordinate vs. time for $b = 4$, $\beta = \frac{b}{8}$.

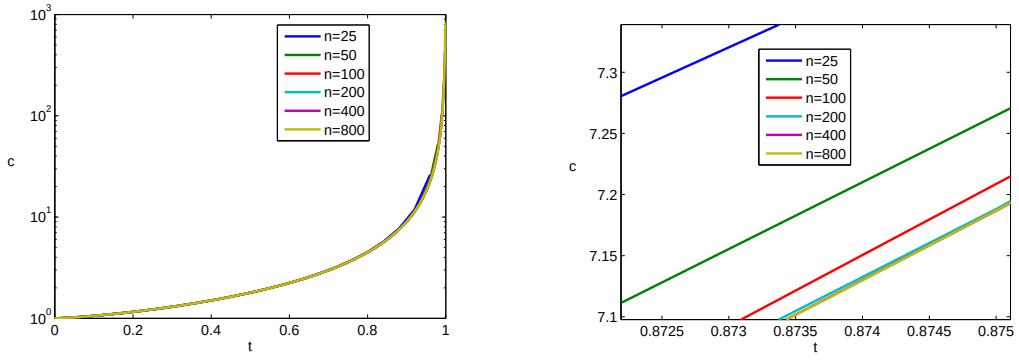

Figure B.4: CZ tip coordinate vs. time for $b = 1.5$, $\beta = \dfrac{b}{2}$.

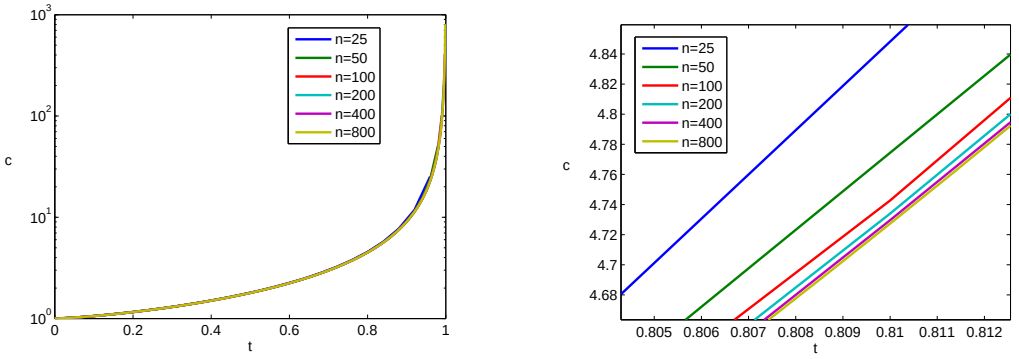

Figure B.5: CZ tip coordinate vs. time for $b = 1.5$, $\beta = \dfrac{b}{4}$.

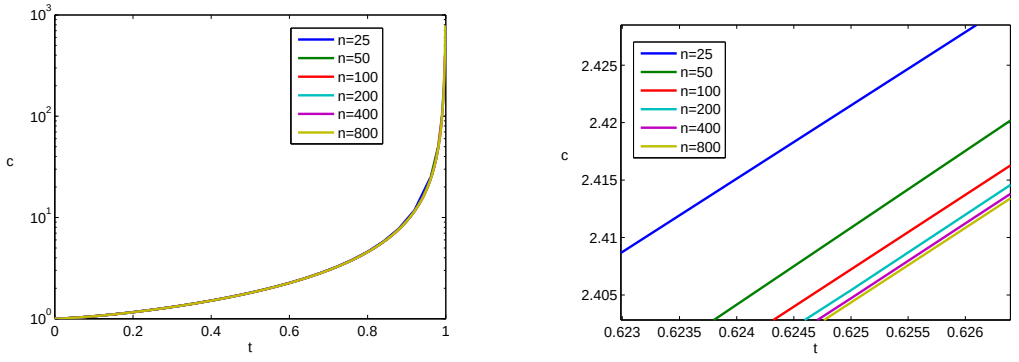

Figure B.6: CZ tip coordinate vs. time for $b = 1.5$, $\beta = \dfrac{b}{8}$.

Stresses

The Case $b = 4$ $\beta = \dfrac{3b}{4}$

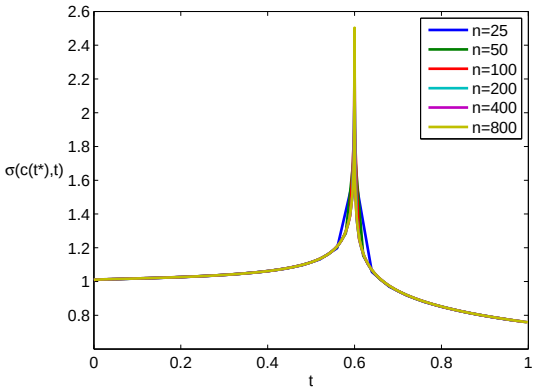

Figure B.7: $\sigma(c(t^*), t)$ vs. time for $b = 4$, $\beta = \dfrac{3b}{4}$, $t^* = 0.6$: global picture.

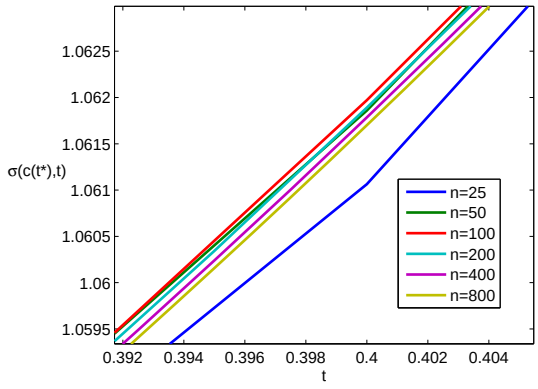

Figure B.8: $\sigma(c(t^*), t)$ for $b = 4$, $\beta = \dfrac{3b}{4}$, $t^* = 0.6$: closer look ahead of the CZ ($t < t^*$).

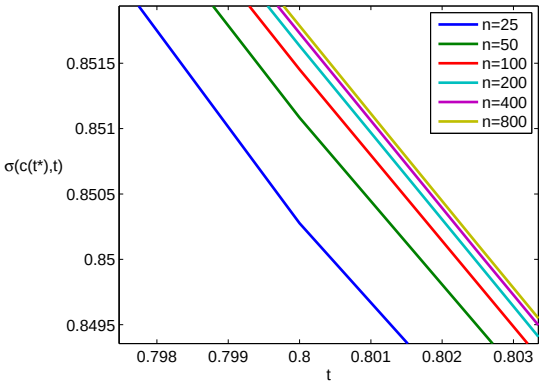

Figure B.9: $\sigma(c(t^*), t)$ for $b = 4$, $\beta = \dfrac{3b}{4}$, $t^* = 0.6$: closer look in the CZ ($t > t^*$).

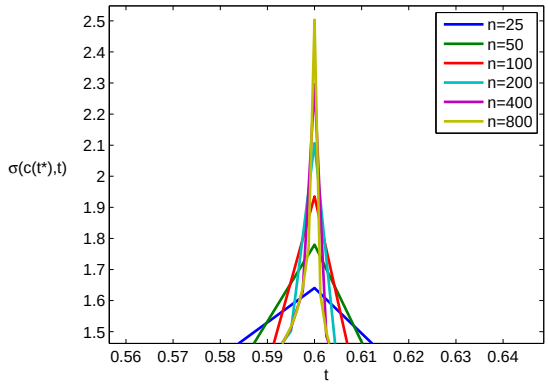

Figure B.10: $\sigma(c(t^*), t)$ for $b = 4$, $\beta = \dfrac{3b}{4}$, $t^* = 0.6$: closer look at the CZ tip (near t^*).

The Case $b = 4$ $\beta = \dfrac{b}{2}$

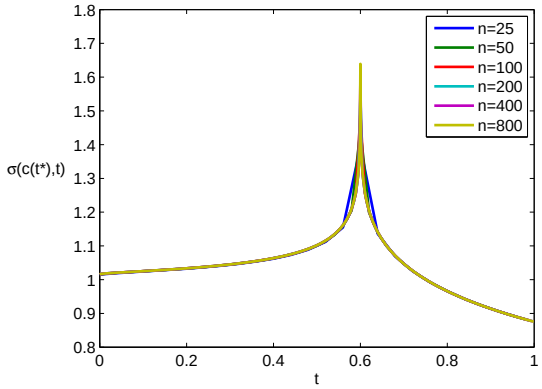

Figure B.11: $\sigma(c(t^*), t)$ vs. time for $b = 4$, $\beta = \dfrac{b}{2}$, $t^* = 0.6$: global picture.

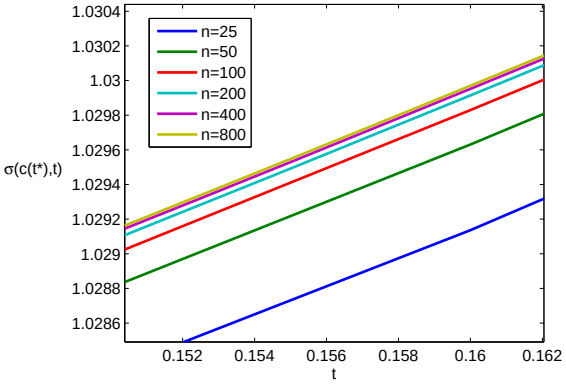

Figure B.12: $\sigma(c(t^*), t)$ for $b = 4$, $\beta = \dfrac{b}{2}$, $t^* = 0.6$: closer look ahead of the CZ ($t < t^*$).

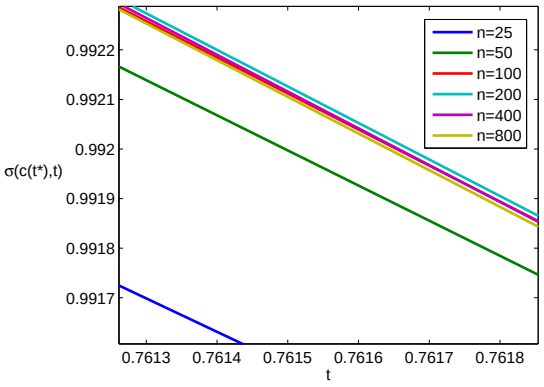

Figure B.13: $\sigma(c(t^*), t)$ for $b = 4$, $\beta = \dfrac{b}{2}$, $t^* = 0.6$: closer look in the CZ ($t > t^*$).

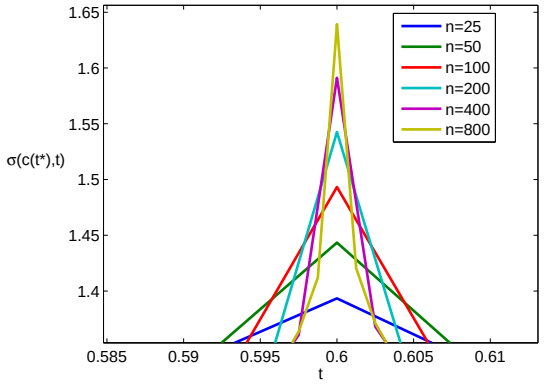

Figure B.14: $\sigma(c(t^*), t)$ for $b = 4$, $\beta = \dfrac{b}{2}$, $t^* = 0.6$: closer look at the CZ tip (near t^*).

The Case $b = 4$ $\beta = \frac{b}{3}$

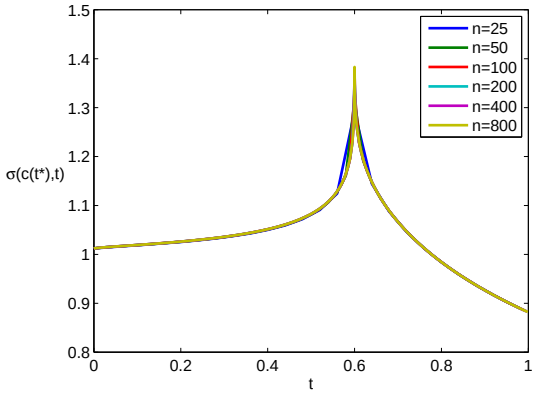

Figure B.15: $\sigma(c(t^*), t)$ vs. time for $b = 4$, $\beta = \frac{b}{3}$, $t^* = 0.6$: global picture.

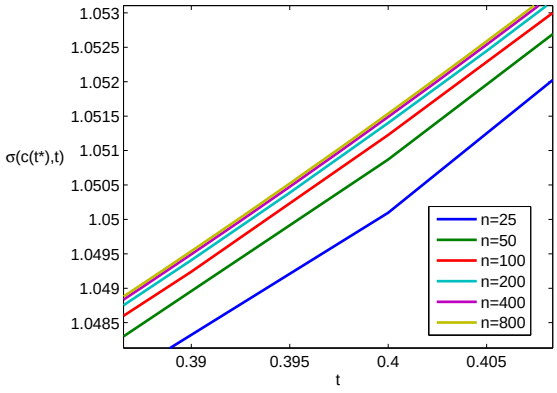

Figure B.16: $\sigma(c(t^*), t)$ for $b = 4$, $\beta = \frac{b}{3}$, $t^* = 0.6$: closer look ahead of the CZ ($t < t^*$).

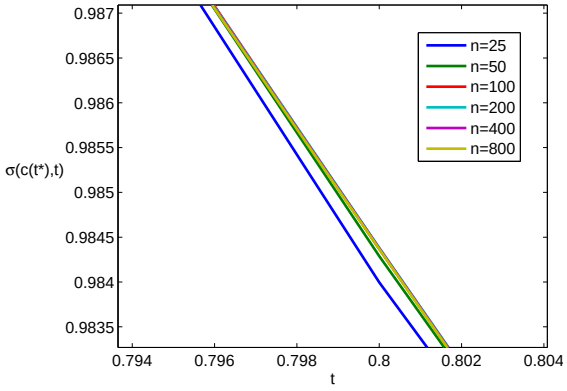

Figure B.17: $\sigma(c(t^*), t)$ for $b = 4$, $\beta = \frac{b}{3}$, $t^* = 0.6$: closer look in the CZ ($t > t^*$).

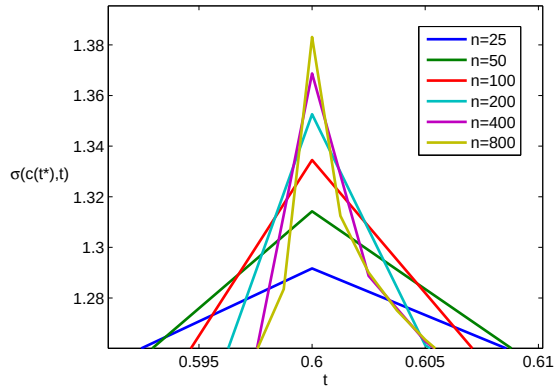

Figure B.18: $\sigma(c(t^*), t)$ for $b = 4$, $\beta = \frac{b}{3}$, $t^* = 0.6$: closer look at the CZ tip (near t^*).

The Case $b = 4$ $\beta = \dfrac{b}{4}$

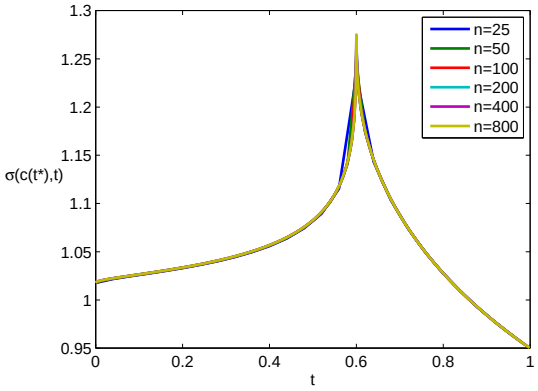

Figure B.19: $\sigma(c(t^*), t)$ vs. time for $b = 4$, $\beta = \dfrac{b}{4}$, $t^* = 0.6$: global picture.

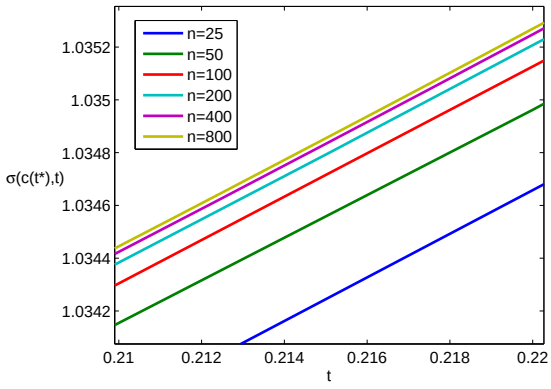

Figure B.20: $\sigma(c(t^*), t)$ for $b = 4$, $\beta = \dfrac{b}{4}$, $t^* = 0.6$: closer look ahead of the CZ ($t < t^*$).

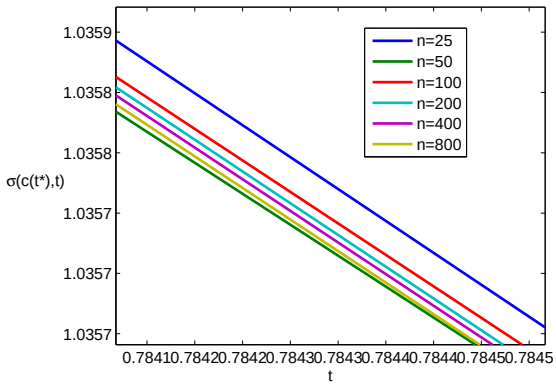

Figure B.21: $\sigma(c(t^*), t)$ for $b = 4$, $\beta = \dfrac{b}{4}$, $t^* = 0.6$: closer look in the CZ ($t > t^*$).

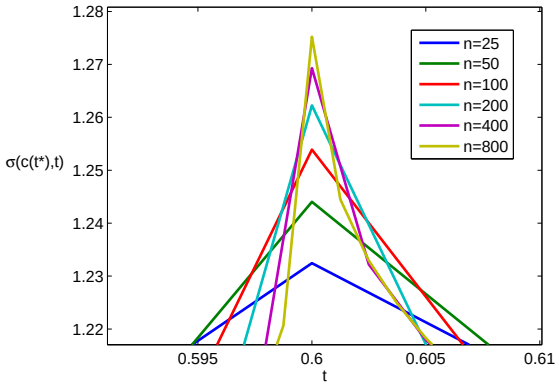

Figure B.22: $\sigma(c(t^*), t)$ for $b = 4$, $\beta = \dfrac{b}{4}$, $t^* = 0.6$: closer look at the CZ tip (near t^*).

The Case $b = 4$ $\beta = \dfrac{b}{8}$

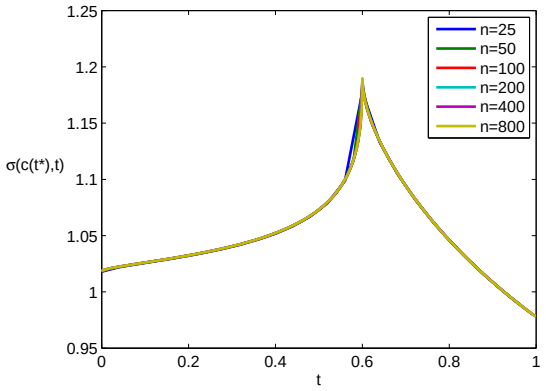

Figure B.23: $\sigma(c(t^*), t)$ vs. time for $b = 4$, $\beta = \dfrac{b}{8}$, $t^* = 0.6$: global picture.

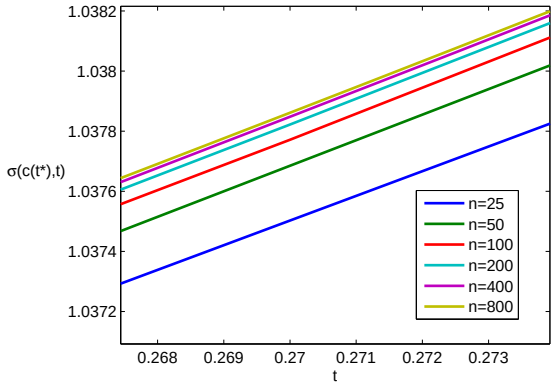

Figure B.24: $\sigma(c(t^*), t)$ for $b = 4$, $\beta = \dfrac{b}{8}$, $t^* = 0.6$: closer look ahead of the CZ ($t < t^*$).

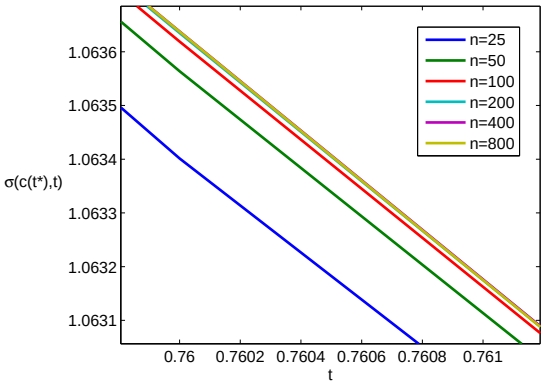

Figure B.25: $\sigma(c(t^*), t)$ for $b = 4$, $\beta = \dfrac{b}{8}$, $t^* = 0.6$: closer look in the CZ ($t > t^*$).

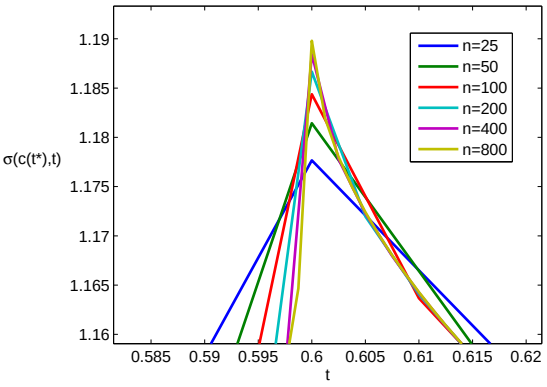

Figure B.26: $\sigma(c(t^*), t)$ for $b = 4$, $\beta = \dfrac{b}{8}$, $t^* = 0.6$: closer look at the CZ tip (near t^*).

The Case $b = 1.5$, $\beta = \dfrac{3b}{4}$

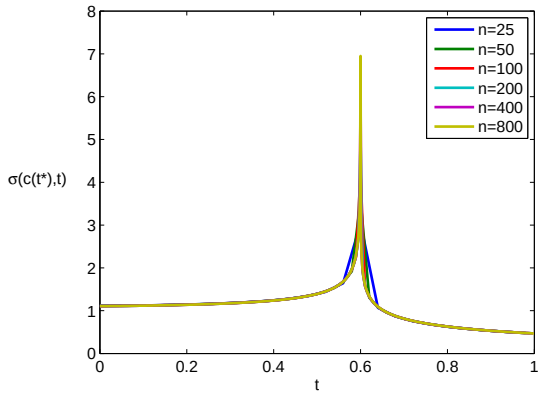

Figure B.27: $\sigma(c(t^*), t)$ vs. time for $b = 1.5$, $\beta = \dfrac{3b}{4}$, $t^* = 0.6$: global picture.

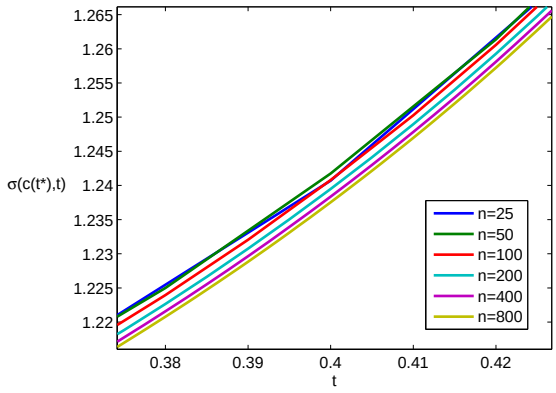

Figure B.28: $\sigma(c(t^*), t)$ for $b = 1.5$, $\beta = \dfrac{3b}{4}$, $t^* = 0.6$: closer look ahead of the CZ ($t < t^*$).

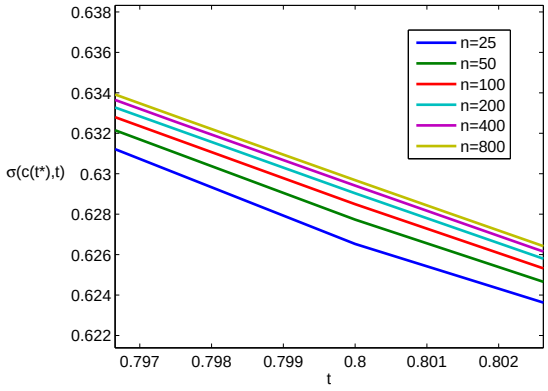

Figure B.29: $\sigma(c(t^*), t)$ for $b = 1.5$, $\beta = \dfrac{3b}{4}$, $t^* = 0.6$: closer look in the CZ ($t > t^*$).

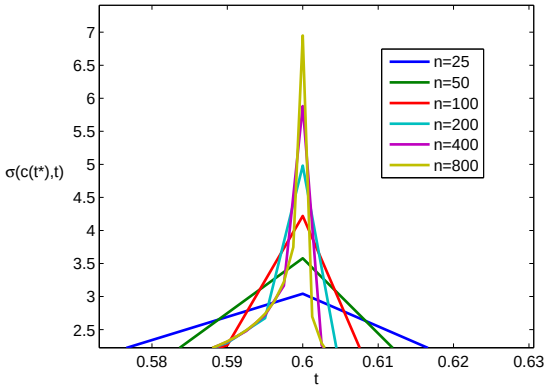

Figure B.30: $\sigma(c(t^*), t)$ for $b = 1.5$, $\beta = \dfrac{3b}{4}$, $t^* = 0.6$: closer look at the CZ tip (near t^*).

The Case $b = 1.5$ $\beta = \dfrac{b}{2}$

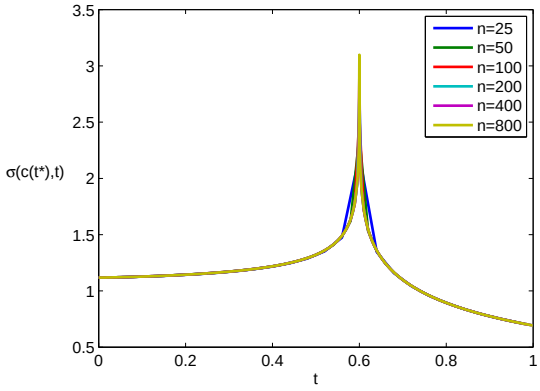

Figure B.31: $\sigma(c(t^*), t)$ vs. time for $b = 1.5$, $\beta = \dfrac{b}{2}$, $t^* = 0.6$: global picture.

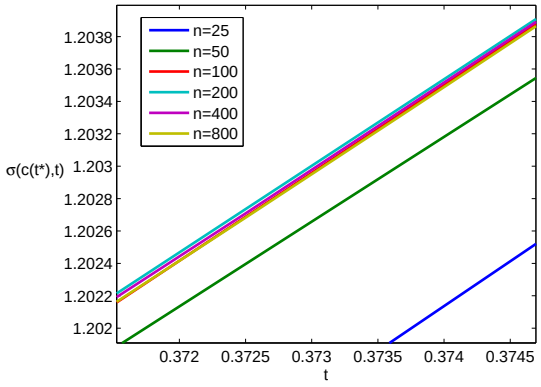

Figure B.32: $\sigma(c(t^*), t)$ for $b = 1.5$, $\beta = \dfrac{b}{2}$, $t^* = 0.6$: closer look ahead of the CZ ($t < t^*$).

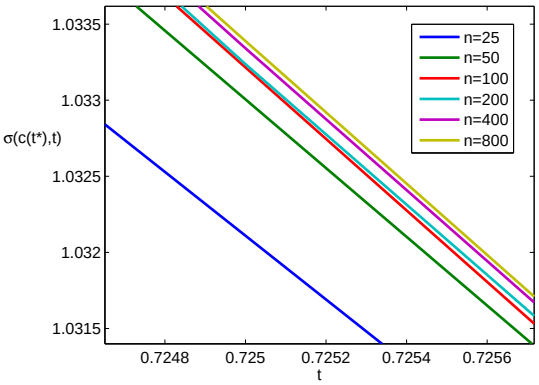

Figure B.33: $\sigma(c(t^*), t)$ for $b = 1.5$, $\beta = \dfrac{b}{2}$, $t^* = 0.6$: closer look in the CZ ($t > t^*$).

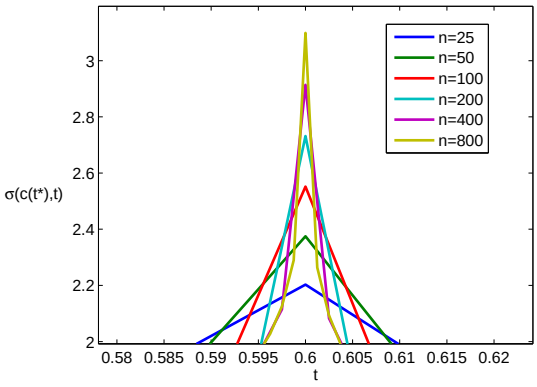

Figure B.34: $\sigma(c(t^*), t)$ for $b = 1.5$, $\beta = \dfrac{b}{2}$, $t^* = 0.6$: closer look at the CZ tip (near t^*).

The Case $b = 1.5$ $\beta = \dfrac{b}{3}$

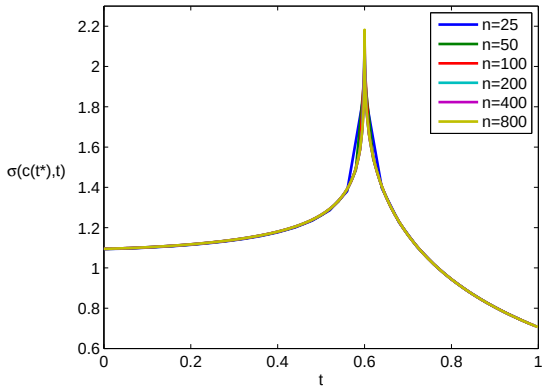

Figure B.35: $\sigma(c(t^*), t)$ vs. time for $b = 1.5$, $\beta = \dfrac{b}{3}$, $t^* = 0.6$: global picture.

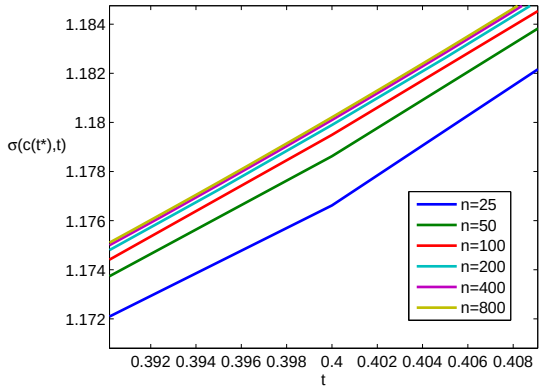

Figure B.36: $\sigma(c(t^*), t)$ for $b = 1.5$, $\beta = \dfrac{b}{3}$, $t^* = 0.6$: closer look ahead of the CZ ($t < t^*$).

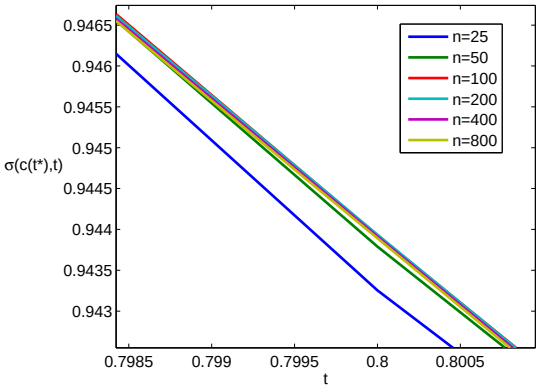

Figure B.37: $\sigma(c(t^*), t)$ for $b = 1.5$, $\beta = \dfrac{b}{3}$, $t^* = 0.6$: closer look in the CZ ($t > t^*$).

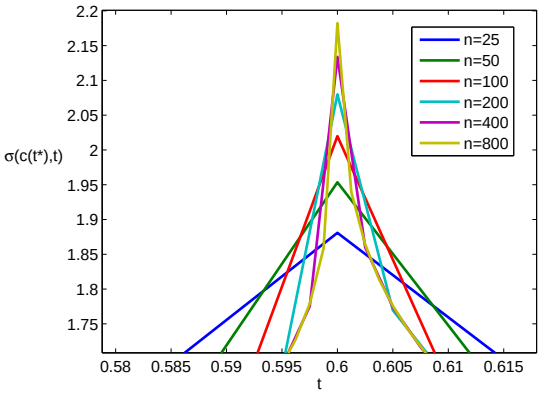

Figure B.38: $\sigma(c(t^*), t)$ for $b = 1.5$, $\beta = \dfrac{b}{3}$, $t^* = 0.6$: closer look at the CZ tip (near t^*).

The Case $b = 1.5$ $\beta = \dfrac{b}{4}$

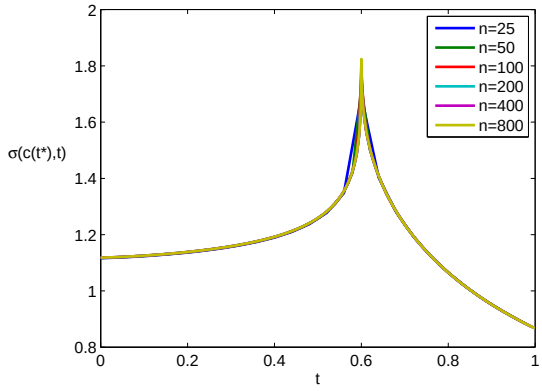

Figure B.39: $\sigma(c(t^*), t)$ vs. time for $b = 1.5$, $\beta = \dfrac{b}{4}$, $t^* = 0.6$: global picture.

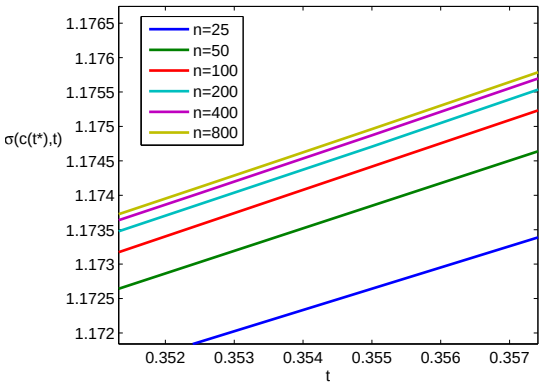

Figure B.40: $\sigma(c(t^*), t)$ for $b = 1.5$, $\beta = \dfrac{b}{4}$, $t^* = 0.6$: closer look ahead of the CZ ($t < t^*$).

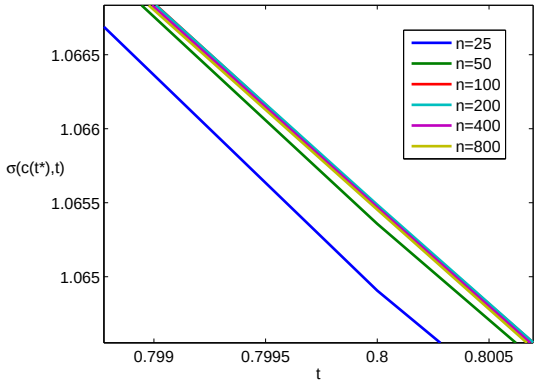

Figure B.41: $\sigma(c(t^*), t)$ for $b = 1.5$, $\beta = \dfrac{b}{4}$, $t^* = 0.6$: closer look in the CZ ($t > t^*$).

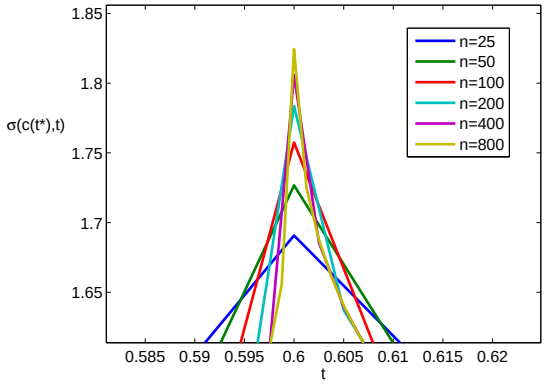

Figure B.42: $\sigma(c(t^*), t)$ for $b = 1.5$, $\beta = \dfrac{b}{4}$, $t^* = 0.6$: closer look at the CZ tip (near t^*).

The Case $b = 1.5$ $\beta = \dfrac{b}{8}$

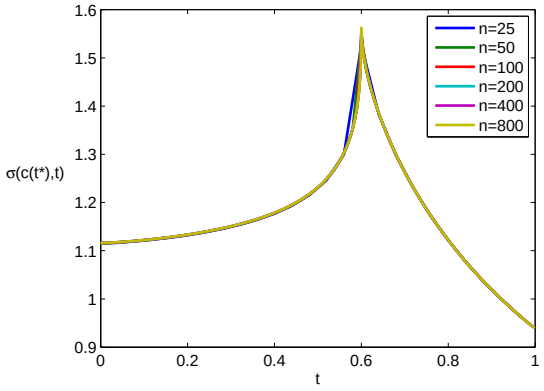

Figure B.43: $\sigma(c(t^*), t)$ vs. time for $b = 1.5$, $\beta = \dfrac{b}{8}$, $t^* = 0.6$: global picture.

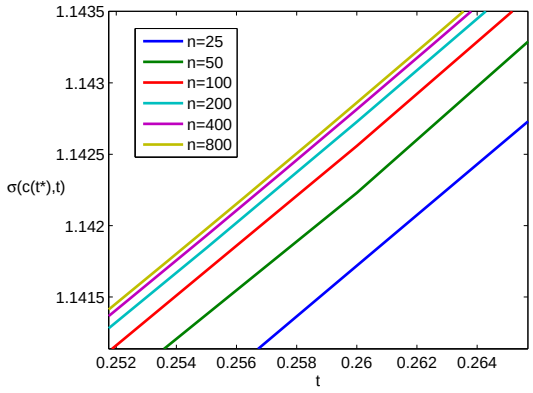

Figure B.44: $\sigma(c(t^*), t)$ for $b = 1.5$, $\beta = \dfrac{b}{8}$, $t^* = 0.6$: closer look ahead of the CZ ($t < t^*$).

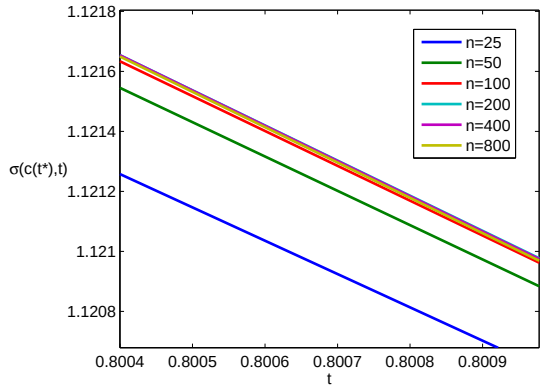

Figure B.45: $\sigma(c(t^*), t)$ for $b = 1.5$, $\beta = \dfrac{b}{8}$, $t^* = 0.6$: closer look in the CZ ($t > t^*$).

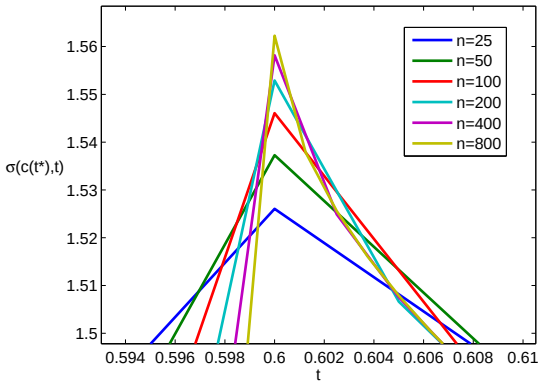

Figure B.46: $\sigma(c(t^*), t)$ for $b = 1.5$, $\beta = \dfrac{b}{8}$, $t^* = 0.6$: closer look at the CZ tip (near t^*).

Crack Tip Opening for the Elastic Case

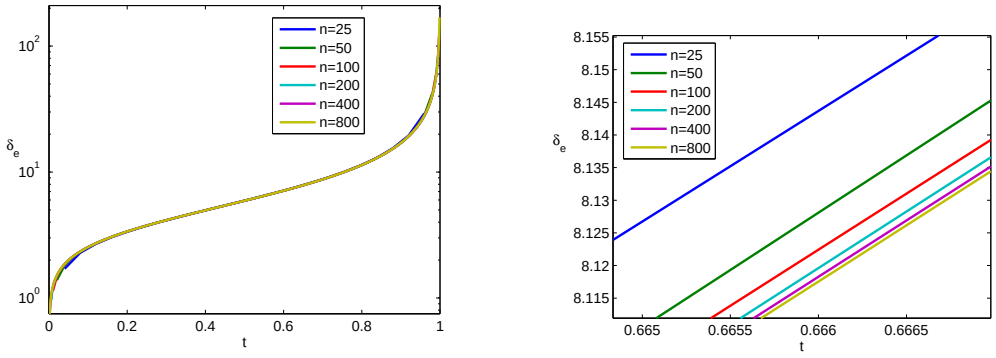

Figure B.47: Crack Opening δ_e vs. time t for $b = 4$, $\beta = \dfrac{b}{2}$.

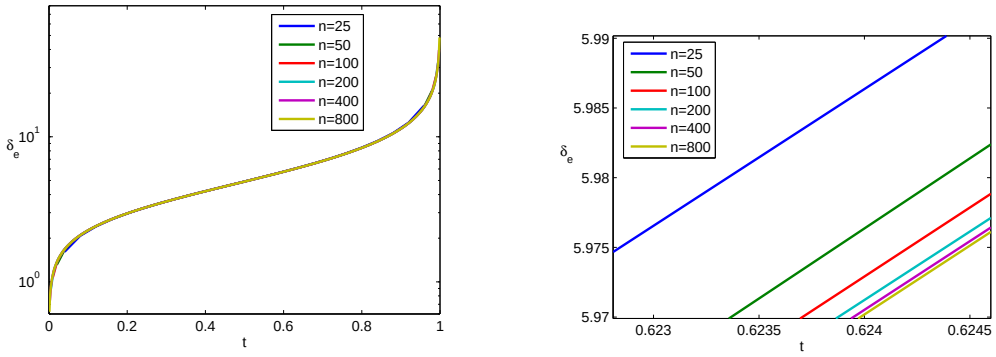

Figure B.48: Crack Opening δ_e vs. time t for $b = 4$, $\beta = \dfrac{b}{4}$.

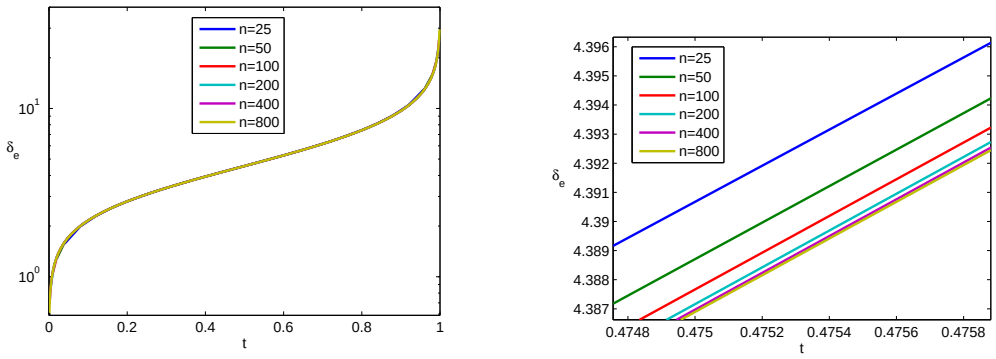

Figure B.49: Crack Opening δ_e vs. time t for $b = 4$, $\beta = \dfrac{b}{8}$.

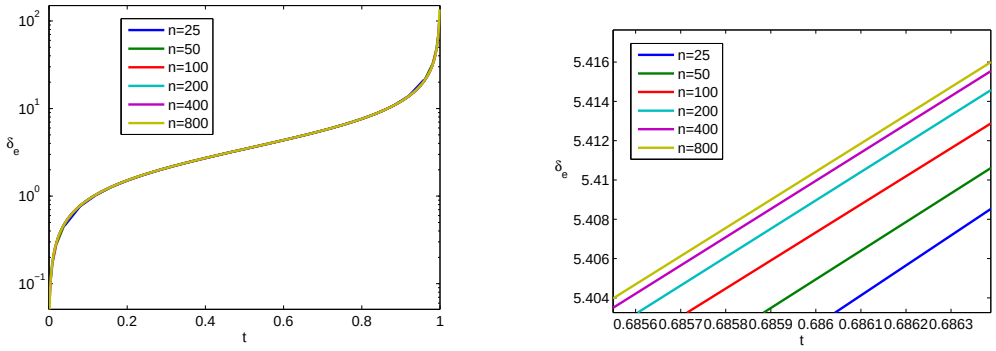

Figure B.50: Crack Opening δ_e vs. time t for $b = 1.5$, $\beta = \dfrac{b}{2}$.

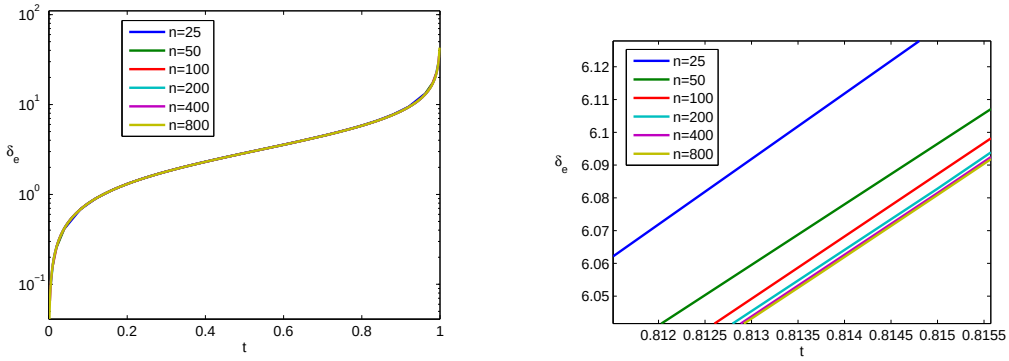

Figure B.51: Crack Opening δ_e vs. time t for $b = 1.5$, $\beta = \dfrac{b}{4}$.

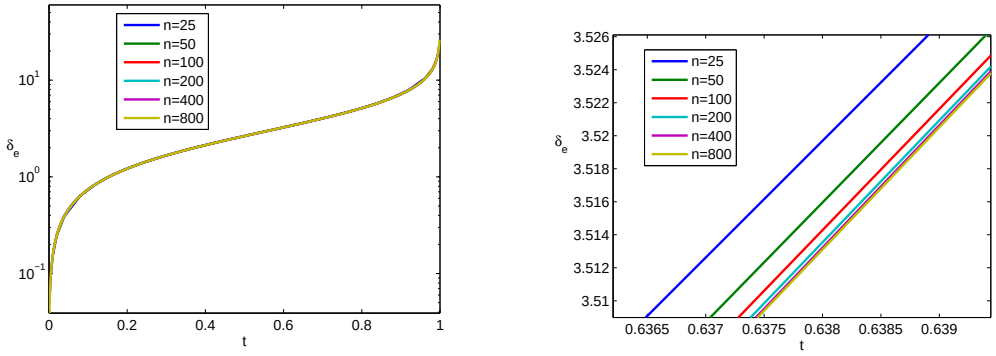

Figure B.52: Crack Opening δ_e vs. time t for $b = 1.5$, $\beta = \dfrac{b}{8}$.

Crack Tip Opening for the Viscoelastic Case

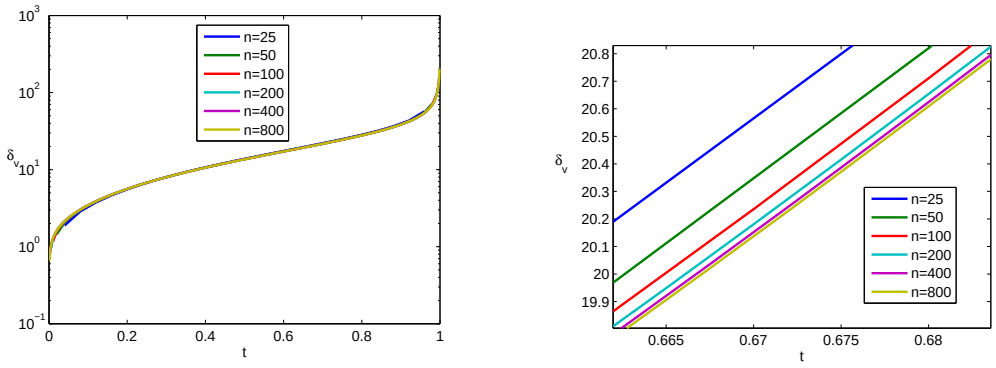

Figure B.53: Crack Opening δ_v vs. time t for $b = 4$, $\beta = \dfrac{b}{2}$.

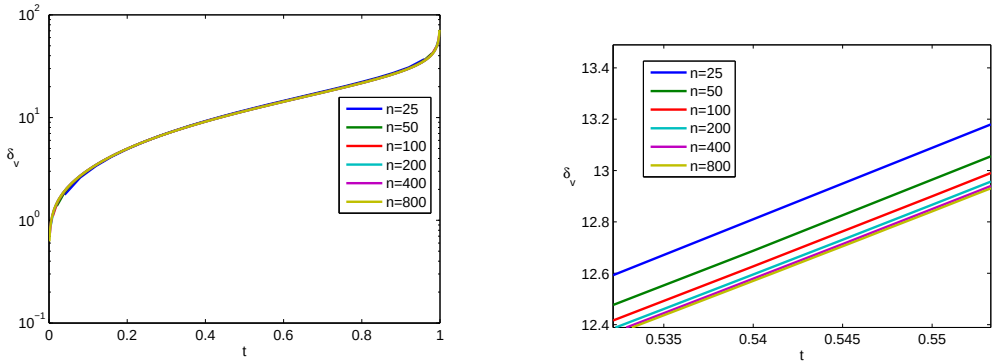

Figure B.54: Crack Opening δ_v vs. time t for $b = 4$, $\beta = \dfrac{b}{4}$.

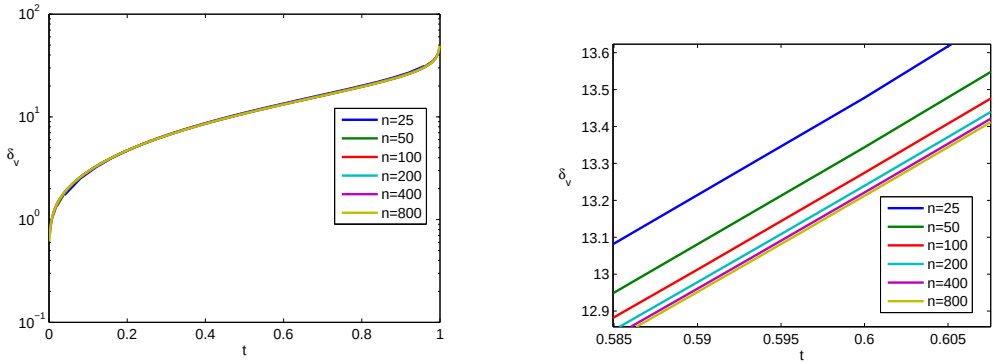

Figure B.55: Crack Opening δ_v vs. time t for $b = 4$, $\beta = \dfrac{b}{8}$.

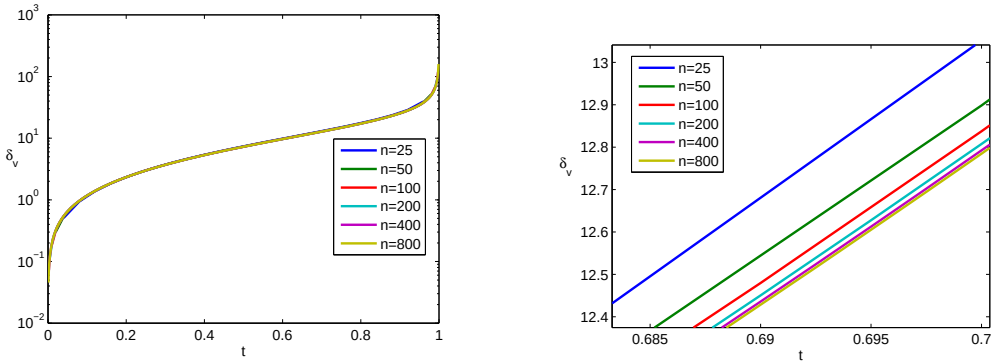

Figure B.56: Crack Opening δ_v vs. time t for $b = 1.5$, $\beta = \dfrac{b}{2}$.

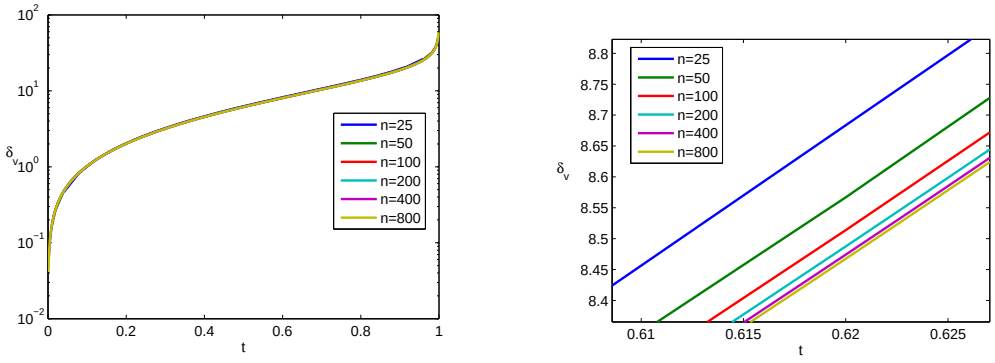

Figure B.57: Crack Opening δ_v vs. time t for $b = 1.5$, $\beta = \dfrac{b}{4}$.

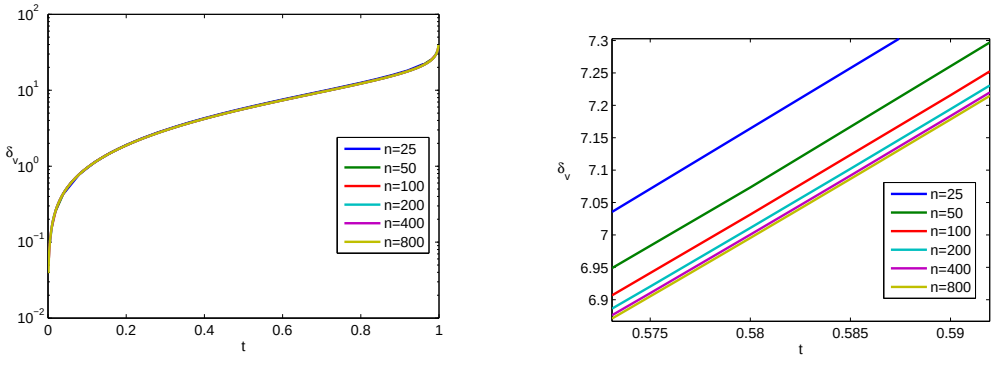

Figure B.58: Crack Opening δ_v vs. time t for $b = 1.5$, $\beta = \dfrac{b}{8}$.

Crack Propagation Stage for the Elastic Case

The Case $b = 4$

Regarding the time mesh of equidistant time steps h, we have considered five cases, namely $h = \frac{1}{500}, \frac{1}{1000}, \frac{1}{2000}, \frac{1}{4000}$ and $\frac{1}{8000}$. We will present in a table the number of time steps before crack growth begins for three cases of β.

Table B.1: Number of time steps $b = 4$ (elastic case).

β \ h	$\frac{1}{500}$	$\frac{1}{1000}$	$\frac{1}{2000}$	$\frac{1}{4000}$	$\frac{1}{8000}$
$b/2$	4	8	15	29	58
$b/4$	6	11	21	41	82
$b/8$	6	12	24	48	95

Now, we will present graphs showing the results obtained.

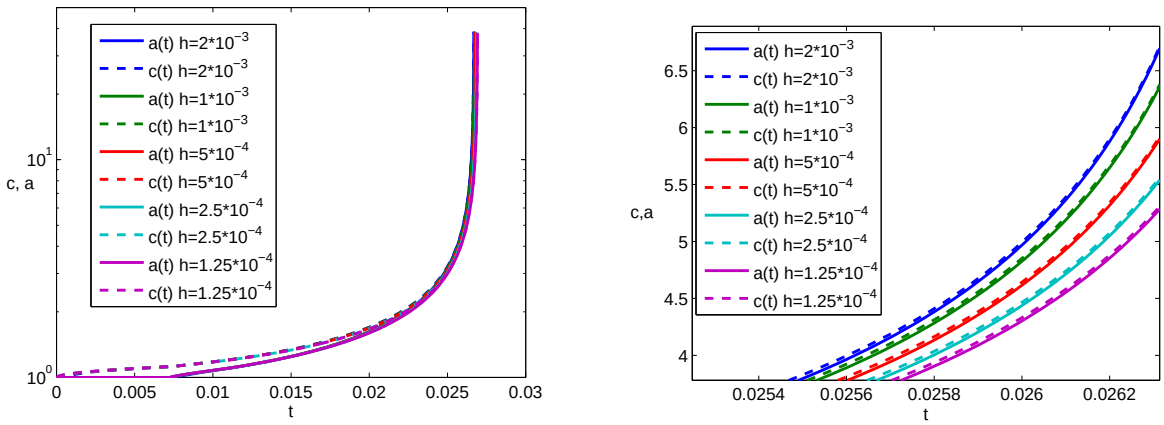

Figure B.59: Length (log scale) vs. time for $b = 4$, $\beta = \frac{b}{2}$.

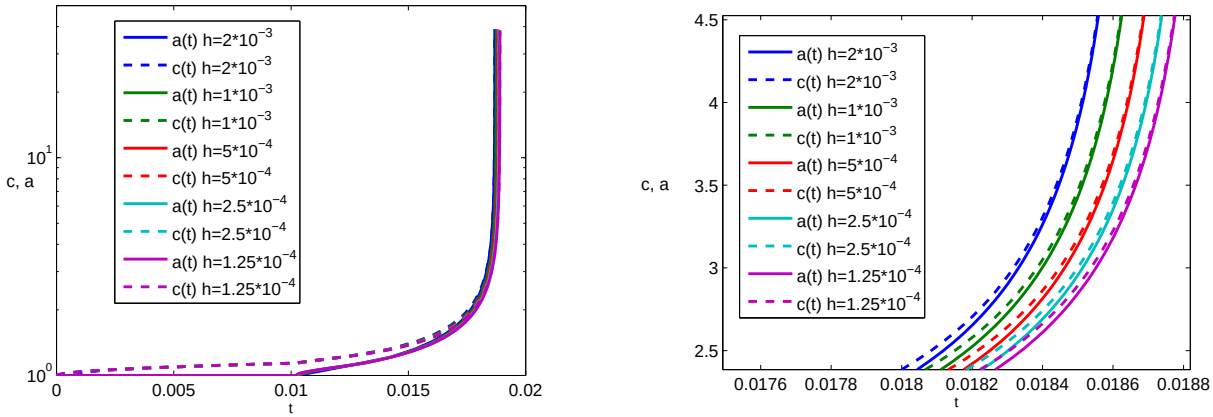

Figure B.60: Length (log scale) vs. time for $b = 4$, $\beta = \dfrac{b}{4}$.

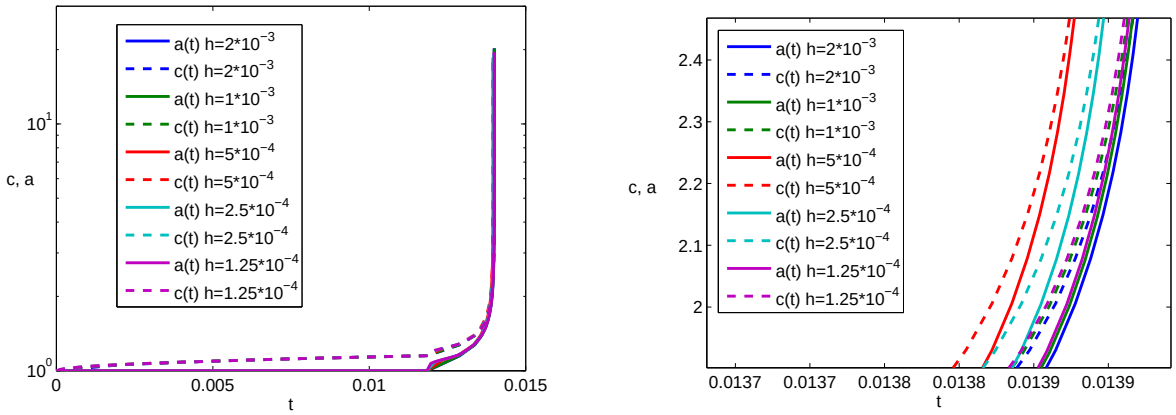

Figure B.61: Length (log scale) vs. time for $b = 4$, $\beta = \dfrac{b}{8}$.

The Case $b = 1.5$

In this case, for the time mesh, we have considered five cases, namely $h = \frac{1}{50}, \frac{1}{100}, \frac{1}{200}, \frac{1}{400}$ and $\frac{1}{800}$. We will present in a table the number of time steps before crack growth begins for three cases of β.

Table B.2: Number of time steps $b = 1.5$ (elastic case).

β \ h	$\frac{1}{50}$	$\frac{1}{100}$	$\frac{1}{200}$	$\frac{1}{400}$	$\frac{1}{800}$
$b/2$	7	14	28	55	109
$b/4$	9	17	33	66	132
$b/8$	10	19	37	73	146

Now, we will present graphs showing the results obtained.

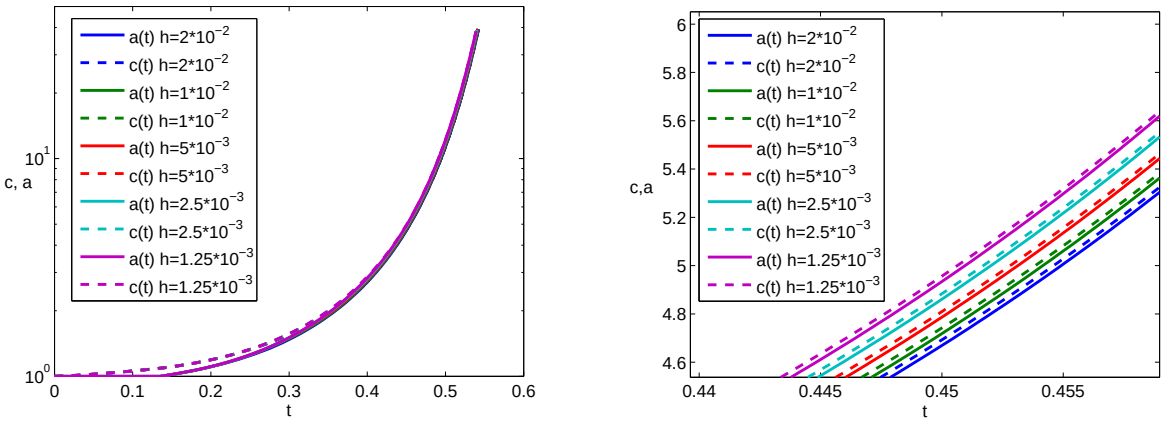

Figure B.62: Length (log scale) vs. time for $b = 1.5$, $\beta = \frac{b}{2}$.

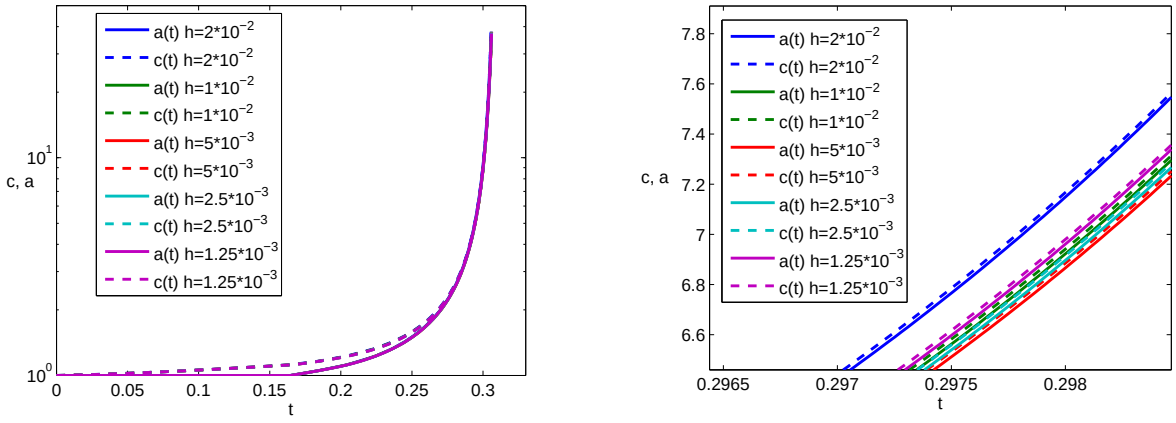

Figure B.63: Length (log scale) vs. time for $b = 1.5$, $\beta = \frac{b}{4}$.

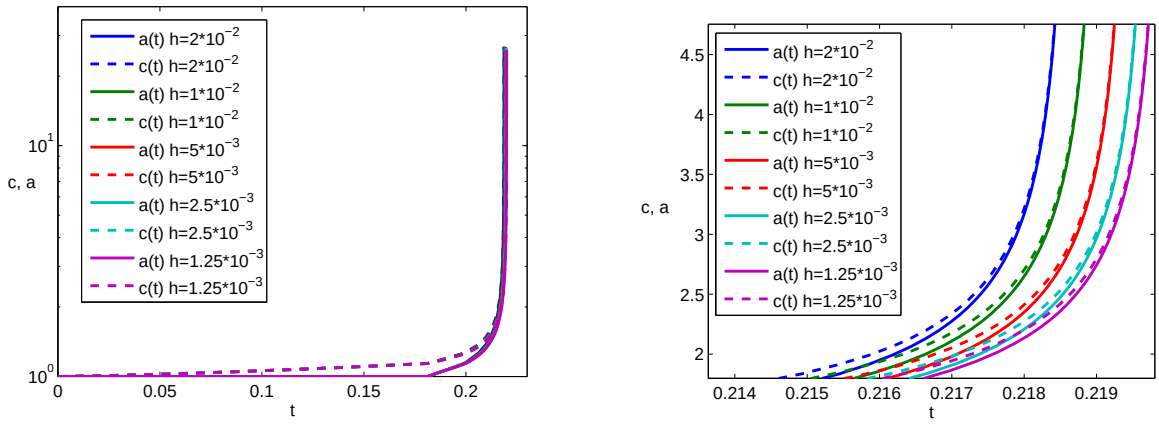

Figure B.64: Length (log scale) vs. time for $b = 1.5$, $\beta = \frac{b}{8}$.

Now we will look at the CZ length with respect to time.

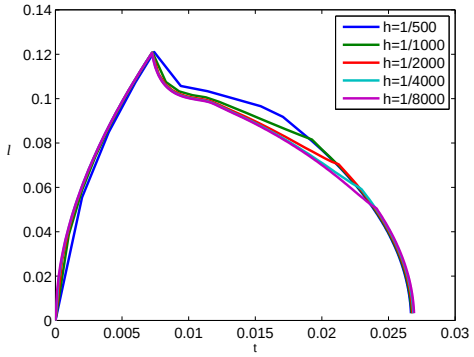

Figure B.65: CZ length vs. t, $b = 4$, $\beta = \frac{b}{2}$.

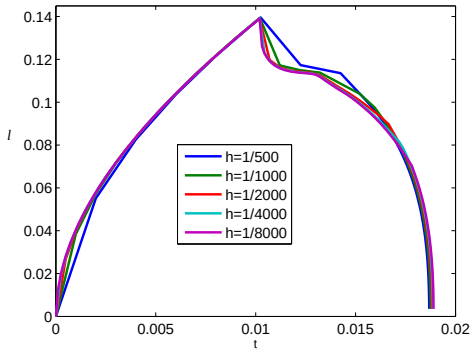

Figure B.66: CZ length vs. t, $b = 4$, $\beta = \frac{b}{4}$.

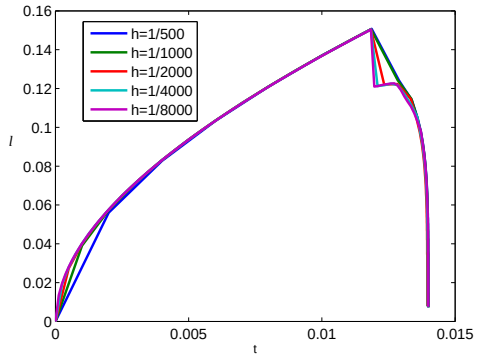

Figure B.67: CZ length vs. t, $b = 4$, $\beta = \frac{b}{8}$.

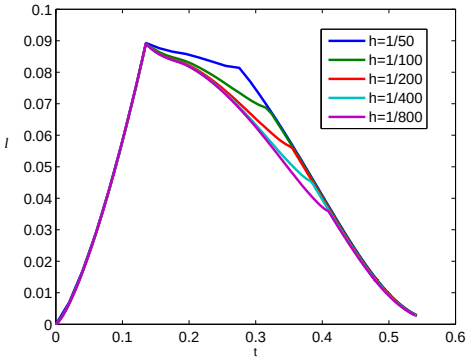

Figure B.68: CZ length vs. t, $b = 1.5$, $\beta = \frac{b}{2}$.

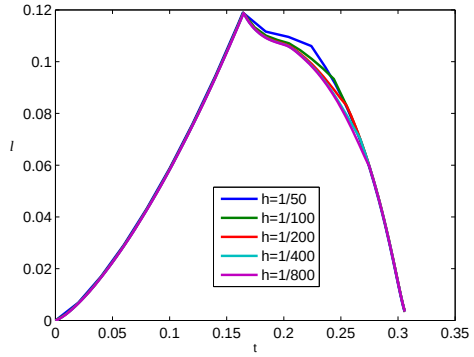

Figure B.69: CZ length vs. t, $b = 1.5$, $\beta = \frac{b}{4}$.

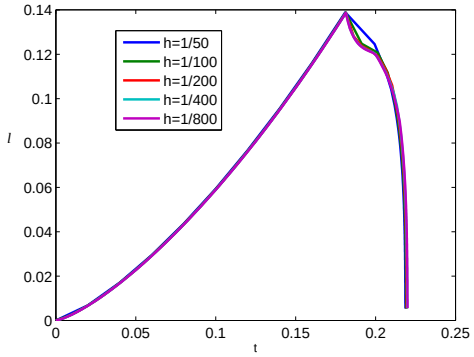

Figure B.70: CZ length vs. t, $b = 1.5$, $\beta = \frac{b}{8}$.

Crack Propagation Stage for the Viscoelastic Case

The Case $b = 4$

Regarding the time mesh of equidistant time steps h, we have considered five cases, namely $h = \frac{1}{500}, \frac{1}{1000}, \frac{1}{2000}, \frac{1}{4000}$ and $\frac{1}{8000}$. We will present in a table the number of time steps before crack growth begins for three cases of β.

Table B.3: Number of time steps $b = 4$ (viscoelastic case).

β \ h	$\frac{1}{500}$	$\frac{1}{1000}$	$\frac{1}{2000}$	$\frac{1}{4000}$	$\frac{1}{8000}$
$b/2$	4	7	14	28	55
$b/4$	5	10	19	38	76
$b/8$	6	11	22	44	87

Now, we will present graphs showing the results obtained.

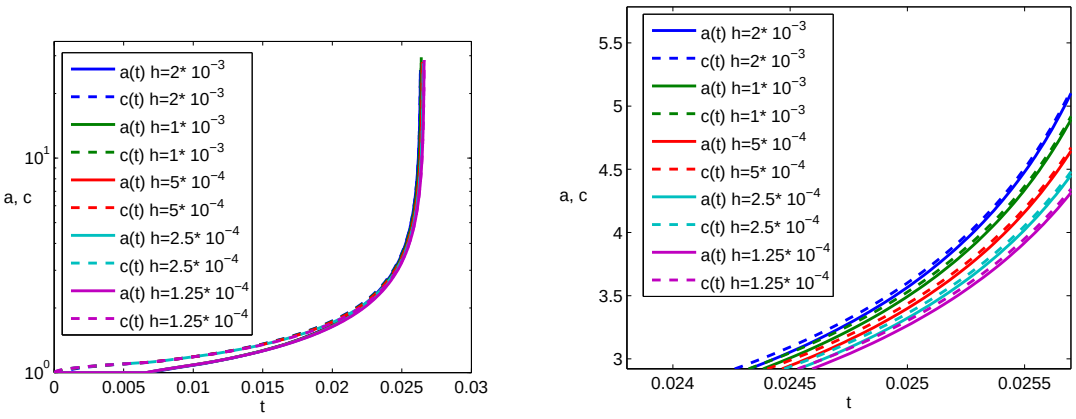

Figure B.71: Length (log scale) vs. time for $b = 4$, $\beta = \frac{b}{2}$.

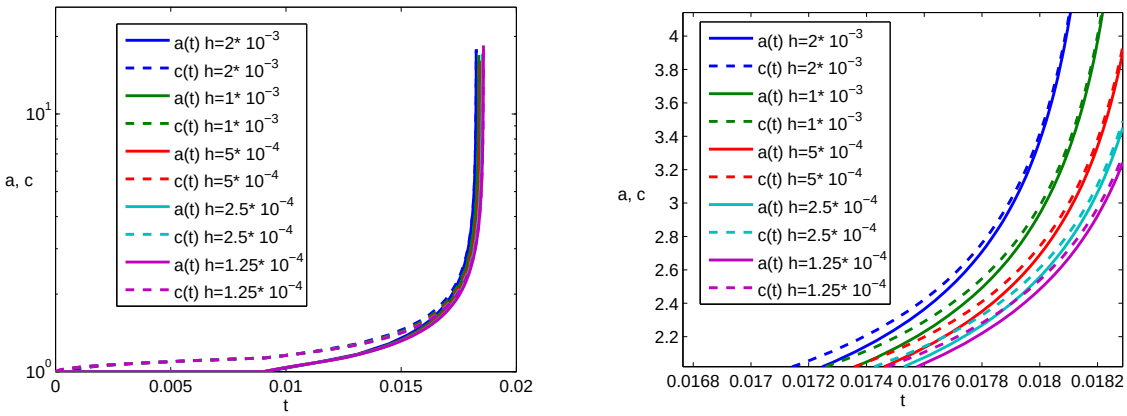

Figure B.72: Length (log scale) vs. time for $b = 4$, $\beta = \frac{b}{4}$.

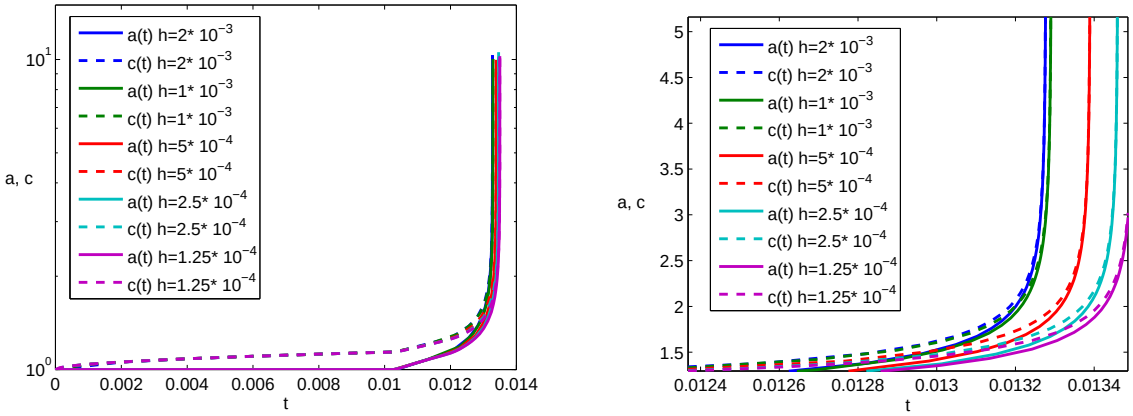

Figure B.73: Length (log scale) vs. time for $b = 4$, $\beta = \frac{b}{8}$.

The Case $b = 1.5$

In this case, for the time mesh, we have considered five cases, namely $h = \frac{1}{50}, \frac{1}{100}, \frac{1}{200}, \frac{1}{400}$ and $\frac{1}{800}$.

Table B.4: Number of time steps $b = 1.5$ (viscoelastic case).

β \ h	$\frac{1}{50}$	$\frac{1}{100}$	$\frac{1}{200}$	$\frac{1}{400}$	$\frac{1}{800}$
$b/2$	6	11	22	44	87
$b/4$	7	13	26	52	103
$b/8$	7	14	28	56	111

Now, we will present graphs showing the results obtained.

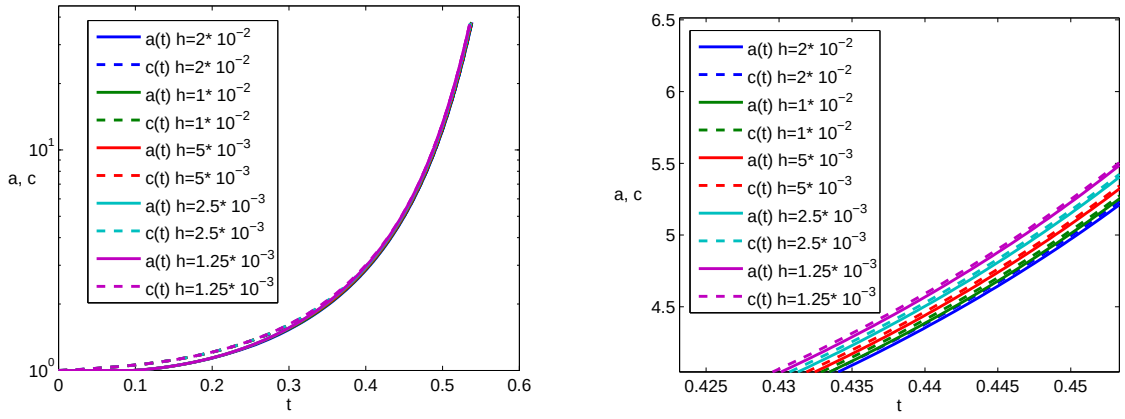

Figure B.74: Length (log scale) vs. time for $b = 1.5$, $\beta = \frac{b}{2}$.

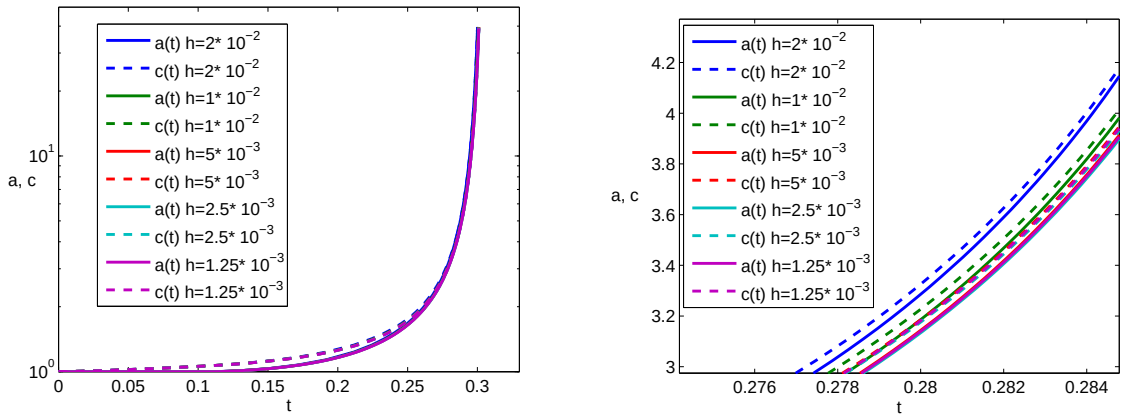

Figure B.75: Length (log scale) vs. time for $b = 1.5$, $\beta = \dfrac{b}{4}$.

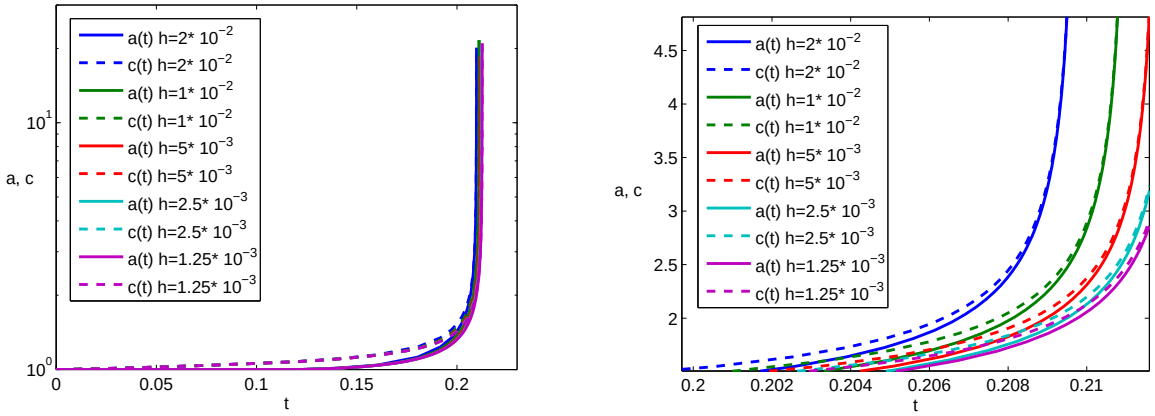

Figure B.76: Length (log scale) vs. time for $b = 1.5$, $\beta = \dfrac{b}{8}$.

Now we will look at the CZ length with respect to time.

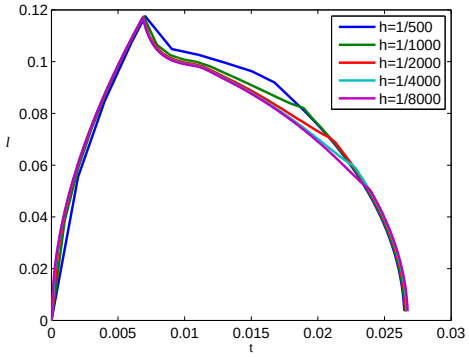

Figure B.77: CZ length vs. t, $b = 4$, $\beta = \frac{b}{2}$.

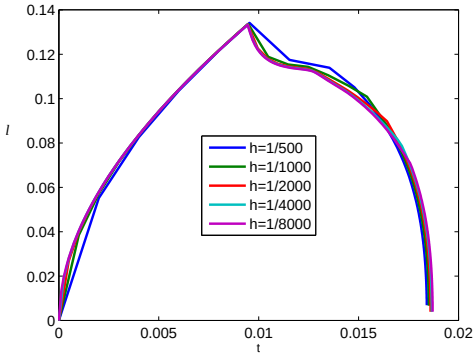

Figure B.78: CZ length vs. t, $b = 4$, $\beta = \frac{b}{4}$.

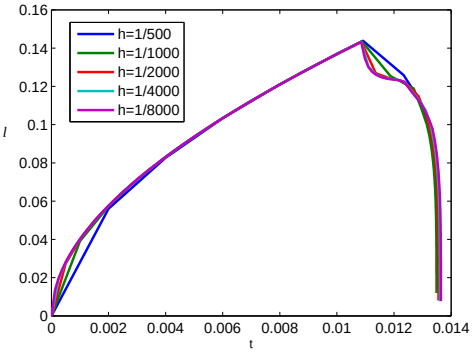

Figure B.79: CZ length vs. t, $b = 4$, $\beta = \frac{b}{8}$.

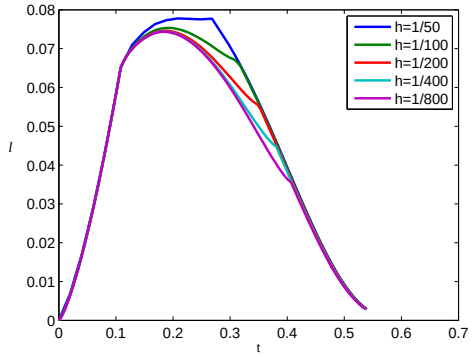

Figure B.80: CZ length vs. t, $b = 1.5$, $\beta = \frac{b}{2}$.

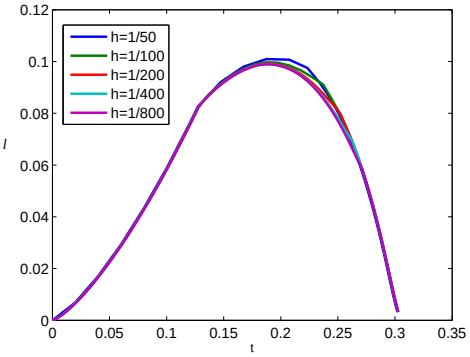

Figure B.81: CZ length vs. t, $b = 1.5$, $\beta = \frac{b}{4}$.

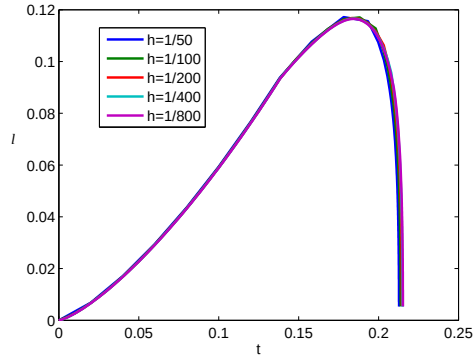

Figure B.82: CZ length vs. t, $b = 1.5$, $\beta = \frac{b}{8}$.

B.2 Variable Loading

CZ Tip Coordinate and Stresses

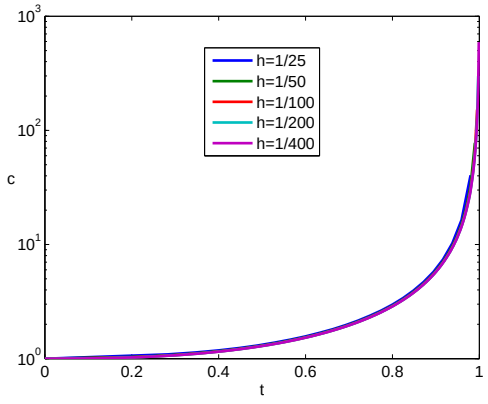

Figure B.83: $c(t)$ vs. t for $b = 4$, $\beta = \dfrac{b}{2}$.

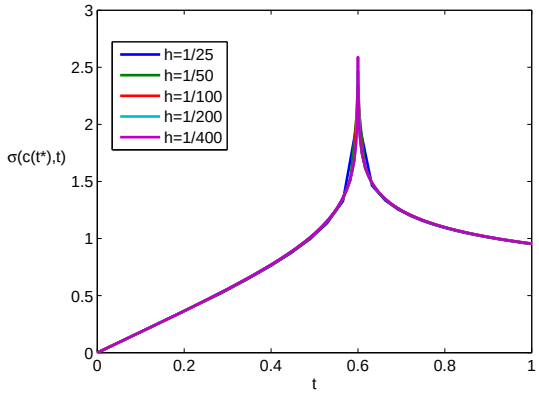

Figure B.84: $\sigma(c(t^*), t)$ vs. t for $b = 4$, $\beta = \dfrac{b}{2}$.

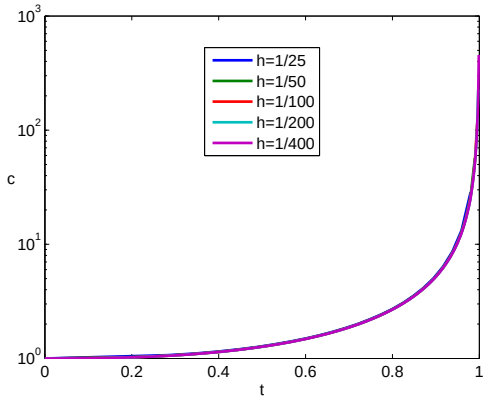

Figure B.85: $c(t)$ vs. t for $b = 4$, $\beta = \dfrac{b}{4}$.

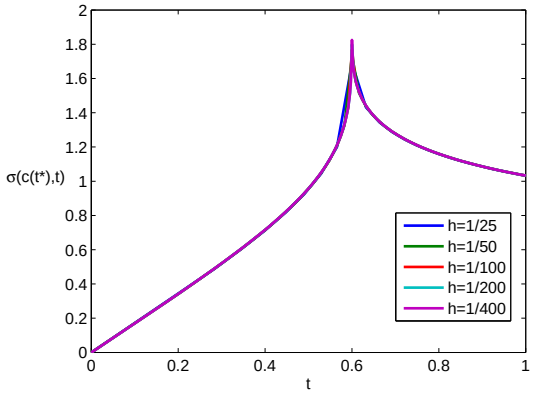

Figure B.86: $\sigma(c(t^*), t)$ vs. t for $b = 4$, $\beta = \dfrac{b}{4}$.

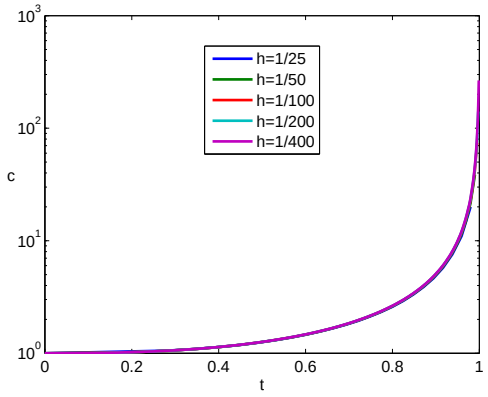

Figure B.87: $c(t)$ vs. t for $b = 4$, $\beta = \dfrac{b}{8}$.

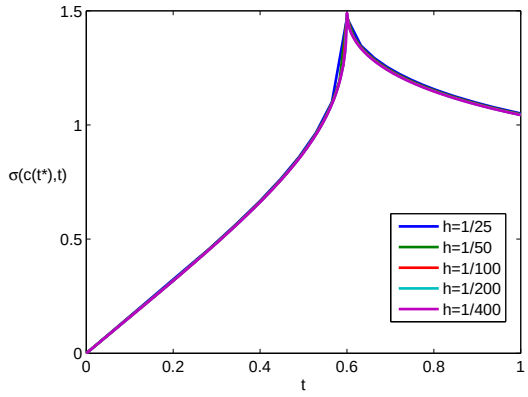

Figure B.88: $\sigma(c(t^*), t)$ vs. t for $b = 4$, $\beta = \dfrac{b}{8}$.

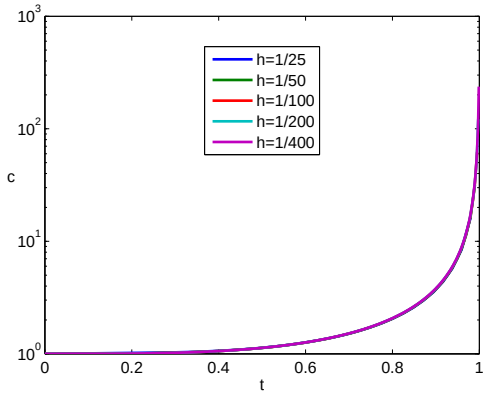

Figure B.89: $c(t)$ vs. t for $b = 1.5$, $\beta = \dfrac{b}{2}$.

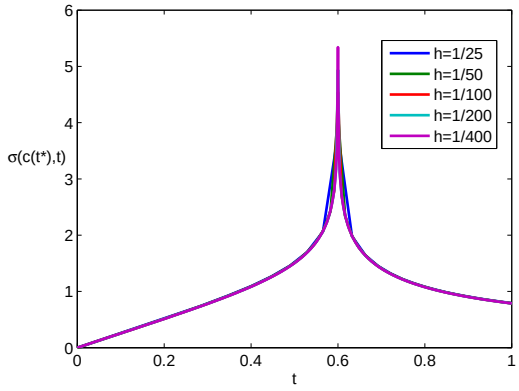

Figure B.90: $\sigma(c(t^*), t)$ vs. t for $b = 1.5$, $\beta = \dfrac{b}{2}$.

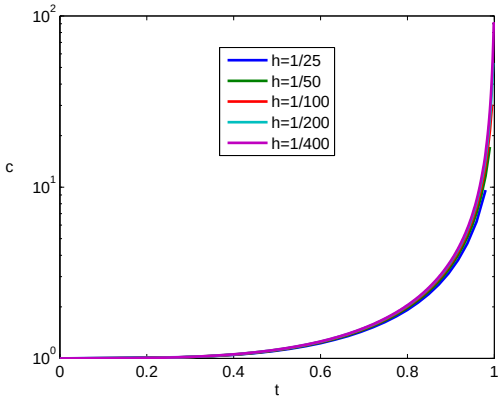

Figure B.91: $c(t)$ vs. t for $b = 1.5$, $\beta = \dfrac{b}{4}$.

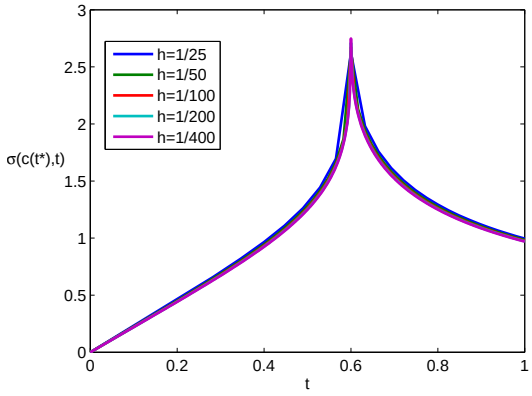

Figure B.92: $\sigma(c(t^*), t)$ vs. t for $b = 1.5$, $\beta = \dfrac{b}{4}$.

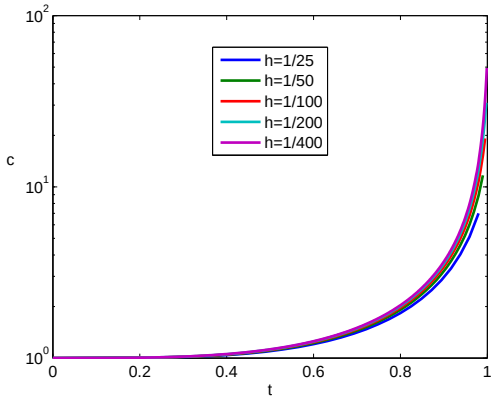

Figure B.93: $c(t)$ vs. t for $b = 1.5$, $\beta = \dfrac{b}{8}$.

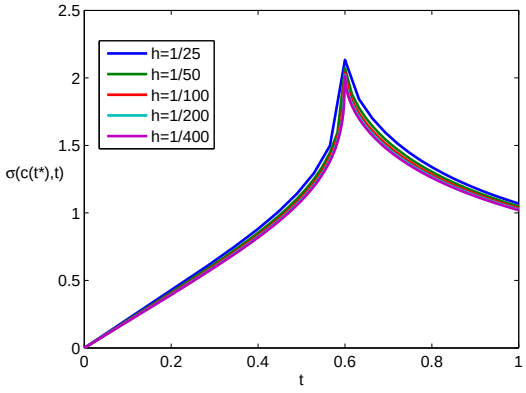

Figure B.94: $\sigma(c(t^*), t)$ vs. t for $b = 1.5$, $\beta = \dfrac{b}{8}$.

Crack Tip Opening for the Elastic Case

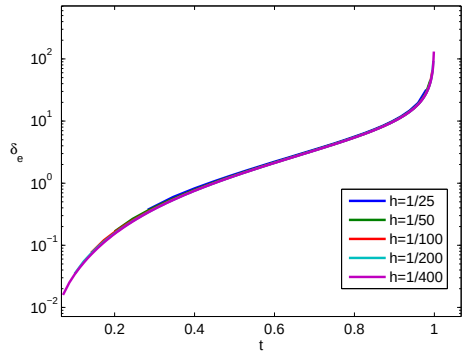

Figure B.95: δ_e vs. t for $b = 4$, $\beta = \dfrac{b}{2}$.

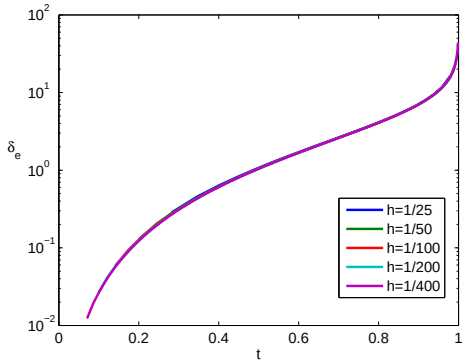

Figure B.96: δ_e vs. t for $b = 4$, $\beta = \dfrac{b}{4}$.

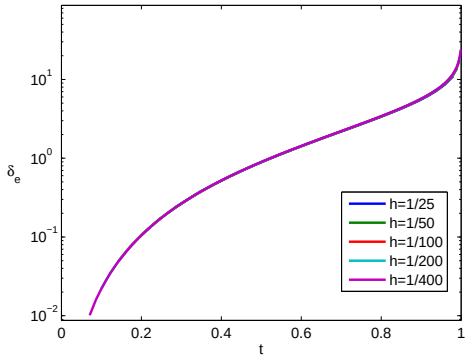

Figure B.97: δ_e vs. t for $b = 4$, $\beta = \dfrac{b}{8}$.

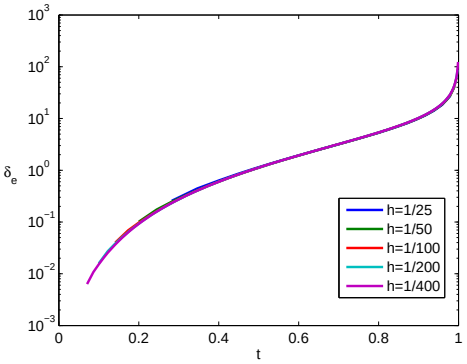

Figure B.98: δ_e vs. t for $b = 1.5$, $\beta = \dfrac{b}{2}$.

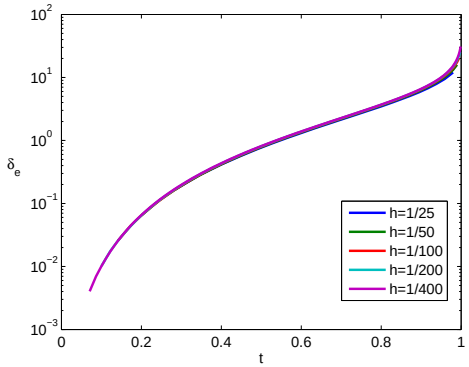

Figure B.99: δ_e vs. t for $b = 1.5$, $\beta = \dfrac{b}{4}$.

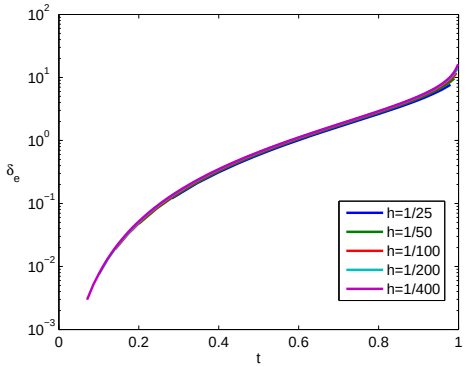

Figure B.100: δ_e vs. t for $b = 1.5$, $\beta = \dfrac{b}{8}$.

Crack Tip Opening for the Viscoelastic Case

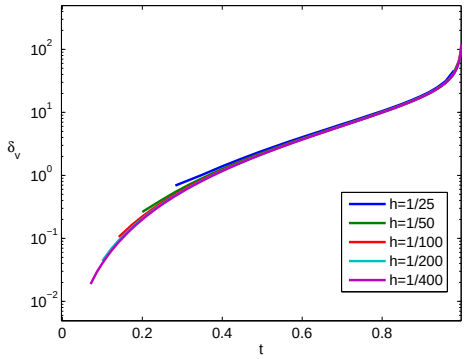

Figure B.101: δ_v vs. t for $b = 4$, $\beta = \dfrac{b}{2}$.

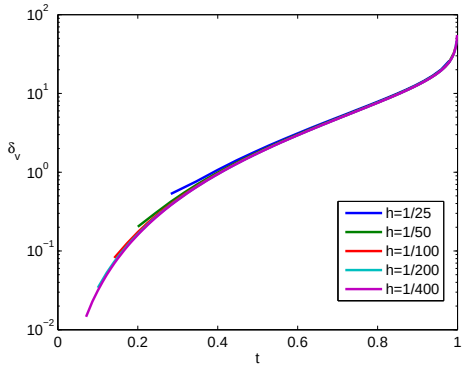

Figure B.102: δ_v vs. t for $b = 4$, $\beta = \dfrac{b}{4}$.

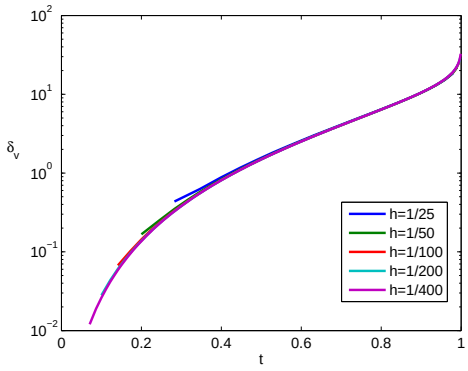

Figure B.103: δ_v vs. t for $b = 4$, $\beta = \dfrac{b}{8}$.

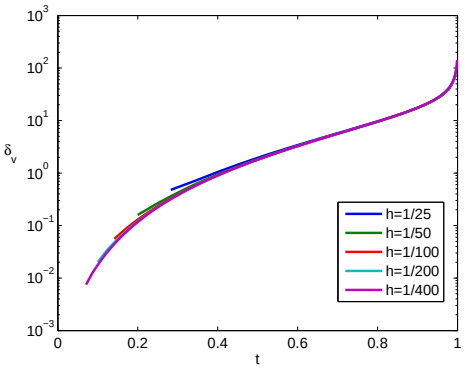

Figure B.104: δ_v vs. t for $b = 1.5$, $\beta = \dfrac{b}{2}$.

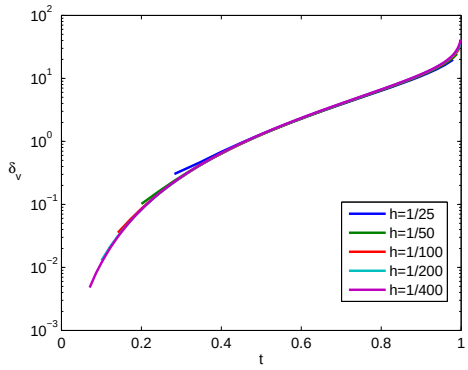

Figure B.105: δ_v vs. t for $b = 1.5$, $\beta = \dfrac{b}{4}$.

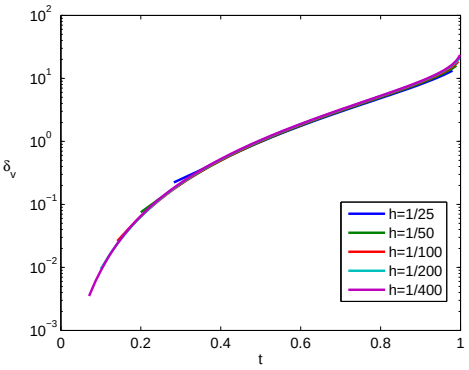

Figure B.106: δ_v vs. t for $b = 1.5$, $\beta = \dfrac{b}{8}$.

CZ Length for a Propagating Crack: Elastic Case

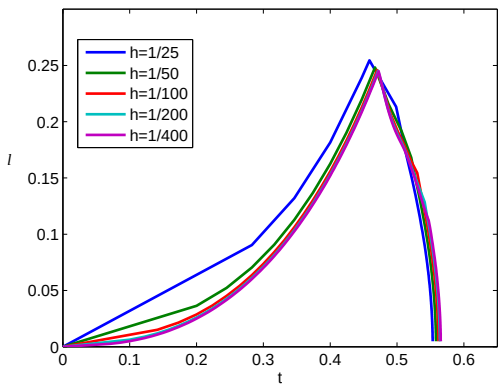

Figure B.107: CZ length vs. t for $b = 4$, $\beta = \dfrac{b}{2}$.

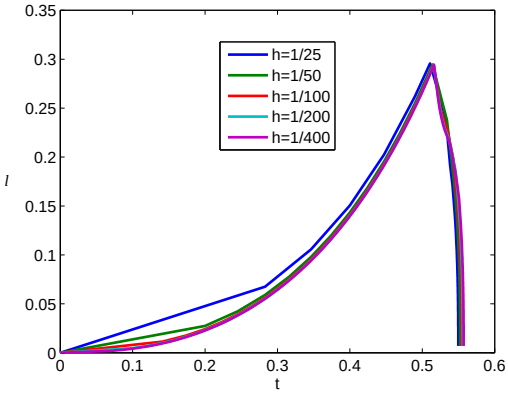

Figure B.108: CZ length vs. t for $b = 4$, $\beta = \dfrac{b}{4}$.

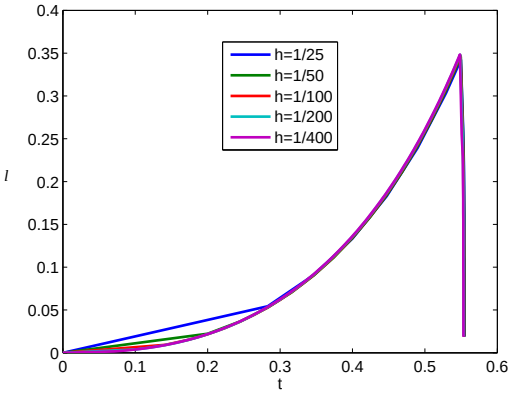

Figure B.109: CZ length vs. t for $b = 4$, $\beta = \dfrac{b}{8}$.

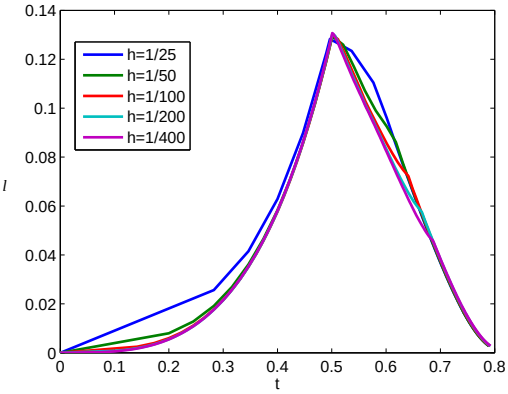

Figure B.110: CZ length vs. t for $b = 1.5$, $\beta = \dfrac{b}{2}$.

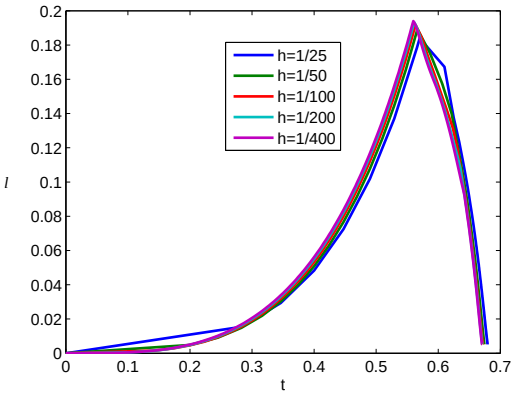

Figure B.111: CZ length vs. t for $b = 1.5$, $\beta = \dfrac{b}{4}$.

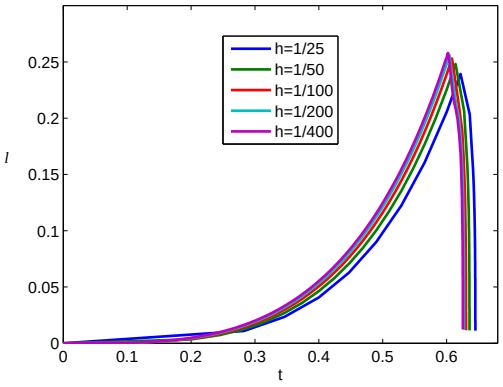

Figure B.112: CZ length vs. t for $b = 1.5$, $\beta = \dfrac{b}{8}$.

CZ Length for a Propagating Crack: Viscoelastic Case

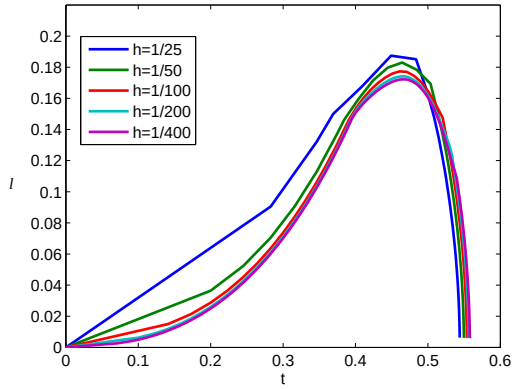

Figure B.113: CZ length vs. t for $b = 4$, $\beta = \dfrac{b}{2}$.

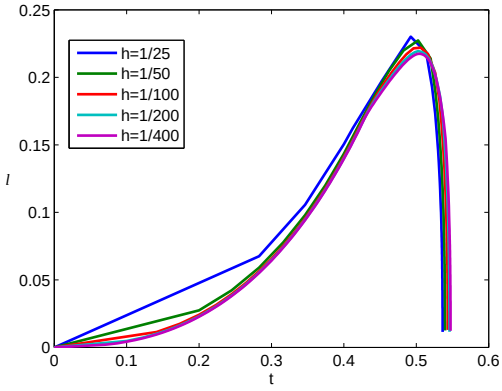

Figure B.114: CZ length vs. t for $b = 4$, $\beta = \dfrac{b}{4}$.

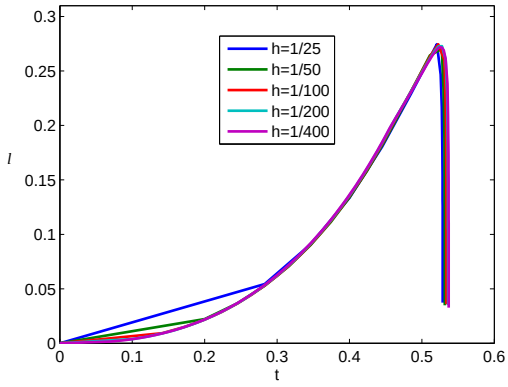

Figure B.115: CZ length vs. t for $b = 4$, $\beta = \frac{b}{8}$.

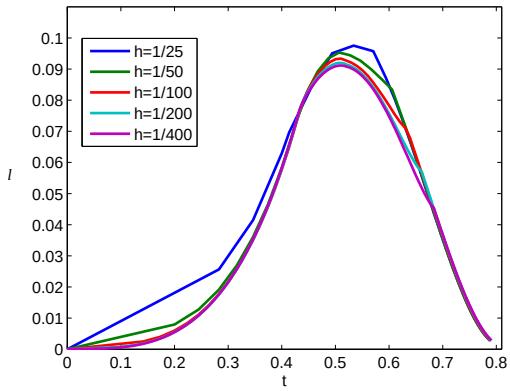

Figure B.116: CZ length vs. t for $b = 1.5$, $\beta = \frac{b}{2}$.

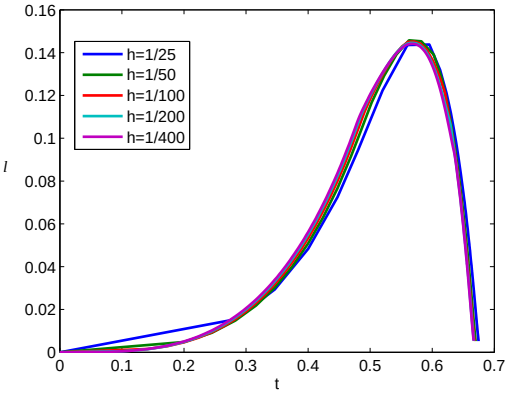

Figure B.117: CZ length vs. t for $b = 1.5$, $\beta = \frac{b}{4}$.

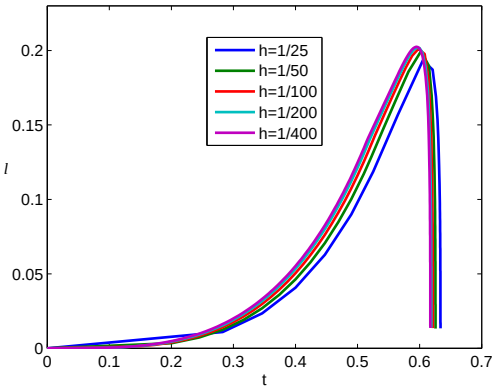

Figure B.118: CZ length vs. t for $b = 1.5$, $\beta = \frac{b}{8}$.

Appendix C

Numerical Convergence Rate for the Variable Loading Case

We will use CR to denote the numerical convergence rate α.

Cohesive Zone Length of a Stationary Crack

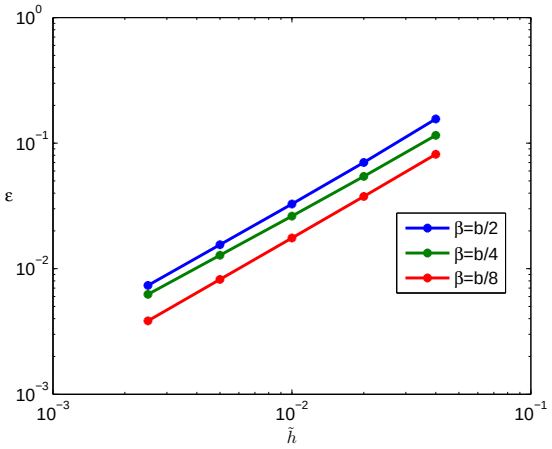

Figure C.1: Error of the CZ length vs. step size for $b = 4$ (stationary crack, variable load).

$\tilde{h}$ \ β	$\frac{b}{2}$	$\frac{b}{4}$	$\frac{b}{8}$
1/25	-	-	-
1/50	1.15325	1.08914	1.11553
1/100	1.09899	1.05023	1.09938
1/200	1.07595	1.03434	1.09730
1/400	1.07595	1.03434	1.09730

Table C.1: CR α of the CZ length for $b = 4$ (stationary crack stage, variable load).

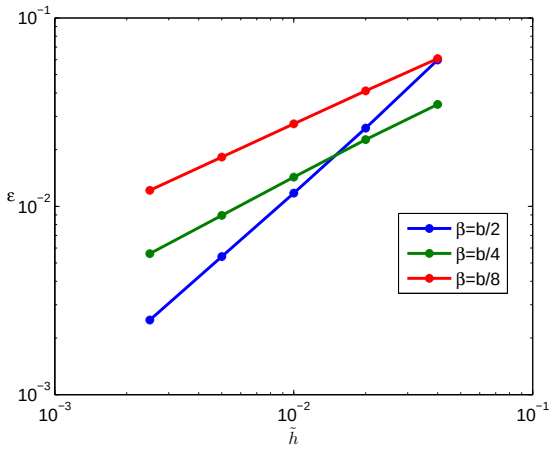

Figure C.2: Error of the CZ length vs. step size for $b = 1.5$ (stationary crack stage, variable load).

$\tilde{h}$ \ β	$\frac{b}{2}$	$\frac{b}{4}$	$\frac{b}{8}$
1/25	-	-	-
1/50	1.20413	0.62096	0.56792
1/100	1.14595	0.66246	0.58262
1/200	1.11929	0.67458	0.58692
1/400	1.11929	0.67458	0.58692

Table C.2: CR α of the CZ length for $b = 1.5$ (stationary crack, variable load).

Stress at the Cohesive Zone Tip

As done for the case of a constant load, we will study the stress at the point $x = c(t^*)$, $t^* = 0.6$. Also, we will use the parameter sets $\beta = \frac{3b}{4}$ and $\beta = \frac{b}{3}$ as well as the usual 3 sets $\beta = \frac{b}{2}$, $\beta = \frac{b}{4}$ and $\beta = \frac{b}{8}$.

β \ $\tilde{h}$	$\frac{1}{25}$	$\frac{1}{50}$	$\frac{1}{100}$	$\frac{1}{200}$	$\frac{1}{400}$	y_a
$3b/4$	2.34684	2.62118	2.90778	3.21403	3.54430	-0.99663
$b/2$	2.056619	2.20209	2.33690	2.46555	2.58998	6.25368
$b/3$	1.82037	1.89511	1.95862	2.01382	2.06232	2.41329
$b/4$	1.68757	1.73202	1.76876	1.79944	1.82514	1.95804
$b/8$	1.46837	1.47359	1.47973	1.48556	1.49065	1.52581

Table C.3: Stress at the CZ tip and its Aitken approximation for $b = 4$, variable load.

Now we will obtain the graph showing the error ε and the table which follows shows the numerical convergence rate at the CZ tip, thus at step $t = 0.6$.

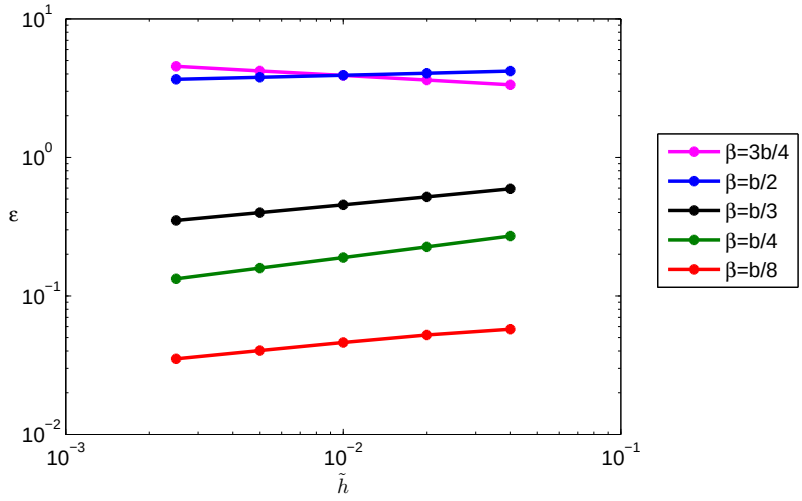

Figure C.3: Error of the stress at the CZ tip vs. step size for $b = 4$ (variable load).

$\tilde{h}$ \ β	$\frac{3b}{4}$	$\frac{b}{2}$	$\frac{b}{3}$	$\frac{b}{4}$	$\frac{b}{8}$
1/25	-	-	-	-	-
1/50	-0.11377	0.05089	0.19440	0.25899	0.13753
1/100	-0.10999	0.04887	0.18863	0.25597	0.18039
1/200	-0.10894	0.048183	0.18673	0.25510	0.19502
1/400	-0.10894	0.04818	0.18673	0.25510	0.19502

Table C.4: CR α for $b = 4$ (stress at the CZ tip, stationary crack, variable load).

β \ $\tilde{h}$	$\frac{1}{25}$	$\frac{1}{50}$	$\frac{1}{100}$	$\frac{1}{200}$	$\frac{1}{400}$	y_a
$3b/4$	5.22639	6.29361	7.54548	9.02099	10.76183	-0.66016
$b/2$	3.78948	4.15634	4.53986	4.93563	5.34045	-12.76732
$b/3$	2.98270	3.08529	3.19467	3.30273	3.40546	5.38498
$b/4$	2.62217	2.64047	2.67340	2.71082	2.74798	8.26950
$b/8$	2.13353	2.07111	2.03855	2.02127	2.01230	2.00261

Table C.5: Stress at the CZ tip and its Aitken approximation for $b = 1.5$, variable load.

Similarly to the case $b = 4$, we will obtain the graph showing the error ε and the table which follows shows the numerical convergence rate at the CZ tip, thus at $t^* = 0.6$.

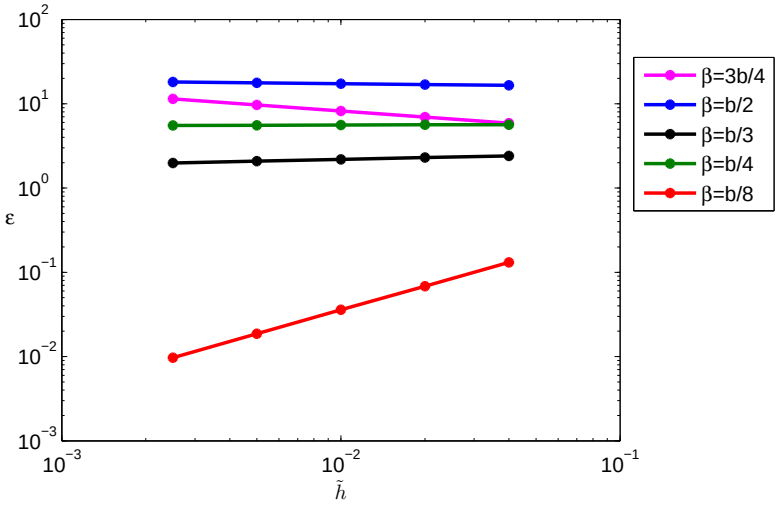

Figure C.4: Error of the stress at the CZ tip vs. step size for $b = 1.5$ (variable load).

$\tilde{h}$ \ β	$\frac{3b}{4}$	$\frac{b}{2}$	$\frac{b}{3}$	$\frac{b}{4}$	$\frac{b}{8}$
1/25	-	-	-	-	-
1/50	-0.24037	-0.03162	0.06296	0.00468	0.93453
1/100	-0.23882	-0.03233	0.07031	0.00846	0.93050
1/200	-0.23856	-0.03262	0.07299	0.00968	0.94530
1/400	-0.23856	-0.03262	0.07299	0.00968	0.94530

Table C.6: CR α for $b = 1.5$ (stress at the CZ tip, stationary crack, variable load).

Crack Tip Opening for the Elastic Case

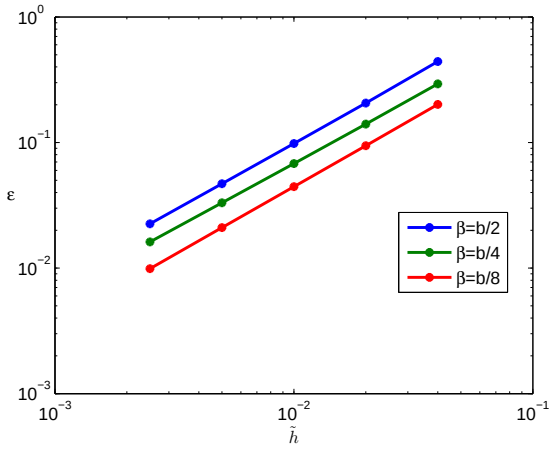

Figure C.5: Error of δ_e vs. step size for $b = 4$ (variable load).

$\tilde{h}$ \ β	$\frac{b}{2}$	$\frac{b}{4}$	$\frac{b}{8}$
1/25	-	-	-
1/50	1.09747	1.06331	1.09249
1/100	1.07247	1.04469	1.08499
1/200	1.06178	1.03648	1.08399
1/400	1.06178	1.03648	1.08399

Table C.7:

CR α of δ_e for $b = 4$ variable load.

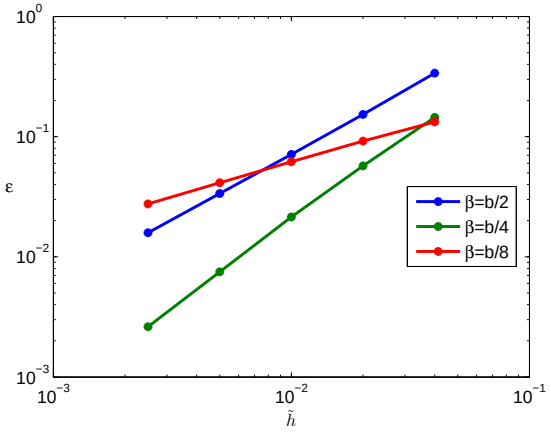

Figure C.6: Error of δ_e vs. step size for $b = 1.5$ (variable load).

$\tilde{h}$ \ β	$\frac{b}{2}$	$\frac{b}{4}$	$\frac{b}{8}$
1/25	-	-	-
1/50	1.14340	1.34027	0.55444
1/100	1.10279	1.41178	0.57297
1/200	1.08322	1.51596	0.57920
1/400	1.08322	1.51596	0.57920

Table C.8: CR α of δ_e for $b = 1.5$, variable load.

Crack Tip Opening for the Viscoelastic Case

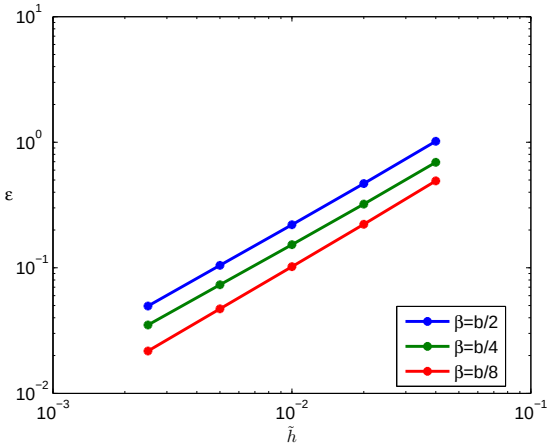

Figure C.7: Error of δ_v vs. step size for $b = 4$ (variable load).

$\tilde{h}$ \ β	$\frac{b}{2}$	$\frac{b}{4}$	$\frac{b}{8}$
1/25	-	-	-
1/50	1.11985	1.10527	1.14557
1/100	1.08832	1.07462	1.12320
1/200	1.07568	1.06124	1.11536
1/400	1.07568	1.06124	1.11536

Table C.9: CR α of δ_v for $b = 4$, variable load.

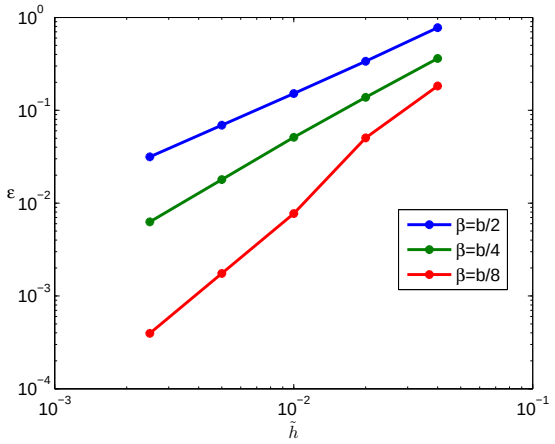

Figure C.8: Error of δ_v vs. step size for $b = 1.5$ (variable load).

$\tilde{h}$ \ β	$\frac{b}{2}$	$\frac{b}{4}$	$\frac{b}{8}$
$1/25$	-	-	-
$1/50$	1.20393	1.38697	1.85606
$1/100$	1.15729	1.43407	2.70668
$1/200$	1.13264	1.51320	2.14398
$1/400$	1.13264	1.51320	2.14398

Table C.10: CR α of δ_v for $b = 1.5$, variable load.

Appendix D

MATLAB Files: Names and Roles

All the algorithms constructed in this thesis were implemented using MATLAB. Table D.1 shows the main MATLAB files used. All the MATLAB files used for this thesis are on a CD which is submitted with the thesis.

Table D.1: Role of main m files used in MATLAB.

File Name	Role of file
nitem9.m	computes the CZ tip coordinate for the stationary crack problem. The stresses ahead of the CZ and in the CZ and at the tip are therefore computed
displ.m	computes the crack tip opening in the elastic case
displvisc.m	computes the crack tip opening in the viscoelastic case
algnewm2.m	computes the crack length and CZ tip coordinate for the propagating crack stage (elastic case)
vvalgnewm2.m	computes the crack length and CZ tip coordinate for the propagating crack stage (viscoelastic case)
crate.m	computes the numerical convergence rates α for specified solutions where the error is also calculated